



City Research Online

City, University of London Institutional Repository

Citation: Xiao, Y. (2018). Quivers, tilings and branes. (Unpublished Doctoral thesis, City, University of London)

This is the accepted version of the paper.

This version of the publication may differ from the final published version.

Permanent repository link: <https://openaccess.city.ac.uk/id/eprint/22113/>

Link to published version:

Copyright: City Research Online aims to make research outputs of City, University of London available to a wider audience. Copyright and Moral Rights remain with the author(s) and/or copyright holders. URLs from City Research Online may be freely distributed and linked to.

Reuse: Copies of full items can be used for personal research or study, educational, or not-for-profit purposes without prior permission or charge. Provided that the authors, title and full bibliographic details are credited, a hyperlink and/or URL is given for the original metadata page and the content is not changed in any way.

Quivers, Tilings and Branes

by

Yan Xiao



Submitted to the Department of Mathematics
in partial fulfillment of the requirements for the degree of

Doctor of Philosophy

at the

CITY, UNIVERSITY OF LONDON

July 2018

*To my wife Sinuo,
whose enduring love and caring support have always guided me in this long journey,
also to my little angels Yoyo and Xiaolu,
who have brought pure joy and happiness to the family,
with love and gratefulness.*

Quivers, Tilings and Branes

by

Yan Xiao

Submitted to the Department of Mathematics
on 30 July, 2018, in partial fulfillment of the
requirements for the degree of
Doctor of Philosophy

Abstract

In this thesis, We review the history behind brane tilings and quiver gauge theories as well as recent developments within this field. The aim of this work is to present a concise introduction towards this field as well as recent new developments on their classifications. In the chapter 3, we present a classification of brane tilings purely from a geometric point of view, *i.e* given a toric diagram of certain area, we find a host of quiver gauge theories that have their vacuum moduli space (VMS) given by the toric geometry.

Brane tilings are bipartite periodic graphs on a torus and they are a graphic representation of $4d \mathcal{N} = 1$ supersymmetric gauge theories originating from D3-braning probing a Calabi-Yau 3-fold singularity. The combinatoric properties of toric diagrams brane tilings/dimer models make themselves the largest and richest set of supersymmetric gauge theories know so far. However, the classification of these theories still remain on the physical side and another classification based on the toric diagram of VMS is developed in this work. In particular, we classified all toric CY 3-folds with toric diagrams up to area 8 and constructed a brane tiling for each of them. To do so, we developed implementations of dimer model techniques specifically tailored for partial resolution. We also created computational modules for a wide range of manipulations and computations involving brane tilings.

Acknowledgments

I would like to express my sincere gratitude towards my supervisor Prof. Yang-Hui He, whose enduring patience and endless discussion have shaped my understanding of physics and research. It would also not be possible to complete this thesis without his numerous enlightening insights. Above all, his cheering and curious attitudes towards life have shown me the glimpse of the working of optimism and great personality.

I also would like to express my sincere thanks to my intellectual brothers Chuang Sun and Da Zhou, whose countless discussion on our collaboration projects have always been interesting and refreshing. I also would like to thank my collaborators Sebastian Franco and Vishnu Jejjala for deepening my knowledge during our collaboration.

I offer my thanks to my fellow students in the Mathematics departments at City, who shared memorable and stimulating times with me.

Lastly, I would like to offer my gratitude towards City Doctoral Studentship funding body, whose generous financial support meant a great deal to me.

Contents

1	Introduction	15
1.1	Historical Aspects of String Theory	16
1.2	Some Elements of String Theory	18
2	Brane Tiling and Quiver Gauge Theory	25
2.1	A List of Geometries	25
2.2	Quiver Gauge Theory	31
2.2.1	Anomaly Cancellation in Quivers	35
2.2.2	Toric Quiver Gauge Theories	36
2.2.3	Quiver Gauge Theories from D-brane Systems	39
2.3	Brane Tiling	45
2.3.1	Brane Tilings and Dimer Models	47
2.3.2	A Short Review on Toric Geometry	53
2.3.3	Dimer Models and Toric Geometry	65
2.4	Forward and Inverse Algorithms	73
2.4.1	Forward Algorithm	73
2.4.2	Inverse Algorithm	77
2.5	Brane Tiling from Brane Construction	84
2.5.1	Relation to D3-Brane Setup	86
3	A Survey of Brane Tilings	89
3.1	Introduction	89
3.2	Brane Tiling Technology	91
3.2.1	D3-Branes Probing Toric CY 3-Folds and Brane Tilings	91
3.2.2	Geometry and Perfect Matchings	93

3.2.3	Partial Resolution and Brane Tilings	96
3.2.4	Brane Tiling Consistency	102
3.3	Existing Classifications	105
3.4	The Geometries	108
3.5	Results	112
3.5.1	Area 6	113
3.5.2	Area 7	117
3.5.3	Area 8	122
3.5.4	Examples: GLSM data for Area 6, 7, 8	131
4	Conclusions	141
A	A	143
A.1	Quick Review on String Theory	143
A.1.1	The Bosonic String	143
A.1.2	Strings with World-Sheet Supersymmetry	149
A.2	Notes on Anomalies in Superstring Theory	168
A.2.1	Chiral Anomaly	168
A.2.2	Anomalies in Gauge Theory	172
A.3	McKay Correspondence	180
A.4	D-branes as Probes of ALE Spaces	182
A.4.1	The Orbifold Spectrum	182
A.4.2	Spectrum on K3 Manifold	184
A.4.3	Singular Limit of K3 Manifold	185
A.5	D-brane Probes	186
A.5.1	ALE Space as the Moduli Space	190
A.5.2	Hyper-Kähler Quotient Construction of ALE Spaces	191
A.6	Computational Modules	195
	Bibliography	197

List of Figures

1-1	An illustration of compactification, where the base manifold is M , where the 2D cylinder looks effectively 1D from a far distance or in low energy limit	18
2-1	The toric diagrams for the classification of Gorenstein singularities of three complex-dimensions by the behaviour of contraction of a single extremal ray. The higher del Pezzo surfaces $dP_{4,\dots,8}$ are not listed since they are non-toric. However, there are the so-called pseudo del Pezzo for dP_4 and dP_5 are studied in [140], which are not generic, smooth dP_4 and dP_5 but degenerate cases with isolated singularities.	31
2-2	Two examples for quiver diagrams.	32
2-3	The quiver diagram for the phase b of the Hirzebruch F_0 model.	34
2-4	The duality between the quiver of A_1 theory and the brane system of D-branes stretching between NS5-branes. They are essentially graph dual of each other viz. the nodes in one are arrows in another and vice versa. The node label in the A_1 quiver becomes the number of D-branes represented by the arrow in the other diagram.	44
2-5	The quiver for D3-branes probing singular metric cone over del Pezzo 1 surface.	49
2-6	The planar quiver for D3-branes probing singular metric cone over del Pezzo 1 surface.	50
2-7	The brane tiling/dimer model for D3-branes probing singular metric cone over del Pezzo 1 surface.	51
2-8	The 8 perfect matchings for D3-branes probing singular metric cone over del Pezzo 1 surface. The weights (h_w, h_z) denotes the intersection of the perfect matching with the boundary of the fundamental region.	54

2-9	The two fans for \mathbb{CP}^2 and $\mathbb{CP}^{(2,3,1)}$. Both of them includes three two-dimensional cones spanned by $v_1 - v_2$, $v_2 - v_3$ and $v_1 - v_3$ and three one-dimensional cones $v_1 v_2$ and v_3 and the origin.	56
2-10	The resolved toric variety for $\mathbb{CP}^{(2,3,1)}$. The added vectors v_4 , v_5 and v_6 , actually correspond to the blown-up exceptional divisors.	59
2-11	The fan for \mathbb{CP}^2 is shown as before as well as the coordinates for the corresponding v_i for $i = 1, 2, 3$. The toric diagram is drawn in thick black lines and it is indeed the dual diagram of the fan.	61
2-12	The diagram on the left is the toric diagram Δ for del Pezzo 1 surface with labels for perfect matchings. The details of the relation between coordinates of the toric diagram and perfect matchings with possible multiplicities are presented in section 2.3.3. The diagram on the right is the complete triangulation of the toric diagram on the left which gives the resolution to the singular metric cone over the del Pezzo 1 surface and the (p, q) -web is given by the thick black lines in it.	63
2-13	The toric diagram of \mathbb{CP}^2 with normals to edges of the shaded triangle giving the degeneration direction of T^3 fibre.	64
2-14	The reduced (p, q) -web diagram and the extended (p, q) -web diagram for dP_1	69
2-15	The two possible partial resolutions of the cone over dP_1 that are realised as linear sigma model with a non-anomalous baryonic $U(1)$: a). $\zeta > 0$ case, representing toric divisors $m_2 = 0$ and m_4 , which can not simultaneously vanish, separated by a blow-up \mathbb{CP}^1 . b). $\zeta < 0$ case, toric divisors $m_1 = 0$ and $m_3 = 0$ are separated by a blow-up \mathbb{CP}^1	73
2-16	The flow-chart for the 'old' forward algorithm that relies on finding the dual cone of K defined by $T = \text{Dual}(K)$. This algorithm is slow as the process of find dual cone has exponential running time.	76
2-17	The toric diagram showing the resolution of the $\mathbb{C}^3/(\mathbb{Z}_2 \times \mathbb{Z}_2)$ singularity on the left to the suspended pinch point (SPP) on the right. The numbers i at the nodes refer to the i -th column of the matrix G_t and physically correspond to the fields m_i in the linear σ -model.	79

2-18	The first diagram is prohibited by the conservation of NS5-charges; The second and the last diagrams represent bound states of N D5-branes and 1 NS5-brane, called the $(N, 1)$ -system. Similarly the third is called $(N, -1)$ -system due to the reversal of orientation of NS5-brane.	85
2-19	The web of connection of brane realisation of D3-brane probing toric Calabi-Yau singular cone over base of SPP. We see that the physical information is fully included in the brane tiling/dimer and the brane construction gives precisely this bipartite tiling on a T^2 , which are the direction we choose to implement the T-dualisation.	87
3-1	Quiver diagram for SPP. Nodes represent gauge groups. The arrow from $i \rightarrow j$ corresponds to the chiral field X_{ij}	94
3-2	Brane tiling for SPP.	95
3-3	Toric diagram for SPP. We indicate the perfect matching associated to each point.	96
3-4	Toric diagrams for: a) $\mathbb{C}^3/(\mathbb{Z}_m \times \mathbb{Z}_n)$ and b) $\mathcal{C}/(\mathbb{Z}_m \times \mathbb{Z}_n)$. We will use the second class of geometries as the starting points for partial resolution.	98
3-5	Brane tiling for $\mathcal{C}/(\mathbb{Z}_2 \times \mathbb{Z}_2)$	99
3-6	Toric diagram for $\mathcal{C}/(\mathbb{Z}_2 \times \mathbb{Z}_2)$ We indicate the perfect matching associated to each point and a possible embedding of the SPP toric diagram (in red).	100
3-7	Toric diagram for SPP obtained by partial resolution of $\mathcal{C}/(\mathbb{Z}_2 \times \mathbb{Z}_2)$	101
3-8	An inconsistent brane tiling for digram 5 in the area 6 list. We see that the number of faces is 7, which is greater than the area of the toric diagram.	104
A-1	Path integral on a torus where the fermions may obey + or - boundary conditions in the σ_1 and σ_2 directions respectively.	159
A-2	The two triangle diagrams to illustrate chiral anomaly. Note that these two diagrams are required by bose statistics and $q = k_1 + k_2$	168
A-3	The Feynman diagram for hexagonal loop amplitude.	173

A-4	The dynkin diagrams for affine simply-laced Lie algebras. The nodes are labelled by comarks of each simple roots. These diagrams have an extra affine node (marked with crosses) due to the central extension.	181
A-5	The quiver diagram for the $U(1) \times U(1)$ gauge theory on D1-brane.	188

List of Tables

2.1	Dictionary for translating between the graph representation of a quiver and the supersymmetric gauge theory that underlies it.	33
2.2	Algebraic singularities describing \mathbb{C}^2/Γ in affine coordinates.	40
2.3	The coordinate arrangement for dual D2-branes and NS5-branes.	41
2.4	The dictionary translating between data in planar quiver and that in brane tiling.	49
2.5	The 5-brane configuration of the NS5-D5 system. We see that the D5 branes break a half of the supercharges and NS5 branes in two directions break the supersymmetry to a quarter resulting 4 supercharges, thus $\mathcal{N} = 1$ in four-dimension.	85
2.6	The brane configuration of a general brane tiling from NS5-D5 brane system. The 5, 7-th directions are compactified and Σ is a holomorphic curve in 4, 5, 6, 7-directions. All the NS5-branes in table 2.5 are merged into a single NS5-brane wrapping holomorphic curve.	86
2.7	The brane configuration after taking T-dualisation in the compactified 5, 7-th directions in the 5-brane system shown in table 2.5. The D5-brane is T-dual to D3-brane and the NS5-brane is dual to the toric Calabi-Yau cone.	86
3.1	The known geometries inside the classification in section 3.4.	107
3.2	Toric diagrams of areas 1, 2 and 3.	108
3.3	Toric diagrams of area 4.	108
3.4	Toric diagrams of area 5.	109
3.5	Toric diagrams of area 6.	109
3.6	Toric diagrams of area 7.	110
3.7	Toric diagrams of area 8.	111

A.1	The classification of discrete subgroups of $SU(2)$. As we can see that this has an ADE pattern. Note the ‘binary’ essentially comes from the fact that $SU(2)$ is a double cover of $SO(3)$	180
A.2	Transformation properties of massless states in the untwisted sector.	183
A.3	Transformation properties of massless states in the untwisted sector.	183
A.4	The bosonic spectrum for the untwisted and twisted sectors.	184
A.5	The coordinate arrangement for D1-brane probing ALE.	187

The author has made the following publications during his Ph.D.:

- Y. H. He, V. Jejjala, L. Pontiggia, Y. Xiao and D. Zhou, “Flatness of Minima in Random Inflationary Landscapes,” arXiv:1704.08351 [hep-th].
- S. Franco, Y. H. He, C. Sun and Y. Xiao, “A Comprehensive Survey of Brane Tilings,” Int. J. Mod. Phys. A **32**, no. 23n24, 1750142 (2017) doi:10.1142/S0217751X17501421 [arXiv:1702.03958 [hep-th]].
- D. Zhou, Y. Xiao and Y. H. He, “Seiberg duality, quiver gauge theories, and Iharas zeta function,” Int. J. Mod. Phys. A **30**, no. 18n19, 1550118 (2015) doi:10.1142/S0217751X15501183 [arXiv:1502.05771 [hep-th]].
- Y. Xiao, Y. H. He and C. Matti, “Standard Model Plethystics,” arXiv:1902.10550 [hep-th].

THIS PAGE INTENTIONALLY LEFT BLANK

Chapter 1

Introduction

Modern theoretic physics has two central pillars: general relativity and quantum mechanics. General relativity affords us the theoretic framework for understanding the large scale of universe. It is understood as perturbative correction to the prediction of Newtonian gravity for the motions of planets and curving of light. It is essentially a geometric view on the universe, where the curvature tells the masses how to move and the masses back-reacts to tell the space how to curve. It changes our fundamental view about space and time: they are dynamical. On the other hand, quantum mechanics is for the microscopic side, where atoms and particles are in the center of the scene. Importantly, evidences continue to show that quantum mechanics is part of the property of the Nature.

The reconciliation and union of general relativity and quantum mechanics are now at the center of modern theoretic physics research due to the common perception that our understanding of the fundamental laws of Nature is only complete when we can derive the two theories from a unified one. However, these two fields have differing concepts, types of calculation and even the definition of observables and they developed almost in parallel until about 1980's. Just to enumerate some of the common issues arise in relativistic quantum mechanics (QFT), one usually has to require two fields defined at two different spacetime points with space-like separation commute. However, gravity dictates that one can only know about the nature of the separation when the metric of the space is defined, which itself is dynamic problem. More importantly, the metric itself is a dynamic object, whose quanta is the famous graviton.

One usually tries to combine quantum mechanics and general relativity within a perturbative regime of quantum field theory. This method runs into the famous ultraviolet divergences at higher order correction. This can be seen from dimensional analysis with knowing the fact that the coupling constant for gravity *i.e.*, Newton's constant in $4D$ is proportional to $(\text{length})^2$ and this gives extra powers of momenta when doing the loop integral and this renders the conventional renormalization methods in QFT unfavourable. However, string theory becomes popular when it purports to provide a consistent quantum theory of gravity.

In next section we review some historical aspects of string theory as well as some basic elements that are relevant to the main focus of this thesis.

1.1 Historical Aspects of String Theory

String theory was first developed to understand the strong nuclear force in 1960's, which is the force holding constituent parts of a nucleus, such as protons, neutrons and quarks. This theory has its basic building block as a string rather than normal particles. Particles inside strong nuclear interaction are represented by different oscillation of strings. In early 1970's, another theory called quantum chromodynamics was developed to solve problems in string theory such as existence of spin-2 particle. However, string theory turned out to be a more ambitious project to unify quantum mechanics with general relativity due to its natural inclusion of the spin-two particle that can be interpreted as graviton. It is important for us to quickly review some well understood salient features of the theory.

Gravity The first is that it naturally includes gravity for the theory to be consistent. Even though the theory has corrections at higher energy, the lower energies the theory gives us Einstein gravity. In contrast, QFT does not allow gravity to exist due to some reasons listed in the previous section.

Yang-Mills Gauge Theory In addition to gravity, present elementary particle physics standard model requires Yang-Mills theory with product gauge group $SU(3) \times SU(2) \times U(1)$ to account for large amount of experimental data. String theory naturally includes gauge

groups of this kind from models such as heterotic string theory and D-brane world volume gauge theories.

Supersymmetry String theory also requires supersymmetry for consistency. Supersymmetry is a symmetry that relates bosons with fermions and it is to be experimentally confirmed. The lack of data for supersymmetry indicates that our probing energy scale is probably below that of supersymmetry breaking and lower than the supersymmetric partners of known particles. One of the major predictions can be made by supersymmetry is spacetime supersymmetry and some argue that the energy scale for supersymmetry breaking is around electroweak scale, *i.e.*, from 100 GeV to a few TeV. The hope is that some superpartners should be observable at Large Hadron Collider.

Extra Dimensions of Spacetime String theory has consistency requirements to predict the dimension of the spacetime it lives in. Specifically, superstring theory is only consistent in a 10 dimensional spacetime. These extra dimensions need to be compactified to make contact with the 4 dimensional world we live in. Therefore, the compactified 6 dimensional space is assumed to be an internal manifold and is small enough to be insensitive to experimental detection. Here we briefly review the initial idea on compact dimension. The original idea was first introduced by Kaluza and Klein in the 1920s. This was developed to unify gravity with electromagnetism in 4 dimension by reducing 5 dimension gravity on a circle. This can be illustrated more clearly in Fig. 1-1, where we can see the top cylinder has its surface being 2 dimensional. Now if we take the radius of the cylinder to extremely small, it effectively becomes 1 dimensional as shown in the bottom of the figure. So one now replaces the long dimension of the cylinder by our ordinary 4 dimensional and the short dimension by a 6 dimensional compact manifold. At large distance or lower energy, the compact internal dimensions “escape” detection and the description becomes a four-dimensional low energy effective theory of the full ten-dimensional one. However, the topological properties of this invisible internal space determine the particle contents and structure of the four-dimensional theory. Calabi-Yau manifolds were first considered for compactification and they have rather attractive phenomenological implications even though it suffers from the problems such as

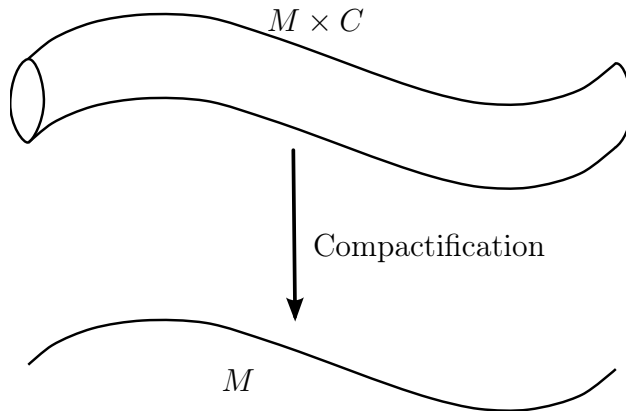


Figure 1-1: An illustration of compactification, where the base manifold is M , where the 2D cylinder looks effectively 1D from a far distance or in low energy limit

moduli space or the string theory landscape.

1.2 Some Elements of String Theory

Before we start discussing brane-tilings and its relation to toric geometry as well as their recent development, it is worthwhile to develop some background from string theory. A more detailed review on bosonic and superstring theories is presented in appendix A.1.

String theory is a theory of quantised, relativistic strings which are controlled by only one free parameter - the string tension T which is related to the Regge slope α' through $T = (2\pi\alpha')^{-1}$. This greatly contrasts with the roughly twenty parameters in Standard Model (coupling constants, fine structure constants, Weinberg angles etc.). Within the theory, there are two topologically different strings, open string with two end points and closed strings which is topologically a circle. The Nambu-Goto action for bosonic string is presented in eq. (A.2). The world-sheet Σ swept out by the string is parametrised by (σ, τ) , which are the spatial and time coordinates on Σ . The integral simply gives the invariant area measured by the induced metric $G_{\alpha\beta} = \partial_\alpha X^\mu \partial_\beta X^\nu \eta_{\mu\nu}$. The spacetime coordinate X^μ is simply a map from world-sheet Σ to the spacetime with Minkowski metric $\eta_{\mu\nu}$. The equation of motion after fixing the gauge is simply a plane wave equation $\partial_\alpha \partial^\alpha X^\mu = 0$, whose solution in light cone coordinates splits into left- and right-moving sectors. Quantisation of the mode expansions of the solutions gives a spectrum that needs to be identified with particles in particle physics.

Schematically, the spectrum is of the form $\alpha' m^2 = n$ for $n \in \mathbb{Z}^+$. Importantly, the spectrum of the closed string always contains a spin two massless mode that can be identified with the graviton. The scattering amplitude of these gravitons up to certain levels are shown to be finite and in such perspective string theory is said to be a potential candidate for quantum gravity. On the other hand, we can impose either Dirichlet or Neumann boundary condition for each end of the open string. Specifically, the Dirichlet boundary condition fixes the end points of an open string, resulting the momentum of the open string not being conserved. However, the Poincaré invariance implies the conservation space-time total momentum, which in turn defines some the hyper-surfaces exchanging momentum with open strings. They are called ‘D-branes’. Since the two ends of open strings are special positions on the string, they can carry charges of fundamental representation of some gauge groups ($SO(32)$) through Chan-Paton factors[12], such that the corresponding gauge group can be thought to reside on the D-branes.

In the bosonic theory, tachyons with imaginary mass are present and their existence within the spectrum indicates instability of the vacuum. Their elimination requires supersymmetry, which is discussed in appendix A.1.2 in more detail. The inclusion of world-sheet fermions ψ_{\pm}^{μ} allows different boundary conditions to be imposed on them *i.e.* Ramond (periodic) or Neveu-Schwarz (anti-periodic) boundary conditions. Since closed string has independent left- and right-movers, there are four different sectors with NS-NS, R-R sectors generating spacetime bosons and NS-R, R-NS leading to spacetime fermions. On the other hand, open strings have fixed ends on D-branes and therefore the modes are standing waves giving only R sector for fermions and NS sector for bosons. The quantisation of this theory requires the superconformal symmetry to decouple the unphysical longitudinal (negative-norm) states, which requires the critical dimension of the theory to be $D = 10$. On top of this, the NS side of the spectrum still contains tachyons and the spectrum must be truncated by Gliozzi-Scherk-Olive projection operator (see appendix A.1.2). Note that the GSO projection is not just an ad-hoc construction to make the spectrum free of tachyon and supersymmetric, it is also a requirement from one or two loop modular invariance of string partition function.

With the previously described features of both open and closed superstrings, we sum-

marise the five consistent string theories as follows. A more detailed construction of these theories is reviewed in appendices A.1.2 to A.1.2. The type I theory has one set of supersymmetry since it can be derived from world-sheet parity projection from type IIB. Therefore, it is a $\mathcal{N} = 1$ theory of both open and closed strings with 16 supercharges. The ends of the open strings are assigned gauge charges by Chan-Paton method [12]. In addition, anomaly cancellation requires the gauge group to be $SO(32)$. If the theory only contains closed strings, they are divided into type II and heterotic theory. The theory with opposite chirality for the R-R ground state is called IIA and the one with same chirality is called IIB. Note here the IIA theory is non-chiral and the IIB theory is chiral. Both theories have 32 supercharges since the Majorana-Weyl fermion in ten dimensions have 16 real components and left- and right-moving sector are independent. The heterotic string theory is also a theory of closed string only and it has 16 supercharges. This theory has its left- and right-moving modes decoupled and the right-moving modes are the same as those in type II, the left-moving modes are used to accommodate gauge symmetry through suitable current algebra. Anomaly cancellation dictates the gauge theory to be $SO(32)$ or $E_8 \times E_8$.

The five string theories are not completely independent and in fact they are related by a web of dualities [13]. For example, T-duality shows that two different geometries are physically equivalent under the transformation of radius $R \rightarrow l_s^2/R$, with $l_s = \sqrt{\alpha'}$. T-duality relates the two type II theories to each other and the two heterotic theories to each other. This duality is a manifestation of the extended nature of the one dimensional string. The S-duality $g_s \rightarrow 1/g_s$ relates the weak coupling regime of one theory to the strong coupling regime of another. This related type I theory to the $SO(32)$ heterotic theory and type IIB to itself. The rest of the two theories, type IIA and heterotic $E_8 \times E_8$ grow an eleventh dimension of size $g_s l_s$ when g_s becomes large. This is the 11-dimensional M-theory [5].

However, for string theory to make contact with the nature, we need to build a 4-dimensional out of the 5 $10D$ critical superstring theories. The idea of *string compactification* was then borne out to solve this dimensional discrepancy. Six dimensions K are ‘compactified’ in a sense they are ‘internal’ and far below current limits of experimental probes, as compared to the current observed macroscopic four dimensions M_4 . Therefore, the 10-dimensional spacetime is a product of geometries of the form $M_4 \times K$. For string

theory to be a theory of gravity, the metric on this 10-dimensional product space has to obey the $10D$ Einstein equation. For the correct amount of supersymmetry, K has to afford a Ricci-flat metric to be a Calabi-Yau (CY) manifold [14]. Calabi-Yau manifolds offer another equivalent definition as a Kähler manifold with vanishing first Chern class. There are various ways of constructing CY manifolds, yet the largest class of non-compact CY manifolds are constructed over toric varieties [15]. These varieties are in the form of weighted projective spaces represented by reflexive polygons in certain lattices. The CY manifolds of such type are the central objects within this thesis and we will develop a more detailed survey later in this chapter.

As strings playing a fundamental role in string theory, D-branes on the other hand serves as a deep connection between algebra and geometry. Since D-branes carry gauge theories in its world-volume, they are a natural starting point for building phenomenological models. Following this route, D-branes are placed on a singularity of type \mathbb{C}^2/Γ (where Γ is a subgroup of $SU(2)$) [16], to produce gauge theories that are captured by affine Dynkin diagrams. The fractional branes are mapped to nodes in the diagrams while strings stretching between fractional branes mapped to lines in the diagram. This relation between affine Dynkin diagrams from Lie algebras and geometry of ALE spaces are known as McKay correspondence [19]. In addition, McKay correspondence can also be realised in Hanany-Witten setup [65]. The NS5-branes in this setting have D-branes stretching between them. The NS5-branes are mapped to lines and D-branes to nodes. The lines and nodes are collected into a graph called *quiver graph*. For such objects, nodes are the gauge groups and the oriented arrows are bifundamental chiral multiplets transforming between the two gauge groups represented by the connected nodes. The gauge invariant operators (terms in the superpotential) from this gauge theory is therefore represented by the closed cycles in the quiver. Phenomenologically, the presence of D-branes breaks supersymmetries as they impose certain boundary conditions to relate left- and right-moving modes. In such sense, the supercharges are reduced from 32 to 8 in this case and we then have a $\mathcal{N} = 2$ four-dimensional theory. Pursuing this path, many have made attempts to generalise this idea to three complex-dimensional spaces [20, 21, 22, 23]. One of methods is to place the D-branes at the singularity of a three-dimensional (complex) Calabi-Yau manifold, *e.g.* conifold and its quotient space by a

finite abelian subgroup of $SU(3)$. The amount of supersymmetry is further reduced by a half to 4 ($\mathcal{N} = 1$ in four dimensions). This construction is the main theme of this article and we shall also cover some more detailed backgrounds and its relation to *brane tiling*.

Therefore, we pause to present a short summary before we plunge into the next part of this article. Having whetted our appetite with some brief comments on string theory, we understand that this is the much pursued goal for theoretical physics/string theory community to reconcile high-energy, supersymmetric and extra-dimensional theories to low-energy four-dimensional gauge dynamics. The reason for one to study supersymmetric gauge theories is that many of their properties can be analysed non-perturbatively. This is then a fertile testing ground for dynamics of gauge theories [66, 67, 65] and a plethora of phenomena such as gauge theory phases and dualities [66, 68, 69, 70, 71, 72]. Thus we would like to construct interesting gauge theories from string theory to study the aforementioned aspects. A powerful way of constructing them is through probing Calabi-Yau singularities with D-branes [27, 28, 29]. Under this particular construction, a deep connection between geometry and physics becomes manifest as different singularities give rise to different conformal field theories. The use of D3-branes is particularly interesting since this engenders unitary gauge group, bifundamental/adjoint matter and superpotentials. The gauge group, matter content and superpotential of a theory of such type can be neatly recorded in a graph known as a *quiver*. This type of gauge theories are referred to as quiver gauge theory [24]. The quiver along with its superpotential are enough to reconstruct the Lagrangian of a $4D$ $\mathcal{N} = 1$ supersymmetric gauge theory [34, 36, 37]. The interplay between geometry and physics in quiver gauge theory is grounded on the geometric structure of moduli space of the gauge theory. The space of solutions of field equations or the moduli space carries intricate structures and they are of great interest to mathematical field such as algebraic geometry. The study of moduli space structure of a supersymmetric quiver gauge theory is deepened with the inclusion of Hilbert series [76, 77, 78, 79, 80]. It is the generating function of holomorphic gauge invariant operators under certain gauge charges and they are closely related to the vacuum of the theory. This function not only carries the information about the spectrum of the theory, it also has criterion on whether the moduli space is Calabi-Yau and its degree and dimension.

The AdS/CFT correspondence [113, 114, 115] has been a powerful toolkit for recent advances in theoretic physics. This correspondence relates weak and strong coupling theories such that the weak (strong) coupling sectors of gravity on anti-de Sitter (AdS) spaces are translated to the strong (weak) limit of a conformal field theory (CFT) living on its boundary of AdS. This duality is absolutely non-trivial since it opens a window to learn about the strong coupling regime by just looking at the weak coupling limit of another theory. Under this correspondence, the $4D \mathcal{N} = 1$ worldvolume gauge theories living on D3-branes probing a Calabi-Yau threefold singularity is dual to IIB string theory living on a geometry of $AdS_5 \times X_5$ with X_5 being a Sasaki-Einstein 5-fold [28, 34, 116]. The gauge theories in this duality are superconformal and can be drawn on a 2-torus as a bipartite graph. This graph is called *brane tiling* [49, 51], which is utilised to make classification [169, 55, 56] of supersymmetric gauge theories with toric Calabi-Yau moduli spaces.

The recent advances in brane tilings are based on the introduction of dimer models into the scene and this is another example of interplay between mathematics and physics. With brane tiling encoding the matter content and superpotential of supersymmetric gauge theory, dimer gives a bipartite graph representation of brane tiling. The nomenclature “brane tiling” actually comes from the early endeavours in brane construction of $4D \mathcal{N} = 1$ superconformal gauge theory [49, 51, 64, 62, 63]. On the other hand, dimer is a term from mathematical community that this bipartite graph has great resemblance of chemical compound with two molecular components. Examples of studies on dimer in mathematical literatures are [62, 63].

The previous paragraphs presented an bird’s-eye view on the main topics of this article: brane tiling and dimer model. It is satisfying to end this lightning introduction with a short summary of brane tiling related topics in string theory/high energy physics:

- Moduli spaces of supersymmetric gauge theories [49, 81, 80, 51, 82, 83, 85, 84]
- Seiberg duality and toric duality [71, 69, 70]
- MSSM and String phenomenology [86]
- Wall-crossing and crystal melting [89, 88, 90]

- Integral systems [91, 92, 93]
- $\mathcal{N} = 4$ Super-Yang-Mills scattering amplitude [94, 95]

The dimers on the other hand, have been used extensively in the following fields of mathematics

- Mirror symmetry [96]
- Graph theory and combinatorics [62, 63]
- Tropical geometry [97]
- Calabi-Yau algebras [98, 99, 100]
- Grothendieck's dessin d'enfant [107, 108, 106]

Lastly, before we plunge into the a more detailed exposition of brane tiling, it is expedient to present the structure of this article:

- Chapter 2 reviews the intricate connections between *quiver gauge theory* and *brane tilings*. This includes the foundation of quiver gauge theory from a physical point of view as well as its original motivation [24]. The essential contents of brane tilings are also reviewed with emphasis on the physical interpretation of brane tilings as brane systems. By passing from the physical view point, we then move onto the contents of toric geometry.
- Chapter 3 develops the main contents of this article, which offers a new classification of brane tilings according to the area of the toric diagrams which underpins the geometry of the VMS of associated gauge theories. The technique used in this thesis is based on the old desire of [71], which initiated the *Inverse Algorithm* to extract the quiver gauge theory as well as superpotential via partial resolution of the orbifold of conifold to desired toric diagram.

Chapter 2

Brane Tiling and Quiver Gauge Theory

In this chapter, we present a short pedagogical introduction to toric quiver gauge theories which live on the world-volume of a stack of coincident D3-branes placed at the singular tip of a toric Calabi-Yau cone. These theories provide us with an infinite class of $4D \mathcal{N} = 1$ superconformal gauge theories which may then be studied in the context of AdS/CFT correspondence. It is now understood that these theories are completely determined by a two-dimensional bipartite graph drawn on a torus *i.e.* the brane tilings and the combinatoric information of the dimer model along with the graph. Therefore, it is useful to review aspects of quiver gauge theory. Along with quiver gauge theory, brane tilings and toric geometry are the related subjects which we shall also review to give a coherent picture.

2.1 A List of Geometries

Before we move onto the main content of this chapter, it is instructive to include a short summary of geometries that will appear in later text for the convenience of the reader as well as the flow of the text. All of these geometries afford a toric description such that they have corresponding toric diagrams, whose definition are presented in section 2.3.2.

Conifold The (singular) conifold is a cone over a five dimensional base and it is a Calabi-Yau threefold. There are two related cases to such singular manifold: one is called a “resolved conifold”, with a blown-up S^2 at the tip of the cone; the other is the “deformed conifold”

whose tip of the cone is blown into an S^3 . All three cases look asymptotically the same as a cone over $S^2 \times S^3$. Their metric takes the form

$$ds^2 = dr^2 + r^2 ds_{\text{base}}^2 .$$

It was shown by Candelas and de la Ossa [170] that all of these three manifolds possess a Ricci flat Kähler metric and one can continuously pass from one geometry to another. This transition is called a *conifold transition*¹. Here we briefly review the geometric properties for all these three manifolds.

- **The singular conifold.** Just as a two-dimensional cone can be embedded in real three dimensional space by $x^2 + y^2 - z^2 = 0$, a real six dimensional conifold can be expressed in terms of three complex coordinates and thus can be embedded in \mathbb{C}^4 as

$$\sum_{i=1}^4 z_i^2 = 0 . \tag{2.1}$$

This gives us a surface that is smooth apart from singularity at $z_i = 0$. This surface has $SO(4) \simeq SU(2) \times SU(2)$ symmetry where z_i are rotated into each other and a $U(1)$ symmetry that rotates z_i by the same phase. There is also a scaling symmetry $z_i \rightarrow tz_i, t \in \mathbb{C}^*$. Let us choose $z_i = x_i + iy_i$ such that

$$\sum_{i=1}^4 x_i y_i = 0 , \quad \sum_{i=1}^4 (x_i^2 - y_i^2) = 0 . \tag{2.2}$$

Thus x_i describe a three-sphere for any y_i with vanishing radius at $y_i = 0$. The coordinates y_i are thus orthogonally fibred to x_i . The total space is thus the cotangent bundle T^*S^3 . To find the base of the conifold, we take the intersection with a three-sphere of radius r :

$$\sum_{i=1}^4 |z_i|^2 = \sum_{i=1}^4 (x_i^2 + y_i^2) = r^2 , \tag{2.3}$$

¹Note that these manifolds are topologically distinct as it can be seen from the Euler characteristics $\chi(S^3) = 0$, $\chi(\text{point}) = 1$ and $\chi(S^2) = 2$

which removes the scaling symmetry $z_i \rightarrow tz_i$. Together with eq. (2.2), we see that x_i in eq. (2.3) describe a three-sphere of radius $r/\sqrt{2}$ and y_i give a two-sphere fibred over S^3 . Since fibrations are trivial, the topology of the base $T^{1,1}$ is $S^2 \times S^3$. In addition, we also see that $T^{1,1}$ affords a coset description as $(SU(2) \times SU(2))/U(1)$. To see this, we first define

$$W = \frac{1}{\sqrt{2}} \sum_n \sigma^n z_n, \quad (2.4)$$

where σ^n are the Pauli matrices. So we have

$$W = \frac{1}{\sqrt{2}} \begin{pmatrix} z_3 + iz_4 & z_1 - iz_2 \\ z_1 + iz_2 & -z_3 + iz_4 \end{pmatrix} \quad (2.5)$$

In such setting, the defining equations for conifold can thus be written as

$$\begin{aligned} \det W &= 0 \\ \text{Tr } W^\dagger W &= r^2. \end{aligned} \quad (2.6)$$

If we make a rescaling $Z = W/r$, we the have

$$\begin{aligned} \det Z &= 0 \\ \text{Tr } Z^\dagger Z &= 1, \end{aligned} \quad (2.7)$$

We see that if we start with a particular solution such as $Z_0 = (\sigma_1 + i\sigma_2)/2$, a general solution $Z = LZ_0R^\dagger$ can be reached for

$$L = \begin{pmatrix} a & -\bar{b} \\ b & \bar{a} \end{pmatrix}, \quad R = \begin{pmatrix} k & -\bar{l} \\ l & \bar{k} \end{pmatrix}, \quad (2.8)$$

where $L, R \in SU(2)$. Thus we have shown that the group $SU(2) \times SU(2)$ acts transitively on the base. When $(L, R) = (\Theta, \Theta^\dagger)$ with

$$\Theta = \begin{pmatrix} e^{i\theta} & 0 \\ 0 & e^{-i\theta} \end{pmatrix}, \quad (2.9)$$

Z_0 is left-fixed. Thus we can identify (L, R) and $(L\Theta, R\Theta^\dagger)$, showing that the base is the coset space $(SU(2) \times SU(2))/U(1) = (S^3 \times S^3)/U(1)$ with topology $S^2 \times S^3$ and symmetry group $SU(2) \times SU(2) \times U(1)$.

- **The deformed conifold** The conifold can have its singularity resolved by deformation near $r = 0$

$$\sum_{i=1}^4 z_i^2 = \mu^2. \quad (2.10)$$

To find the base, we again intersect it with three sphere to find that, $2x_i^2 = \mu^2 + r^2$, which is a finite S^3 at $r = 0$. This is the *deformed conifold*. The $U(1)$ symmetry of the singular conifold $z_i \rightarrow e^{i\alpha} z_i$ is broken to a \mathbb{Z}_2 that sends $z_i \rightarrow -z_i$. In terms of matrix defined in eq. (2.5), the deformed conifold is

$$\det W = -\mu^2/2;. \quad (2.11)$$

A radius coordinate can be also defined as $r^2 = \text{Tr}(W^\dagger W)$. If we split z_i into real and imaginary parts, we see that

$$r^2 = \sum_{i=1}^4 (x_i^2 + y_i^2), \quad \mu^2 = \sum_{i=1}^4 (x_i^2 - y_i^2), \quad (2.12)$$

which implies that r takes value from μ to infinity. It is also clear that the deformed conifold is still a cotangent bundle of S^3 but with the S^3 having a minimal size prescribed by μ . Similarly, we can find a particular solution as

$$W_\mu = \begin{pmatrix} \frac{\mu}{2} & \sqrt{r^2 - \mu^2} \\ 0 & -\frac{\mu}{2} \end{pmatrix}, \quad (2.13)$$

where a general solution is obtained by $W = LW_\mu R^\dagger$ for $L, R^\dagger \in SU(2)$. For $r \neq \mu$, the stability group is $U(1)$ and for each $r = \text{constant}$, the surfaces are given by $S^2 \times S^3$. For $r = \mu$, the W matrix is proportional to σ_3 and is invariant under the entire $SU(2)$. Thus the ‘‘origin’’ of coordinates $r = \mu$ is $SU(2) \simeq S^3$.

- **The resolved conifold** The alternative to fix the singularity is to blow it up to a two-sphere. If we define a new set of variables by

$$x = z_1 + iz_2, y = z_2 + iz_1, u = z_3 - iz_4, v = z_4 - iz_3 \quad (2.14)$$

the conifold equation in 2.1 is rephrased as

$$xy - uv = 0, \quad (2.15)$$

which is equivalent to requiring non-trivial solution of matrix equation

$$\begin{pmatrix} x & u \\ v & y \end{pmatrix} \begin{pmatrix} \xi_1 \\ \xi_2 \end{pmatrix} = 0, \quad (2.16)$$

where ξ_1 and ξ_2 are not both zero. So for points away from the tip $(x, y, u, v) \neq 0$, this describes a conifold as usual. But at the tip $(x, y, u, v) = 0$, this equation is solved by (ξ_1, ξ_2) , which admits an overall scaling $(\xi_1, \xi_2) \sim (\lambda\xi_1, \lambda\xi_2)$. Therefore, we mod out this equivalence and see that (ξ_1, ξ_2) actually describes a two-sphere $\mathbb{CP}^1 \sim S^2$ at the tip of the cone.

Suspended pinch point (SPP) This geometry was first introduced by [28] in the context of compactifying M-theory on three complex-dimensional canonical Gorenstein singularities. Such singularities have a classification based on the behaviour of contraction of a single extremal ray (*i.e.* those which can be resolved by a single blow-up). The SPP geometry is within in the class of a surface “contracting” to a curve. More explicitly, it affords the following definition

Definition 2.1.1. *A rational ruled surface whose ruling has $n \geq 0$ degenerate fibres is contracted to a curve.*

We also note that since the singularities are not isolated in this case and there are only two isomorphisms of local singularities, corresponding to

- Contraction at a non-singular fibre of the ruling on the surface (the generic case). This

is a quotient singularity of the form $\mathbb{C}^3/\mathbb{Z}_2$, where the quotient only acts on two of the three complex coordinates, which is locally described by $xy = z^2$. This has a horizon of S^5/\mathbb{Z}_2 .

- Contraction at a singular fibre (the special case). This is the *suspended pinch point* with local equation $xy = z^2t$. The horizon of SPP is a circle bundle over weighted projective spaces² $\mathbb{WCP}^{1,2} \times \mathbb{WCP}^{1,2}$.

Del Pezzo surfaces Del Pezzo surfaces also falls in to the classification of three complex-dimensional canonical Gorenstein singularities as described in our discussion on SPP in the last paragraph. Generically, these singularities are formed by contracting a surface to a point. More specifically, the surfaces have the following definition.

Definition 2.1.2. *A (complex) del Pezzo surface is a smooth projective complex surface with ample anticanonical line bundle. These surfaces have a degree defined as the self-intersection of the canonical divisor. The possible degree takes value between $d = 1$ and $d = 9$.*

Remark. Topologically, del Pezzo surfaces are determined by their degrees except for the case of $d = 8$. If $d \neq 8$, a del Pezzo surface of degree d is a generic blow-up of projective plane \mathbb{CP}^2 at $9 - d$ points. If $d = 8$, then there are two choices: \mathbb{CP}^2 blown up at one point and $\mathbb{CP}^1 \times \mathbb{CP}^1$. All of these surfaces admit metrics of positive scalar curvature and a complex cone over these surfaces gives potential candidates for non-compact Calabi-Yau varieties. For surfaces formed by blowing up $9 - d$ points, no three may be collinear, no six lie on a conic, and no eight of them lie on a cubic having a node at one of them. Conversely any blowup of the plane in points satisfying these conditions is a del Pezzo surface.

Having briefly summarised the details on the geometries that will appear as examples in the later text, we present their toric diagrams in fig. 2-1 for the completeness of this discussion.

²The definition of weighted projective space is presented in section 2.3.2

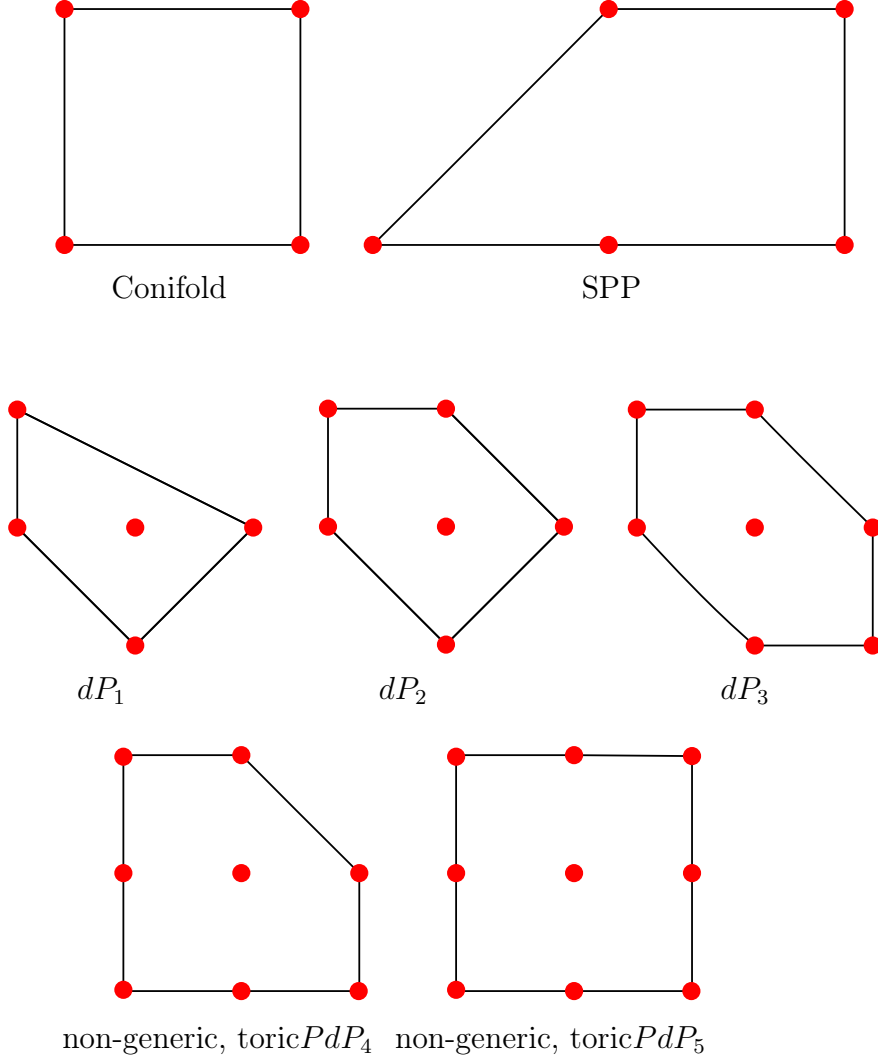


Figure 2-1: The toric diagrams for the classification of Gorenstein singularities of three complex-dimensions by the behaviour of contraction of a single extremal ray. The higher del Pezzo surfaces $dP_{4,\dots,8}$ are not listed since they are non-toric. However, there are the so-called pseudo del Pezzo for dP_4 and dP_5 are studied in [140], which are not generic, smooth dP_4 and dP_5 but degenerate cases with isolated singularities.

2.2 Quiver Gauge Theory

In this section, we present a quick review of $\mathcal{N} = 1$ superconformal quiver gauge theories as well as their string theory realisation in terms of D3-branes and Calabi-Yau manifolds. For more comprehensive review addressed to physicist, see [41, 42] and that addressed to mathematician [43].

The name ‘quiver’ was first introduced into the scene by [40]³. In physics, we take quiver to represent a collection of vertices (nodes) and oriented edges (arrows). Examples of quivers are shown in fig. 2-2. In some cases, we can have arrows starting and ending on the same

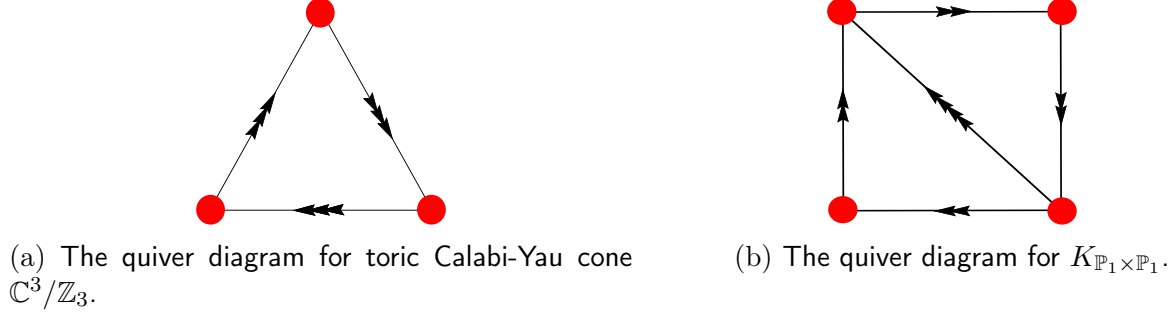


Figure 2-2: Two examples for quiver diagrams.

node, which simply means we have an adjoint field represented by that arrow. To represent a gauge theory, the quiver diagrams need to have their constituents endowed with physical meaning. We briefly summarise its physical data as follows:

Definition 2.2.1. *A quiver $\mathcal{Q} = (\mathcal{Q}_0, \mathcal{Q}_1, W)$ is a finite directed graph with a set of nodes \mathcal{Q}_0 and arrows \mathcal{Q}_1 , whose cardinalities are N_0 and N_1 respectively. The following points need to be taken into consideration with this definition:*

- \mathcal{Q} engenders a representation such that we attach a vector space $V_i \sim \mathbb{C}^{n_i}$ to node i with some positive integer n_i , where each arrow $(X_{ij} \in \mathcal{Q}_1) \in \text{Hom}(V_i, V_j)$ is then an $n_i \times n_j$ matrix. Self-adjoint arrows are also allowed $\phi_i = X_{ii}$, as well as cycles that are formed from closed loops of arrows $X_{i_1 i_2} X_{i_2 i_3} \cdots X_{i_k i_1}$.
- \mathcal{Q} is constrained by relations derived from superpotential W which is a polynomial in fields X_{ij} (arrows) as formal matrix variables:

$$W = \sum_{k=1}^{N_2} c_k \text{Tr}(\prod X_{ij}) \cdots \text{Tr}(\prod X_{i'j'}) , \quad (2.17)$$

where the sum runs over nodes inside possible cycles with coefficients $c_k \in \mathbb{C}$. The

³The German word of quiver, ‘Köcher’ was used in this literature. Quiver has a lexicographical meaning of ‘portable case for holding arrows’.

relation that restricts the superpotential is derived from the vanishing of the Jacobian $\partial_{X_{ij}} W$.

Remark. The following remarks should be added to the previous definition:

- The closed loops in the quiver complicate the representation theory but it is a necessary requirement from physics as the vacuum moduli space of the gauge theory from the quiver is exactly carved out by these relations.
- The number of nodes N_0 , number of arrows N_1 and number of monomial terms in superpotential W will have a combinatoric relation *i.e.* the Euler characteristic for a torus, that arises from the dimer representation of quiver on a drawn on a torus.
- The above data is associated to a four-dimensional supersymmetric gauge theory with product group $\mathcal{G} = \prod_{i=1}^{N_0} U(n_i)$. The translation between the above data and the gauge theory is recorded in table 2.1

Node i	Gauge factor $U(n_i)$
Arrow $i \rightarrow j$	Bi-fundamental field X_{ij} transforming as $(\square, \bar{\square})$ of $U(n_i) \times U(n_j)$
loop $i \rightarrow i$	Adjoint field $\phi_i = X_{ii}$ of group $U(n_i)$
Cycle $i_1 \rightarrow i_2 \rightarrow \dots \rightarrow i_k \rightarrow i_1$	Gauge invariant operator (GIO) $\text{Tr}(X_{i_1 i_2} X_{i_2 i_3} \dots X_{i_k i_1})$
$\text{Tr}(\prod X_{ij})$	Single-trace GIO
$\text{Tr}(\prod X_{ij}) \dots \text{Tr}(\prod X_{i'j'})$	Multi-trace GIO
2-Cycle $X_{ij} X_{jk}$	Mass term
Superpotential in eq. (2.17)	Superpotential in Lagrangian with coupling c_i
$\{\partial_{X_{ij}} W\}$	F-term relations

Table 2.1: Dictionary for translating between the graph representation of a quiver and the supersymmetric gauge theory that underlies it.

- The vector $\vec{n} = (n_1, n_2, \dots, n_{N_0})$ has its components as the ranks of the factors of the product gauge group, meaning we have the arrows being complex numbers when $n_i = 1$.

- The *incidence matrix* of a quiver is $d_{i\alpha}$, with $i = 1, \dots, N_0$ labelling the nodes and $\alpha = 1, \dots, N_1$ referring to the arrows, such that an arrow from node i to node j gives a column in $d_{i\alpha}$ with -1 at row i and $+1$ at row j , and 0 otherwise. This can be seen as a bifundamental field X_{ij} give -1 for $U(n_i)$ and $+1$ for $U(n_j)$. An example for incidence matrix for phase b of the Hirzebruch F_0 model [49, 51, 74, 73] shown in fig. 2-3 is given by eq. (2.18).

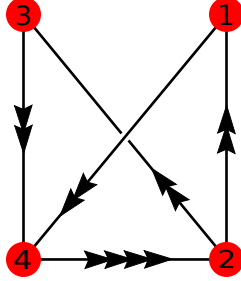


Figure 2-3: The quiver diagram for the phase b of the Hirzebruch F_0 model.

$$d = \left(\begin{array}{c|cccccccccccc} & X_{14}^1 & X_{14}^2 & X_{21}^1 & X_{21}^2 & X_{23}^1 & X_{23}^2 & X_{34}^1 & X_{34}^2 & X_{42}^1 & X_{42}^2 & X_{42}^3 & X_{42}^4 \\ \hline U(n_1) & -1 & -1 & 1 & 1 & 0 & 0 & 0 & 0 & 0 & 0 & 0 & 0 \\ U(n_2) & 0 & 0 & -1 & -1 & -1 & -1 & 0 & 0 & 1 & 1 & 1 & 1 \\ U(n_3) & 0 & 0 & 0 & 0 & 1 & 1 & -1 & -1 & 0 & 0 & 0 & 0 \\ U(n_4) & 1 & 1 & 0 & 0 & 0 & 0 & 1 & 1 & -1 & -1 & -1 & -1 \end{array} \right) \quad (2.18)$$

Note here the columns in the matrix are not linearly independent due to the fact that all the entries in each row sum up to 0 since each node has equal amounts of incoming and outgoing arrows. This is from the anomaly cancellation condition since incoming and outgoing arrows contribute to the anomaly with opposite sign, whereby requiring the number of fundamental and anti-fundamental chiral fields to be equal. Note that this equality is only for the case when ranks on all the nodes are equal. Other cases will be discussed in next section. Thus the incidence matrix in in fact a matrix of the form $d_{(N_0-1) \times N_1}$.

- Since we have a chiral gauge theory for each quiver, it is important to have anomaly

cancelled. The anomaly cancellation [44] can be written as follows

$$\sum_{a=(i,j)} d_{i\alpha} n_j = 0 \quad (2.19)$$

where the sum goes over all arrows labelled by $a = (i, j)$ that are between node i and j . n_j is the rank of group $U(n_j)$ as j -th node in the quiver. We will expand more on this in section 2.2.1. The D-terms are then give by $\sum_{\alpha} d_{j\alpha} |X_{ij}|^2 - \zeta_i$ with $\zeta_i \in \mathbb{C}$ being the Fayet-Iliopolous (FI) parameter.⁴ Here the D-terms are non-holomorphic as opposed to the F-terms.

2.2.1 Anomaly Cancellation in Quivers

As we have eluded in the previous section, the structure of a quiver for $\mathcal{N} = 1$ superconformal gauge theory is constrained by the anomaly cancellation condition. It is therefore satisfactory to expand on it for a bit more detail for completeness.

In general, quiver gauge theories are chiral and anomaly cancellation is essential for consistency of such theories. In order to elucidate eq. (2.19), we define the incidence matrix $\sigma_{i\alpha}$ as follows

$$\sigma_{\alpha i} = \begin{cases} +1 & \text{arrow } \alpha \text{ ends at node } i, \\ -1 & \text{arrow } \alpha \text{ starts at node } i, \end{cases} \quad (2.20)$$

where $\alpha = 1, \dots, N_0$ and $i = 1, \dots, N_1$. Suppose we have node i and want to check anomaly cancellation at this node, then we have

$$\sum_{\alpha_{ij}} \sigma_{\alpha i} n_j = 0 \quad (2.21)$$

where we sum over all arrows which start from node i and end on node j . The rank of the gauge group at node j is denoted by n_j ⁵. We have to make a note here that the ranks of

⁴Generically, one usually assigns a charge q_{α} to the fields and sum over $q_{\alpha} |X_{i\alpha}|^2$. Since FI parameters only exist for $U(1)$ groups and we only talk about $U(1)^{N_0}$ in our case here, the charge is set to 1 for every field.

⁵In general, the ranks of the $U(n_i)$ gauge groups are $n_i \geq 1$. For most of the examples discussed in this article, we consider all gauge groups to be equal. If not explicitly stated otherwise, the quiver is considered to be Abelian where for all i , $n_i = 1$, as we want to work in the regime of toric quiver gauge theories, whose

the gauge groups residing on the nodes of the quiver diagram can not be captured by the incidence matrix defined here. This is essentially the same as eq. (2.19). Let us rewrite this in another form by

$$\sigma_{ij} = \sigma_{\alpha i} , \tag{2.22}$$

where arrow α starts on node i and ends on node j . With this equation, we can write eq. (2.21) as

$$\sum_{j \in i} \sigma_{ij} n_j = 0, \tag{2.23}$$

where node j is connected to i by arrows. Therefore, the summation over edges connecting nodes i and j is implicitly built in it.

Schematically, an arrow starting at node i and ending at node j is a bifundamental field transforming in (\bar{n}_i, n_j) under group $U(n_i) \times U(n_j)$. Viewing from $U(n_i)$, this bifundamental is a set of n_j anti-fundamental fields, which contribute to the gauge anomaly by $-n_j = \sigma_{\alpha i} n_j$. An arrow in opposite direction then contributes with opposite sign by $\sigma_{\alpha i} n_j$. The vanishing of anomaly is then given by eq. (2.21). Let us consider the case where all gauge groups have the same rank. The anomaly cancellation condition then requires that each node i to have the same number of incoming and outgoing arrows. This condition is met in quiver fig. 2-3. We will see that this condition is satisfied for all quiver gauge theories built out of brane tilings by the very definition of toric condition and combinatoric properties of dimer models reviewed in section 2.3.1.

2.2.2 Toric Quiver Gauge Theories

Before moving onto the discussion of brane tiling, we present a few remarks on *toric* quiver gauge theory, which is a special class of gauge theories in contrast to the general definition of quiver gauge theory in definition 2.2.1. $\mathcal{N} = 1$ quiver gauge theories were first studied by Douglas and Moore [24] and later clarified by Douglas, Greene and Morrison [27]. The toric structure of the moduli space of the constructed quiver theories was studied by a change of variable to parametrise it as the moduli space of an Abelian linear sigma model. Ensuing

gauge group essentially descend from the algebraic toric action by \mathbb{C}^* . In other words, the toric description is only possible iff all nodes are of rank one, *i.e.* $U(1)$.

works were then dedicated to study more general toric singularities and the corresponding linear sigma models.

In addition to the definition 2.2.1, we supplement it with other properties that the quiver holds.

- The quiver graph also specifies the D-terms of the gauge theory since we have $U(1)$ factors coming from $U(n_a)$. The Abelian factors thus give rise to the D-term constraints on the vacuum moduli space as

$$\sum_i Q_i^a |X_i|^2 = \zeta^a, \quad (2.24)$$

where the sum is over all quiver fields X_i and Q_i^a is the charge for field X_i (note this is exactly the incidence matrix we defined in section 2.2) under a -th gauge group $U(1) \subset U(n_a)$. In this charge matrix, the fields in fundamental representation (incoming arrow) of $U(n_a)$ have charge $+1$, those in the anti-fundamental (outgoing arrow) has charge -1 and those in adjoint or which are uncharged under this gauge group have charge 0 thus not seen by the D-term condition. The FI parameter ζ^a is real whose vanishing is required by supersymmetric vacuum as $\sum \zeta^a = 0$.

- As first described in [34], the quiver gauge theory becomes meaningful when we start considering non-trivial conformal fixed points thereof. Such conformal IR fixed points give us the corresponding CFT that are strongly coupled. Thus the exact NSVZ beta function [75] for gauge coupling g_a of gauge factor labelled by a is

$$\beta(g_a) = \frac{d}{d \ln \mu} \frac{1}{g_a^2} = \frac{N}{1 - \frac{g_a^2 N}{8\pi^2}} \left(3 - \frac{1}{2} \sum_{i \in a} (1 - \gamma_i) \right), \quad (2.25)$$

where the sum is over all fields transform under gauge group a and γ_i is the anomalous dimension of the field X_i . Thus we have the conformal dimension to be

$$\Delta(X_i) = 1 + \frac{1}{2} \gamma_i = \frac{3}{2} R(X_i), \quad (2.26)$$

where $R(X_i)$ is the R-charge of field X_i . The conformal invariance thus requires van-

ishing beta function

$$\sum_{i \in a} (1 - \gamma_i) = 6 \implies \sum_{i \in a} (1 - R(X_i)) = 2. \quad (2.27)$$

The points to note here is that, in the context of AdS/CFT correspondence, the dual CFT is obtained as the IR fixed point of the D-brane world-volume gauge theory. The $U(1)$ gauge group factors couple to charged matter (bifundamentals in quiver) and they are IR free. Thus in the IR fixed point the $U(1)$ gauge couplings are zero and the gauged $U(1)$ factors become global symmetries of the CFT. The second is that the some of the $U(1)$ of the classical Lagrangian are anomalous, these anomalous $U(1)$ are cancelled in string theory and the $U(1)$ fields become massive. The non-anomalous $U(1)$ symmetries survive the RG flow and become global symmetries in the IR. In such scenario, we will refer to the D3-brane world-volume gauge theory (D3-branes probing the toric CY cone) with gauged $U(1)$ factors as the ‘‘UV’’ theory. The IR limit is obtained by going to the near horizon limit of the D3-branes to produce $AdS_5 \times X^5$ geometry with X^5 being the SE manifold. The type IIB theory on this near horizon geometry is equivalent to the CFT sitting at the IR fixed point, which is an $SU(N)$ quiver gauge theory. This is essentially the picture in AdS-CFT correspondence.

The quiver theories living on the stack of D3-branes at singularities of the CY cone have additional structures that highly constrain both the quiver and the superpotential thereof. *Each bifundamental field of the quiver theory appears linearly in superpotential W , and precisely in two terms of opposite sign.* This structure of superpotential directly follows from that of $\mathcal{N} = 4$ Yang-Mill superpotential $W = \text{Tr}[[X, Y], Z]$. This property is also inherited in the Abelian orbifold of type $\mathbb{C}^3/(\mathbb{Z}_n \times \mathbb{Z}_m)$; and is also preserved by partial resolution/Higgsing of the singularity, which we use to obtain any toric theory for suitable m and n . Upon Higgsing, the vacuum expectation values play the roles of couplings in the superpotential. With such toric structure, the F-term condition, namely

$$\frac{\partial W}{\partial X} = 0 \quad (2.28)$$

has the form of *monomial = monomial*. As we know that $\mathcal{N} = 1$ SCFT has a global $U(1)$

R-symmetry that is dual to a $U(1)$ isometry of the SE manifold X_5 . However, the toric cases actually have larger isometry group (at least $U(1)^2$) that corresponds to a product of R-symmetry and global flavour symmetries. On top of this, there are additional global “baryonic” symmetries in the CFT which are gauged on the CFT. They descend from the reduction of R-R 4-form on 3-cycles of X_5 thereby producing gauge fields on the AdS. Most importantly, these symmetries will give rise to the dimer models.

2.2.3 Quiver Gauge Theories from D-brane Systems

After reviewing the basic setup for (toric) quivers, we now move onto a concrete example. One of the most crucial point is that quiver gauge theories find their abundant appearances in string theory compactification, which essentially, paves the way for high energy, extra-dimensional $10D$ string theory to make contact with $4D$ gauge dynamics in our everyday experiences. The celebrated work of Douglas and Moore [24] in 1994 showed that we can obtain $\mathcal{N} = 2$ superconformal quiver gauge theories on world-volume of D-branes which probe the ALE spaces. In particular, let Γ be a discrete subgroup of $SU(2)$. We consider the orbifold space of \mathbb{C}^2/Γ which is singular and whose resolution gives the Asymptotically Locally Euclidean spaces (ALE). The natural question to ask is that what gauge theories do we have on the D-branes? The solution to this question is given by [24, 25, 26] that the theories are quiver gauge theories. The diagrams are constructed as follows.

Consider discrete subgroup Γ of $SU(2)$ and the set of all irreducible representations $\{R_i\}$. The tensor products of such representations with defining representation $\mathbf{2}$ then decompose as:

$$\mathbf{2} \otimes R_i = \bigoplus_j a_{ij}^{\mathbf{2}} R_j \tag{2.29}$$

Now we take the matrix $a_{ij}^{\mathbf{2}}$ as the adjacency matrix⁶ for a finite directed graph *i.e.*, a quiver labelled by the dimensions of the irreps. Each node represents an irreducible representation R_i . Then McKay’s theorem states that the $a_{ij}^{\mathbf{2}}$ of the finite group is precisely the Dynkin diagrams of the affine ADE Lie algebra and they correspond to the comarks⁷ of the algebra.

⁶The *adjacency matrix* a_{ij} is a matrix with ij -th entry being the number of arrows going from node i to node j .

⁷The comarks a_i^\vee are the expansion coefficients of the highest root θ into simple coroots $\alpha_i^\vee := 2\alpha_i/|\alpha_i|^2$

$$\begin{aligned}
A_n &: & xy + z^n &= 0 \\
D_n &: & x^2 + y^2z + z^{n-1} &= 0 \\
E_6 &: & x^2 + y^3 + z^4 &= 0 \\
E_7 &: & x^2 + y^3 + yz^3 &= 0 \\
E_8 &: & x^2 + y^3 + z^5 &.
\end{aligned}$$

Table 2.2: Algebraic singularities describing \mathbb{C}^2/Γ in affine coordinates.

The diagrams are presented in fig. A-4. This is the remarkable observation made by McKay in [19], which is then dubbed as McKay Correspondence. Thus the supersymmetric quiver gauge theories specified by quivers in fig. A-4 are precisely the ones living on the D-branes probing singular \mathbb{C}^2/Γ . Lastly, we note that only the A-type quiver among all the ADE quivers affords toric description since only the $A_n \simeq \mathbb{Z}_{n+1}$ is Abelian. Other ADE quiver are constructed from quotient of \mathbb{C}^2 by non-Abelian group, thus giving non-toric VMS for the corresponding quiver gauge theories.

Before we move onto other aspects of quiver gauge theories, we should mention the connection between the ADE classification of discrete subgroups of $SU(2)$ and that of semisimple simply-laced Lie algebras. We refer a more detailed exposition to appendix A.3 on this surprising connection between classifications of finite groups and that of Lie algebras. With such hindsight, it is therefore natural for us to name the groups in table A.1 with such ADE structure. After this discovery, people considered the crepant resolution of \mathbb{C}^2/Γ , which gives the K3 surface that are the only Calabi-Yau two-fold other than the trivial T^4 . In terms of affine coordinates, the orbifold are described by algebraic singularities in table 2.2. In the work by González-Springberg and Verdier [121], the crepant resolution of these singularities gives the -2 exceptional curves, *i.e.* the \mathbb{P}^1 blow-ups, with intersection matrices. These matrices correspond exactly to the McKay's adjacency matrix a_{ij}^2 in eq. (2.29). We include some details of this construction in appendix A.5.2 for completeness of this article.

Now we move onto the prototypical example of quiver gauge theory first initialised by Douglas and Moore [24]. Here we review an example⁸ of type II string propagating on the

with α_i being simple roots.

$$\theta = \sum_i^r a_i^\vee \alpha_i^\vee,$$

where r is the rank of the algebra or simply the number of nodes in Dynkin diagram.

⁸For the details of this example, see appendix A.4.

smooth ALE background from resolving singular $\mathbb{R}^6 \times T^4/\mathbb{Z}^2$. Two D1-branes are introduced in this orbifold in order to keep in line the action of orbifold, which in turn produces spectrum that includes both twisted and untwisted sectors. The additional twisted sector is unique to theories on orbifold and this additional part of the spectrum with the untwisted case contain just the enough information to specify the smoothed version of the $\mathbb{R}^6 \times T^4/\mathbb{Z}_2$, the K3 manifold. K3 manifold can always be tuned to resemble ALE spaces locally by shrinking some of the two-cycles of K3. More importantly, the gauge theory on the pair of the D1-branes is $U(1) \times U(1)$ and the moduli space of this theory has the metric of ALE space.

Since this section focuses on the emergence of quiver gauge theories from D-brane system. The earliest example for such setup is through the T-dualisation of $\mathbb{C}^2/\mathbb{Z}_2$, the example we referred to in the preceding paragraph. This dualisation gives n NS5-branes placed in a ring; the world-volume theory of D4-branes stretched between these branes, the so-called elliptic model, is the $\mathcal{N} = 2$ A-type orbifold theory above. Such equivalence is actually between the D-brane probe picture and the Hanany-Witten setup [65]. We briefly recount some of the contents of this equivalence here.

The final part of discussion on quiver gauge theory will be about its connection to its construction using D-brane system. First, up to a change of variables in the supergravity background in eq. (A.119), \mathbf{y} can be taken to be a vector $\mathbf{y} = (x^7, x^8, x^9)$ with x^6 being the periodic coordinate z . It is easier to visualise if we draw a table 2.3 to keep a note on the coordinate arrangement.

	x^0	x^1	x^2	x^3	x^4	x^5	x^6	x^7	x^8	x^9
D2	—	—	×	×	×	×	—	×	×	×
NS5	—	—	—	—	—	—	×	×	×	×

Table 2.3: The coordinate arrangement for dual D2-branes and NS5-branes.

Since we have a compact direction in x^6 , we can perform a T dualisation and arrive at

another background with the metric

$$\begin{aligned}
ds^2 &= -dt^2 + \sum_{m=1}^5 dx^m dx^m + V(y)(dx^6 dx^6 + d\mathbf{y} \cdot d\mathbf{y}) \\
e^{2\Phi} = V(\mathbf{y}) &= \sum_{i=0}^{N-1} \frac{\sqrt{\alpha'}}{|\mathbf{y} - \mathbf{y}_i|},
\end{aligned} \tag{2.30}$$

which is a $10D$ solution if we take the non-trivial background fields [48] $H_{mns} = \epsilon_{mns}{}^r \partial_r \Phi$, which defines the potential B_{6i} ($i = 7, 8, 9$) as a vector A_i satisfying $\nabla V = \nabla \times \mathbf{A}$. The non-zero B_{6i} is because the T-dual theory has non-zero G_{6i} as T-duality relates these two-forms. This solution is actually independent of direction x^6 . However, a full solution should have structures in x^6 since translation invariance is broken in this direction. This is due to the fact that the x^6 -circle of the ALE space has fixed-points due the orbifold action, *i.e.* circle shrinks away at those points. Therefore, we expect the winding modes to behave differently at those points as well as the T-dual momentum states. Localised solutions in the directions x^6, x^7, x^8, x^9 can be thought of being harmonic at those points. In such setting, we take $\mathbf{x} = (x^6, \mathbf{y})$ to denote the coordinates in the \mathbb{R}^4 and replace $V(\mathbf{y})$ by

$$V(\mathbf{x}) = 1 + \sum_{i=0}^{N-1} \frac{\alpha'}{(\mathbf{x} - \mathbf{x}_i)^2}. \tag{2.31}$$

By adding 1 to the solution, we add the solution an asymptotically flat region while keeping $V(\mathbf{x})$ harmonic in \mathbb{R}^4 . This solution comprises of a chain of N objects that are point-like in x^6, x^7, x^8, x^9 and are magnetic sources of the $B_{\mu\nu}$ NS-NS potential. These are actually the NS5-brane arranged in the x^6 -circle.

Keeping up with such spirit, we would like to realise our quiver gauge theories in this dual picture. From appendix A.4, we have D1-brane along the x^1 direction probing ALE space. If we T-dualise on this D1-brane, it becomes a D2-brane with an extra leg extended along the compact x^6 direction. Therefore, the D2-brane intersects with the two NS5-brane as it winds around x^6 . The point at which it passes through an NS5-brane is characterised by four numbers \mathbf{x}_i for the i -th brane. The intersection point can be located anywhere inside the NS5-brane's worldvolume in the directions x^2, x^3, x^4, x^5 . If we start with 32 supercharges

in IIA supersymmetry, the presence of NS5-brane breaks half of the SUSY and the D2-brane breaks another half, thus leaving eight supercharges in total. The infinite part of the probe, as an effective one-brane, has a $U(1)$ on its worldvolume. Then tension is given by $2\pi l\mu_2$ with μ_2 being the charge of D2-brane, with length of l unspecified for the compact direction x^6 . The size of the compact direction can take on different values thus giving different densities of branes in the dual picture.

For our case, we focus on the case of $N = 2$. If we take the two NS5-branes to have the same $\mathbf{y} = x^{7,8,9}$, then the D2-brane is broken into two segments in the x^6 direction giving a $U(1) \times U(1)$ on the effective 1-brane in the infinite x^1 direction. The two segments can move independently within the NS5-brane worldvolume and preserve supersymmetry. This is precisely the Coulomb branch we encountered in the D1-brane probing ALE space. The hypermultiplets come from the fundamental strings stretching between the NS5-branes in the x^6 direction. The differences of the other three coordinates in the \mathbb{R}^4 are the T-dual of the NS-NS parameters controlling the size and orientation of the \mathbb{CP}^1 blow-up. The x^6 separation between the two NS5-branes is thus dual to the flux $2\pi l\Phi_B$ ⁹.

Now if we change the relative position of the two NS5-branes, and say, make them coincident in x^6 direction. One of the fundamental strings stretching between them becomes tensionless, we obtain an A_1 enhancement of the gauge symmetry carried by the two-form potential living on the type IIA NS5-brane. If we have IIB NS5-branes with D1-branes stretching between them instead, we obtain massless particles with enhanced $SU(2)$ gauge symmetry. There is also an interesting duality between the quiver diagram we obtained in fig. A-5 and the brane configuration we just arrived. It is shown in fig. 2-4.

If the NS5-branes become separated in x^6 and are at different positions in $\mathbf{y} = x^{7,8,9}$ directions, the D1-brane segments must become tilted to remain stretched between two NS5-branes. The segments thus have to be oriented differently from each other and supersymmetry is then broken. This corresponds to the ‘lifting’ of the Coulomb branch. To recover the supersymmetric vacua when NS5-branes are at different positions in $\mathbf{y} = x^{7,8,9}$, the brane segments need to be rejoined to give a single D-brane. In such setting, the single

⁹ Φ_B is proportional to the charge induced by $B_{\mu\nu}$ on the one-brane inside the NS5-brane worldvolume *i.e.* $\Phi_B \sim \int_{\Sigma} B$.

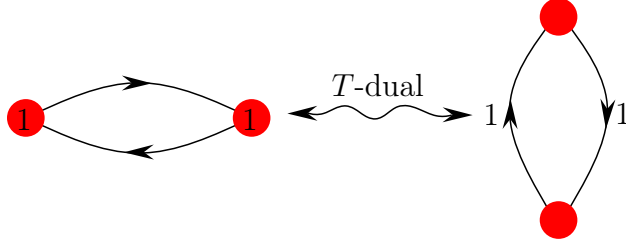


Figure 2-4: The duality between the quiver of A_1 theory and the brane system of D-branes stretching between NS5-branes. They are essentially graph dual of each other viz. the nodes in one are arrows in another and vice versa. The node label in the A_1 quiver becomes the number of D-branes represented by the arrow in the other diagram.

D-brane does not need to move with the NS5-brane and supersymmetry is preserved. This signifies turning on the FI parameter and moving from the Coulomb branch to the Higgs branch of the vacua. The \mathbf{y} position and x^6 Wilson line correspond to the Higgs branch parameters.

The fractional branes and their T-duals stretched brane segments are less mobile than a complete D-brane as they are ‘anchored’ between the NS5 branes and can not move in certain directions. For such properties, they are used extensively in the study of gauge theories on branes with reduced supersymmetries – the Hanany-Witten setup [65]. As we shall see that this serves the foundation of our next topic **Brane Tiling**, which uses certain brane construction to obtain $4D \mathcal{N} = 1$ superconformal quiver gauge theories in the similar spirit we have just recounted.

2.3 Brane Tiling

Since the advent of AdS/CFT correspondence, efforts are devoted to investigate theories with fewer supersymmetries than the paragon $AdS_5 \times S^5$ $\mathcal{N} = 4$ theory first studied by Maldacena [113]. One important approach to obtain such set of theories is to break supersymmetries by changing the topology of the string theory background, thereby replacing the $AdS_5 \times S^5$ by a different manifold $AdS_5 \times X^5$. To preserve the $\mathcal{N} = 1$ supersymmetry in the resulting four-dimensional theory, the X^5 has to be a Sasaki-Einstein (SE) manifold. The reason for choosing such manifold is that the metric cone over X^5

$$ds^2 = dr^2 + r^2 dX_5^2 \tag{2.32}$$

is **Ricci flat**. Thus the metric cone is a Calabi-Yau three-fold with $SU(3)$ holonomy. For generic $\mathcal{N} = 1$ case, $U(1)$ R-symmetry is thus dual to the isometry of SE manifold X^5 [28].

One important class of such manifold is the **toric SE manifolds**: both SE manifold and its Calabi-Yau cone have $U(1)^3$ isometries. These toric geometries produce infinitely many such SE manifolds, which themselves may have complicated topology and offer a window to study such a plethora of $\mathcal{N} = 1$ supersymmetric gauge theories in the context of AdS/CFT correspondence. In the past decade, there are new tools developed called **brane tiling** and **dimer model** to study the structure of $4D$ superconformal gauge theory whose moduli spaces are given by certain toric varieties/SE spaces. These CFTs are quiver gauge theory in type, with $U(1)_R \times U(1)_F^2$ global symmetry *i.e.* a subgroup of R-symmetry group times a non-baryonic flavour symmetry group. In such framework, the prime example are the familiar Abelian orbifolds S^5/Γ , $\Gamma \sim \mathbb{Z}_n$ or $\mathbb{Z}_n \times \mathbb{Z}_m$, which are conifolds and its orbifolds. The next ones are the $Y^{p,q}$ and $L^{a,b,c}$ [60, 58]. These SE manifolds have their metrics explicitly constructed and offer direct computation for checking AdS/CFT correspondence, such as correlation functions. Generic SE manifolds do not have known metric and such direct computation is not possible. However, CFTs built out of toric manifolds are completely defined without referring to the knowledge of metrics by relying on brane tiling reformulation of the gauge theory data and the associated dimer models.

For a particular toric Calabi-Yau threefold constructed as the metric cone over SE toric

base, one would like to know the gauge theories that live in the worldvolume of D3-branes at the tip of the cone ¹⁰. However, such IR theories are not in one to one correspondence with the vacuum geometry as gauge theories are related by Seiberg duality [68, 69, 70]. Such gauge theories are of quiver type and flow to a non-trivial conformal fixed point. In the string dual picture, this means the D3-branes taking near-horizon limit to replace $\mathbb{R}^{3,1} \times \text{CY}_3$ by $AdS_5 \times X^5$. Thus the problem of identifying quiver gauge theories with a given Calabi-Yau cone was first discussed in [69] using D3-brane linear sigma model in [27]. The idea behind this is that we can always obtain the desired singularity by embedding it inside a “larger” singularity and then perform a stepwise partial resolution of the parent singularity until we reach the embedded one. This partial resolution on the quiver gauge theory corresponds to turning on the FI parameters to Higgs certain fields. This algorithm is well-defined but it requires exponential running-time as the number of generators of the Calabi-Yau cone increases. Therefore it is relatively restricted to simple singularities. However, this algorithm is significantly enhanced with the tools from brane tiling and dimer models as this article tries to expand the classification of the quiver gauge theories according to some combinatoric properties of the moduli spaces which are captured inside planar diagrams called toric diagrams. This deeper combinatoric structure underlying the toric gauge theories was first noted in [49]. The dimer models were used to compute the charges and field content of the D3-brane linear sigma models for arbitrary *toric* Calabi-Yau spaces. The relation between quiver gauge theory and this dimer model was then clarified and made precise in [51].

In this section, we review how the data of toric quiver gauge theory maybe more elegantly rephrased by another construction called brane tiling, which is a bipartite tiling of a torus. The brane tiling is also shown to encode the global $U(1)$ of the CFT inside the combinatoric data of the dimer on the edges of the brane tiling. Some tools from mathematical physics will also be used to solve the underlying combinatoric problems and show how they are relevant to the classification of properties of gauge theories. We also review how dimer model provides a simple realisation of moduli space of the D3-brane worldvolume theory

¹⁰D3-branes at non-singular point only see a local geometry of \mathbb{C}^3 and this gives rises to $\mathcal{N} = 4$ super-Yang-Mills in the IR where all the curvature corrections can be neglected

and an efficient reconstruction of D3-brane linear sigma model in [27] as compared to the algorithm presented in [69].

2.3.1 Brane Tilings and Dimer Models

In this subsection, we start to look into the additional structures inside toric quiver gauge theories by first combining the quiver and its associating superpotential inside a bipartite tiling of a 2-torus by polygons – brane tiling. Secondly, we then relate the set of $U(1)$ symmetries of the quiver theories to the combinatorics of the dimer model on the brane tiling. We also give a justification of the nomenclature “brane tiling” by showing that all the physical data inside these graphs arise from certain D-brane constructions in string theory. More specifically, we make ourselves an example of D-brane construction to engineer the quiver gauge theories in string theory. In addition, these models have their worldvolumes wrapping a T^2 and reproduce the brane tiling dictionary. With the data from toric quiver gauge theory and its superpotential, we can immediately write down the corresponding brane tiling. The inverse direction, that is to construct the quiver gauge theories and its superpotential from a given singularity, becomes tractable with the aid of dimer model. An extension of this inverse direction to expand the classification of quiver gauge theories based on the singular geometry they probe will be the main result of this article.

If a toric quiver gauge theory and its superpotential is known, the brane tiling that they represent becomes immediately clear. We shall discuss this in more detail now.

Planer Quivers and Brane Tilings: a pair of graph duals. The key observation to combine matter contents and superpotential of a quiver theory into a single object is to define the individual terms in the superpotential by plaquettes *i.e.* representing boundaries of polygons. When a bifundamental field appears twice in the superpotential, the plaquettes containing that field are glued together on that edge. In general, quivers and superpotentials combined this way do not give interesting structure. However, it is the toric condition that makes this construction obvious since this gives a planar structure for toric cases. In addition, the toric condition forces the planar structure a *periodic polygonal tiling* of a Riemann surface. This is the object called **planar quiver** and we use it to obtain brane tiling.

Recall that we have \pm signs in front of each term in the superpotential. This can be implemented by demanding neighbouring plaquettes have opposite orientation signalled by the directions of the bounding arrows. This shows that the Riemann surface also has orientation. Furthermore, the genus of the Riemann surface can be uncovered from the superconformality condition of the gauge theory. Recall that the vanishing of NSVZ beta function requires

$$\sum_{e \in V_i} (1 - R_e) = 2, \quad (2.33)$$

where the sum is over the edges connected to the gauge node i . The requirement of superpotential having charge 2 can be written as

$$\sum_{e \in F_i} R_e = 2, \quad (2.34)$$

where the sum is over all edges surrounding a plaquette. Now we can sum over all nodes and plaquettes

$$\begin{aligned} \sum_{V_i \in V} \sum_{e \in V_i} (1 - R_e) &= 2N_V \\ \sum_{F_i \in F} \sum_{e \in F_i} R_e &= 2N_F, \end{aligned} \quad (2.35)$$

where N_F, N_V are the number of nodes and faces in the planar quiver. This is because each edge connects 2 nodes and is shared by 2 faces. We also have

$$\begin{aligned} 2 \sum_e (1 - R_e) &= 2N_E - 2 \sum_e R_e = 2N_V \\ 2 \sum_e R_e &= 2N_F, \end{aligned} \quad (2.36)$$

where the sum is over all edges. We then have the relation for Euler characteristic $N_F - N_E + N_V = 0$ for planar diagram. This is also equivalent to $2 - 2g$ with g being the number of handles, or genus. So we have the Riemann surface of genus one, or simply topologically a T^2 . Therefore, we have combined the quiver and superpotential into an embedding of the

quiver into a torus T^2 with the aid of R-symmetry and conformal symmetry. The faces in the planar quiver can have labels from the coupling constant in front the term in superpotential, but with alternating sign due to the toric condition. The alternating signs can be better presented by passing to the dual diagram for the planar quiver: each face is replaced by a node; two faces adjacent along an edge are replaced by two nodes connected by the dual edge (perpendicular to the original one); nodes are replaced by the new faces and are enclosed by new edges. The dual graph is also embedded in T^2 . The alternating sign of the nodes actually turn the dual graph into a *bipartite graph* where each node is only connected to nodes that have opposite sign, or “colour”. Our convention is to refer the nodes with positive sign as “black” and negative ones as “white”. Now we summarise the dictionary between planar quiver and brane tiling in table 2.4.

Gauge Theory	Planar Quiver	Brane Tiling
$SU(N)$ or $U(N)$	Node	Polygonal face
Chiral multiplet	Edge/Arrow	Edge/Arrow
Superpotential term	Polygonal face	Node

Table 2.4: The dictionary translating between data in planar quiver and that in brane tiling.

Now it is probably a good place to introduce an example to illustrate the web of connections. We take the del Pezzo 1 singularity [69]. We have the quiver of dP_1 given by fig. 2-5

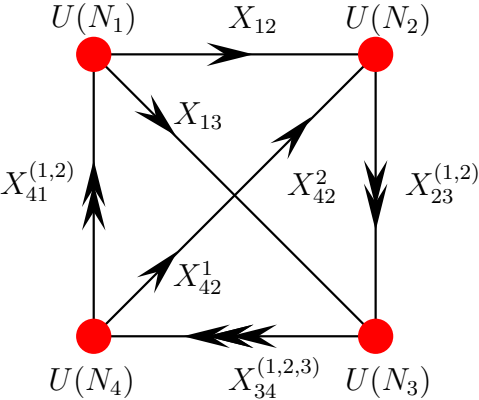


Figure 2-5: The quiver for D3-branes probing singular metric cone over del Pezzo 1 surface.

The superpotential for this quiver theory is given by

$$W = \text{Tr} X_{13} X_{34}^2 X_{41}^2 - \text{Tr} X_{13} X_{34}^1 X_{41}^1 + \text{Tr} X_{12} X_{23}^2 X_{34}^3 X_{41}^1 \quad (2.37)$$

$$- \text{Tr} X_{12} X_{23}^1 X_{34}^3 X_{41}^2 + \text{Tr} X_{23}^1 X_{34}^1 X_{42} - \text{Tr} X_{23}^2 X_{34}^2 X_{42} , \quad (2.38)$$

where the trace is over the gauge group indices since the superpotential is made up by gauge invariant operators. With the explicit superpotential written down, we can draw the planar quiver as shown in fig. 2-6. Using the dictionary in table 2.4, the brane tiling is drawn in

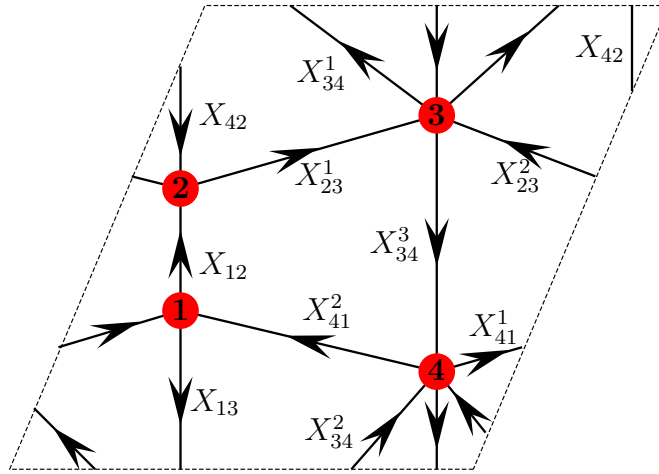


Figure 2-6: The planar quiver for D3-branes probing singular metric cone over del Pezzo 1 surface.

fig. 2-7.

We can see that the region bounded by the dashed lines has exactly 6 nodes representing the 6 terms in superpotential. Each term in the superpotential is obtained by tracing clockwise around black nodes and anti-clockwise around white nodes and collecting edges that are connected to the node in consideration.

Dimer Models and Classical $U(1)$ Symmetries of Toric Quiver. Now we look at the set of $U(1)$ symmetries on the bifundamental fields X_{ij}^k under which the superpotential transforms homogeneously. The D-terms and kinetic terms are automatically invariant since they are quadratic in fields *i.e.* they combine holomorphic fields and its complex conjugate together. Once the superpotential transforms homogeneously under $U(1)$, we can find $U(1)$ symmetries of the Lagrangian by taking quotients of two such $U(1)$ with certain weights

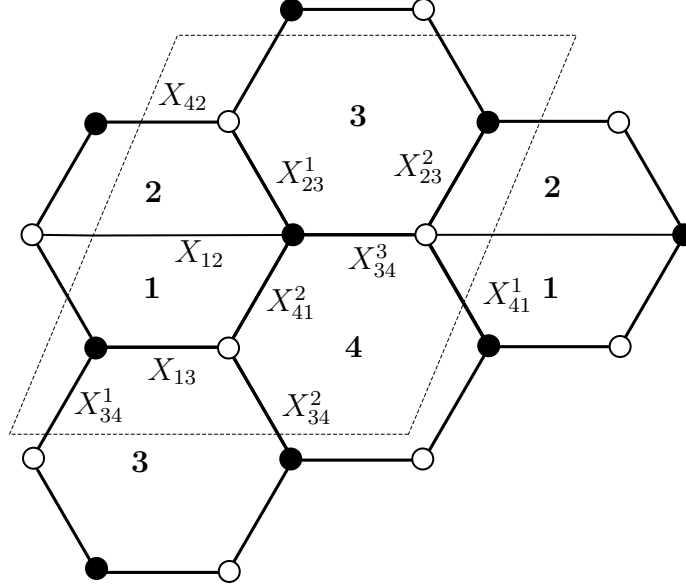


Figure 2-7: The brane tiling/dimer model for D3-branes probing singular metric cone over del Pezzo 1 surface.

such that the superpotential is invariant. This question has a natural combinatoric solution within the structure of **dimer model**, which we shall describe now.

For bipartite graph, a *dimer* is a marked edge and a *dimer configuration* or *perfect matching* is a collection of dimers/marked edges such that every node of the graph has connectivity one, or is covered exactly by one dimer. The bipartite graph with its set of dimer configuration is call a *dimer model*. Now we turn to our dictionary between physics and brane tiling and see that the nodes in the dimer are the terms of superpotential for the gauge theory represented by the quiver. A dimer configuration in this sense is a choice of exactly one field in every term of the superpotential. Thus action of $U(1)$ on this set of fields is homogeneous on the superpotential W . We have transformed the problem of finding homogeneous $U(1)$ action on the superpotential into one that enumerating possible dimer configuration/perfect matching of the bipartite graph. This enumerative problem is exactly the contents of Kasteleyn matrix [63]. We will use the notation for Kasteleyn matrix that is a modified version of [57].

For a bipartite graph Γ , the **weighted adjacency matrix** A , whose rows and columns

label the black and white nodes, has entries K_{ij}

$$A_{ij} = \begin{cases} \sum_k a_{ij}^k & \text{for each edge } k \text{ connecting black node } i \text{ to white node } j \\ 0 & \text{otherwise} \end{cases} \quad (2.39)$$

where $a_{ij}^k \in \mathbb{R}^*$ are **edge weights**, formal variables labelling the edges. The matrix A only specifies the connectivity of the graph and contains no information about the embedding on the torus. We now define another matrix called **Kasteleyn matrix** to encode the information of embedding $\Gamma \in T^2$. To define such matrix, we choose two primitive winding cycles for the torus γ_w and γ_z , which can be seen as carving out the fundamental domain of the periodic tiling of the T^2 . The Kasteleyn matrix $K(w, z)$ is then defined by

$$K_{ij} = \sum_k a_{ij}^k z^{\langle a_{ij}^k, \gamma_z \rangle} w^{\langle a_{ij}^k, \gamma_w \rangle}, \quad (2.40)$$

where $\langle a_{ij}^k, \gamma \rangle$ is the signed intersection number of the edge a_{ij}^k and the boundary of the fundamental domain, which is an oriented contour γ in our case. In this chapter, we will take the a_{ij}^k to be 1 to enumerate all possible perfect matchings with certain rules of assigning \pm to the entries of K [63, 57] to avoid any accidental cancellation. However, in next chapter, we will take the entries explicitly to be the fields when we consider the *Inverse Algorithm*. Since edges can only cross the contour once, the intersection number can only be $\pm 1, 0$ meaning if the edge crosses γ with positive orientation or negative orientation or does not cross at all. The Kasteleyn matrix is the basic tool we will need to recover the D3-brane linear sigma modes, which give the classical and semiclassical (anomaly-free) moduli space of the quiver gauge theory. If we take the determinant of the Kasteleyn matrix, we see that it enumerates all possible perfect matchings by construction: the rows and columns are labelled by black and white nodes, the cofactor expansion of determinant takes only one edge for all possible choices of row and column. We include the fugacities z and w in the determinant to give a bi-grading $z^a w^b$ to make connection with toric geometry as we shall explain in next paragraph.

Before we move on to review toric geometry, we take a look at the Kasteleyn matrix for

del Pezzo 1.

$$K(w, z) = \begin{pmatrix} a_{13} & a_{41}^1 z & a_{34}^1 w^{-1} \\ a_{41}^2 & a_{34}^3 + a_{12} z & a_{23}^1 \\ a_{34}^2 w & a_{23}^2 & a_{42} z^{-1} \end{pmatrix} \quad (2.41)$$

Its determinant is

$$\begin{aligned} \det K(w, z) = & -a_{13} a_{23}^1 a_{23}^2 - a_{34}^1 a_{34}^2 a_{34}^3 + a_{12} a_{13} a_{42} - a_{41}^1 a_{41}^2 a_{42} \\ & + a_{23}^2 a_{34}^1 a_{41}^2 w^{-1} + a_{13} a_{34}^3 a_{42} z^{-1} - a_{12} a_{34}^1 a_{34}^2 z + a_{23}^1 a_{34}^2 a_{41}^1 w z \end{aligned} \quad (2.42)$$

This corresponds to the 8 perfect matchings as shown in fig. 2-8.

Other examples between dimer models and toric geometry can be found in [49, 51]. In next subsection, we take a small detour to cover some background in toric geometry as all of the model we refer to are based on this vast class of geometry.

2.3.2 A Short Review on Toric Geometry

For a standard introduction to toric geometry, the reader can refer to the mathematical textbook [129], as well as physical introductions [130, 131, 132].

A **toric variety** is defined by an integer lattice $N \simeq \mathbb{Z}^n$, and a **fan** of strongly convex rational polyhedra cones generated by N . These cones are defined by having apex at the origin and are generated by elements of N as a vector space over \mathbb{R} . Toric varieties are special as they provide an elementary entry into understanding many abstract concepts of algebraic geometry. Due to its simplicity, many non-trivial results in string theory can be computed that are otherwise impossible.

Toric varieties can be accessed in different approaches. The definition using fans and cones is one of them. There are others such as homogeneous coordinates, symplectic manifold or physically, the Higgs branch of the space of supersymmetric vacua of some gauged linear sigma model. They can even be associated to convex polytopes in integral lattices. The simplest of all would be through the route of homogeneous coordinate, which we shall describe now. In fact, toric varieties look similar to our usual complex (weighted) projectives space when using homogeneous coordinates. With such point of view, we can see toric varieties as

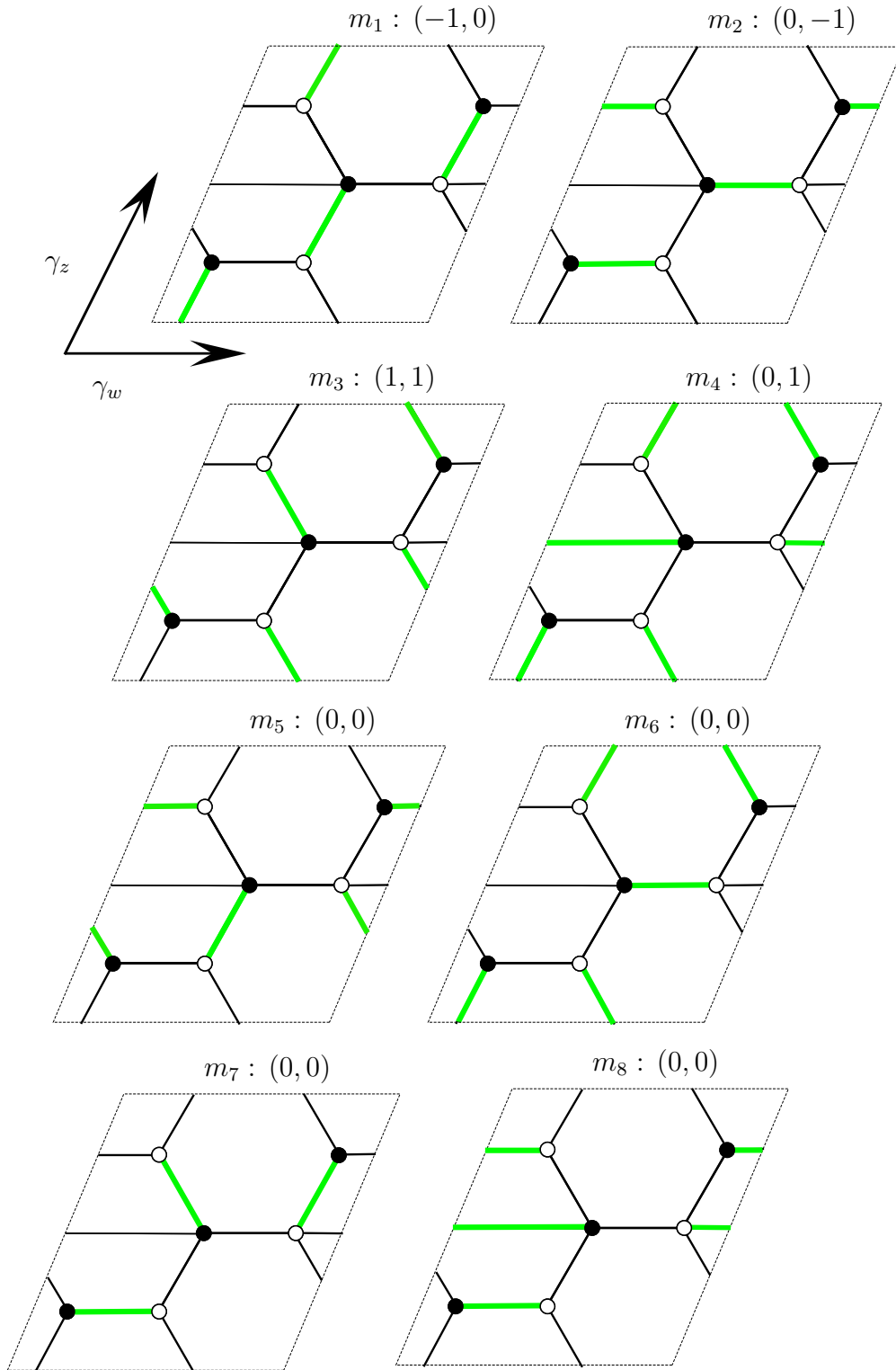


Figure 2-8: The 8 perfect matchings for D3-branes probing singular metric cone over del Pezzo 1 surface. The weights (h_w, h_z) denotes the intersection of the perfect matching with the boundary of the fundamental region.

an algebraic generalisation of (weighted) complex projective spaces.

Homogeneous Coordinates Recall that the projective space \mathbb{CP}^2 has definition as a quotient space in \mathbb{C}^3

$$\mathbb{CP}^2 = (\mathbb{C}^3 \setminus \{0\}) / \mathbb{C}^* , \quad (2.43)$$

where the quotient is through modding out the equivalence relation

$$(x, y, z) \sim \lambda(x, y, z) \quad \text{with} \quad \lambda \in \mathbb{C}^* . \quad (2.44)$$

This can be generalised into weighted case by assigning weights for modding of individual coordinate. For example, the weighted projective space $\mathbb{CP}^{(2,3,1)}$ is given by

$$\begin{aligned} \mathbb{CP}^2 &= (\mathbb{C}^3 \setminus \{0\}) / \mathbb{C}^* , \\ (x, y, z) &\sim (\lambda^2 x, \lambda^3 y, \lambda z) \quad \text{with} \quad \lambda \in \mathbb{C}^* . \end{aligned} \quad (2.45)$$

The toric varieties can be seen as a further generalisation of the weighted case, where we quotient by more than one \mathbb{C}^* action. Consider \mathbb{C}^m and an action by an algebraic torus $(\mathbb{C}^*)^p, p < m$. First we subtract a subset U that is fixed by the action of the continuous subgroup of $(\mathbb{C}^*)^p$, which is the generalisation of taking out the origin in previous two examples. This essentially removes any fix points that become singular after the quotient action. A toric variety \mathcal{M} is then defined by

$$\mathcal{M} = (\mathbb{C}^m \setminus U) / (\mathbb{C}^*)^p . \quad (2.46)$$

The reasoning behind such a nomenclature is based on the fact that it still has an algebraic torus action by the group $(\mathbb{C}^*)^{m-p}$ descending from the natural action of $(\mathbb{C}^*)^m$ on \mathbb{C}^m .

Cones and Fans Toric variety also affords definition by combinatoric lattices. This entails the definition of cones and fans from integral lattices. Now let M and N be a dual pair of lattices, taken as subsets of vector spaces $M_{\mathbb{R}} = M \otimes_{\mathbb{Z}} \mathbb{R}$ and $N_{\mathbb{R}} = N \otimes_{\mathbb{Z}} \mathbb{R}$. The pairing $(u, v) \rightarrow \langle u, v \rangle$ is equivalent to the mapping $M \times N \rightarrow \mathbb{Z}$ and $M_{\mathbb{R}} \times N_{\mathbb{R}} \rightarrow \mathbb{R}$.

Definition 2.3.1. A strongly convex rational polyhedral cone $\sigma \in N_{\mathbb{R}}$ is a set

$$s = \{a_1v_1 + a_2v_2 + \cdots + a_kv_k | a_i \geq 0\} , \tag{2.47}$$

generated by a finite set of vectors v_1, \dots, v_k in N such that $\sigma \cap (-\sigma) = \{0\}$.

Let us clarify this definition. If the lattice N is n -dimensional *i.e.* $N \simeq \mathbb{Z}^n$, a rational polyhedral cone is a cone of dimension not greater than n , with its apex sitting at the origin ($\sigma \cap (-\sigma) = \{0\}$) such that it is bounded by finitely many hyperplanes ('polyhedra'), its edges spanned by lattice vectors ('rational') and it contains no complete line ('strongly convex'). A *face* of a cone σ is either σ itself or the intersection of the cone with one of the hyperplanes bounding σ .

Definition 2.3.2. A collection Σ of cones in $N_{\mathbb{R}}$ is called a fan if each face of a cone in Σ is also a cone in Σ and the intersection of two cones in Σ is a face of each.

There are two examples shown in fig. 2-9. Now we can move the definition of toric

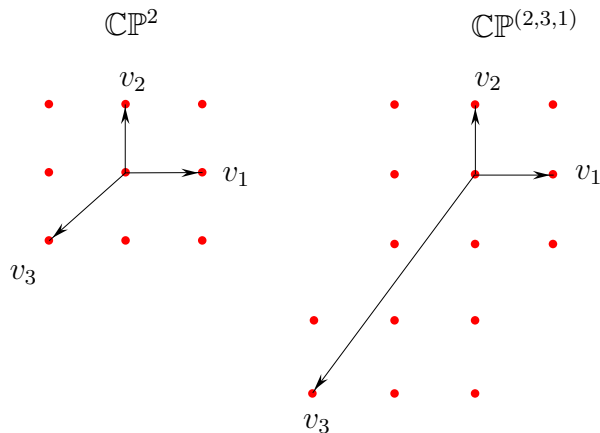


Figure 2-9: The two fans for \mathbb{CP}^2 and $\mathbb{CP}^{(2,3,1)}$. Both of them includes three two-dimensional cones spanned by $v_1 - v_2$, $v_2 - v_3$ and $v_1 - v_3$ and three one-dimensional cones v_1 , v_2 and v_3 and the origin.

varieties using fans and cones. In particular, we are interested in three-dimensional toric varieties *i.e.* $M, N \in \mathbb{Z}^3$.

Let Σ be a fan in N and $\Sigma(1)$ be the set of one-dimensional cones in Σ with cardinality k . We associate each vector v_i in $\Sigma(1)$ with a homogeneous coordinate $w_i \in \mathbb{C}$. Then remove

the set from the resulting \mathbb{C}^k

$$Z_\Sigma = \bigcup_I \{(w_1, \dots, w_k) : w_i = 0 \forall i \in I\}, \quad (2.48)$$

where the union is taken for all sets $I \subseteq 1, \dots, k$ for which $\{w_i : i \in I\}$ does not belong to a cone in Σ . This means several w_i 's are allowed to vanish simultaneously only the corresponding v_i 's all belong to the same cone in Σ .

The toric variety is thus defined by

$$\mathcal{M}_\Sigma = \frac{\mathbb{C}^k \setminus Z(\Sigma)}{G}, \quad (2.49)$$

where G is a product group of $(\mathbb{C}^*)^{k-3}$ and a finite abelian group. The finite group is trivial for our cases here. See [132] for more discussion on this group. The quotient is implemented as the following equivalence relation among the homogeneous coordinates w_i

$$(w_1, \dots, w_k) \sim (\lambda^{Q_a^1} w_1, \dots, \lambda^{Q_a^k} w_k), \quad (2.50)$$

where $\lambda \in \mathbb{C}^*$ and $\sum_{i=1}^k Q_a^i v_i = 0$. Note that this sum essentially parametrises the linear relations between the k one-dimensional cones and among these, $k-3$ are independent.

Let us take the example of \mathbb{CP}^2 , whose fan is given by the first diagram in fig. 2-9. The three one-dimensional cones are $v_1 = (1, 0)$, $v_2 = (0, 1)$ and $v_3 = (-1, -1)$, which represent three homogeneous coordinates w_1, w_2 and w_3 in \mathbb{C}^3 . The set $Z_\Sigma = 0$ is simply the origin. The toric variety is then give by

$$\mathcal{M}_\Sigma = \frac{(\mathbb{C}^3 \setminus \{0\})}{(\mathbb{C}^*)}. \quad (2.51)$$

The linear relation between the generators are $1 \times (1, 0) + 1 \times (0, 1) + 1 \times (-1, -1) = (0, 0)$. Therefore, the equivalence relation is given by $(w_1, w_2, w_3) \sim \lambda(w_1, w_2, w_3)$.

In addition, let us consider a less trivial example of $\mathbb{CP}^{(2,3,1)}$, whose fan is given by the

second diagram in fig. 2-9. This again has Z_Σ to be $\{0\}$. The toric variety is given by

$$M_\Sigma = \frac{(\mathbb{C}^3 \setminus \{0\})}{(\mathbb{C}^*)}. \quad (2.52)$$

The linear relation between generators is now $2 \times (1, 0) + 3 \times (0, 1) + 1 \times (-2, -3) = (0, 0)$. Thus the equivalence relation is $(w_1, w_2, w_3) \sim (\lambda^2 w_1, \lambda^3 w_2, \lambda w_3)$.

Here are few properties of toric varieties that are easy to visualise in the diagram.

Proposition 1. *A toric variety \mathcal{M}_Σ is compact if and only if its fan Σ fills $N_{\mathbb{R}}$.*

For a formal proof of this, see [129]. This gives a straight visualisation of the compactness of toric varieties – both examples in fig. 2-9. In addition, it is also easy to check whether a toric manifold is singular or not. We need some auxiliary definitions for this criterion of smoothness. An r -dimensional cone is called *simplicial* if it is generated by r one-dimensional vectors. A fan is simplicial if all of its constituting cones are simplicial. Given a simplicial fan Σ , it can be shown that the corresponding toric variety can have at most orbifold singularities. In addition, if every n -dimensional cones are generated by the vectors generating the whole lattice N , then the variety \mathcal{M}_Σ is smooth.

Let us check these propositions against the examples in fig. 2-9. We see that both varieties $\mathbb{C}\mathbb{P}^2$ and $\mathbb{C}\mathbb{P}^{(2,3,1)}$ are compact since all of their fans fill up the $N_{\mathbb{R}}$. However, we also see that for $\mathbb{C}\mathbb{P}^{(2,3,1)}$, two of its cones are not generated by the vectors generating N and it indeed has orbifold singularities which locally are $\mathbb{C}^2/\mathbb{Z}_2$ and $\mathbb{C}^2/\mathbb{Z}_2$ and $\mathbb{C}^2/\mathbb{Z}_3$ [132]. To resolve the singularities, we keep adding one-dimensional cones to the fan until all two-dimensional cones are generated by vectors generating N . For example, we can resolve the \mathbb{Z}_2 and \mathbb{Z}_3 singularities as shown in fig. 2-10.

Before we implement the condition for toric Calabi-Yau three-fold, it is expedient to introduce the definition of a toric divisor.

Definition 2.3.3. *Let \mathcal{M}_Σ be a toric variety defined by the fan Σ and $\Sigma(1)$ be the set of one-dimensional cones. We associate each vector v_i in $\Sigma(1)$ with a homogeneous coordinate w_i . The toric divisor D_i is defined by the hypersurfaces $w_i = 0$ in \mathcal{M}_Σ .*

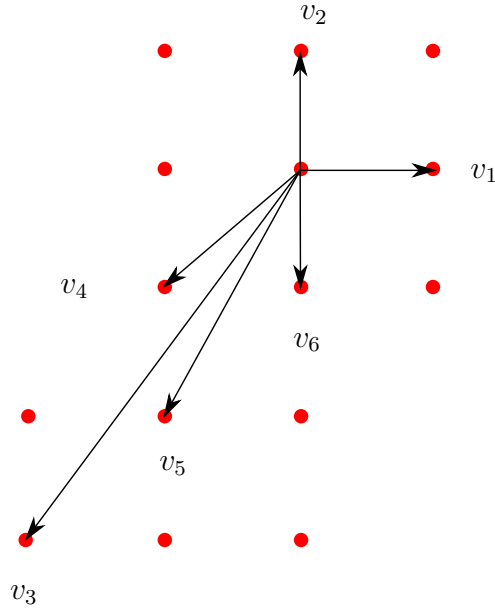


Figure 2-10: The resolved toric variety for $\mathbb{C}\mathbb{P}^{(2,3,1)}$. The added vectors v_4 , v_5 and v_6 , actually correspond to the blown-up exceptional divisors.

It can also be shown [129] that the canonical bundle of \mathcal{M}_Σ is given by

$$K_{\mathcal{M}_\Sigma} = \mathcal{O}\left(-\sum_i D_i\right). \quad (2.53)$$

This result is crucial in checking whether a toric variety is Calabi-Yau or not. Specifically, these toric divisors play an important role in AdS/CFT correspondence for our non-compact toric CY3 cases. As we have mentioned in preceding sections that the singular CY3 is a real metric cone over a Sasaki-Einstein 5-fold. However, when CY3 is toric, the SE manifold is itself a $U(1)$ bundle over a toric base admitting a $U(1)^3$ isometry. In this case, the non-compact four-dimensional (real) toric divisors restrict to compact 3-cycles in SE 5-fold. These 3-cycles correspond to toric divisors (holomorphic curves) of the toric base with $U(1)$ fibre over them.

Toric Calabi-Yau Threefolds

As we know that we can associate a line bundle with meromorphic section to a divisor $D = \sum_i a_i N_i$, such that the meromorphic section has a pole of order $-a_i$ along N_i when

$a_i < 0$ and a zero of order a_i along N_i if $a_i > 0$. N_i are irreducible hypersurfaces for the base of the bundle. Now for our toric case, the divisors are defined by $w_i = 0$ which are also irreducible. Therefore, a toric divisor D_i is associated to a line bundle with a section s which has a zero of order one along D_i . The section is simply w_i . We see that each homogeneous coordinate w_i corresponds to a section of a line bundle associated to a toric divisor D_i .

Now let us consider the monomial $w_1^{a_1} \cdots w_k^{a_k}$. we see that from previous discussion that this monomial has zero of order a_i along D_i if $a_i > 0$ and pole of order $-a_i$ if $a_i < 0$ along D_i . Thus it is a section of line bundle $\mathcal{O}(\sum_i D_i)$. Now let us take $\langle v_i, m \rangle = a_i$, $i = 1, \dots, k$ for $m \in M$ with M being the dual lattice of N . The equivalence under which toric variety is defined now becomes

$$(\lambda^{Q_a^1} w_1)^{\langle v_1, m \rangle} \cdots (\lambda^{Q_a^k} w_k)^{\langle v_k, m \rangle} = \lambda^{\langle \sum_{i=1}^k Q_a^i v_i, m \rangle} w_1^{\langle v_1, m \rangle} \cdots w_k^{\langle v_k, m \rangle} . \quad (2.54)$$

But we have the definition of toric variety: $\sum_{i=1}^k Q_a^i v_i = 0$, which means this monomial is invariant under the equivalence relation. Thus we have a globally defined meromorphic function of our toric variety, which must be a section of the trivial line bundle

$$\sum_{i=1}^k \langle v_i, m \rangle D_i \sim 0 \quad \text{for any } m \in M . \quad (2.55)$$

If $\sum_{i=1}^k a_i D_i \sim 0$, then there exists an $m \in M$ such that $a_i = \langle v_i, m \rangle$ for all i . Recall that the canonical line bundle of a toric variety is given by $K_{\mathcal{M}_\Sigma} \simeq \mathcal{O}(-\sum_{i=1}^k D_i)$ and a Kähler manifold is Calabi-Yau if and only if its canonical line bundle is trivial. Thus for the canonical line bundle to be trivial, we need to have $\sum_i D_i \sim 0$. Then there exists an $m \in M$ such that $a_i = \langle v_i, m \rangle = 1$ for all i . So we have to following condition for a toric variety to be Calabi-Yau

Definition 2.3.4. *Let \mathcal{M}_Σ be a toric variety defined by a fan Σ . \mathcal{M}_Σ is Calabi-Yau if and only if all the vectors generating the fan lie in the same affine hyperplane in the fan Σ .*

So there are some immediate consequences as follows:

Proposition 1. *A toric Calabi-Yau manifold is non-compact.*

As all the vectors v_i lie in the same hyperplane, they can not fill $N_{\mathbb{R}}$. Thus by proposition 1, the variety is not compact. There is another form of CY condition for toric variety that we will refer to more often. As we have the toric variety to satisfy $\sum_i Q_a^i v_i = 0$ for the charges Q_a^i . It is obvious that $\sum_i Q_a^i \langle v_i, m \rangle$ for any $m \in M$ and particularly, there is a choice of m such that $\langle v_i, m \rangle = 1$ if and only if $\sum_{i=1}^k Q_a^i = 0$ for all a . So we have the following for CY condition on toric variety

Proposition 2. *A toric manifold is Calabi-Yau if and only if the charges Q_a^i satisfy the condition $\sum_{i=1}^k Q_a^i = 0$ for all a .*

The CY threefolds in toric case are especially easy to visualise if we define the so called “toric diagram”. These are the diagrams dual to the two-dimensional hypersurface in which all of the one-dimensional cones reside. Therefore, if we intersect the fan Σ representing the toric CY threefold with the plane P in which all the vectors v_i lie, we obtain the two-dimensional diagram $\tilde{\Gamma}$. The dual diagram Γ of $\tilde{\Gamma}$ is drawn such that every edge in Γ is the normal of the edge in $\tilde{\Gamma}$ and vice versa. The diagram Γ is called the toric diagram of the toric Calabi-Yau threefold \mathcal{M}_{Σ} . An example is shown fig. 2-11.

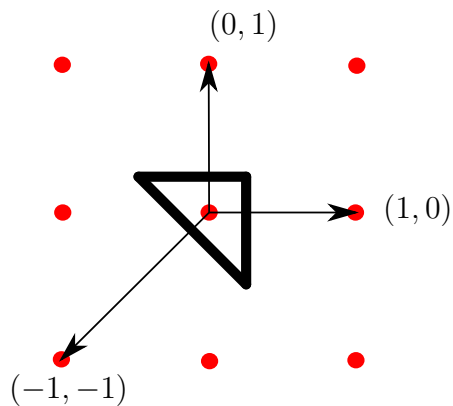


Figure 2-11: The fan for $\mathbb{C}\mathbb{P}^2$ is shown as before as well as the coordinates for the corresponding v_i for $i = 1, 2, 3$. The toric diagram is drawn in thick black lines and it is indeed the dual diagram of the fan.

Toric CY3 as Symplectic Quotients and Fibrations Before we move back to discussion on brane tilings, we describe the construction of toric varieties as symplectic quotients and see the connection between toric varieties and gauged sigma linear models.

Now let z_1, \dots, z_k be coordinates on \mathbb{C}^k and $\mu_a : \mathbb{C}^k \rightarrow \mathbb{C}$, $a = 1, \dots, k-3$ be $k-3$ moment maps defined by

$$\sum_{i=1}^k Q_a^i |z_i|^2 = \text{Re}(t_a), \quad (2.56)$$

where t_a are some complex numbers and are called the ‘level’ for the a -th moment map. The charges Q_a^i are the same as before and they satisfy $\sum_{i=1}^k Q_a^i = 0$ for all a . Also consider the group action $G = U(1)^{k-3}$ on the coordinates governed by

$$z_j \rightarrow \exp(iQ_a^j \alpha_a) z_j, \quad a = 1, \dots, k-3, \quad (2.57)$$

it can be shown that the quotient

$$\mathcal{M} = \frac{\bigcap_{a=1}^{k-3} \mu^{-1}(\text{Re}(t_a))}{G}, \quad (2.58)$$

is also a toric Calabi-Yau threefold. The $k-3$ t_a parameters are the complex Kähler parameters of the Calabi-Yau. We note that this construction also arises in gauged linear sigma models. This model is a two dimensional gauge theory with $U(1)^{k-3}$ gauge group. There are k chiral superfields Φ_i with scalar components denoted by complex variables z_i . The charges of the superfields under gauge group $U(1)^{k-3}$ are denoted by Q_a^i , $a = 1, \dots, k-3$. This justifies the nomenclature ‘charge’ for matrix Q_a^i . Since we have abelian gauge factors here, the supersymmetric vacua are thus constrained by the D-terms equation, which are precisely the moment maps defined in eq. (2.56). Here we see that these toric Calabi-Yau threefolds can be interpreted physically as the Higgs branch of the supersymmetric vacua of a gauge linear sigma model.

As the title suggests, there is another more geometric interpretation of toric CY3 as $U(1)^3 \simeq T^3$ bundle over a real linear subspace (parametrised by the $|z_i|^2$ variables) formed by the intersection of hyperplanes in eq. (2.56) with $(\mathbb{R}^+)^d$. More specifically, we introduce coordinates on the toric manifolds as those z_i in eq. (2.56) for a threefold. These coordinates are not all independent, there are $k-3$ relations imposed by the moment maps. We can rewrite the coordinates as $|z_j|e^{i\theta_j}$ and introduce a new set of coordinates $\{(p_1, \theta_1), (p_2, \theta_2), \dots, (p_k, \theta_k)\}$ with $p_i = |z_i|^2$, $i = 1, \dots, k$. Thus the base is the parametrised

by the $p_i \in \mathbb{R}^+$ and the fibres by the phases θ_i .

Since the coordinates p_i are non-negative, thus the boundaries of the base are place where some of the p_i vanish. However, when $p_j = 0$, the circle $|z_j|e^{i\theta_j}$ degenerates to a point. Therefore, the boundary of the base denotes the degeneration of the fiber θ_j . Geometrically, the fiber degenerates in the direction normal to the boundary. Thus the toric diagram can be drawn as follows. First, express p_j , $j = 4, \dots, k$ in terms of p_1, p_2, p_3 and Kähler parameters using the moment map in eq. (2.56). Each boundary is a plane in the space generated by p_1, p_2 and p_3 . Intersections of these boundary planes give the edges of the toric diagram. On the other hand, there is a relation between the toric diagram and the so called (p, q) -web in physics literature [38]. In the dual picture, the edges of this web correspond to 5-branes carrying (p, q) D5- and NS5-brane charges. This web diagram is graph dual to the triangulation of the toric diagram as shown in fig. 2-12.

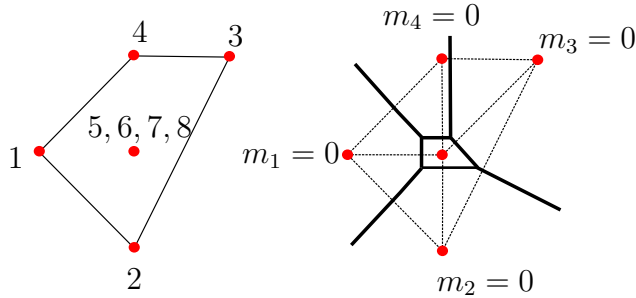


Figure 2-12: The diagram on the left is the toric diagram Δ for del Pezzo 1 surface with labels for perfect matchings. The details of the relation between coordinates of the toric diagram and perfect matchings with possible multiplicities are presented in section 2.3.3. The diagram on the right is the complete triangulation of the toric diagram on the left which gives the resolution to the singular metric cone over the del Pezzo 1 surface and the (p, q) -web is given by the thick black lines in it.

In this picture, the toric diagram is visualised as the boundary of the three-dimension base parametrised by p_1, p_2 and p_3 . There is a T^3 fibre over a generic point of the base with degeneration specified by the direction normal to the boundary. For generic choices of t_a the resulting space is smooth. When all $t_a = 0$, the origin $(z_1, \dots, z_k) = 0$ is a solution of eq. (2.56) and the Calabi-Yau space is a complex cone over a toric surface, with a Gorenstein canonical singularity at the origin. Other values of the Kähler parameter t_a give partial resolution of this singularity. An example of this T^3 fiber construction can be seen for $\mathcal{O}(-3) \rightarrow \mathbb{CP}^2$.

This toric variety is defined by the moment map $p_1 + p_2 + p_3 - 3p_4 = t$, which gives p_4 as $p_4 = (p_1 + p_2 + p_3 - t)/3$. The boundary planes are given by $p_1 = 0, p_2 = 0, p_3 = 0$ and $p_1 + p_2 + p_3 = t$. We see that the intersection of these planes give the toric diagram of \mathbb{CP}^2 as shown in fig. 2-13. Note here the Kähler parameter t controls the size of \mathbb{CP}^2 .

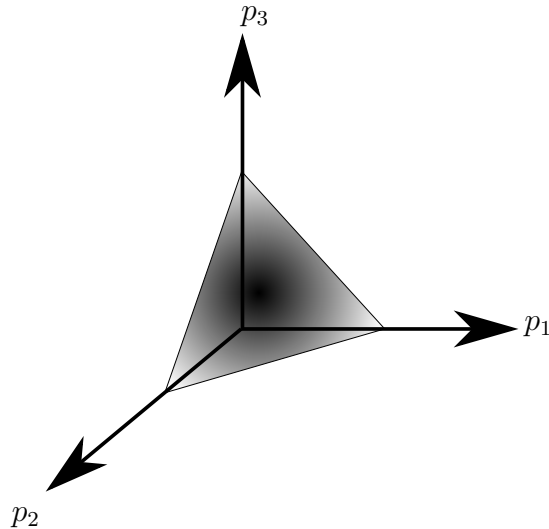


Figure 2-13: The toric diagram of \mathbb{CP}^2 with normals to edges of the shaded triangle giving the degeneration direction of T^3 fibre.

There is also another construction of toric diagram as the degeneration locus of $T^2 \times \mathbb{R}$ fibration over \mathbb{R}^3 base manifold. It is covered in topological vertex formalism developed in [133] for toric CY3. The basic idea behind this formalism is that we can build a toric CY3 by gluing together local \mathbb{C}^3 patches. First, we take \mathbb{C}^3 as a fibration $T^2 \times \mathbb{R}$ and describe its degeneration locus in a two dimensional diagram Γ , which is a trivalent vertex. Then we glue different patches of \mathbb{C}^3 /trivalent vertices specified by the moment map in eq. (2.56). On the other hand, if we are given a toric CY3, we can group the coordinates in triplets which is the same as splitting the CY3 into patches of \mathbb{C}^3 . The moment map in eq. (2.56) then specifies how trivalent vertices of each \mathbb{C}^3 patch is glued together to form the toric diagram of the CY3.

2.3.3 Dimer Models and Toric Geometry

As we shall see in this section: there is a direct translation between the Newton polygon obtained from the Kastelyn matrix of a dimer model and the associated toric diagram. This in fact allows us to construct a series of quiver gauge theories with certain prescribed toric moduli space.

The determinant of the Kasteleyn matrix has the expansion

$$\det K(w, z) = \sum_{(a,b) \in \Delta} f_{ab}(a_{ij}^k) w^a z^b, \quad (2.59)$$

where Δ is the set for all possible exponents (a, b) and $f_{ab}(a_{ij}^k)$ is a function of edge weights a_{ij}^k , which is linear when written in terms of matchings. If we define the matching variables m_i , we have

$$f_{ab}(a_{ij}^k) = \sum_{l \in M_{ab}} m_l, \quad (2.60)$$

where the sum runs over a subset of matchings $M_{ab} \in M$. The assignment of matchings is dictated by their intersection with the contours γ_w and γ_z in eq. (2.40). See fig. 2-12 for the Newton polygon for the cone over dP_1 surface. Each lattice point has perfect matchings m_i residing on it. The coordinates of the lattice points (a, b) are precisely the exponents of the $w^a z^b$ and perfect matchings are their coefficients in the expansion of $\det K(w, z)$.

To expand the previous paragraph in more details, we form the Newton polygon Δ of $\det K(w, z)$ by taking the convex hull of the exponents $(a, b) \in \Delta$. The lattice points in \mathbb{Z}^2 correspond to the individual exponents (a, b) . In [49], it was observed that this lattice polygon is closely related to the toric CY3 which the D3-branes probe. If we append the lattice points with an additional coordinate

$$(a, b) \mapsto (1, a, b), \quad (2.61)$$

we see that these are exactly the complete set of one-dimensional cone of the fan that represents the resolved toric Calabi-Yau. Therefore, Δ is simply the toric diagram of the Calabi-Yau.

However, there are some redundancies in the presentation of the toric diagram since different choices of γ_w and γ_z act as $SL(3, \mathbb{Z})$ on the set of lattice vectors. Translated onto the toric diagram, it acts by $SL(2, \mathbb{Z})$ (shear and rotation) and an integer shift. This transformation is then a change of basis in the charge matrix Q . We see that these redundancies clearly do not change the geometry that the toric diagram represents.

The connection between dimer model and toric Calabi-Yau geometry is based on the simple idea that the D3-branes are probes on the CY geometry and they are free to explore the cone geometry and their moduli space reflects the fact that the D3-branes can explore the neighbourhood of the singularity. The dimer model connects to the geometry by giving a natural parametrisation of the moduli space of toric structure. One aspect of the dimer model is that the lattice points $(1, a, b)$ of the toric diagram usually have multiplicities greater than one. This comes from the fact that there are usually several summands in the coefficients of $z^a w^b$ in expansion of $\det K(w, z)$. This seems like an overkill for representation of the CY geometry, however, it is these multiplicities that give rise to a class of quiver gauge theories of the same moduli space, as we will see in the next chapter.

Bases of Perfect Matching

Recall that a perfect matching in a dimer model correspond to a set of fields that makes the superpotential transform homogeneously under $U(1)$. Therefore, any pairwise difference of perfect matchings generates $U(1)$ symmetries of the theory. The differences of matching also give closed, oriented path on the dimer graph. We shall classify these symmetries according to the homology of these paths and find some distinguished bases for these symmetries. We can treat the $U(1)$ symmetries more precisely by recast them into one-forms [53]. A one-form ϵ is a function defined on the edges of the graph

$$\epsilon = \sum_{i=1}^{N_E} \epsilon_i \delta(i), \quad (2.62)$$

where $\delta(i)$ is a delta-function on i -th edge with canonical orientation from black node to white node. This one-form is anti-symmetric under exchange of orientation of the edge and

it is defined up to a gauge transformation

$$\epsilon \sim \epsilon + df, \quad (2.63)$$

with

$$df(e) = f(F_L) - f(F_R). \quad (2.64)$$

This means each edge gets a contribution from the difference of an integer-valued function evaluated on the faces on the left and on the right of the edge with respect to a canonical orientation from black to white. Now we can assign $U(1)$ charges to the fields which translates to putting these one-forms on the edges. The superpotential has charge zero under these $U(1)$ symmetries apart from the $U(1)_R$. The invariance of superpotential then demands the closure of the one-form $d\epsilon = 0$. This shows that the $U(1)$ symmetries are classified by the cohomology $H^1(\Gamma, \mathbb{Z})$.

With such definitions, we proceed to characterise the baryonic and mesonic $U(1)$ symmetries. A mesonic operator M is a closed path γ_M on T^2 , comprised of a set of edges. Thus the charge is a sum of charges over all fields in the path

$$Q_\epsilon(M) = \oint_{\gamma_M} \epsilon. \quad (2.65)$$

By definition, the baryonic $U(1)$ symmetries are those under which all mesons are uncharged. Therefore the one-form ϵ is exact such that $\epsilon = d\eta$, with $\eta \in H^0(\Gamma, \mathbb{Z})$. A basis for $H^0(\Gamma, \mathbb{Z})$ can be taken as delta functions $\delta(F_i)$ with support on i -th face. This delta function then assigns charges to the edges through the one-form $d\delta(F_i)$, where the exterior derivative is given by the eq. (2.64). This assignment of charges alternates between ± 1 since the canonical orientation of the edges alternates. But the charge is 0 when two adjacent faces are identified due to the periodic tiling on the T^2 . This assignment of charges are precisely the incidence matrix in section 2.2 and it can be interpreted as the ‘‘baryonic’’ $U(1)$ symmetry of the fields in the CFT limit. This is because all mesonic operators are formed by taking traces of the gauge indices, thus all fields in the operators should enter a gauge node as many times as they leave the node. With such configuration, all mesonic operators are uncharged under

this $U(1)$ symmetry. But if an operator is comprised of unequal number of incoming and outgoing fields of a gauge node, it is then charged under this $U(1)$ and hence justifies the name “baryonic”. This is also called the face symmetry, signifying that they come from the contours surrounding faces.

The “mesonic” symmetry on the other hand, are generated by the two non-trivial generators of one-forms corresponding to paths winding the two non-trivial cycles of the torus. These are the mesonic flavour symmetries under which the mesons are charged. It is known that the mesonic “flavour” symmetry corresponds to the $U(1)^2$ isometries of the toric surface at the base of toric Calabi-Yau cone.

As we saw earlier, the perfect matchings parametrise the set of $U(1)$ symmetries under which the superpotential transforms homogeneously. It is therefore worthwhile to construct the “perfect matching matrix” as

$$P_{i\alpha} = \begin{cases} 1 & \text{if } i\text{-th edge is contained in } \alpha\text{-th perfect matching} \\ 0 & \text{otherwise} \end{cases} \quad (2.66)$$

Therefore, the differences of the columns of this matrix generate the $U(1)$ symmetries of the W . It can be seen that the charge assignments differences of columns of P agree the previous one-form parametrisation. There is a preferred basis of matchings that generate contours surrounding the faces of the dimer. Also note that this basis is over-complete as the perfect matchings are not all independent.

Zig-Zag symmetries There is another set of one-forms that will be useful for accounting non-anomalous $U(1)$ symmetries of the quiver gauge theory. These are the one-forms generated by the perfect matchings residing on the boundary points of the toric diagram. For convention, we may take the points in anti-clockwise orientation on the boundary and take successive differences $m_i - m_{i+1}$ [50]. The path is such that it makes precisely one maximal clockwise turn around a white node and then a maximal anti-clockwise turn around the next black node before reaching the next edge and node in the sequence. A fundamental cell of a brane tiling has always a finite number of zig-zag paths. They correspond to the closed

curves wrapped by the NS5-branes and the 46 torus cycles along which the NS5-branes intersect the D5-branes, which we will give a description in next section [56, 42]. We see that these paths have non-trivial winding (p, q) and are subject to some linear constraint among the vectors (p, q) . These are therefore some linear combination of the above baryonic and mesonic symmetries. In fact, these paths have a direct relation to the (p, q) -web diagram which we referred to briefly in the previous section. Every zig-zag path has a winding number in relation to a reference fundamental cell of the brane tiling. The winding numbers of the zig-zag paths of a brane tiling can be drawn as rays from the origin of a \mathbb{Z}^2 lattice. The resulting fan is called *reduced (p, q) -web diagram*, whose origin is N -valent with N being the total number of zig-zag paths in the fundamental cell. The reduced (p, q) -web diagram can be refined by decomposing the N -valent origin into 3-valent vertices. [38, 39]. The dual of the resulting extended (p, q) -web diagram is precisely the toric diagram of the non-compact Calabi-Yau 3-fold. The different ways of decomposing the N -valent origin of the reduced diagram correspond precisely to the different ways of triangulating the convex toric diagram. The example for the dP_1 surface is shown in fig. 2-14. Note here the dP_1 toric diagram only

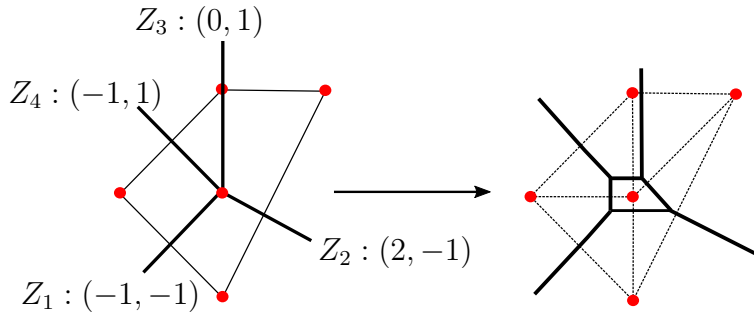


Figure 2-14: The reduced (p, q) -web diagram and the extended (p, q) -web diagram for dP_1 .

has one unique triangulation and thus there is only one dual extended (p, q) -web diagram. The coordinates for the perfect matchings in the first diagram correspond to exactly the winding (p, q) with respect to the fundamental domain.

There is the associated notion of *consistency* related to brane tiling and zig-zag paths [50]. A consistent brane tiling is expected to flow to a superconformal fixed point in the IR with a preferred $U(1)$ R-symmetry, which becomes a part of the superconformal algebra and determines the scaling dimension of BPS operators. If the brane tiling is not consistent,

one normally expect 0 superconformal R-charges to be assigned to the bifundamental fields under a-maximisation [134, 135, 136]. With such assignment, some dibaryon operators would violate the unitarity bound on the scaling dimension. Graphically, this condition on a brane tiling is

- No self-intersection zig-zag paths.
- No edges are multi-bonded, meaning no faces are two-sided.
- No extremal (corner) correspond to more than one perfect matching on the toric diagram.

In terms of toric diagram, a brane tiling is *inconsistent* when

- The area of the toric diagram as measured by the number of fundamental triangles is *NOT* the number of gauge groups in the brane tiling. This condition is important when we start collecting consistent brane tilings generated from certain singular geometry.

Example: dP_1 Now let us take the example of del Pezzo surface 1. The perfect matching matrix is give by the determinant of Kasteleyn matrix

$$M = \left(\begin{array}{c|cccc|cccc} & m_1 & m_2 & m_3 & m_4 & m_5 & m_6 & m_7 & m_8 \\ \hline X_{12} & 0 & 0 & 0 & 1 & 0 & 0 & 0 & 1 \\ X_{23}^1 & 0 & 0 & 1 & 0 & 0 & 0 & 1 & 0 \\ X_{23}^2 & 1 & 0 & 0 & 0 & 0 & 0 & 1 & 0 \\ X_{34}^1 & 1 & 0 & 0 & 1 & 0 & 1 & 0 & 0 \\ X_{34}^2 & 0 & 0 & 1 & 1 & 0 & 1 & 0 & 0 \\ X_{34}^3 & 0 & 1 & 0 & 0 & 0 & 1 & 0 & 0 \\ X_{42} & 0 & 1 & 0 & 0 & 1 & 0 & 0 & 1 \\ X_{13} & 0 & 1 & 0 & 0 & 0 & 0 & 1 & 1 \\ X_{41}^1 & 0 & 0 & 1 & 0 & 1 & 0 & 0 & 0 \\ X_{41}^2 & 1 & 0 & 0 & 0 & 1 & 0 & 0 & 0 \end{array} \right) \quad (2.67)$$

Note that we have split the perfect matchings into external (m_1, \dots, m_4) and internal (m_5, \dots, m_8) in toric diagram Δ . The baryonic face symmetries are given by the linear combination as

$$Q_D = \left(\begin{array}{c|cccc|cccc|c} F_1 & 0 & 0 & 0 & 0 & -1 & 0 & 0 & 1 & \zeta_1 \\ F_2 & 0 & 0 & 0 & 0 & 0 & 0 & 1 & -1 & \zeta_2 \\ F_3 & 0 & 0 & 0 & 0 & 0 & 1 & -1 & 0 & \zeta_3 \\ F_4 & 0 & 0 & 0 & 0 & 1 & -1 & 0 & 0 & \zeta_4 \end{array} \right) \quad (2.68)$$

Note here we included the FI parameter ζ^a accounting the $U(1)$ factor for each face/gauge node. Note that not all face symmetries are independent and we see that this essentially comes from the linear relations among perfect matchings themselves. We can demand an extra relation between the FI parameters to signify this dependence by $\sum_a \zeta^a = 0$.

The zig-zag symmetries are

$$Q_Z = \left(\begin{array}{c|cccccccc} Z_1 & 1 & -1 & 0 & 0 & 0 & 0 & 0 & 0 \\ Z_2 & 0 & 1 & -1 & 0 & 0 & 0 & 0 & 0 \\ Z_3 & 0 & 0 & 1 & -1 & 0 & 0 & 0 & 0 \\ Z_4 & -1 & 0 & 0 & 1 & 0 & 0 & 0 & 0 \end{array} \right). \quad (2.69)$$

These basis can be used to construct anomaly-free baryonic symmetries (c.f. §3.8 [41]). Lastly, the redundancies are given by the kernel of perfect matching matrix M

$$Q_F = \text{Ker}(M) = \left(\begin{array}{cccccccc|c} 0 & 1 & 0 & 1 & 0 & -1 & 0 & -1 & 0 \\ 1 & 1 & 1 & 0 & -1 & -1 & -1 & 0 & 0 \end{array} \right) \quad (2.70)$$

Note that the last column has all entries as 0. This is due to the fact that these choice of perfect matchings do not correspond to physical symmetries hence do not have corresponding FI parameter.

Anomalous $U(1)$ Symmetries $U(1)$ symmetries that become anomalous in the IR limit of the CFT should be singled out. In general, there are two such symmetries. The anomalies in string theory are cancelled by a generalised version of Green-Schwarz mechanism [24, 137]. The $U(1)$ gauge fields of D3-brane worldvolume theory couple to the closed string fields and become massive to decouple from the IR gauge dynamics. As in [138], The anomalous $U(1)$ D-term should not be considered when computing the vacuum. The anomaly-free baryonic $U(1)$ symmetries remain gauged in the AdS model and the gauge fields come from reduction of R-R four-form on the 3-cycles of Sasaki-Einstein 5-fold. These gauge fields couple to the global $U(1)$ currents on the boundary of the AdS. The corresponding dibaryons in the CFT are dual to the wrapped D3-brane, which are charged under these $U(1)$. The 3-cycles in the Sasaki-Einstein 5-fold are from the toric divisors of the Calabi-Yau cone. This gives us a direct way to get the non-anomalous $U(1)$ symmetries from the dimer alone.

The external matchings on the dimer correspond to points on the boundaries of the Newton polygon. We used pairwise difference between perfect matchings to define the zig-zag $U(1)$ symmetries of the CFT. These symmetries can be shown [53, 135] to be exactly the $U(1)$ anomaly-free baryonic symmetries. The number of symmetries is $N_d - 1$ with N_d being the integer length of the boundary of the toric diagram. The two primitive winding cycles are dual to mesonic symmetries, so the baryonic combination of symmetries should

have zero winding number. This imposes another two constrains, making total of $N_d - 3$ baryonic combinations of zig-zag paths.

From fig. 2-14, we read off the winding numbers of zig-zag paths for dP_1 :

$$(-1, -1), (2, -1), (0, 1), (-1, 1).$$

Only three of them are independent as they have a relation $a(-1, 1) + b(2, -1) + c(0, 1) = (0, 0)$ for integers $a = 2, b = 1$ and $c = 3$. This choice of corresponds to the linea combination of charges

$$2Z_1 + Z_2 + 3Z_3 = (2, 1, 2, 3, 0, 0, 0, 0|\zeta) ,$$

where the new FI parameter will be determined by expressing this symmetry as the classical symmetries recorded in eq. (2.68):

$$(2, 1, 2, 3, 0, 0, 0, 0) = (-2, 1, -1, -3, 2) \cdot Q_t . \quad (2.71)$$

Thus $\zeta_{\text{new}} = -2\zeta^1 + \zeta^2 + -\zeta^3$. This $U(1)$ symmetry is the only non-anomalous one of dP_1 theory. In such sense, the anomalous ζ^a should not be treated as fixed number thus constraining the allow values of $|m_i|^2$, but rather defined to be equal to the linear combination of $|m_i|^2$. However, the two redundant ζ^4 and ζ^5 still constrain the VEVs of the fields and thus give relations

$$\begin{aligned} |m_8|^2 &= |m_2|^2 + |m_4|^2 - |m_6|^2 \\ |m_7|^2 &= |m_1|^2 + |m_2|^2 + |m_3|^2 - |m_5|^2 - |m_6|^2 . \end{aligned} \quad (2.72)$$

We then use the remaining three ζ^a 's to define the relation

$$\begin{aligned} \zeta^1 &= |m_8|^2 - |m_5|^2 = |m_2|^2 + |m_4|^2 - |m_5|^2 - |m_6|^2 \\ \zeta^2 &= |m_7|^2 - |m_8|^2 = |m_1|^2 + |m_3|^2 - |m_4|^2 |m_5|^2 \\ \zeta^3 &= |m_6|^2 - |m_7|^2 = -|m_1|^2 - |m_2|^2 - |m_3|^2 + |m_5|^2 + 2|m_6|^2 \end{aligned} \quad (2.73)$$

The non-anomalous combination is then $-2\zeta^1 + \zeta^2\zeta^3 = 2|m_1|^2 - |m_2|^2 + 2|m_3|^2 - 3|m_4|^2$. Thus the non-anomalous baryonic symmetries correspond to the sigma model defined only by the *external* matchings only, with charges $Q = (2 \ -1 \ 2 \ -3|\zeta)$ and $\zeta = -2\zeta^1 + \zeta^2\zeta^3$.

When $\zeta = 0$, the moduli space is the singular cone over dP_1 . For the case when $\zeta \neq 0$ The singularity is (partially) resolved. There are two partial resolutions of the singularity corresponding to the two possible triangulation of the toric diagram as shown in fig. 2-15.

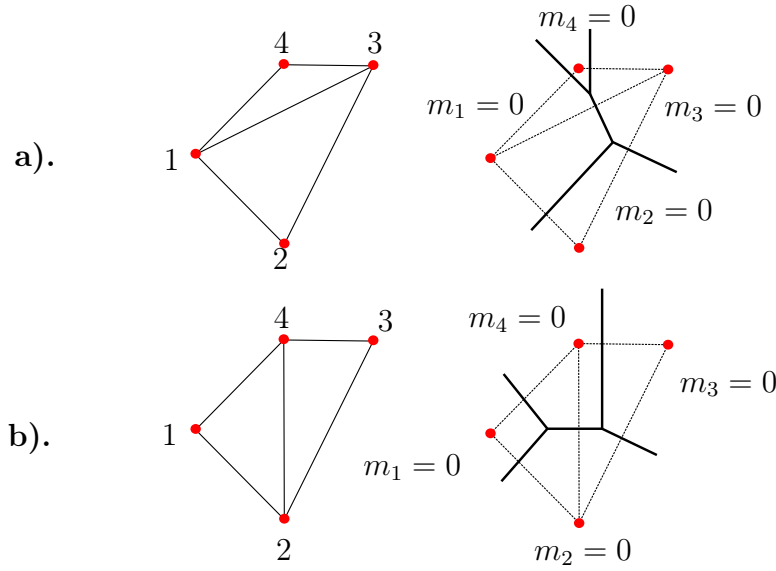


Figure 2-15: The two possible partial resolutions of the cone over dP_1 that are realised as linear sigma model with a non-anomalous baryonic $U(1)$: **a).** $\zeta > 0$ case, representing toric divisors $m_2 = 0$ and m_4 , which can not simultaneously vanish, separated by a blow-up $\mathbb{C}P^1$. **b).** $\zeta < 0$ case, toric divisors $m_1 = 0$ and $m_3 = 0$ are separated by a blow-up $\mathbb{C}P^1$.

In both resolutions, $|\zeta|$ is the Kähler parameter of the blow-up $\mathbb{C}P^1$. When $\zeta > 0$, there is a $\mathbb{C}^2/\mathbb{Z}_2$ singularity at every point on the $\mathbb{C}P^1$, and when $\zeta < 0$, there is a point on the $\mathbb{C}P^1$ with an isolated singularity of the form $\mathbb{C}^3/\mathbb{Z}_3$.

2.4 Forward and Inverse Algorithms

2.4.1 Forward Algorithm

In previous sections, we consider the UV theory of gauge group $U(N)$ and D-terms in the classical limit. The solutions to the F-flatness in eq. (2.28) give an affine toric cone and

D-flatness in eq. (2.24) gives a non-compact toric variety. The intersection of these two spaces can then be constructed as a symplectic quotient or a gauge linear sigma model. This construction was first studied in [27] runs into practical difficulties due to the exponential running time of computing certain dual cone. With the combinatoric tools developed in preceding sections, we review an alternative construction that utilises dimer configurations as natural variables. This construction in fact trivialises the problem [139, 49, 67, 51, 73, 140, 141]. Within this construction, a new basis of fields can be defined from the set of quiver fields. The motivation of this new basis is to put the F-terms and D-terms relation on the same footing. The news fields are the gauged linear sigma model fields and they are precisely the perfect matchings in the brane tiling.

Here we take a pragmatic approach into constructing the sigma model from brane tiling. For the equivalence between dimer model and the formulation in [27], we refer to [141]. This approach has the advantage of dramatically simplifying the computation of moduli space.

In section 2.3.3, we see that the dimer configurations can be used to implement the D-term relations through closed contours enclosing faces in the dimer. In fact, these configurations can also be used to implement the F-term conditions as follows.

Assign each quiver field the product perfect matchings

$$X_i = \prod_{\alpha=1}^m m_{\alpha}^{P_{i\alpha}} , \quad (2.74)$$

where the product is over all perfect matchings and $P_{i\alpha}$ are the entries of the matching matrix. This simply multiplies together all perfect matchings m_{α} that contains quiver field X_i . The F-flatness condition in eq. (2.28) is

$$\prod_{i \in V_i} X_i = \prod_{j \in V_j} X_j , \quad (2.75)$$

where the product is over the edges of adjacent nodes and the product omits the edge connecting i -th and j -th node since the partial derivative w.r.t field X_{ij} in F-flatness condition gets rid of it (note this is only true in toric case). This equation is simply the F-flatness constraint associated to this field. By the definition in eq. (2.74), a field that appears on the

LHS must also be on the RHS since a perfect matching has to cover all nodes in the dimer. Therefore, the F-flatness condition is trivially satisfied by eq. (2.74). Also note that not all perfect matchings are linear independent and the relation among them is recorded in the charge matrix Q_F as in the example eq. (2.70). We can then concatenate the matrices as

$$Q_t = \begin{pmatrix} Q_F \\ Q_D \end{pmatrix} \quad (2.76)$$

and regard Q_t as the charge matrix for the corresponding gauged linear sigma model. The toric variety corresponding moduli space for this model is then obtained by finding the kernel of the matrix Q_t , whose columns gives the lattice vectors for the toric diagram.

Example: dP_1 By concatenating the F-term and D-term matrix for dP_1 , we have the charge matrix to be

$$Q_t = \left(\begin{array}{cccccccc|c} 0 & 0 & 0 & 0 & -1 & 0 & 0 & 1 & \zeta_1 \\ 0 & 0 & 0 & 0 & 0 & 0 & 1 & -1 & \zeta_2 \\ 0 & 0 & 0 & 0 & 0 & 1 & -1 & 0 & \zeta_3 \\ 0 & 1 & 0 & 1 & 0 & -1 & 0 & -1 & 0 \\ 1 & 1 & 1 & 0 & -1 & -1 & -1 & 0 & 0 \end{array} \right) \quad (2.77)$$

Here the eight GLSM fields (perfect matchings) are charged under five gauge groups. The D-term constrains then give a 3-dimensional vacuum space

$$\sum_{i=1}^8 Q_i^a |m_i|^2 = \zeta^a, \quad (2.78)$$

where $a = 1, \dots, 5$ labels the 5 gauge groups. Then we obtain the kernel of Q_t to be

$$\ker Q_t = G = \left(\begin{array}{cccccccc} m_1 & m_2 & m_3 & m_4 & m_5 & m_6 & m_7 & m_8 \\ 1 & 1 & 1 & 1 & 1 & 1 & 1 & 1 \\ -1 & 0 & 1 & 0 & 0 & 0 & 0 & 0 \\ 0 & -1 & 1 & 1 & 0 & 0 & 0 & 0 \end{array} \right) \quad (2.79)$$

The columns are the coordinates for the toric diagram of the moduli space. We see that the multiplicities are not always one directly from this matrix.

To make comparison with the algorithm we just described, we briefly summarise the ‘old’ algorithm first developed in [27] and used in literatures such as [24, 29, 33], in a flow-chart shown in fig. 2-16.

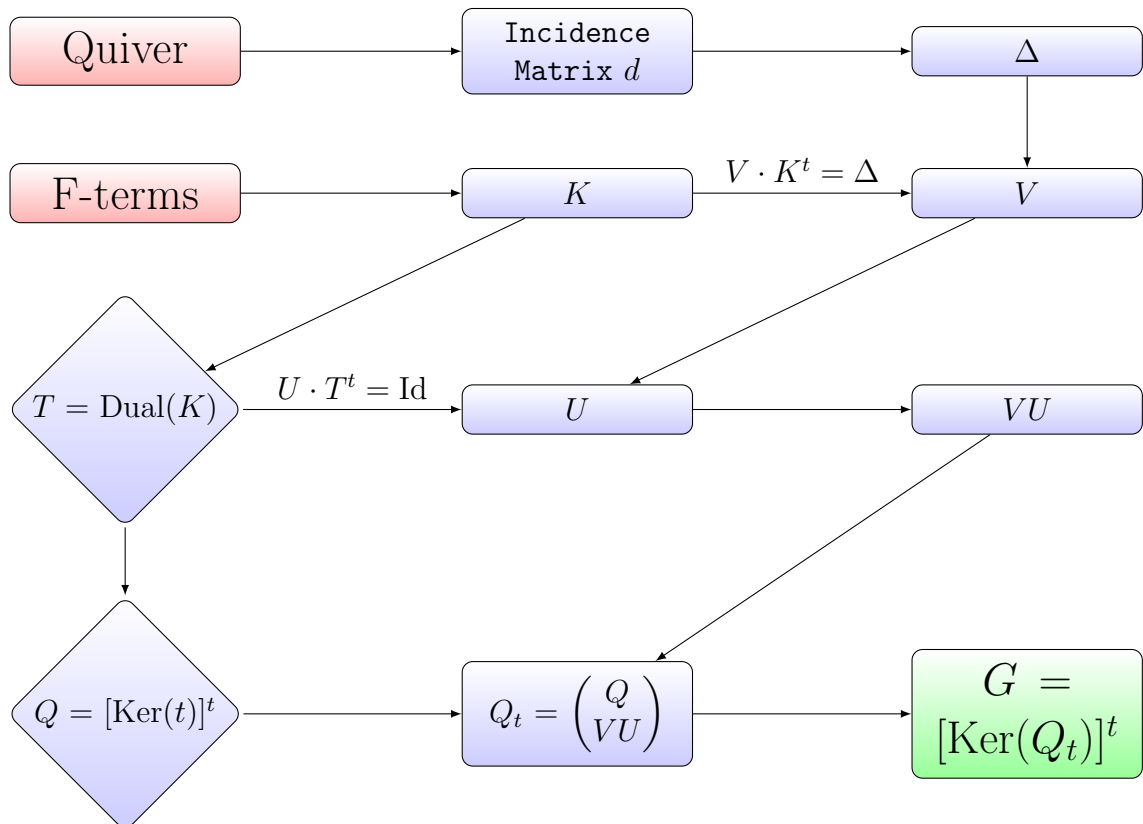


Figure 2-16: The flow-chart for the 'old' forward algorithm that relies on finding the dual cone of K defined by $T = \text{Dual}(K)$. This algorithm is slow as the process of find dual cone has exponential running time.

2.4.2 Inverse Algorithm

As we see from the last section, the gauge theory on the D-brane probing the singularities such as Abelian orbifolds, conifolds, etc., can be systematically encoded into the matrix Q_t , which essentially encapsulates the information from F-term and D-term. The kernel of this matrix then is a list of vectors that records the information of the coordinates of the corresponding toric diagram of the corresponding singularity. Thus it is a natural question to ask: whether given an arbitrary singularity which affords a toric description, we could obtain the gauge theory living on the D-brane probing the singularity. This is the *Inverse Problem* we wish to solve as the foundation of our classification in next chapter.

The solution to this problem must be two-fold: the quiver and its associating superpotential, which correspond to D-term that gives the matter content and gauge group, the F-term that gives the superpotential when integrated back. The general methodology is thus

1. Read the column vectors describing the coordinates of the points in the toric diagram, repeat the appropriate columns when needed and then set $Q_t = \text{Coker}(G_t)$.
2. Separate the D-term ($V \cdot U$) and F-term Q_t contributions from Q_t .
3. Obtain $T = \text{Ker}(Q)$ from Q .
4. The theorem due to Farka [129] guarantees that the dual cone of a convex polytope is still convex. Thus we have $K = \text{Dual}(T^t)$. In addition, the duality theorem gives $\text{Dual}(\text{Dual}(K)) = K$ thus engenders the inverse procedure.
5. Since $U \cdot T^t = \text{Id}$ and $V \cdot K^t = \Delta \implies (V \cdot U) \cdot (T^t \cdot K^t) = \Delta$. Once we can obtain Q_t from the toric diagram, the relations

$$K = \text{Dual}(T^t) \quad \Delta = (V \cdot U) \cdot (T^t \cdot K^t), \quad (2.80)$$

gives our desired K and Δ representing F-terms and D-terms constraints.

However, there are immediate indeterminacies in arriving at a unique Q_t from the given toric diagram.

- In step (1) above, we do not know *a priori* which column vector to repeat when writing the coordinates of the toric diagram into matrix Q_t .
- In step (2), we do not know which vectors constitute Q and which constitute $V \cdot Q$ within Q_t .

On top of these ambiguities, we are faced with one more difficulty: tracing back the arrows in fig. 2-16 does not guarantee us a gauge theory living on the D-branes probing the singularity we started with. Therefore, we need to find a canonical method to avoid the described difficulties, thus giving us consistent gauge theories with only bifundamentals etc. This is where we resort to the method of **partial resolution**. The physical interpretation of partial resolution is simple: starting with abelian orbifolds which are toric, we tune the FI parameters of the theory while staying in the cone partition of these parameters to avoid flop-transition, to obtain a physical resulting theory [29]. In other words, we carefully tune the FI parameters in the allowed region for the parent orbifold theory to reach subsector theories that still live on the D-brane and is well-behaved.

Partial Resolution

The orbifold singularities of the form $\mathbb{C}^k/\Gamma(k, n)$ for $\Gamma(k, n) = \mathbb{Z}_n \times \mathbb{Z}_n \times \dots \times \mathbb{Z}_n$ ($(k-1)$ -th product) have been well studied. The complete information as well as the charge matrix Q_t for $\Gamma(k, n)$ is known: $k=2$ is the elliptic model, $k=3$ the brane-box model *etc.* [30, 31, 32] and $k=3, n=3$ in [29].

Now if we have any toric diagram of dimension k , we can embed it into such a $\Gamma(k, n)$ -orbifold toric diagram for sufficiently large n , for which we choose the smallest case that suffices. This embedding is always possible as the $\Gamma(k, n)$ -orbifold is a k -complex of length n and any toric diagrams can be obtained by deletion of a subset of lattice points. This procedure of node deletion is called **partial resolution** of $\Gamma(k, n)$ -orbifold. This essentially gives us a method to turn on the FI parameters thus enabling us to determine the Q_t from the orbifold singularity.

We turn the the classical example of partial resolution of $\Gamma(3, 2) = \mathbb{Z}_2 \times \mathbb{Z}_2$ to obtain conifold and SPP [32]. The SPP defined by $xy = zw^2$ can be obtained from $\Gamma(3, 2)$ defined

that D-term conditions are linear systems in modulus-squared of quiver fields, we can make the definition $x_i = |m_i|^2$. Then solving all GLSM fields in terms of x_7 is done through Gaussian row reduction: $\vec{x} = \{x_1, x_2, x_1 + \zeta_2 + \zeta_3, \frac{2x_1 - x_2 + x_7 - \zeta_1 + \zeta_2}{2}, 2x_1 - x_2 + \zeta_2 + \zeta_3, \frac{2x_1 - x_2 + x_7 + \zeta_1 + \zeta_2 + 2\zeta_3}{2}, x_7, \frac{x_2 + x_7 - \zeta_1 - \zeta_2}{2}, \frac{x_2 + x_7 + \zeta_1 + \zeta_2}{2}\}$. We see from this reduction that the nodes away from m_7 are unaffected by the resolution, thus fields residing on those nodes continue to have zero vev. Now we can set the ones unaffected by resolution to zero giving $\vec{x} = \{0, 0, 0, \frac{x_7 - \zeta_1 - \zeta_3}{2}, 0, \frac{x_7 + \zeta_1 + \zeta_3}{2}, x_7, \frac{x_7 - \zeta_1 + \zeta_3}{2}, \frac{x_7 + \zeta_1 - \zeta_3}{2}\}$. Now we have an arbitrary choice to make m_4 and m_8 have zero vev by choosing $\zeta_3 = 0$ and $x_7 = \zeta_1$. Thus $x_{6,7,9}$ have vev equal to ζ_1 as shown in fig. 2-17.

3. **Solving for G_t :** Now we see that by deleting column m_7 , we must also resolve m_6 and m_9 . So we have

$$Q_t = \text{Coker}(Q_t) = \begin{pmatrix} m_1 & m_2 & m_3 & m_4 & m_5 & m_8 \\ 0 & 1 & 0 & 0 & -1 & 1 \\ 1 & 1 & 1 & 0 & 1 & 0 \\ 1 & 1 & 1 & 1 & 1 & 1 \end{pmatrix}, \quad (2.81)$$

where we see here these are the coordinates of toric diagram D on the right of fig. 2-17.

4. **Solving for Q_t :** Now we need to make linear combinations of columns of Q'_t to obtain Q_t as to force columns 6, 7, 9 zero. Note that G_t has 6 columns and 3 rows and it is in the nullspace of Q_t , which must have $9 - 3 = 6$ columns and we then must have $6 - 3 = 3$ rows for Q_t . In addition, row containing ζ_1 must be eliminated since it is the resolved and needs to be removed from D-terms constraints. Now we define variables $\{a_{i=1,\dots,6}\}$ such that $\sum_i a_i \text{row}_i(Q'_t)$ is a row of Q_t . Firstly, (a) the 6, 7, 9-th columns of y must be set to 0 since these are the m_i GLSM fields that obtain vev. Secondly, (b) after removing these columns, y must be in the nullspace spanned by the rows of G_t . Since by definition, Q'_t is in the nullspace of G'_t and the row-combination operator is closed in the nullspace, and columns to be set to 0 in Q_t to give Q_t are precisely those removed in G'_t to give G_t . Then (a) implies (b). Condition (a) gives the equations $\{a_1 + a_6 = 0, -a_1 + a_2 - a_6 = 0, -a_2 + a_4 = 0\}$ which afford the solution $a_1 = -a_6$; $a_2 = a_4 = 0$. $a_4 = 0$ eliminates the row containing ζ_1 . We choose $a_1 = 1$ and $a_5 = 1$ as ζ_5 is unresolved. This gives the tree rows for D-term relations: row₁, row₅ and row₆. The remaining must be the F-term relations: $a_3 = 1$. Therefore, we have the matrix

$$Q_t = \left(\begin{array}{cccccc|c} m_1 & m_2 & m_3 & m_4 & m_5 & m_8 & \\ \hline 1 & -1 & 1 & 0 & -1 & 0 & 0 \\ -1 & 1 & 0 & 1 & 0 & -1 & \zeta_2 \\ -1 & 0 & 0 & -1 & 1 & 1 & \zeta_3 \end{array} \right) \quad (2.82)$$

5. **Δ and K Matrices:** From Q_t , we have $Q = (1, -1, 1, 0, -1, 0)$, giving

$$T_{j\alpha} := \text{Ker}(Q) = \begin{pmatrix} 0 & 0 & 0 & 0 & 0 & 1 \\ 1 & 0 & 0 & 0 & 1 & 0 \\ 0 & 0 & 0 & 1 & 0 & 0 \\ -1 & 0 & 1 & 0 & 0 & 0 \\ 1 & 1 & 0 & 0 & 0 & 0 \end{pmatrix} \quad \text{and} \quad K^t := \text{Dual}(T^t) = \begin{pmatrix} 1 & 0 & 0 & 0 & 0 & 0 \\ 0 & 0 & 1 & 0 & 1 & 0 \\ 0 & 1 & 0 & 0 & 0 & 0 \\ 0 & 0 & 1 & 1 & 0 & 0 \\ 0 & 0 & 0 & 1 & 0 & 1 \end{pmatrix}.$$

We then obtain

$$T^t \cdot K^t = \begin{pmatrix} 0 & 0 & 0 & 0 & 1 & 1 \\ 0 & 0 & 0 & 1 & 0 & 1 \\ 0 & 0 & 1 & 1 & 0 & 0 \\ 0 & 1 & 0 & 0 & 0 & 0 \\ 1 & 0 & 0 & 0 & 0 & 0 \end{pmatrix}.$$

From Q_t , we also have

$$V \cdot U = \begin{pmatrix} -1 & 1 & 0 & 1 & 0 & -1 \\ -1 & 0 & 0 & -1 & 1 & 1 \end{pmatrix}. \quad (2.83)$$

Using eq. (2.80), we obtain at last

$$\Delta = \begin{pmatrix} -1 & 1 & 0 & 1 & -1 & 0 \\ 1 & -1 & 1 & 0 & 0 & -1 \end{pmatrix} \implies d = \left(\begin{array}{c|cccccc} & X_1 & X_2 & X_3 & X_4 & X_5 & X_6 \\ \hline U(1)_A & -1 & 1 & 0 & 1 & -1 & 0 \\ U(1)_B & 1 & -1 & 1 & 0 & 0 & -1 \\ \hline U(1)_C & 0 & 0 & -1 & -1 & 1 & 1 \end{array} \right), \quad (2.84)$$

which is precisely the incidence matrix obtained from the quiver of SPP that encodes the gauge groups and matter content.

6. **Superpotential** To obtain the superpotential, the natural place to start is the K matrix we previously arrived – it should integrate back to a single function: the superpotential. However, there are subtleties in finding the correct candidate in all possible linear combinations. Note that K is a matrix of dimension $m \times (r - 2)$ with m fields that appear in the final superpotential and $(r + 2)$ linear combinations of the said m fields, as well as $m \geq r + 2$. Thus we have $(r + 2)$ vectors in \mathbb{Z}^m with generic $m - r - 2$ linear relations among them. For example, if we have $\text{row}_1 + \text{row}_3 = \text{row}_7$, we can write down $X_1 X_3 = X_7$ as a potential F-terms condition. In general, $\sum_i a_i K_{ij} = 0$ with $a_i \in \mathbb{Z}$ gives a F-term as $\prod_i X_i^{a_i} = 1$ for $X_i = \prod_j v_j^{K_{ij}}$, where v_i are the $r + 2$ parameters used to solve the system of F-term relations. Thus we need to find all linear relations by finding the \mathbb{Z} -nullspace of K^t of dimension $m - r - 2$.

However, this procedure has some ambiguities as any new linear combination will result in some new terms in the F-term relations. So there are some guess work involved to find the most convenient set of linear combinations to integrate back to the superpotential. We first wish to have this back-integration gives no fields other than the m fields contained in the K matrix. But sometimes this is not possible as we shall see that some new fields need to be included and the moduli space of such theory is larger than that encoded in our toric data: the new fields parametrise the new branch

of the moduli space.

We take our SPP example and recall that the K matrix is give by

$$K = \left(\begin{array}{c|ccccc} & v_1 & v_2 & v_3 & v_4 & v_5 \\ \hline X_1 & 1 & 0 & 0 & 0 & 0 \\ X_2 & 0 & 0 & 1 & 0 & 0 \\ X_3 & 0 & 1 & 0 & 1 & 0 \\ X_4 & 0 & 0 & 0 & 1 & 1 \\ X_5 & 0 & 1 & 0 & 0 & 0 \\ X_6 & 0 & 0 & 0 & 0 & 1 \end{array} \right),$$

where we see that the relation $X_3X_6 = X_4X_5$ is immediate. Since $m - r - 2 = 1$, we see that is only one such linear relation. Now we check the gauge charge that this term carries to make sure it is gauge invariant. Since the charges of the fields under the gauge groups are give by incidence matrix d :

$$d = \left(\begin{array}{c|cccccc} & X_1 & X_2 & X_3 & X_4 & X_5 & X_6 \\ \hline U(1)_A & -1 & 1 & 0 & 1 & -1 & 0 \\ U(1)_B & 1 & -1 & 1 & 0 & 0 & -1 \\ U(1)_C & 0 & 0 & -1 & -1 & 1 & 1 \end{array} \right),$$

we have the charge of X_3X_6 to be $(q_A, q_B, q_C) = (0+0, 1+(-1), (-1)+1) = (0, 0, 0)$ as expected. And by construction, X_4X_5 has the same charge. To integrate this F-term back, we now are presented with two choice:

- Write the superpotential using only X_i for $i = 1, \dots, 6$. For such case, we can try ansatz $W = X_1X_2(X_3X_6 - X_4X_5)$, which gives back the F-term when taking partial derivative w.r.t X_1 or X_2 . This gives us a new F-term $X_1X_2X_3$ upon the action of $\partial/\partial X_6$. This term is inconsistent since the corresponding rows do not add up to zero. So we move the another option.
- We introduce another field ϕ that is invariant under all the gauge group to the superpotential. We have $W = \phi(X_3X_6 - X_4X_5)$. When $\phi = 0$, we have our original moduli space and matter content. When $\phi \neq 0$, we must have $X_3 = X_4 = X_5 = X_6 = 0$ and the D-term relations read $|X_1|^2 - |X_2|^2 = -\zeta_1 = \zeta_2$, giving us the moduli space $\{\phi \in \mathbb{C}, X_1 \in \mathbb{C}\}$ with constraint $\zeta_1 + \zeta_2 = 0$. Hence, we obtain a new moduli space.

We can take on a less trivial example from dP_1 :

$$\begin{aligned}
d &= \left(\begin{array}{c|cccccccccc} & X_1 & X_2 & X_3 & X_4 & X_5 & X_6 & X_7 & X_8 & X_9 & X_{10} \\ \hline U(1)_A & -1 & 0 & 0 & -1 & 0 & 0 & 0 & 1 & 0 & 1 \\ U(1)_B & 1 & -1 & 0 & 0 & 0 & -1 & 0 & 0 & 1 & 0 \\ U(1)_C & 0 & 0 & 1 & 0 & 1 & 0 & 1 & -1 & -1 & -1 \\ U(1)_D & 0 & 1 & -1 & 1 & -1 & 1 & -1 & 0 & 0 & 0 \end{array} \right) \\
K &= \left(\begin{array}{c|cccccccccc} & X_1 & X_2 & X_3 & X_4 & X_5 & X_6 & X_7 & X_8 & X_9 & X_{10} \\ \hline v_1 & 1 & 0 & 1 & 0 & 0 & 0 & 1 & 0 & 0 & 0 \\ v_2 & 0 & 1 & 1 & 0 & 0 & 0 & 0 & 1 & 0 & 0 \\ v_3 & 1 & 0 & 0 & 1 & 0 & 0 & 0 & 0 & 1 & 0 \\ v_4 & 0 & 1 & 0 & 1 & 0 & 1 & 0 & 0 & 0 & 0 \\ v_5 & 0 & 0 & 1 & 0 & 1 & 0 & 1 & 0 & 0 & 0 \\ v_6 & 0 & 0 & 0 & 0 & 0 & 1 & 1 & 0 & 0 & 1 \end{array} \right). \tag{2.85}
\end{aligned}$$

The nullspace of K is $10 - 6 = 4$ dimensional and one relation can be obtain straight away $X_2X_7 = X_3X_6$. The charge is $(q_A, q_B, q_C, q_D) = (0 + 0, -1 + 0, 0 + 1, 1 + (-1)) = (0, -1, 1, 0)$, which precisely cancels that of X_9 . Therefore, the term $X_9(X_2X_7 - X_3X_6)$ can be a term of W . Now acting with ∂/∂_{X_2} , we have X_7X_9 , which is equal to $X_1X_5X_{10}$ as seen from K . Thus we can add $-X_1X_2X_5X_{10}$ to W . Thus we can repeat this procedure and add in new fields if necessary and we finally arrive at $W = X_2X_7X_9 - X_3X_6X_9 - X_4X_8X_7 - X_1X_2X_5X_{10} + X_3X_4X_{10} + X_1X_5X_6X_8$.

Before ending this section, we make a few general remarks on obtaining the superpotential. Since we are within the toric regime, each field appears exactly twice with opposite signs in different terms in the superpotential. Thus the F-terms can be written as

$$\prod_i X_i^{a_i} = \prod_j X_j^{b_j}, \tag{2.86}$$

with $a_i, b_j \in \mathbb{Z}^+$. If we were to have another field X_k that $k \notin \{i\}, \{j\}$, then the term $X_k(\prod_i X_i^{a_i} - \prod_j X_j^{b_j})$ must appear in W only this once for it to be additive in W . Sometimes, this field X_k may not be possible to find and new fields need to be introduced, thus giving a moduli space that is larger than that described by the toric data. On top of this, we need to make sure each term in W to be invariant under the product gauge groups. This means we must have $Q^s(X_k) + \sum_i Q^s(X_i) = 0$ for $s = 1, \dots, r$ labelling the gauge groups. If we can not find such X_k , we have to introduce new fields with appropriate charge. Therefore, for each relation we read from matrix K , we proceed in such manner until we reach the final superpotential.

From previous points, we note that we need to have educated guesses to decide if we need to include new fields when integrating back the F-terms. It seems rather cumbersome if we want to find the gauge theories living on the D-brane probing toric Calabi-Yau singularities. However, we shall see in the last chapter that the dimer and brane tiling interpretation of combining quiver and its associated superpotential, make the aforementioned *Inverse Algorithm* a streamlining procedure. The *partial resolution* as stated above corresponds to edge deletion in the brane tiling/dimer, which physically means giving vevs (higgsing) to certain fields thereby deleting perfect matchings that contain these fields. The superpotential of the resulting theory is therefore automatic from the construction of dimer. We shall see more of this technique in action in Chapter 3.

2.5 Brane Tiling from Brane Construction

In the last section, we focused on the interpretation of brane tiling as a combinatoric object that encodes the corresponding physical contents. It is important for us to make reference to the five-brane construction of brane tiling and see how the combinatoric properties of bipartite graph embedded on T^2 arise from such construction. In particular, we shall use the NS5-D5 brane system for string theory realisation of $\mathcal{N} = 1$ superconformal quiver gauge theory.

First, let us consider type IIB theory with a stack of N D5-branes. Then as the D-branes are hyperplanes on which the open strings terminate, we have $U(N)$ gauge theory living on the worldvolume of D5-branes. Our goal is to construct four-dimensional theory, therefore two of the D5-directions are redundant. We thus choose two of its directions x^5 and x^7 to be compactified on T^2 with radius R . Now we have N D5-branes wrapping T^2 cycles whence Kaluza-Klein modes must decouple when radius R is small. We thus have four-dimensional $\mathcal{N} = 4$ supersymmetric Yang-Mills theory as the introduction of D5-brane breaks half of the supersymmetry. The need to have $\mathcal{N} = 1$ theory, we further introduce NS5-branes to break the supersymmetry. The five-brane system is shown in table 2.5. With such brane configuration, we see that the D5-branes are divided into chambers in the x^5 and x^7 directions by the presence of NS5-branes. The gauge groups are then separated into

	x^0	x^1	x^2	x^3	x^4	x^5	x^6	x^7	x^8	x^9
D5	-	-	-	-		-			-	
NS5	-	-	-	-	-	-				
NS5'	-	-	-	-			-	-		

Table 2.5: The 5-brane configuration of the NS5-D5 system. We see that the D5 branes break a half of the supercharges and NS5 branes in two directions break the supersymmetry to a quarter resulting 4 supercharges, thus $\mathcal{N} = 1$ in four-dimension.

factor gauge group where each chamber represents a single factor. As we can see here, the D5-branes and NS5-branes have junction in this configuration and it was pointed out in [53] that gauge anomaly cancellation implies the conservation of NS5-charge, which then restricts the structure of NS5-D5 junction. This separates the T^2 into different regions differentiated by the relative orientations of NS5- and D5-branes at the junction. Such a separation of the T^2 is called the fivebrane diagram [54]. In addition to the structure we described above, we can put the NS5-branes to be parallel to the D5-branes as it is allowed by the conservation of NS5-charges as shown in fig. 2-18. These different NS5-branes can now join to form a single

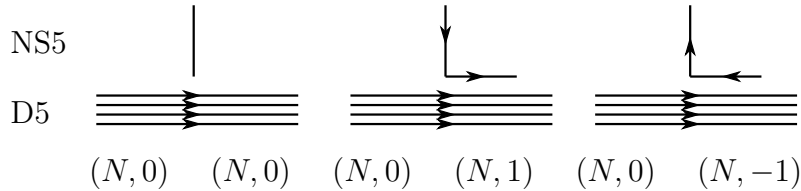


Figure 2-18: The first diagram is prohibited by the conservation of NS5-charges; The second and the last diagrams represent bound states of N D5-branes and 1 NS5-brane, called the $(N, 1)$ -system. Similarly the third is called $(N, -1)$ -system due to the reversal of orientation of NS5-brane.

NS5-brane. Note in fig. 2-18 that the NS5-branes seem to bend at 90 degrees at the junction due to fact it is at the strong coupling limit. The shape of NS5-brane is in fact smooth at string general coupling constant. Since we have a single NS5-brane, the worldvolume of it is therefore a product $\mathbb{R}^{3,1} \times \Sigma$, where Σ intersects with the T^2 with one-cycle: one of its two directions is in the compact 5, 7-direction and the other in the non-compact 4, 6-direction. The brane configuration is therefore more generalised as shown in table 2.6.

	x^0	x^1	x^2	x^3	x^4	x^5	x^6	x^7	x^8	x^9
D5	—	—	—	—		—		—		
NS5	—	—	—	—	— Σ —					

Table 2.6: The brane configuration of a general brane tiling from NS5-D5 brane system. The 5, 7-th directions are compactified and Σ is a holomorphic curve in 4, 5, 6, 7-directions. All the NS5-branes in table 2.5 are merged into a single NS5-brane wrapping holomorphic curve.

2.5.1 Relation to D3-Brane Setup

As shown in table 2.5, the compact 5, 7-directions give us the choice to T-dualise. This turns the D5-branes into D3-brane and the NS5-branes into a Calabi-Yau manifold. This is because one of the compact 5, 7-directions is orthogonal to the NS5-brane and taking T-duality along the direction perpendicular to NS5-brane turns it into CY3. Note that the T-duality exchanges momentum and winding modes, which in the case of NS5-brane, it also has to exchange corresponding gauge fields: metric and B-field. After T-duality, we have a non-trivial B-field that becomes the source of NS5-brane. The details of this are the content of Busher’s rule [142]. The brane configuration is shown in table 2.7. At this point,

	x^0	x^1	x^2	x^3	x^4	x^5	x^6	x^7	x^8	x^9
D3	—	—	—	—						
CY3					—	—	—	—	—	—

Table 2.7: The brane configuration after taking T-dualisation in the compactified 5, 7-th directions in the 5-brane system shown in table 2.5. The D5-brane is T-dual to D3-brane and the NS5-brane is dual to the toric Calabi-Yau cone.

it becomes clear why we started with D5-branes with two directions compactified. From the D3-brane picture, the T^2 of 5, 7-th directions form a sub-torus of the $U(1)^3$ isometry of the toric Calabi-Yau cone and we have T-dualised along the sub- T^2 to reach from Calabi-Yau to NS5-brane. As another generic example, consider $\mathbb{C} \times \mathbb{C}^2/\mathbb{Z}_2$, the T-duality maps it into two parallel NS5-branes. Note that this construction of NS5-D5 system is a natural generalisation of brane interval [65] and brane box model [64]. To summarise, we present this web of connections in fig. 2-19.

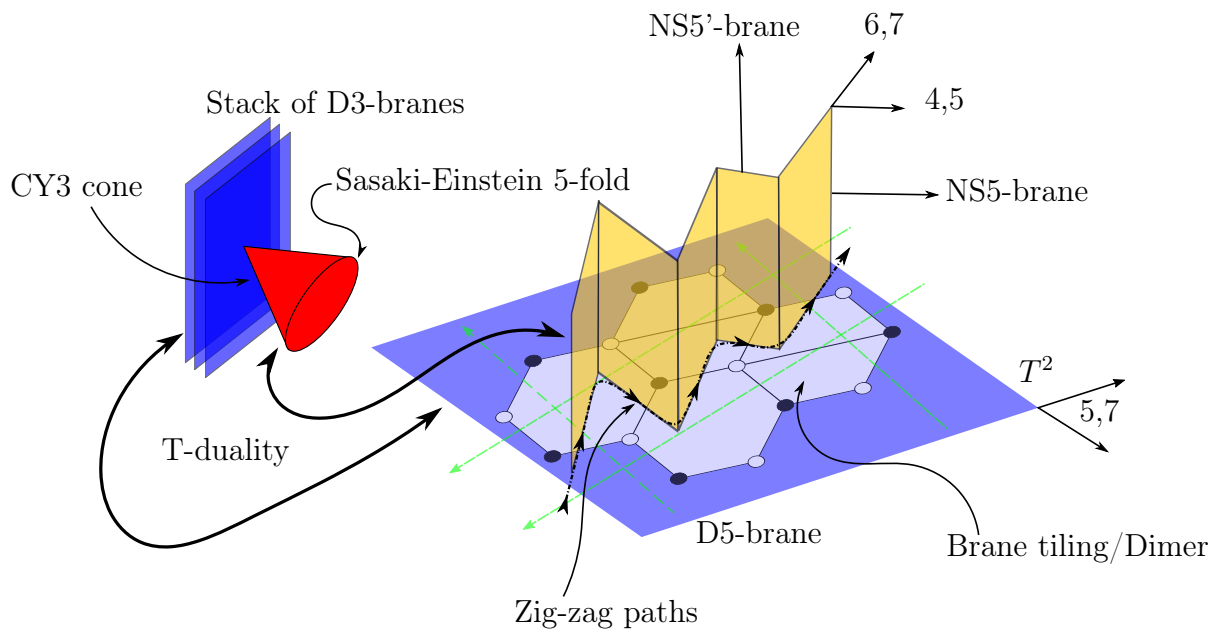


Figure 2-19: The web of connection of brane realisation of D3-brane probing toric Calabi-Yau singular cone over base of SPP. We see that the physical information is fully included in the brane tiling/dimer and the brane construction gives precisely this bipartite tiling on a T^2 , which are the direction we choose to implement the T-dualisation.

THIS PAGE INTENTIONALLY LEFT BLANK

Chapter 3

A Survey of Brane Tilings

Having reviewed the essential backgrounds in quiver gauge theories and brane tilings as well as their relations to each other and their connections to toric geometry, we see that An infinite class of $4d \mathcal{N} = 1$ gauge theories can be engineered on the worldvolume of D3-branes probing toric Calabi-Yau 3-folds. This kind of setup has multiple applications, ranging from the gauge/gravity correspondence to local model building in string phenomenology. Brane tilings fully encode the gauge theories on the D3-branes and have substantially simplified their connection to the probed geometries. The purpose of this chapter is to push the boundaries of computation and to produce as comprehensive a database of brane tilings as possible. We develop efficient implementations of brane tiling tools particularly suited for this search. We present the first complete classification of toric Calabi-Yau 3-folds with toric diagrams up to area 8 and the corresponding brane tilings. This classification is of interest to both physicists and mathematicians alike.

3.1 Introduction

A powerful approach for engineering $4d \mathcal{N} = 1$ gauge theories in string theory consists of realizing them on the worldvolume of D3-branes probing singular Calabi-Yau (CY) 3-folds. The case in which the CY 3-fold is toric is extremely rich, yet particularly tractable.

More than a decade has passed since the first systematic treatment of the question “what is the gauge theory given an arbitrary toric CY_3 ?” [69]. A first approach for addressing

this problem was the *Inverse Algorithm* (the details are review in section 2.4.2), which generates the quiver and superpotential for a given toric singularity via partial resolution of an appropriate $\mathbb{C}^3/(\mathbb{Z}_N \times \mathbb{Z}_M)$ orbifold. In practice, a chief bottleneck of this method was the exponential running time necessary for finding dual cones needed for partial resolution. Later, the connection between toric geometry and gauge theory was tremendously simplified with the advent of *brane tilings* [49, 51, 52], which have become the standard tools in this field. Brane tilings are Type IIB configurations of branes related to D3-branes at toric singularities by T-duality, see section 2.5 for more details of this string theory realisation of brane tiling. Throughout this paper, we will equivalently refer to brane tilings as dimer models.

obing toric CY 3-folds have found a myriad of applications. In physics, they include: the understanding that toric duality is Seiberg duality [71, 70], one of the most fertile grounds for testing the AdS/CFT correspondence [117, 52, 118, 119], connections to mirror symmetry and tropical geometry [96, 97], local string phenomenology [86, 87], and bipartite field theories [143, 144, 145, 146, 147, 148, 149].

In parallel, in mathematics, the dialogue between gauge theory and the geometry and combinatorics of toric CY 3-folds also engendered numerous developments, including: new directions in Calabi-Yau algebras and quiver representations [104, 105, 101, 99, 100, 98, 102, 103], non-commutative crepant resolutions of toric singularities [150, 151, 152, 153], connections with Grothendieck’s dessins d’enfants and certain isogenies of elliptic curves [109, 110, 111, 112, 106, 107, 108] and a geometric perspective on cluster algebras [154, 155, 156, 157].

The purpose of this chapter is to push the boundaries of computation and to produce as comprehensive a database of brane tilings as possible. We will develop efficient implementations of dimer model tools particularly suited for this search and develop a catalogue of explicit brane tilings for a large class of toric geometries. We will also generate new computational tools, in the form of *Mathematica* modules, which we will make publicly available [158]. We expect a wide range of researchers will find this novel toolkit useful. A short summary of the logic of the codes is presented in appendix A.6.

Until now, a large database of explicit brane tilings was lacking and we envision many

applications for such a catalogue in both physics and mathematics. In our case, we plan to use these theories in the near future as starting points for a systematic and large scale investigation of phenomenological local models in string theory, following [86, 87].

The organization of this chapter is as follows. section 3.2 reviews brane tilings and outlines how to construct new ones by means of partial resolution. We will see that how this technique is easier computational-wise as the exponential running-time step of finding dual cone is not necessary and this allows us to expand the search of quiver gauge theories from more complex toric geometries. section 3.3 summarises the existing classifications of brane tilings. section 3.4 classifies all independent toric diagrams up to area 8. section 3.5 presents brane tilings for all toric CY 3-folds with toric diagrams of area 6, 7 and 8. ¹ We collect our conclusions and directions for future research in chapter 4. appendix A.6 explains the *Mathematica* modules we created for manipulating brane tilings.

3.2 Brane Tiling Technology

In this section we present a lightning review of brane tiling technology. In order to set up the stage for our computations, we also review the basics of the connection between brane tilings and geometry and the implementation of partial resolution in terms of them. We refer the interested reader to [51, 52, 41, 42] and references therein for further details.

3.2.1 D3-Branes Probing Toric CY 3-Folds and Brane Tilings

The $4d \mathcal{N} = 1$ gauge theories living on the worldvolume of D3-branes probing affine toric CY 3-folds are described by bipartite graphs on T^2 called *brane tilings*. A more detailed review is in section 2.3 [49, 51, 52]. In fact a brane tiling is a physical brane configuration, related to the D3-branes at a toric singularity by T-duality, consisting of an NS5-brane wrapping a holomorphic surface from which D5-branes are suspended (see section 2.5 for more details). The geometry of a non-compact toric CY 3-fold is captured by a *toric diagram*, which is

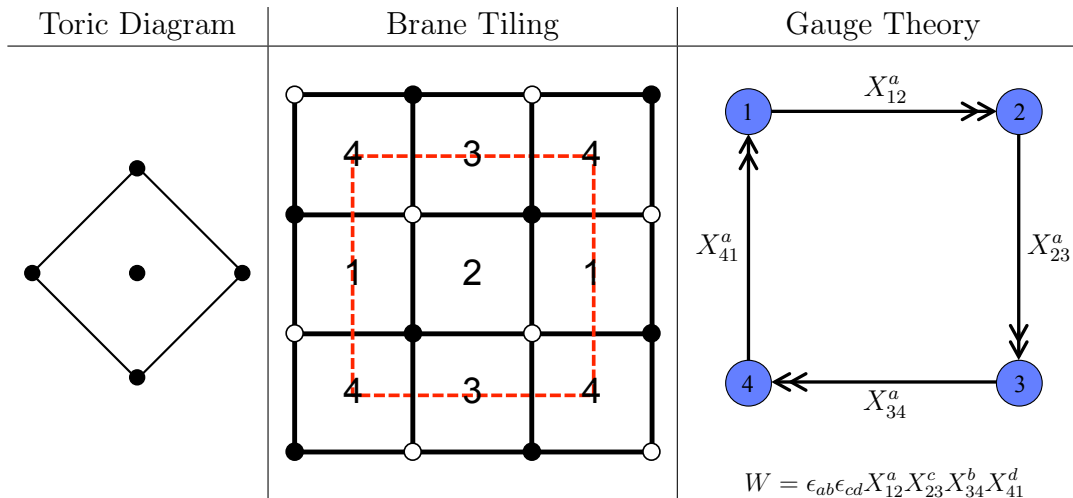
¹All the brane tilings for lower toric diagram areas can be found in [51, 52]. The few missing cases can be immediately determined from gauge theory information presented in [74].

convex lattice polygon.² The probed CY_3 arises as the vacuum moduli space of the gauge theory on the D3-branes, which is defined by the vanishing of D - and F -terms.

The dictionary between $4d \mathcal{N} = 1$ quiver gauge theory and brane tiling is presented in table 2.4. For the convenience of the reader, we reiterate them here as follows:

1. Every face (say labeled by i) corresponds to a $U(N_i)$ gauge group factor in a product gauge group structure.
2. Every edge between faces i and j corresponds to a bifundamental chiral field X_{ij} of $U(N_i) \times U(N_j)$. If i is equal to j , then X_{ii} is an adjoint field of $U(N_i)$. The orientation of fields is a convention, e.g. clockwise and counterclockwise around black and white nodes of the tiling, respectively.
3. Every node corresponds to a monomial term in the superpotential, obtained by multiplying all the edges adjacent to the node. Like the orientation of chiral fields, the sign of the monomial is controlled by the color of the node.

In order to illustrate these ideas, below we present an explicit example that corresponds to the complex cone over F_0 .³ The red dashed lines indicate the boundary of the unit cell.



²An affine toric variety of complex dimension n is usually described by a convex polyhedral cone in \mathbb{R}^n but the Calabi-Yau condition imposes the extra condition that the endpoints of the vector generators of the cone are co-hyperplanar. Thus for 3-folds, the toric diagram can be taken to be a convex lattice polygon in $2d$.

³In fact there are two toric phases, i.e. two theories described by brane tilings, for this geometry. They are related by Seiberg duality [71].

3.2.2 Geometry and Perfect Matchings

In this section, we reiterate some of the definition made in section 2.3.3 and make small changes to the Kasteleyn matrix defined in eq. (2.40) to suit the purpose of our later classification procedure. *Perfect matchings* are combinatorial objects that play a central role in the study of bipartite graphs. A perfect matching p is defined as a collection of edges in the brane tiling such that every node is the endpoint of exactly one edge in p .

Perfect matching substantially simplify the connection between brane tilings and geometry. Let us consider the following map between chiral fields in the quiver X_α , equivalently edges in the brane tiling, and perfect matchings p_μ

$$X_\alpha = \prod_{\mu=1}^c p_\mu^{P_{\alpha\mu}}, \quad (3.1)$$

where c is the total number of perfect matchings. The P -matrix summarizes the edge content of perfect matchings and is defined as follows

$$P_{\alpha\mu} = \begin{cases} 1 & \text{if } X_\alpha \in p_\mu \\ 0 & \text{if } X_\alpha \notin p_\mu \end{cases} \quad (3.2)$$

A remarkable feature of the map in (3.1) is that when chiral fields are expressed in terms of perfect matching variables in this way, all F -terms automatically vanish as we saw in section 2.4.1. Perfect matchings are thus in one-to-one correspondence with fields in the GLSM description of the toric CY 3-fold, namely points in its toric diagram [51].

Perfect matchings and the toric diagram can be efficiently determined using the *Kasteleyn matrix* K . We define K as the adjacency matrix of the graph in which rows are indexed by black nodes and columns are indexed by white nodes, i.e. for every edge X_α in the bipartite graph between nodes \mathbf{b}_μ and \mathbf{w}_ν , we introduce a contribution X_α to the $K_{\mu\nu}$ entry. In addition, whenever an edge crosses the boundary of the unit cell in the x and/or y directions, we multiply the contribution by $x^{\pm 1}$ and $y^{\pm 1}$ weights, respectively. The exponents are positive or negative depending on whether the crossing occurs in the positive or negative direction, which is determined by conventionally orienting edges from white to black nodes. Note here

we defined a slight different version of K-matrix than that in eq. (2.40) by explicitly writing out the field variables. This seems rather like a redundancy as we expect the determinant of K matrix $\det K$ to be the generating function for perfect matchings labelled by their winding number relative to the fundamental domain, in fact we shall see that this explicit inclusion of field variables makes the partial resolution/higgsing procedure manifest and it allows us to choose precisely which choice of fields to participate in the higgsing process. This explicit choice therefore gives us the ability to find all possible quiver gauge theories filtered by consistency conditions from a given singularity.

Let us consider a concrete example. fig. 3-1 shows the quiver diagram for the suspended pinch point (SPP). The corresponding superpotential is

$$W = X_{12}X_{21}X_{22} - X_{22}X_{23}X_{32} + X_{13}X_{23}X_{31}X_{32} - X_{12}X_{13}X_{21}X_{31}. \quad (3.3)$$

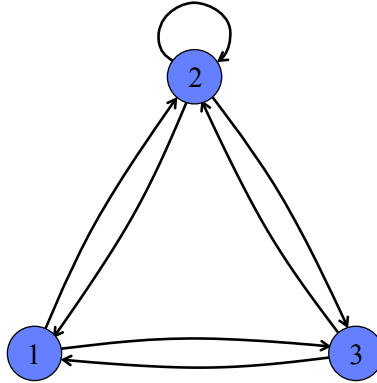


Figure 3-1: Quiver diagram for SPP. Nodes represent gauge groups. The arrow from $i \rightarrow j$ corresponds to the chiral field X_{ij} .

All this information is encoded in the brane tiling shown in fig. 3-2.

The superpotential has four terms, which are represented in the brane tiling by two white and two black nodes. We have labeled the nodes in blue to facilitate the construction of the Kasteleyn matrix, which is given by

$$K = \left(\begin{array}{c|cc} & w[1] & w[2] \\ \hline b[1] & X_{22} x & X_{23} + X_{32} x \\ \hline b[2] & X_{12} + X_{21} x & X_{31} y + X_{13} xy \end{array} \right). \quad (3.4)$$

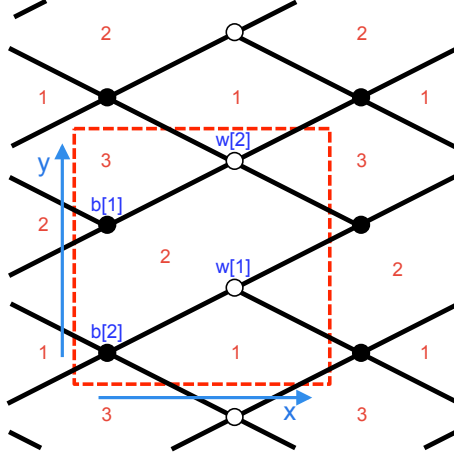


Figure 3-2: Brane tiling for SPP.

The determinant of the Kasteleyn matrix generates the perfect matchings. In this case, we get

$$\det K = -X_{12}X_{23} - (X_{21}X_{23} + X_{12}X_{32})x - X_{21}X_{32}x^2 + X_{22}X_{31}xy + X_{13}X_{22}x^2y. \quad (3.5)$$

Every monomial in this expression corresponds to a perfect matching. Furthermore, the powers of x and y indicate their position in the toric diagram, as shown in fig. 3-3. The perfect matching can be summarized in the P -matrix as follows

$$P = \left(\begin{array}{c|cccccc} & p_1 & p_2 & p_3 & p_4 & p_5 & p_6 \\ \hline X_{22} & 0 & 0 & 0 & 0 & 1 & 1 \\ X_{12} & 1 & 0 & 1 & 0 & 0 & 0 \\ X_{21} & 0 & 1 & 0 & 1 & 0 & 0 \\ X_{23} & 1 & 1 & 0 & 0 & 0 & 0 \\ X_{32} & 0 & 0 & 1 & 1 & 0 & 0 \\ X_{31} & 0 & 0 & 0 & 0 & 1 & 0 \\ X_{13} & 0 & 0 & 0 & 0 & 0 & 1 \end{array} \right). \quad (3.6)$$

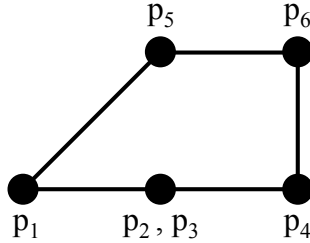


Figure 3-3: Toric diagram for SPP. We indicate the perfect matching associated to each point.

3.2.3 Partial Resolution and Brane Tilings

Brane tilings completely solved the problem of finding the gauge theory associated to a generic toric CY 3-fold and vice versa. There are well established procedures for going from brane tilings to geometry and in the opposite direction: the *fast forward* [51] and *fast inverse algorithms* [50, 96], respectively. One of the main goals to this paper is to develop a practical approach to determine the brane tiling associated to a general toric diagram. While the fast inverse algorithm provides an answer to this question, its automation remains challenging. We thus opt for an alternative approach, which admits a rather simple computer implementation.

Our strategy will be to perform partial resolution, which translates to higgsing in the gauge theory. In terms of brane tilings, it corresponds to removing the edges associated to the fields acquiring non-zero vacuum expectation values (vevs). We will exploit the map between perfect matchings and fields in the gauge theory to systematically identify the vevs that are turned on when certain points in the toric diagram are deleted.

Any geometry for which the brane tiling is known can be used as the starting point for partial resolution. There are two canonical classes of initial theories that have been broadly used in the literature for this purpose. The first one is $\mathbb{C}^3/(\mathbb{Z}_m \times \mathbb{Z}_n)$ orbifolds, with the two generators of the orbifold group acting on \mathbb{C}^3 as: $(X, Y, Z) \mapsto (e^{i2\pi/N} X, e^{-i2\pi/N} Y, Z)$ and $(X, Y, Z) \mapsto (X, e^{i2\pi/M} Y, e^{-i2\pi/M} Z)$. The resulting toric diagram is shown in fig. 3-4.a, and the corresponding brane tiling is an hexagonal lattice with an $N \times M$ unit cell. The second standard class of starting points are $\mathbb{Z}_m \times \mathbb{Z}_n$ orbifolds of the conifold \mathcal{C} . As we know that

the conifold is a three dimensional hypersurface singularity defined in \mathbb{C}^4 by

$$\mathcal{C} : \quad xy - uv = 0 .$$

It can also be realised as a holomorphic quotient of \mathbb{C}^4 by \mathbb{C}^* action given by

$$(A_1, A_2, B_1, B_2) \rightarrow (\lambda A_1, \lambda A_2, \lambda^{-1} B_1, \lambda^{-1} B_2) \quad \text{for } \lambda \in \mathbb{C}^* .$$

The charge matrix is the transpose of $Q' = (1, 1, -1, -1)$ and $\Delta = \sigma$ is a convex polyhedral cone in $\mathbb{N}'_{\mathbb{R}} = \mathbb{R}^3$ generated by vectors $v_1, v_2, v_3, v_4 \in \mathbb{N}' = \mathbb{Z}^3$ with

$$v_1 = (1, 0, 0), \quad v_2 = (0, 1, 0), \quad v_3 = (0, 0, 1), \quad v_4 = (1, 1, -1) .$$

The correspondence between the two representation of \mathcal{C} is given by

$$x = A_1 B_1, \quad y = A_2 B_2, \quad u = A_1 B_2, \quad v = A_2 B_1 .$$

Now we can take quotient of the conifold \mathcal{C} by product group of the form $\mathbb{Z}_m \times \mathbb{Z}_n$. The \mathbb{Z}_m acts on A_i and B_j through

$$(A_1, A_2, B_1, B_2) \rightarrow (e^{-2\pi i/m} A_1, A_2, e^{2\pi i/m} B_1, B_2) , \quad (3.7)$$

and \mathbb{Z}_n acts through

$$(A_1, A_2, B_1, B_2) \rightarrow (e^{-2\pi i/n} A_1, A_2, B_1, e^{2\pi i/n} B_2) . \quad (3.8)$$

Therefore, the action of these groups on conifold \mathcal{C} is then given by

$$(x, y, u, v) \rightarrow (x, y, e^{-2\pi i/m} u, e^{2\pi i/m} v) \quad (3.9)$$

and

$$(x, y, u, v) \rightarrow (e^{-2\pi i/n} x, e^{2\pi i/n} y, u, v) . \quad (3.10)$$

Now we define the orbifold of conifold to be $\mathcal{C}/(\mathbb{Z}_m \times \mathbb{Z}_n)$. There are still only four vectors inherited from \mathcal{C} to define the orbifold. There is only a single relation among these vectors, and thus it has a single Kähler class which is not enough to smooth out $\mathcal{C}/(\mathbb{Z}_m \times \mathbb{Z}_n)$. So if we consider a finer lattice $\mathbb{N} = \mathbb{N}' + \frac{1}{m}(v_3 - v_1) + \frac{1}{n}(v_4 - v_1)$, we see that the lattice points $\sigma \cap \mathbb{N}$ of σ in \mathbb{N} are generated by $(m+1)(n+1)$ lattice points as a semigroup. We that the toric diagram of $\mathcal{C}/(\mathbb{Z}_m \times \mathbb{Z}_n)$ is shown in fig. 3-4.

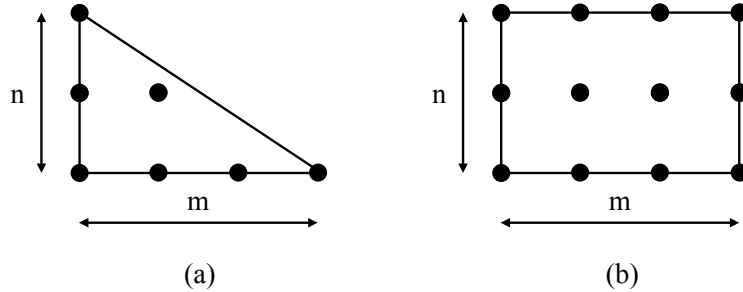


Figure 3-4: Toric diagrams for: a) $\mathbb{C}^3/(\mathbb{Z}_m \times \mathbb{Z}_n)$ and b) $\mathcal{C}/(\mathbb{Z}_m \times \mathbb{Z}_n)$. We will use the second class of geometries as the starting points for partial resolution.

With such construction of $\mathcal{C}/(\mathbb{Z}_m \times \mathbb{Z}_n)$ at our disposal, we can obtain any toric diagram with sufficiently large m and n . However, we have to determine the minimal size of numbers m and n such that it contains the desired toric diagram as a subset. To find the correct m and n , we first find the longest span of the diagram across the two directions $(1,0)$ and $(0,1)$. Then m and n can be found easily.

For example, diagram 3 in the area 8 list has its lengths along $(1,0)$ and $(0,1)$ directions to be 3 and 5. Then we have $m = 5 - 1$ and $n = 3 - 1$ as shown in previous paragraph. Similarly, diagram 1 in the same list has length 4 across both directions, resulting $m = n = 3$.

We now illustrate the dimer implementation of partial resolution with an explicit example. Let us derive the brane tiling for the SPP from a $\mathcal{C}/(\mathbb{Z}_m \times \mathbb{Z}_n)$ orbifold. Considering the toric diagrams, it is clear that it would be sufficient to start from \mathcal{C}/\mathbb{Z}_2 . However, in order to demonstrate the methods in a more involved partial resolution, let us use $\mathcal{C}/(\mathbb{Z}_2 \times \mathbb{Z}_2)$ as the initial theory. The brane tiling for $\mathcal{C}/(\mathbb{Z}_2 \times \mathbb{Z}_2)$ is shown in fig. 3-5.⁴

⁴There are other brane tilings for $\mathcal{C}/(\mathbb{Z}_2 \times \mathbb{Z}_2)$, which correspond to additional toric phases obtained from this one by Seiberg duality.

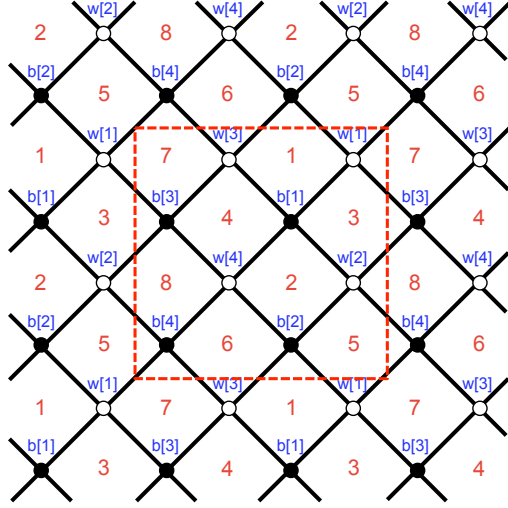


Figure 3-5: Brane tiling for $\mathcal{C}/(\mathbb{Z}_2 \times \mathbb{Z}_2)$.

The Kasteleyn matrix is given by

$$K = \begin{pmatrix} & w[1] & w[2] & w[3] & w[4] \\ b[1] & X_{13} & X_{32} & X_{41} & X_{24} \\ b[2] & X_{51} y & X_{25} & X_{16} y & X_{62} \\ b[3] & X_{37} x & X_{83} x & X_{74} & X_{48} \\ b[4] & X_{75} xy & X_{58} x & X_{67} y & X_{86} \end{pmatrix}. \quad (3.11)$$

We obtain the perfect matchings by computing the determinant of the Kasteleyn matrix. They are summarized in the following P -matrix:

	(0, 0)		(1, 0)		(2, 0)		(1, 1)		(2, 1)										(2, 2)		(0, 2)		(1, 2)		(2, 2)	
	p_1	p_2	p_3	p_4	p_5	p_6	p_7	p_8	p_9	p_{10}	p_{11}	p_{12}	p_{13}	p_{14}	p_{15}	p_{16}	p_{17}	p_{18}	p_{19}	p_{20}	p_{21}	p_{22}	p_{23}	p_{24}		
X_{13}	1	1	0	0	1	0	1	0	0	0	0	0	0	0	1	0	1	0	0	0	0	0	0	0	0	
X_{16}	0	0	0	0	0	0	1	0	0	0	0	0	0	0	1	1	0	0	1	0	0	1	0	1	1	
X_{24}	0	0	0	0	0	0	0	0	1	0	1	0	1	0	0	0	0	0	1	0	0	0	1	1	1	
X_{25}	1	0	1	0	1	0	0	0	1	0	0	1	1	0	0	0	0	0	0	0	0	0	0	0	0	
X_{32}	0	0	0	0	0	1	0	0	0	1	0	0	0	1	0	1	0	0	0	0	1	1	0	0	0	
X_{37}	0	0	1	1	0	0	0	0	1	1	0	0	0	0	0	1	0	0	1	0	0	0	0	0	0	
X_{41}	0	0	1	1	0	0	0	1	0	0	0	1	0	0	0	0	0	1	0	1	0	0	0	0	0	
X_{48}	0	0	0	0	1	0	1	1	0	0	0	1	0	0	0	0	0	0	0	0	1	1	0	0	0	
X_{51}	0	0	0	0	0	1	0	1	0	0	1	0	0	0	0	0	0	1	0	0	1	0	1	0	0	
X_{58}	0	1	0	1	0	0	1	1	0	0	1	0	0	0	0	0	0	0	1	0	0	0	0	0	0	
X_{62}	0	1	0	1	0	0	0	0	0	1	0	0	0	1	1	0	0	0	0	1	0	0	0	0	0	
X_{67}	0	0	0	0	1	0	0	0	1	1	0	0	0	1	0	0	0	0	0	0	1	0	1	0	0	
X_{74}	1	1	0	0	0	1	0	0	0	0	1	0	1	1	0	0	0	0	0	0	0	0	0	0	0	
X_{75}	0	0	0	0	0	0	0	0	0	0	1	1	1	0	0	0	0	0	0	1	0	1	0	1	1	
X_{83}	0	0	0	0	0	0	0	0	0	0	0	0	0	0	1	0	1	1	0	1	0	0	1	1	1	
X_{86}	1	0	1	0	0	1	0	0	0	0	0	0	0	0	0	1	1	1	0	0	0	0	0	0	0	

where in the top row we have indicated the corresponding point in the toric diagram, which is shown in fig. 3-6. The significance of the rows that are highlighted in blue will be discussed soon.

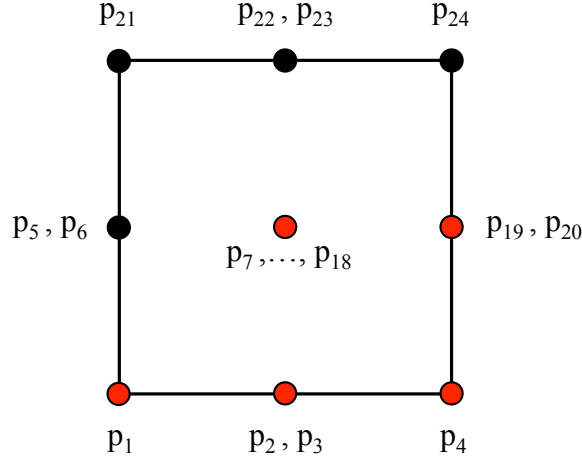


Figure 3-6: Toric diagram for $\mathcal{C}/(\mathbb{Z}_2 \times \mathbb{Z}_2)$. We indicate the perfect matching associated to each point and a possible embedding of the SPP toric diagram (in red).

Figure 3-6 shows a possible way of embedding the toric diagram of SPP, shown in red, into the one for $\mathcal{C}/(\mathbb{Z}_2 \times \mathbb{Z}_2)$. According to eq. (3.2), we should regard chiral fields as products of perfect matchings. The vev of a chiral field results from the product of the vevs of its perfect matching constituents. Then, a chiral field gets a vev and is removed from the brane tiling only when all the perfect matchings that contain it are deleted. Even after picking an embedding of the final toric diagram into the parent one there are, in general, multiple ways of achieving the desired partial resolution. For the embedding in Figure 3-6, one possibility is to turn on vevs for $\{X_{16}, X_{24}, X_{32}, X_{48}, X_{51}\}$. The corresponding rows in the P -matrix are highlighted in blue in eq. (3.12). It is straightforward to verify that this set of vevs achieves the desired resolution. Some perfect matchings can be removed from the surviving points in the toric diagram. For example, all but p_{15} are deleted in the point that originally contains p_7, \dots, p_{18} . Similarly, p_{19} is removed while leaving p_{20} for that point. fig. 3-7 shows the final toric diagram.

Having established the vevs that implement the desired partial resolution to the SPP, the associated brane tiling is obtained by deleting the corresponding edges in Figure 3-5. When doing so, a pair of 2-valent nodes is generated. Such nodes correspond to mass terms

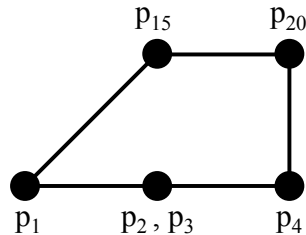


Figure 3-7: Toric diagram for SPP obtained by partial resolution of $\mathcal{C}/(\mathbb{Z}_2 \times \mathbb{Z}_2)$.

in the superpotential. Massive fields are easily integrated out in terms of brane tilings [51]. The final result is precisely the brane tiling in Figure 3-2, which corresponds to the quiver in fig. 3-1 and the superpotential eq. (3.3).

Therefore, we briefly summarize a general procedure of the above said partial resolution. This is exactly the content of the function `RemovePoints2PNew[]` inside the `MATHEMATICA` package of the algorithmic implementation. The flow of the general process is as follows:

1. Function takes in the Kasteleyn matrix of the $\mathcal{C}/(\mathbb{Z}_m \times \mathbb{Z}_n)$ and the coordinates of the points to be removed from the parent toric diagram.
2. The perfect matchings and the set of all fields from the $\mathcal{C}/(\mathbb{Z}_m \times \mathbb{Z}_n)$ are obtained from the Kasteleyn matrix.
3. For a given set of toric points to be removed, all the perfect matchings residing on such points should be removed. For the set of perfect matchings to be removed \mathcal{P} , we can easily find the set \mathcal{F} of constituent fields for \mathcal{P} . Since each field in \mathcal{F} can be in multiple perfect matchings, we have to start building the set of correct fields to be removed by adding candidates to an empty set one at a time.
4. Since deleting a field can result in deleting multiple perfect matching, therefore leading to the removal of the wrong toric point. Hence, for adding any new fields into the set of fields to be integrated out, the resulting toric points are checked each time to make sure no unwanted deletion of points takes place.

3.2.4 Brane Tiling Consistency

Not every bipartite graph on a 2-torus corresponds to a *consistent brane tiling* and hence defines a well-behaved $4d \mathcal{N} = 1$ gauge theory (cf. see section 2.3.3). In fact, higgsing of consistent brane tilings can lead to inconsistent ones. This It thus becomes imperative to check the consistency of the brane tilings generated via partial resolution. Inconsistent brane tilings may naively seem to correspond to toric CY_3 's, but fail more subtly. The problems of inconsistent tilings manifest at all levels: the gauge theory, the D-brane configuration and its algebraic description. By now, this subject has been studied in depth and is well understood. We refer the interested readers to [50, 56, 98, 159, 160, 161, 162] and references therein for detailed discussions.

Consistency can be determined using multiple diagnostics, all of which are closely related. They range from physical considerations regarding the positivity of R -charges to graph-theoretic tests based on intersection properties of zig-zag paths. The latter condition is closely related to the concept of *reducibility* of brane tilings. A brane tiling is reducible, or equivalently inconsistent, if the number of faces can be decreased by deleting edges while preserving the toric diagram. On the other hand, the number of gauge groups should be equal to the area of the toric diagram, measured in terms of elementary triangles. These two points lead to a simple criterion for consistency of brane tilings, which is particularly well-suited for partial resolution. A brane tiling is inconsistent whenever the number of faces is larger than the area of the toric diagram. When this occurs, the brane tiling can be cured and turned into a consistent one by removing certain edges, i.e. by turning on vevs, without modifying the toric diagram.

This clarifies how inconsistent brane tilings can arise when partial resolution is not properly implemented. Sometimes, given an initial toric diagram and its corresponding brane tiling, a target toric diagram may be obtained by turning on an incomplete collection of vevs.⁵ To avoid inconsistent tilings we should make sure that the set of vevs not only gives rise to the desired toric diagram but that it is also *maximal*. Algorithmically, it is most easily implemented by checking the number of gauge groups against the number of fundamental triangles after triangulation. Therefore, a brane tiling is inconsistent whenever its number of

⁵This was not a possibility in the example discussed in the previous section.

faces is larger than the area of toric diagram. Once an inconsistent brane tiling is detected, it can be repaired by deleting certain edges while maintaining the toric diagram.

This is best illustrated by looking at the diagram 5 in area 6 list. This toric diagram can be reached from $\mathcal{C}/\mathbb{Z}_3 \times \mathbb{Z}_2$. The parent toric diagram has toric points:

$$\{(0, 0), (1, 0), (2, 0), (3, 0), (0, 1), (1, 1), (2, 1), (3, 1), (0, 2), (1, 2), (2, 2), (3, 2)\} ,$$

wherein the set $\{(0, 1), (0, 2), (1, 2), (3, 2), (3, 1)\}$ needs to be removed. In addition, we have Kasteleyn matrix for the parent theory to be

$$K = \begin{pmatrix} X_{1,3} & 0 & X_{3,2} & X_{4,1} & 0 & X_{2,4} \\ X_{6,1} & X_{5,6} & 0 & X_{1,7} & X_{7,5} & 0 \\ 0 & yX_{8,5} & X_{2,8} & 0 & yX_{5,9} & X_{9,2} \\ xX_{3,10} & 0 & xX_{11,3} & X_{10,4} & 0 & X_{4,11} \\ xX_{10,6} & xX_{6,12} & 0 & X_{7,10} & X_{12,7} & 0 \\ 0 & xyX_{12,8} & xX_{8,11} & 0 & yX_{9,12} & X_{11,9} \end{pmatrix} , \quad (3.13)$$

where we can see that the deletion of fields $\{X_{1,7}, X_{3,2}, X_{4,11}, X_{9,12}, X_{10,6}\}$ gives us the correct toric diagram, as one can check this easily by computing the determinant of Kasteleyn matrix and find the Newton polygon. However, the presence of 7 gauge group in the quiver signals that this choice of deletion of fields gives inconsistent brane tiling. This can be remedied by deleting one more fields $X_{8,5}$. The inconsistent brane tiling is shown in fig. 3-8. After deleting $X_{8,5}$, the brane tiling is thus the same as the one in diagram 6 of the list of section 3.5.1.

Lastly, we would like to expand on how this new algorithm is much less complex to implement algorithmically comparing to the previous versions. We see that the old inverse algorithm is also based on partial resolution. It has exactly the same procedure that requires finding the dual cone of a given cone: $T = \text{Dual}(K)$ such that $K \cdot T \geq 0$ for all entries. For the completeness of discussion about the complexity of the old algorithm, we present the standard algorithm of finding dual cone here.

Let us begin with a convex polytope C , with edges given by the matrix M whose columns are the vectors corresponding to these edges. We need to find the dual cone \tilde{C} of C , or

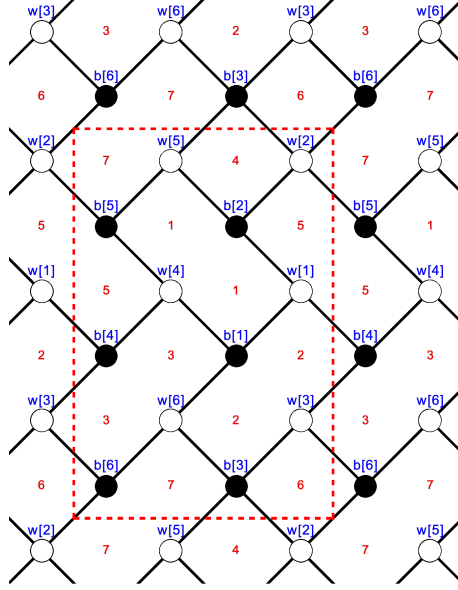


Figure 3-8: An inconsistent brane tiling for digram 5 in the area 6 list. We see that the number of faces is 7, which is greater than the area of the toric diagram.

alternatively matrix N such that

$$N^t \cdot M \geq 0 \quad \text{for all entries.}$$

This algorithm is standard and presented in [129]. Let M be $n \times p$ i.e., there are p n -dimensional vectors spanning C . Note here $p \geq n$ is required for convex polytope. Now we choose $n - 1$ vectors out of the p candidates. We have a matrix of $n \times (n - 1)$ of co-rank 1, whence we extract a 1-dimensional null space described by a single vector u .

Next we check the dot product with the remaining $p - (n - 1)$ vectors. If all dot products are positive, we keep vector u , and if all products are negative, we keep $-u$, we discard it if otherwise.

We then choose another $n - 1$ vectors and repeat above until all combinations are exhausted. The set of vectors that are kept, either u 's or $-u$'s should form the columns of N and span the dual cone \tilde{C} . Thus the complexity of the algorithm depends on the choice

$$\binom{p}{n-1},$$

which has exponential growth as a function of n and p . This can be seen by the following bounds on binomial coefficients

$$\frac{p^{n-1}}{(n-1)^{n-1}} \leq \binom{p}{n-1} \leq \frac{p^{n-1}}{(n-1)!} < \left(\frac{p \cdot e}{n-1}\right)^{n-1},$$

where we see that it is exponential because $p/(n-1) > 1$ and we have $(p/(n-1))^{n-1}$. This clearly has exponential growth. Since both the old forward and inverse algorithm require the computation of a dual cone of certain input, this inevitably prohibits the algorithm to work with any larger toric diagrams or quiver gauge theories.

The procedure involving brane tiling and refined Kasteleyn matrix has much better performance since the dual cone calculation is circumvented and is embedded inside the calculation of perfect matching matrix. For the old inverse algorithm described in [69], a lot of arbitrary choices are involved to determine the correct fields to be resolved by turning on FI parameters. On top of this, the K matrix, encoding the F-term equations is not enough to integrate back to superpotential. Extra guesses in the linear relations among column vectors in the K matrix are sometimes required. In addition, the back-integration procedure might involve extraneous fields that are not easy to implement algorithmically.

The other partial resolution using dimers in [49] also suffers some drawbacks as we shall describe now. In this method, bipartite graphs are obtained given certain toric singularity. This method is also computationally expensive since it was unknown how to identify the desired Higgsing on the quiver side. But with the correspondence between quiver with superpotential and brane tiling elucidated as in table 2.4, we can easily identify the edge of brane tiling to be removed that corresponds to the Higgsing of any given field in the quiver. Lastly, with the dimer in the calculation, we do *not* need to calculate any dual cone as the determinant of the Kasteleyn matrix has its Newton polygon giving the toric diagram.

3.3 Existing Classifications

A plethora of explicit brane tilings have been constructed in the literature. Below we summarize the existing systematic classifications of *classes* of models. Several additional scattered

examples exist.

- Del Pezzo surfaces [51]. The brane tilings for all toric phases for cones over toric del Pezzo surfaces dP_n , $n = 0, \dots, 3$, have been classified. Even before the development of brane tilings, the corresponding gauge theories were determined in [29, 69, 73, 71, 70].
- Abelian orbifolds of \mathbb{C}^3 [163, 164, 165, 166, 167]. It is straightforward to construct the brane tilings for abelian orbifolds of arbitrary geometries by appropriately enlarging the unit cell. The geometric action of the orbifold group is encoded in the periodicity conditions. However, a systematic classification of the orbifold possibilities of geometries beyond \mathbb{C}^3 does not currently exist.
- The $Y^{p,q}$ [117] and $L^{a,b,c}$ [52, 118, 119] infinite families. In fact the $Y^{p,q}$ theories are fully contained within the $L^{a,b,c}$ class. The toric diagrams for these geometries have four external edges. Explicit metrics for the $Y^{p,q}$ and $L^{a,b,c}$ Sasaki-Einstein manifolds were introduced in [59, 58, 60, 61]. The construction of the gauge theories for these geometries had a substantial impact on the AdS₅/CFT₄ correspondence with $\mathcal{N} = 1$ supersymmetry. It allowed refined tests of the correspondence for the infinite classes of dual pairs.
- The $X^{p,q}$ family [168]. The toric diagrams for these geometries have five external edges. While this classification was not performed in the language of brane tilings, it is straightforward to translate it.
- [169] classified all brane tilings up to six superpotential terms. These theories are substantially simpler than the ones studied in this paper.
- We also briefly tabulate which diagrams among the results are known geometries inside $L^{a,b,c}$, $Y^{p,q}$ and $X^{p,q}$ in table 3.1. For obvious reasons, geometries such as orbifold of \mathbb{C}^3 and conifolds, del Pezzo surfaces are not tabulated. The toric diagrams are labelled according to tables 3.2 to 3.7.
- Lastly, we present the GLSM data or the charge matrices Q_t for area 6, 7, 8 diagrams from the classification in section 3.4 in this link. The file is called `GLSMData.nb` and

it requires MATHEMATICA to open. The reason that these matrices are not presented here is because some of matrices are rather large and the space here is rather limited. This should complete the description on the geometry side of the story here. The GLSM data is mainly centred on the charge matrix Q_t , which acts as the central connection between the symplectic quotient construction of a toric variety and Higgs branch of supersymmetric vacua of certain GLSM. We see that the torus action for a toric diagram is given by the eq. (2.57) and the charge matrix Q_t records how the torus action is performed on each coordinate.

	Area 4	Area 5	Area 6	Area 7	Area 8
Geometry	$6 : L^{2,2,2}$ $7 : L^{1,3,2}$	$4 : L^{1,4,2}$	$9 : L^{2,4,3}$ $10 : Y^{3,0}$ $12 : L^{1,5,3}$ $13 : L^{1,5,2}$	$7 : X^{3,1}$ $8 : X^{3,2}$	$1 : L^{1,7,3}$ $3 : Y^{4,0}$ $4 : L^{1,7,2}$ $5 : L^{2,6,4}$ $7 : L^{1,7,4}$ $8 : L^{3,5,4}$ $14 : L^{2,6,3}$ $16 : L^{4,4,4}$

Table 3.1: The known geometries inside the classification in section 3.4.

3.4 The Geometries

A primary goal of this paper is to construct brane tilings for all toric CY 3-folds with toric diagrams up to area 8. The relative simple cases of area 1 to 5 have been extensively studied and brane tilings are known for all of them. We will thus concentrate on areas 6 to 8. As mentioned earlier, part of our motivation for focusing on these geometries has to do with applications to local string phenomenology along the lines of [86, 87].

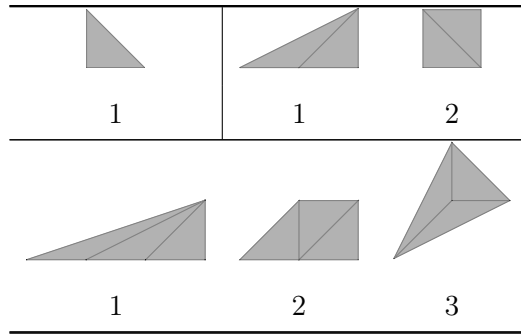


Table 3.2: Toric diagrams of areas 1, 2 and 3.

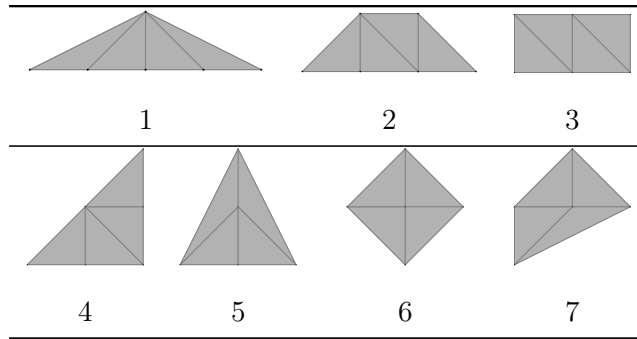


Table 3.3: Toric diagrams of area 4.

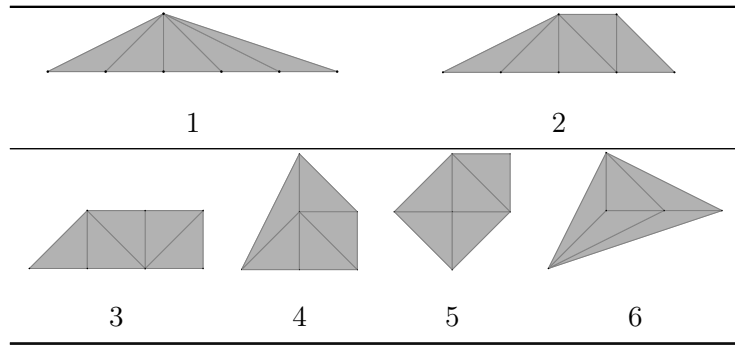


Table 3.4: Toric diagrams of area 5.

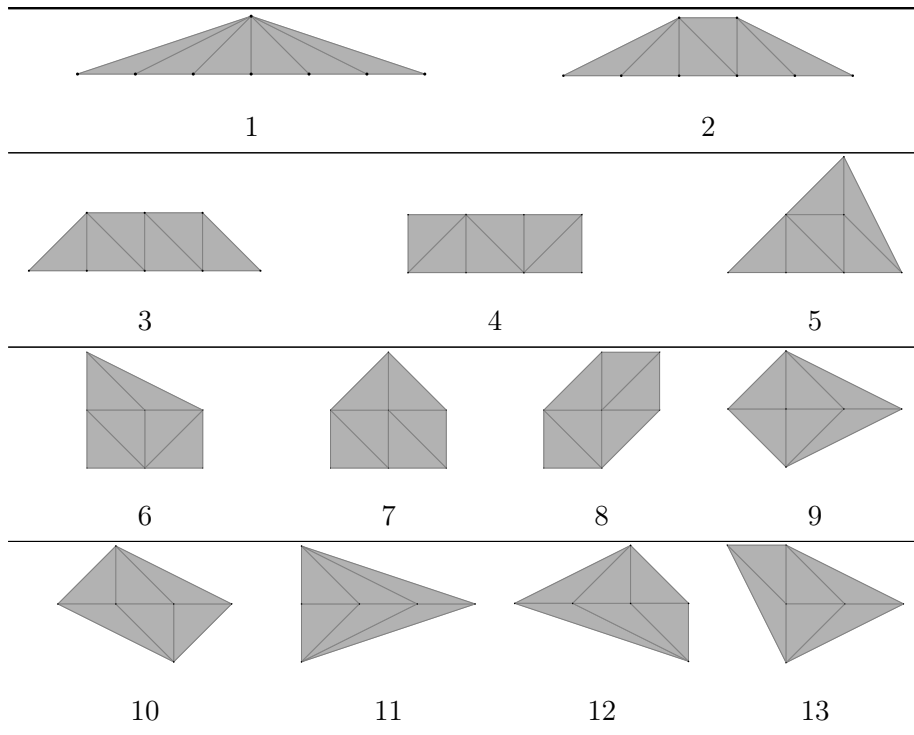


Table 3.5: Toric diagrams of area 6.

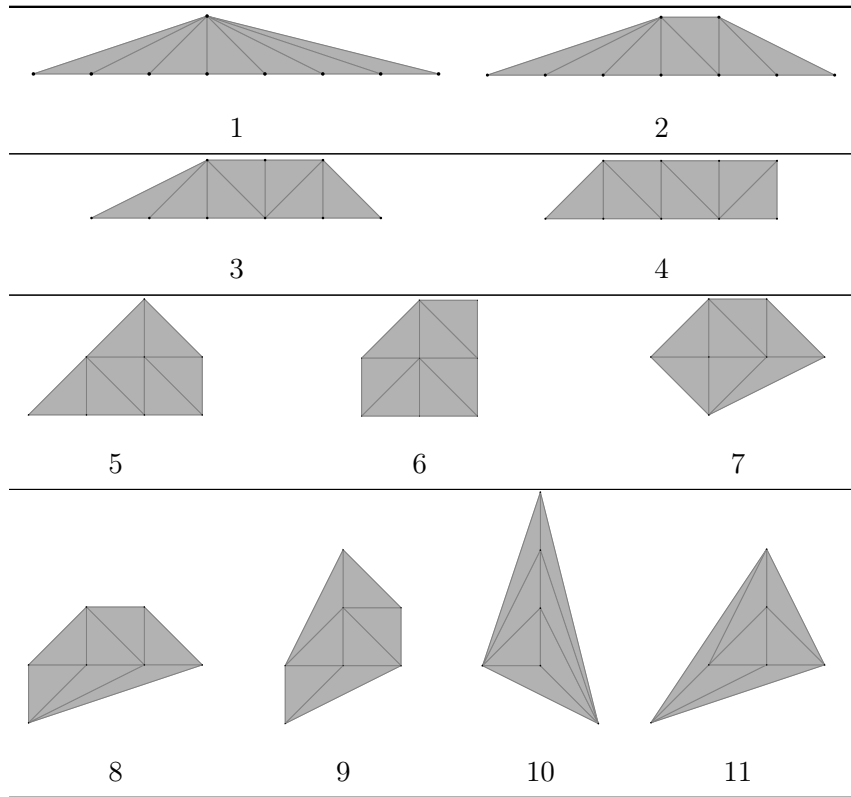


Table 3.6: Toric diagrams of area 7.

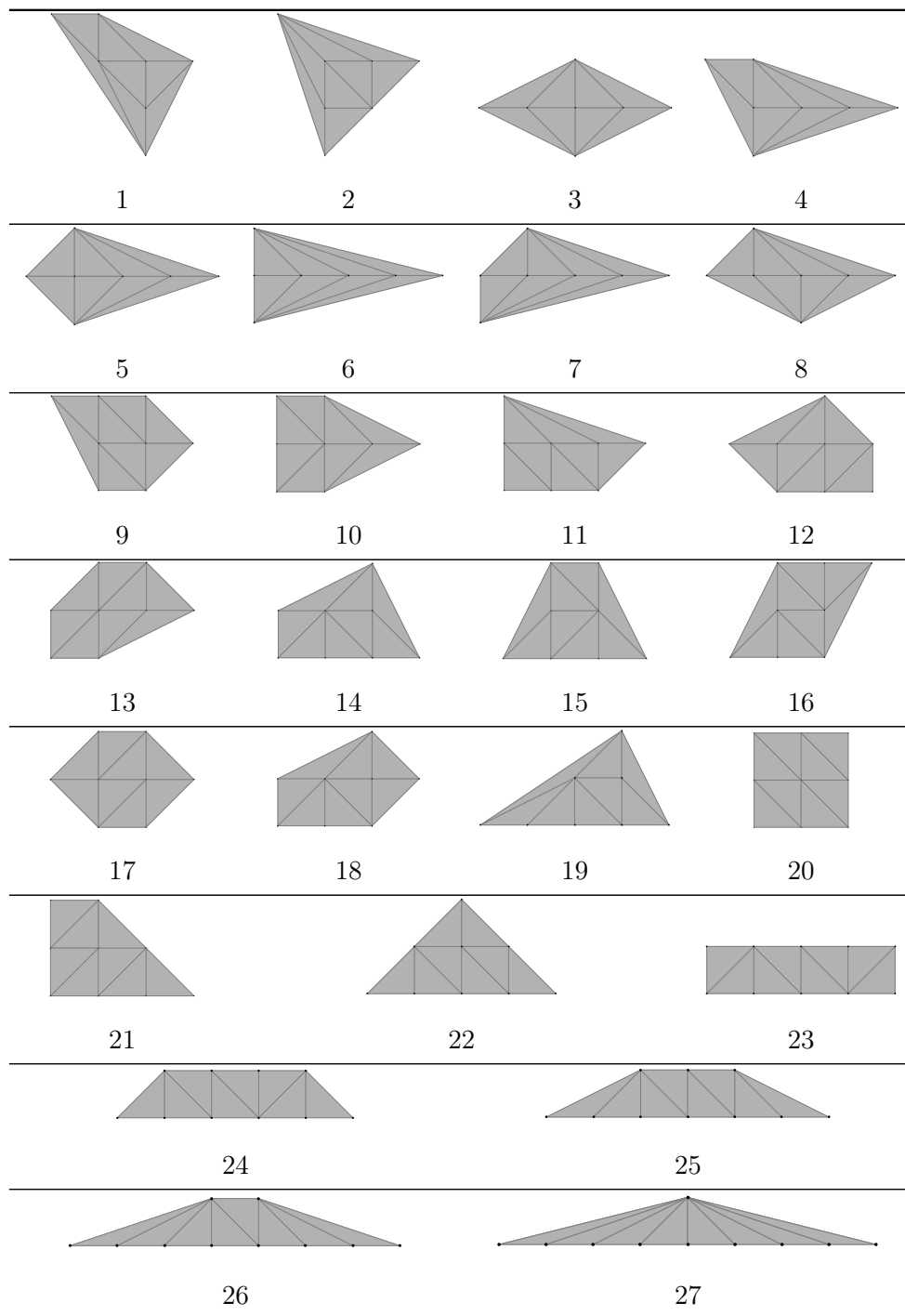


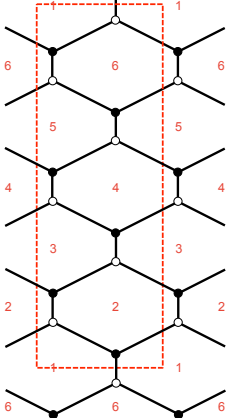
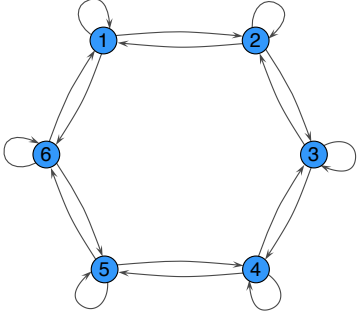
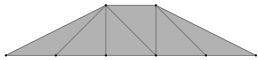
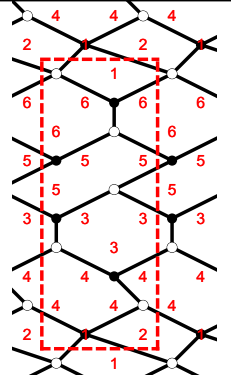
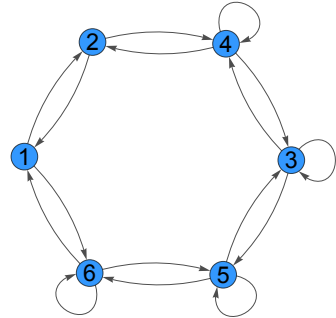
Table 3.7: Toric diagrams of area 8.

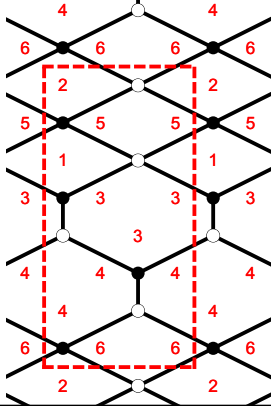
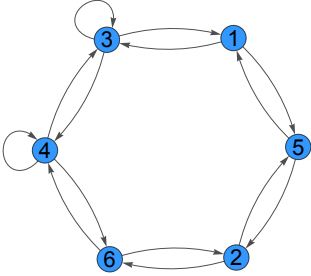
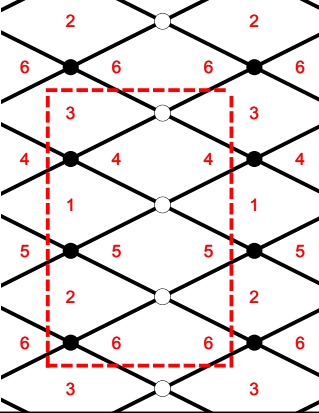
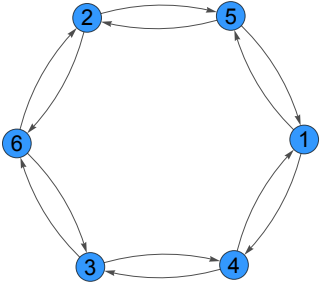
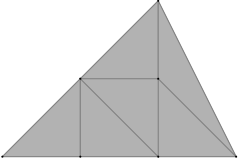
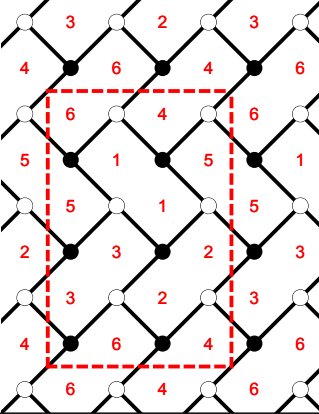
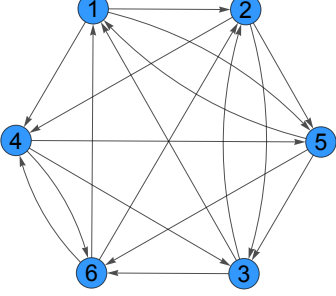
3.5 Results

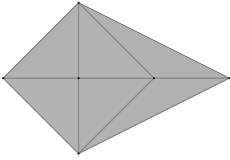
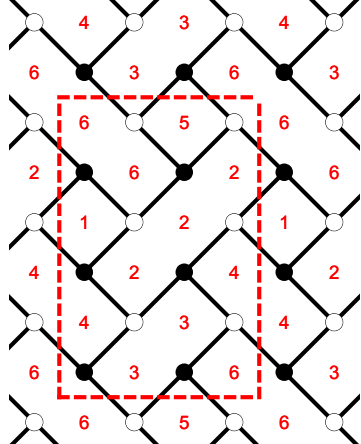
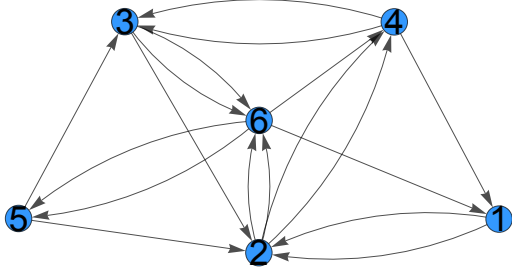
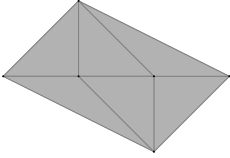
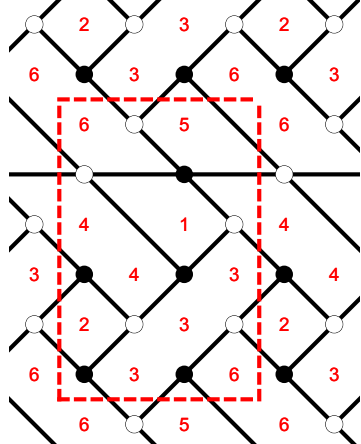
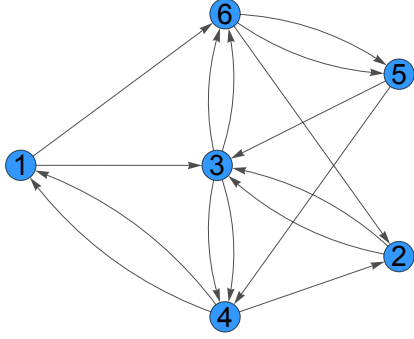
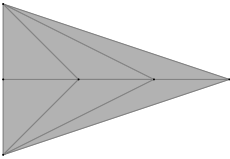
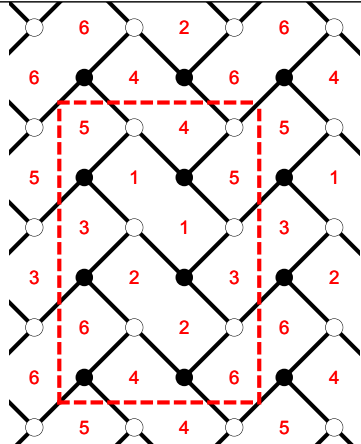
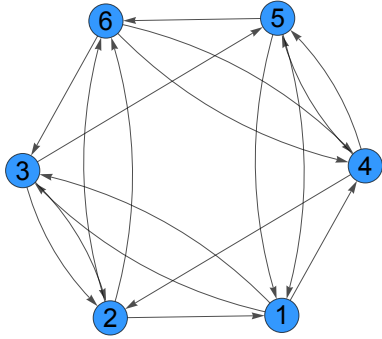
We now present the classification of brane tilings obtained when implementing the ideas outlined in section 3.2 to the geometries presented in section 3.4. We provide one brane tiling per geometry for toric diagrams with areas 6 to 8. Below, the order of toric diagrams is as given in Tables 4, 5 and 6. While some of these theories have previously appeared in the literature, ours is the first exhaustive classification. Generically, there can be multiple brane tilings for a given CY_3 . It is straightforward to generate all of them by systematically acting with Seiberg duality on the brane tilings that we present.

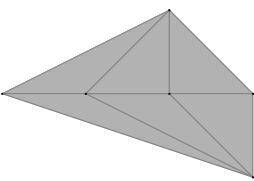
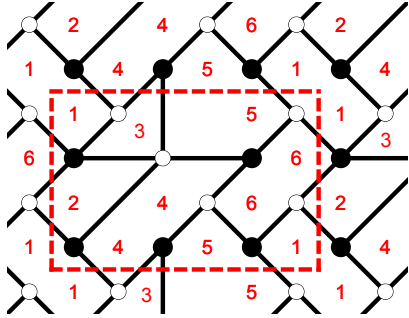
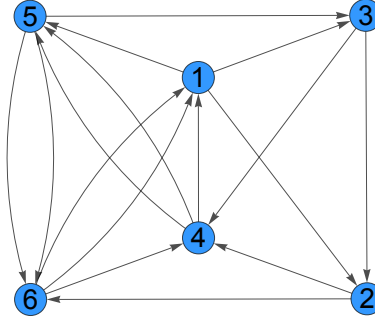
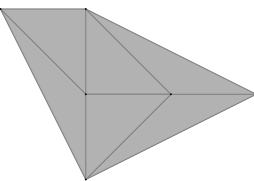
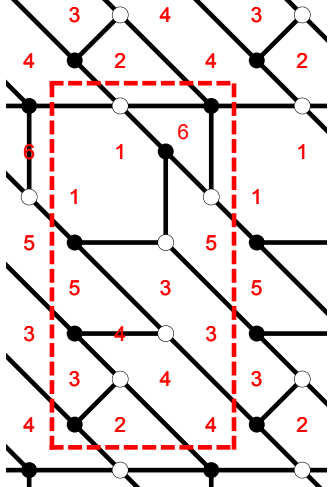
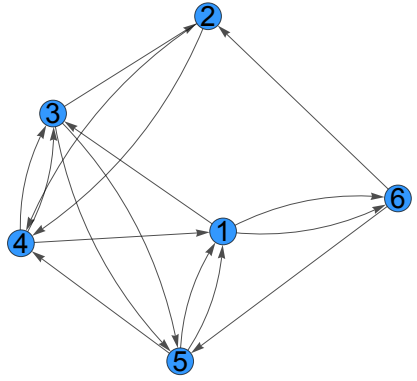
The geometries associated to toric diagrams without internal points give rise to non-chiral gauge theories, which are not so interesting from a model building point of view. For areas 6 to 8, they correspond to cones over $L^{a,b,a}$ manifolds [52].

3.5.1 Area 6

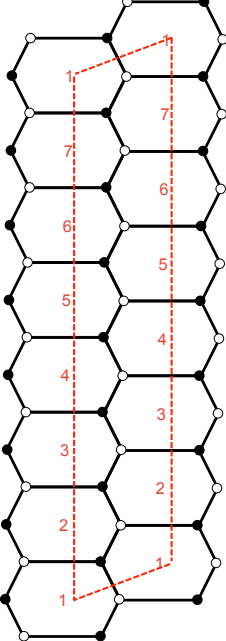
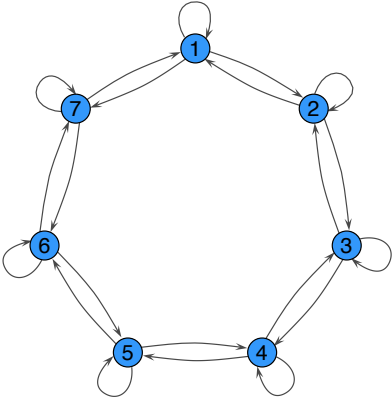
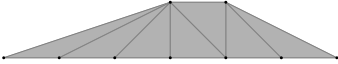
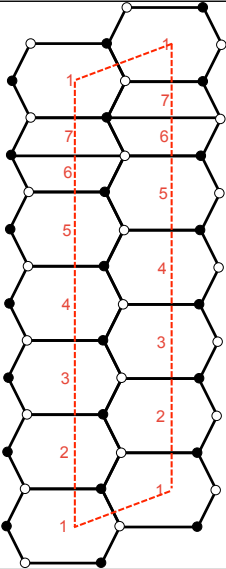
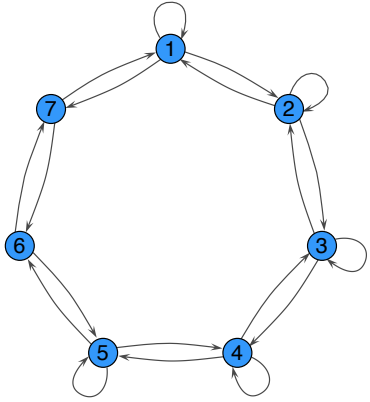
Toric Diagram	Brane Tiling	Quiver
		
$W = -X_{11}X_{12}X_{21} - X_{22}X_{23}X_{32} - X_{33}X_{34}X_{43} - X_{44}X_{45}X_{54} - X_{55}X_{56}X_{65} - X_{66}X_{61}X_{16} \\ + X_{11}X_{16}X_{61} + X_{22}X_{21}X_{12} + X_{33}X_{32}X_{23} + X_{44}X_{43}X_{34} + X_{55}X_{54}X_{45} + X_{66}X_{65}X_{56}$		
		
$W = -X_{34}X_{44}X_{43} - X_{16}X_{66}X_{61} - X_{12}X_{24}X_{42}X_{21} - X_{33}X_{35}X_{53} - X_{55}X_{56}X_{65} \\ + X_{33}X_{34}X_{43} + X_{35}X_{53}X_{55} + X_{56}X_{66}X_{65} + X_{12}X_{21}X_{16}X_{61} + X_{24}X_{44}X_{42}$		

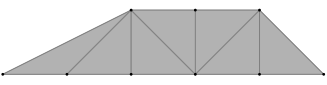
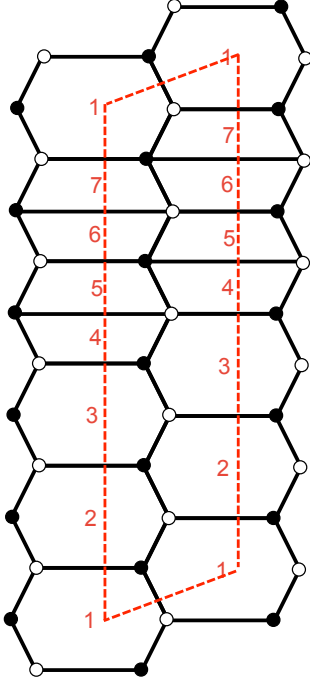
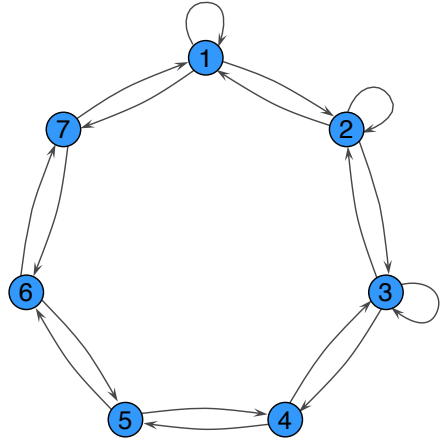
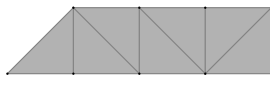
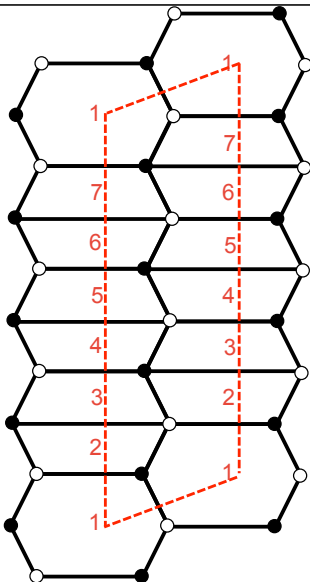
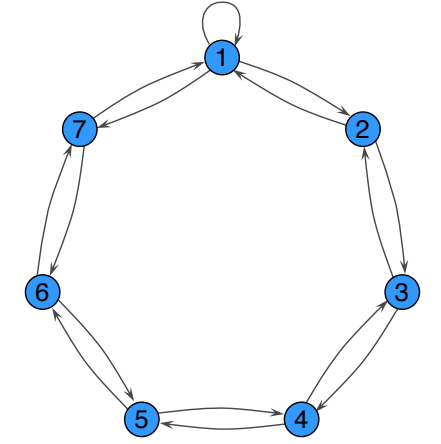
Toric Diagram	Brane Tiling	Quiver
		
$W = -X_{34}X_{44}X_{43} - X_{13}X_{33}X_{31} - X_{15}X_{52}X_{25}X_{51} - X_{26}X_{64}X_{46}X_{62} + X_{33}X_{34}X_{43} + X_{13}X_{31}X_{15}X_{51} + X_{25}X_{52}X_{26}X_{62} + X_{44}X_{46}X_{64}$		
		
$W = -X_{15}X_{52}X_{25}X_{51} - X_{14}X_{43}X_{34}X_{41} - X_{26}X_{63}X_{36}X_{62} + X_{14}X_{41}X_{15}X_{51} + X_{34}X_{43}X_{36}X_{63} + X_{25}X_{52}X_{26}X_{62}$		
		
$W = -X_{12}X_{23}X_{31} - X_{14}X_{45}X_{51} - X_{24}X_{46}X_{62} - X_{25}X_{53}X_{32} - X_{15}X_{56}X_{61} - X_{36}X_{64}X_{43} + X_{12}X_{25}X_{51} + X_{45}X_{56}X_{64} + X_{24}X_{43}X_{32} + X_{15}X_{53}X_{31} + X_{14}X_{46}X_{61} + X_{23}X_{36}X_{62}$		

Toric Diagram	Brane Tiling	Quiver
		
$W = -X_{24}X_{43}X_{32} - X_{26}X_{65}X_{52} - X_{36}X_{65}X_{53} - X_{12}X_{24}X_{41} - X_{12}X_{26}X_{61} - X_{36}X_{64}X_{43} \\ + X_{12}X_{24}X_{41} + X_{26}X_{65}X_{52} + X_{36}X_{64}X_{43} + X_{12}X_{26}X_{61} + X_{36}X_{65}X_{53} + X_{24}X_{43}X_{32}$		
		
$W = -X_{13}X_{34}X_{41} - X_{16}X_{65}X_{54}X_{41} - X_{36}X_{65}X_{53} - X_{23}X_{34}X_{42} - X_{23}X_{36}X_{62} \\ + X_{13}X_{34}X_{41} + X_{16}X_{65}X_{54}X_{41} + X_{23}X_{36}X_{62} + X_{36}X_{65}X_{53} + X_{23}X_{34}X_{42}$		
		
$W = -X_{13}X_{32}X_{21} - X_{14}X_{45}X_{51} - X_{26}X_{64}X_{42} - X_{26}X_{63}X_{32} - X_{13}X_{35}X_{51} - X_{45}X_{56}X_{64} \\ + X_{13}X_{35}X_{51} + X_{45}X_{56}X_{64} + X_{26}X_{63}X_{32} + X_{13}X_{32}X_{21} + X_{14}X_{45}X_{51} + X_{26}X_{64}X_{42}$		

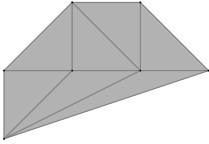
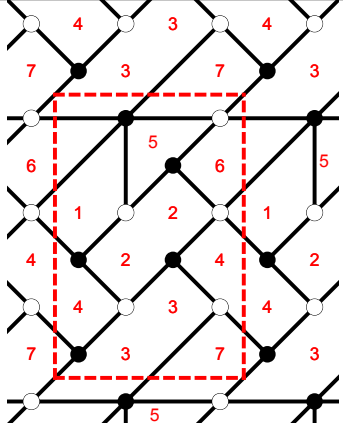
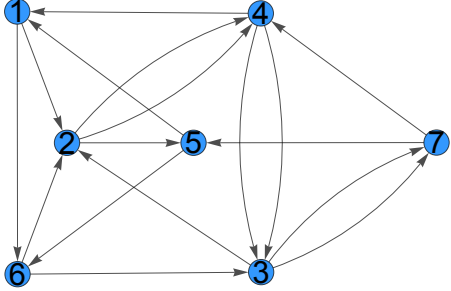
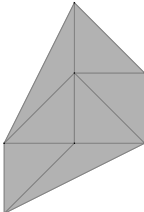
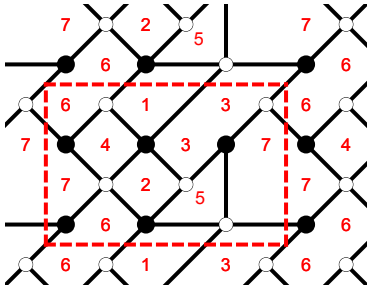
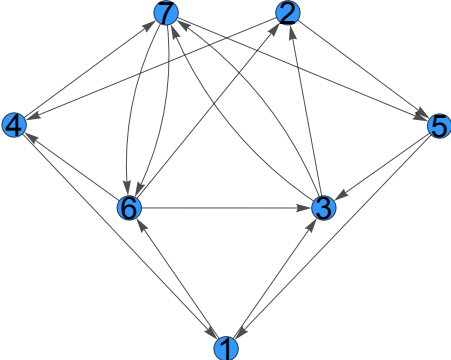
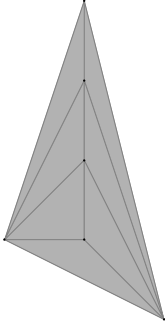
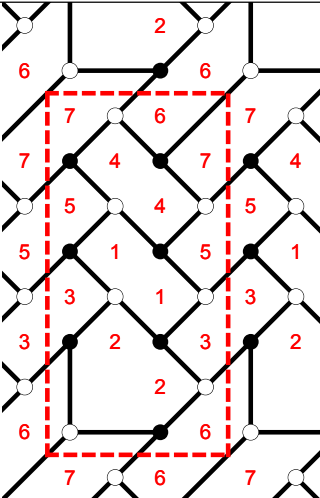
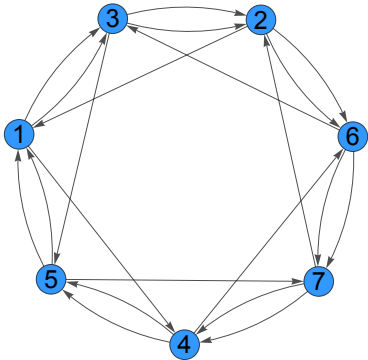
Toric Diagram	Brane Tiling	Quiver
		
$W = -X_{34}X_{45}X_{53} - X_{45}X_{56}X_{64} - X_{15}X_{56}X_{61} - X_{13}X_{32}X_{26}X_{61} - X_{12}X_{24}X_{41} \\ + X_{24}X_{45}X_{53}X_{32} + X_{45}X_{56}X_{64} + X_{15}X_{56}X_{61} + X_{12}X_{26}X_{61} + X_{13}X_{34}X_{41}$		
		
$W = -X_{16}X_{65}X_{51} - X_{25}X_{54}X_{43}X_{32} - X_{12}X_{25}X_{51} - X_{16}X_{64}X_{41} - X_{36}X_{64}X_{43} \\ + X_{12}X_{25}X_{51} + X_{16}X_{65}X_{51} + X_{36}X_{64}X_{43} + X_{25}X_{54}X_{43}X_{32} + X_{16}X_{64}X_{41}$		

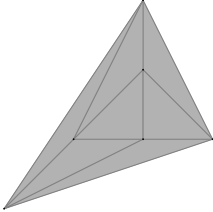
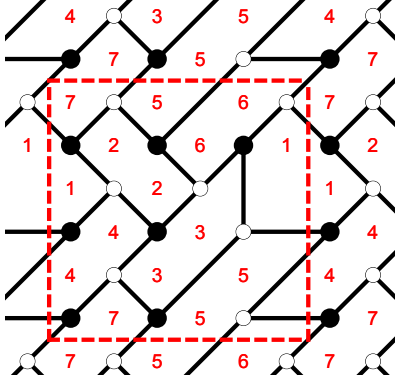
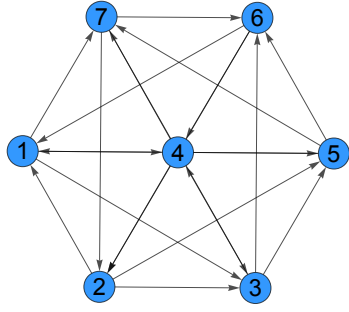
3.5.2 Area 7

Toric Diagram	Brane Tiling	Quiver
		
$ \begin{aligned} W = & -X_{11}X_{12}X_{21} - X_{22}X_{23}X_{32} - X_{33}X_{34}X_{43} - X_{44}X_{45}X_{54} \\ & -X_{55}X_{56}X_{65} - X_{66}X_{67}X_{76} - X_{77}X_{71}X_{17} \\ & +X_{11}X_{17}X_{71} + X_{22}X_{21}X_{12} + X_{33}X_{32}X_{23} + X_{44}X_{43}X_{34} \\ & +X_{55}X_{54}X_{45} + X_{66}X_{65}X_{56} + X_{77}X_{76}X_{67} \end{aligned} $		
		
$ \begin{aligned} W = & -X_{11}X_{12}X_{21} - X_{22}X_{23}X_{32} - X_{33}X_{34}X_{43} - X_{44}X_{45}X_{54} - X_{55}X_{56}X_{65} - X_{67}X_{71}X_{17}X_{76} \\ & +X_{11}X_{17}X_{71} + X_{22}X_{21}X_{12} + X_{33}X_{32}X_{23} + X_{44}X_{43}X_{34} + X_{55}X_{54}X_{45} + X_{67}X_{76}X_{65}X_{56} \end{aligned} $		

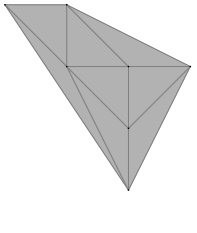
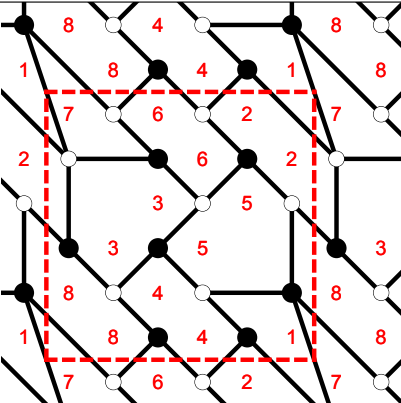
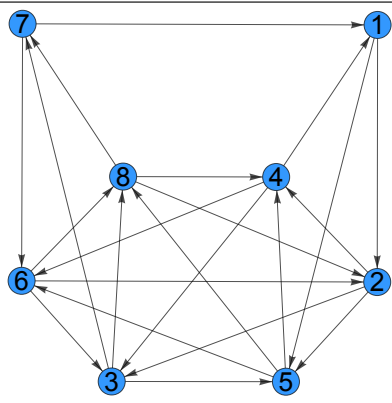
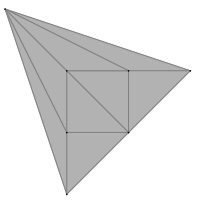
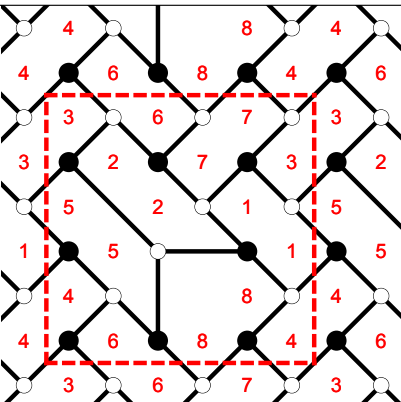
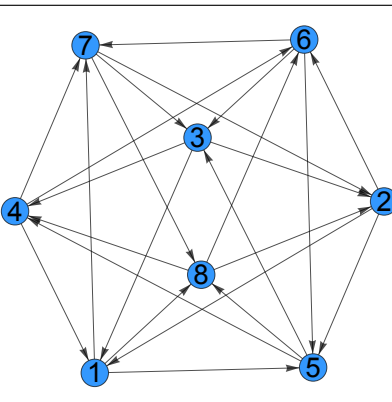
Toric Diagram	Brane Tiling	Quiver
		
$W = -X_{11}X_{12}X_{21} - X_{22}X_{23}X_{32} - X_{33}X_{34}X_{43} - X_{45}X_{56}X_{65}X_{54} - X_{67}X_{71}X_{17}X_{76} \\ + X_{11}X_{17}X_{71} + X_{22}X_{21}X_{12} + X_{33}X_{32}X_{23} + X_{34}X_{45}X_{54}X_{43} + X_{56}X_{67}X_{76}X_{65}$		
		
$W = -X_{11}X_{12}X_{21} - X_{23}X_{34}X_{43}X_{32} - X_{45}X_{56}X_{65}X_{54} - X_{67}X_{71}X_{17}X_{76} \\ + X_{11}X_{17}X_{71} + X_{12}X_{23}X_{32}X_{21} + X_{34}X_{45}X_{54}X_{43} + X_{56}X_{67}X_{76}X_{65}$		

Toric Diagram	Brane Tiling	Quiver
$W = -X_{23}X_{34}X_{42} - X_{14}X_{43}X_{31} - X_{25}X_{56}X_{62} - X_{16}X_{67}X_{72}X_{21} - X_{35}X_{57}X_{73} - X_{47}X_{75}X_{54} \\ + X_{14}X_{42}X_{21} + X_{35}X_{54}X_{43} + X_{16}X_{62}X_{23}X_{31} + X_{25}X_{57}X_{72} + X_{34}X_{47}X_{73} + X_{56}X_{67}X_{75}$		
$W = -X_{36}X_{67}X_{75}X_{53} - X_{16}X_{62}X_{25}X_{51} - X_{37}X_{74}X_{43} - X_{13}X_{32}X_{24}X_{41} \\ + X_{25}X_{53}X_{32} + X_{13}X_{37}X_{75}X_{51} + X_{16}X_{67}X_{74}X_{41} + X_{24}X_{43}X_{36}X_{62}$		
$W = -X_{24}X_{43}X_{32} - X_{25}X_{56}X_{62} - X_{35}X_{57}X_{73} - X_{27}X_{74}X_{46}X_{62} - X_{15}X_{56}X_{61} - X_{15}X_{57}X_{71} \\ + X_{24}X_{46}X_{62} + X_{15}X_{56}X_{61} + X_{35}X_{57}X_{74}X_{43} + X_{25}X_{56}X_{62} + X_{15}X_{57}X_{71} + X_{27}X_{73}X_{32}$		

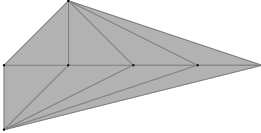
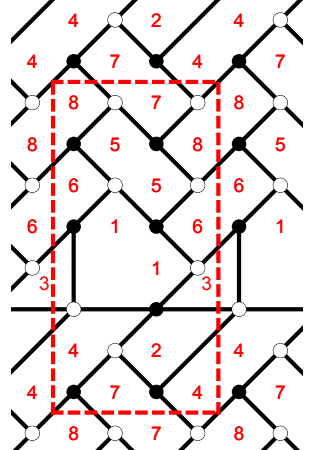
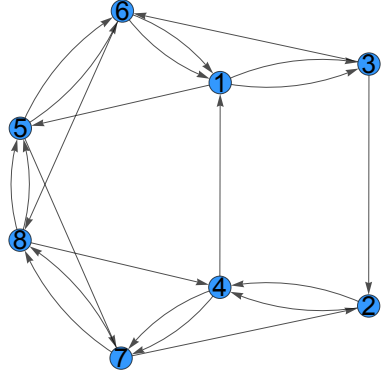
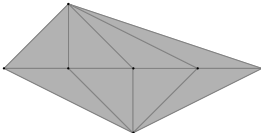
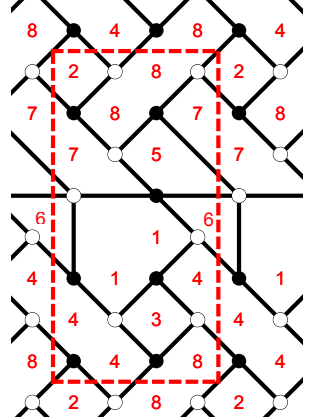
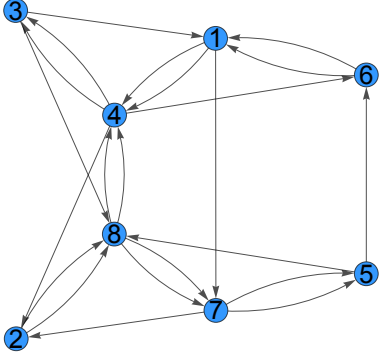
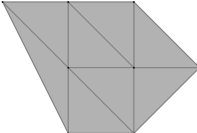
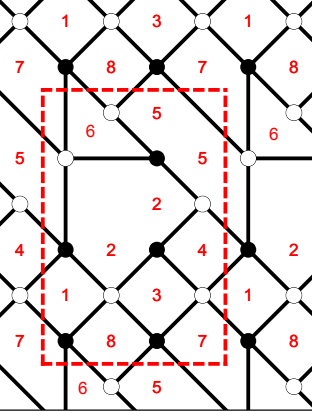
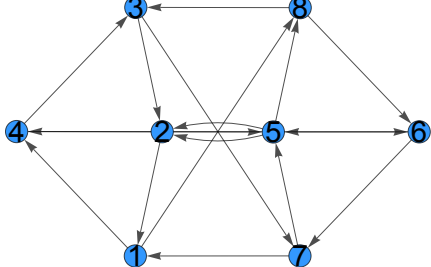
Toric Diagram	Brane Tiling	Quiver
		
$W = -X_{24}X_{43}X_{32} - X_{25}X_{56}X_{62} - X_{16}X_{63}X_{37}X_{75}X_{51} - X_{12}X_{24}X_{41} - X_{37}X_{74}X_{43} + X_{16}X_{62}X_{24}X_{41} + X_{37}X_{75}X_{56}X_{63} + X_{37}X_{74}X_{43} + X_{12}X_{25}X_{51} + X_{24}X_{43}X_{32}$		
		
$W = -X_{13}X_{32}X_{24}X_{41} - X_{16}X_{62}X_{25}X_{51} - X_{37}X_{75}X_{53} - X_{47}X_{76}X_{64} - X_{37}X_{76}X_{63} + X_{13}X_{37}X_{75}X_{51} + X_{25}X_{53}X_{32} + X_{37}X_{76}X_{63} + X_{16}X_{64}X_{41} + X_{24}X_{47}X_{76}X_{62}$		
		
$W = -X_{13}X_{32}X_{21} - X_{14}X_{45}X_{51} - X_{46}X_{67}X_{74} - X_{26}X_{67}X_{72} - X_{26}X_{63}X_{32} - X_{13}X_{35}X_{51} - X_{45}X_{57}X_{74} + X_{13}X_{35}X_{51} + X_{45}X_{57}X_{74} + X_{26}X_{67}X_{72} + X_{26}X_{63}X_{32} + X_{13}X_{32}X_{21} + X_{14}X_{45}X_{51} + X_{46}X_{67}X_{74}$		

Toric Diagram	Brane Tiling	Quiver
		
$W = -X_{23}X_{34}X_{42} - X_{25}X_{56}X_{62} - X_{35}X_{57}X_{73} - X_{13}X_{36}X_{61} - X_{14}X_{45}X_{51} - X_{17}X_{72}X_{21} - X_{47}X_{76}X_{64} \\ + X_{23}X_{36}X_{62} + X_{45}X_{56}X_{64} + X_{13}X_{35}X_{51} + X_{17}X_{76}X_{61} + X_{14}X_{42}X_{21} + X_{25}X_{57}X_{72} + X_{34}X_{47}X_{73}$		

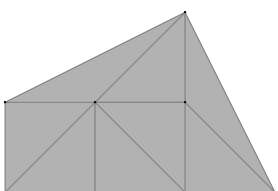
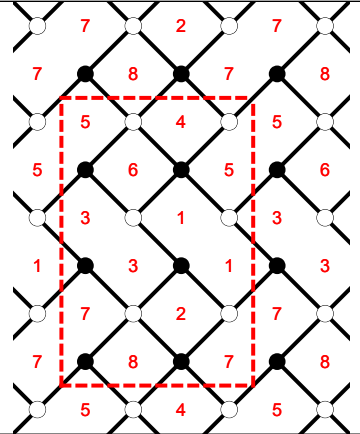
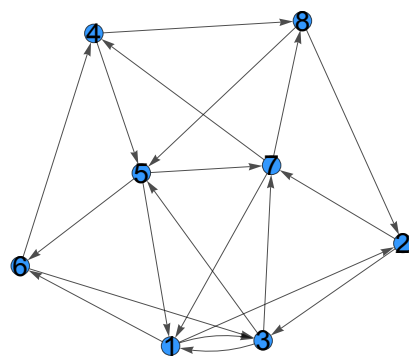
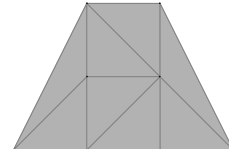
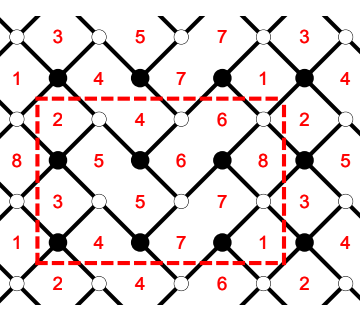
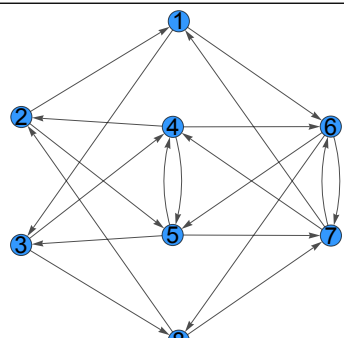
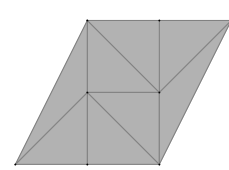
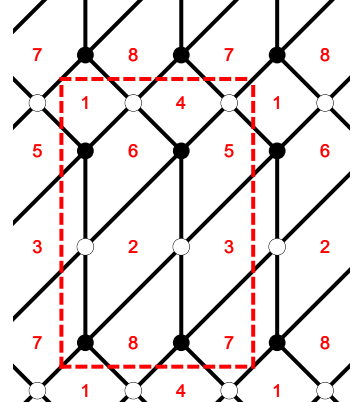
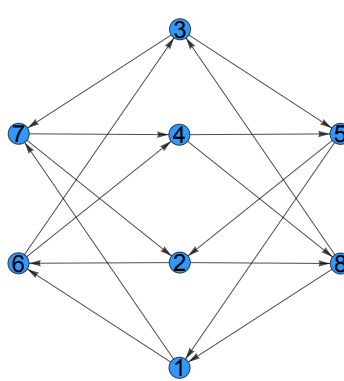
3.5.3 Area 8

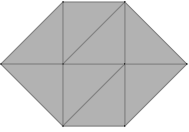
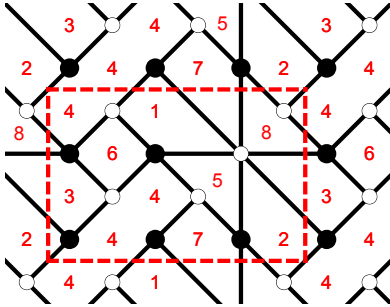
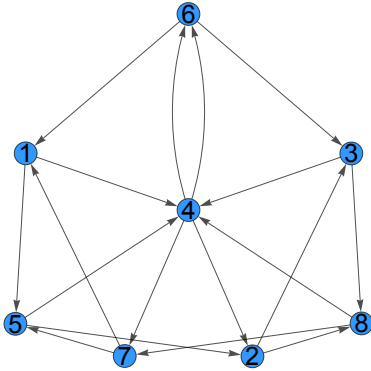
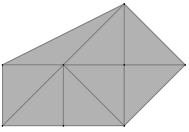
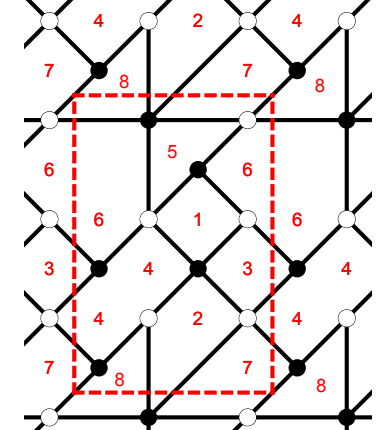
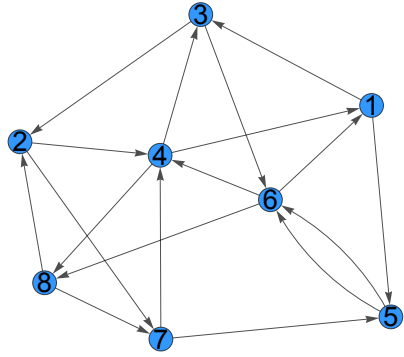
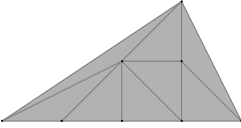
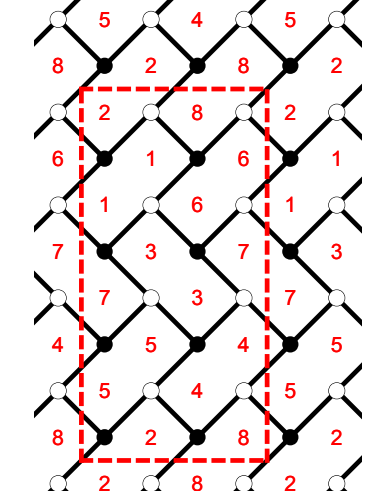
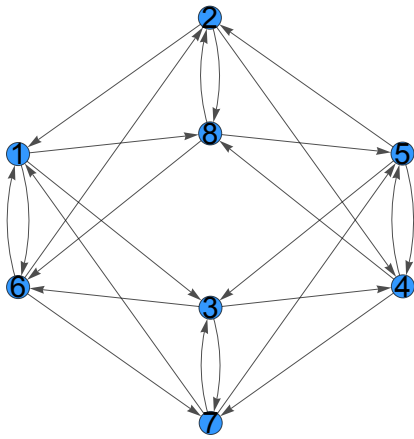
Toric Diagram	Brane Tiling	Quiver
		
$W = -X_{35}X_{54}X_{43} - X_{37}X_{76}X_{63} - X_{46}X_{68}X_{84} - X_{15}X_{58}X_{87}X_{71} - X_{25}X_{56}X_{62} - X_{12}X_{24}X_{41} - X_{23}X_{38}X_{82} + X_{35}X_{56}X_{63} + X_{24}X_{46}X_{62} + X_{15}X_{54}X_{41} + X_{25}X_{58}X_{82} + X_{12}X_{23}X_{37}X_{71} + X_{68}X_{87}X_{76} + X_{38}X_{84}X_{43}$		
		
$W = -X_{26}X_{67}X_{72} - X_{58}X_{86}X_{65} - X_{18}X_{82}X_{21} - X_{17}X_{73}X_{31} - X_{47}X_{78}X_{84} - X_{15}X_{54}X_{41} - X_{25}X_{53}X_{32} - X_{34}X_{46}X_{63} + X_{17}X_{72}X_{21} + X_{67}X_{78}X_{86} + X_{25}X_{58}X_{82} + X_{15}X_{53}X_{31} + X_{34}X_{47}X_{73} + X_{18}X_{84}X_{41} + X_{26}X_{63}X_{32} + X_{46}X_{65}X_{54}$		

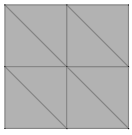
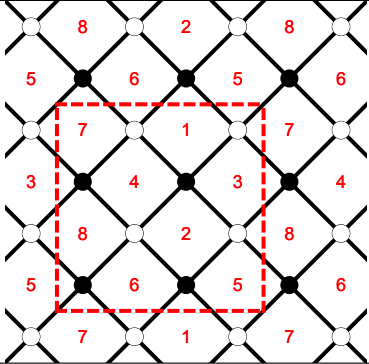
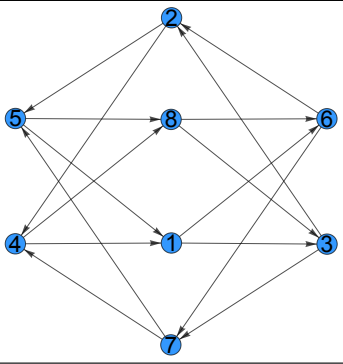
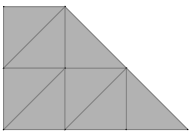
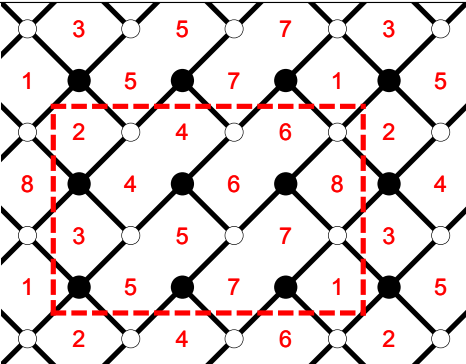
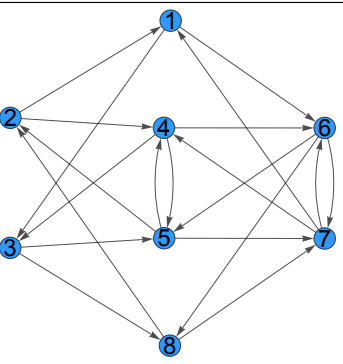
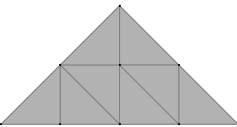
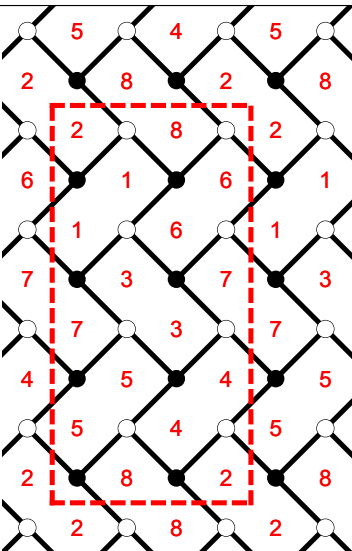
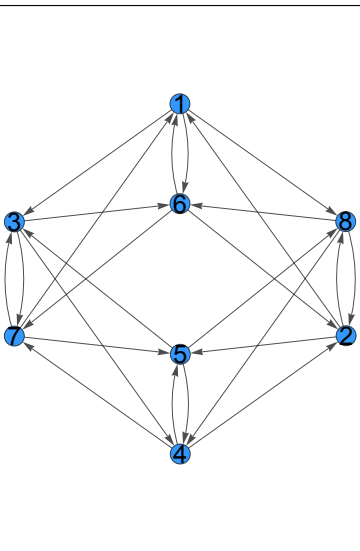
Toric Diagram	Brane Tiling	Quiver
$W = -X_{35}X_{54}X_{43} - X_{36}X_{64}X_{43} - X_{15}X_{57}X_{78}X_{81} - X_{35}X_{57}X_{73} - X_{16}X_{62}X_{28}X_{81} - X_{23}X_{36}X_{62} \\ + X_{35}X_{57}X_{73} + X_{35}X_{54}X_{43} + X_{15}X_{57}X_{78}X_{81} + X_{16}X_{62}X_{28}X_{81} + X_{23}X_{36}X_{62} + X_{36}X_{64}X_{43}$		
$W = -X_{45}X_{56}X_{64} - X_{56}X_{68}X_{87}X_{75} - X_{16}X_{67}X_{71} - X_{12}X_{28}X_{81} - X_{12}X_{23}X_{31} - X_{23}X_{34}X_{42} - X_{34}X_{45}X_{53} \\ + X_{45}X_{56}X_{64} + X_{56}X_{67}X_{75} + X_{16}X_{68}X_{81} + X_{12}X_{28}X_{87}X_{71} + X_{12}X_{23}X_{31} + X_{23}X_{34}X_{42} + X_{34}X_{45}X_{53}$		
$W = -X_{15}X_{54}X_{46}X_{61} - X_{15}X_{57}X_{71} - X_{57}X_{78}X_{85} - X_{27}X_{78}X_{82} - X_{23}X_{38}X_{82} - X_{23}X_{34}X_{46}X_{62} \\ + X_{15}X_{57}X_{71} + X_{57}X_{78}X_{85} + X_{27}X_{78}X_{82} + X_{23}X_{38}X_{82} + X_{23}X_{34}X_{46}X_{62} + X_{15}X_{54}X_{46}X_{61}$		
Toric Diagram	Brane Tiling	Quiver
$W = -X_{24}X_{43}X_{32} - X_{25}X_{56}X_{62} - X_{57}X_{78}X_{85} - X_{17}X_{73}X_{31} - X_{14}X_{43}X_{31} - X_{24}X_{46}X_{62} - X_{56}X_{68}X_{85} - X_{17}X_{78}X_{81} \\ + X_{24}X_{46}X_{62} + X_{56}X_{68}X_{85} + X_{17}X_{78}X_{81} + X_{14}X_{43}X_{31} + X_{24}X_{43}X_{32} + X_{25}X_{56}X_{62} + X_{57}X_{78}X_{85} + X_{17}X_{73}X_{31}$		

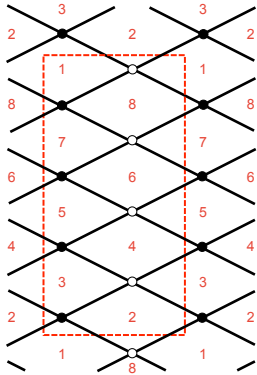
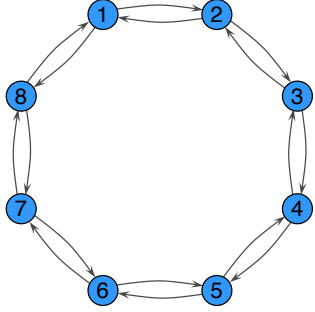
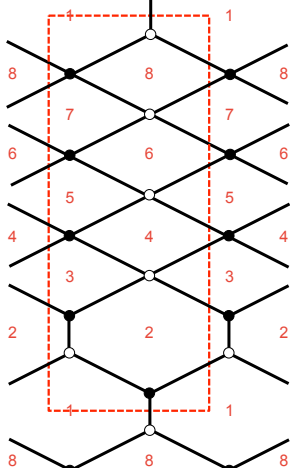
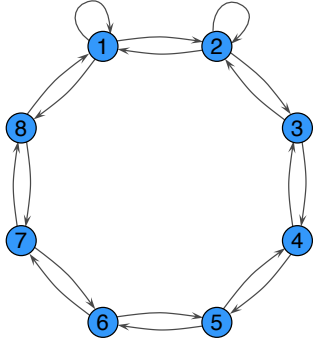
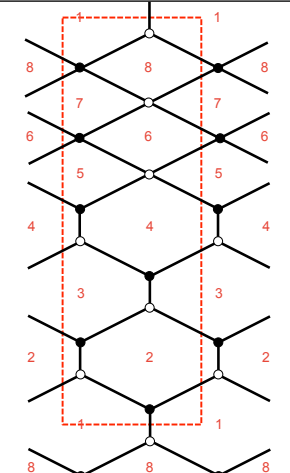
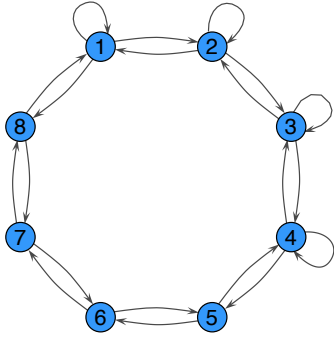
<p>Toric Diagram</p> 	<p>Brane Tiling</p> 	<p>Quiver</p> 
$W = -X_{13}X_{32}X_{24}X_{41} - X_{15}X_{56}X_{61} - X_{57}X_{78}X_{85} - X_{24}X_{47}X_{72} - X_{13}X_{36}X_{61} - X_{56}X_{68}X_{85} - X_{47}X_{78}X_{84} + X_{13}X_{36}X_{61} + X_{56}X_{68}X_{85} + X_{47}X_{78}X_{84} + X_{13}X_{32}X_{24}X_{41} + X_{15}X_{56}X_{61} + X_{57}X_{78}X_{85} + X_{24}X_{47}X_{72}$		
<p>Toric Diagram</p> 	<p>Brane Tiling</p> 	<p>Quiver</p> 
$W = -X_{14}X_{43}X_{31} - X_{17}X_{75}X_{56}X_{61} - X_{58}X_{87}X_{75} - X_{38}X_{84}X_{43} - X_{14}X_{46}X_{61} - X_{28}X_{87}X_{72} - X_{28}X_{84}X_{42} + X_{14}X_{46}X_{61} + X_{17}X_{75}X_{56}X_{61} + X_{28}X_{87}X_{72} + X_{38}X_{84}X_{43} + X_{58}X_{87}X_{75} + X_{28}X_{84}X_{42} + X_{14}X_{43}X_{31}$		
<p>Toric Diagram</p> 	<p>Brane Tiling</p> 	<p>Quiver</p> 
$W = -X_{24}X_{43}X_{32} - X_{26}X_{65}X_{52} - X_{37}X_{75}X_{58}X_{83} - X_{14}X_{45}X_{52}X_{21} - X_{18}X_{86}X_{67}X_{71} + X_{24}X_{45}X_{52} + X_{26}X_{67}X_{75}X_{52} + X_{14}X_{43}X_{37}X_{71} + X_{58}X_{86}X_{65} + X_{18}X_{83}X_{32}X_{21}$		

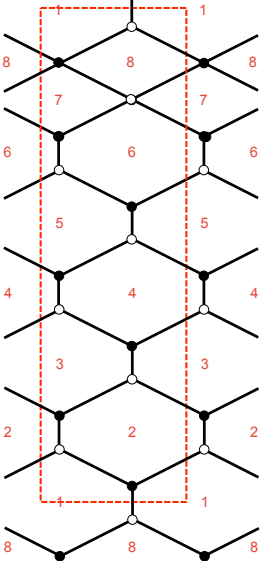
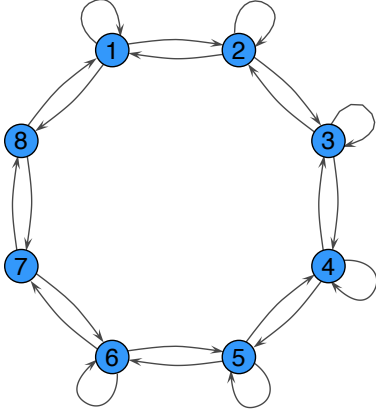
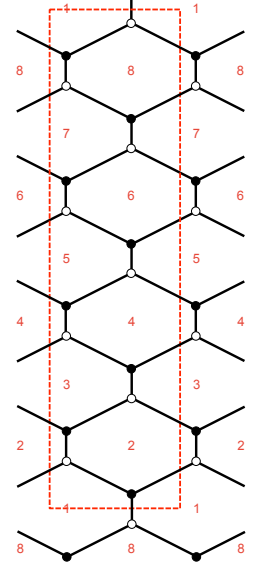
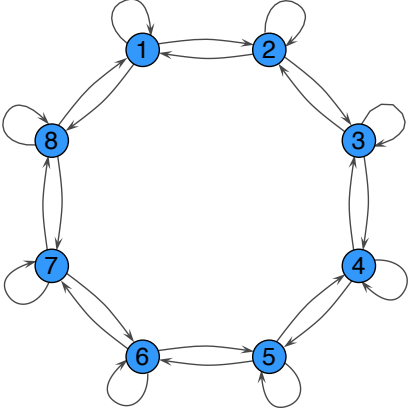
Toric Diagram	Brane Tiling	Quiver
$W = -X_{34}X_{45}X_{53} - X_{37}X_{74}X_{46}X_{63} - X_{38}X_{86}X_{63} - X_{18}X_{86}X_{61} - X_{18}X_{82}X_{25}X_{51} - X_{17}X_{72}X_{21} + X_{38}X_{86}X_{63} + X_{34}X_{46}X_{63} + X_{18}X_{82}X_{21} + X_{18}X_{86}X_{61} + X_{25}X_{53}X_{37}X_{72} + X_{17}X_{74}X_{45}X_{51}$		
$W = -X_{35}X_{54}X_{43} - X_{36}X_{67}X_{73} - X_{48}X_{86}X_{64} - X_{15}X_{54}X_{41} - X_{23}X_{35}X_{57}X_{72} - X_{16}X_{62}X_{28}X_{81} + X_{35}X_{57}X_{73} + X_{28}X_{86}X_{67}X_{72} + X_{15}X_{54}X_{48}X_{81} + X_{35}X_{54}X_{43} + X_{23}X_{36}X_{62} + X_{16}X_{64}X_{41}$		
$W = -X_{35}X_{54}X_{43} - X_{37}X_{74}X_{46}X_{63} - X_{56}X_{68}X_{85} - X_{16}X_{68}X_{81} - X_{13}X_{32}X_{28}X_{81} - X_{12}X_{27}X_{71} + X_{35}X_{56}X_{63} + X_{46}X_{68}X_{85}X_{54} + X_{16}X_{68}X_{81} + X_{12}X_{28}X_{81} + X_{13}X_{37}X_{71} + X_{27}X_{74}X_{43}X_{32}$		
$W = -X_{24}X_{43}X_{35}X_{52} - X_{26}X_{63}X_{32} - X_{14}X_{47}X_{78}X_{86}X_{61} - X_{24}X_{47}X_{72} - X_{15}X_{58}X_{81} + X_{24}X_{47}X_{72} + X_{24}X_{43}X_{32} + X_{14}X_{47}X_{78}X_{81} + X_{15}X_{52}X_{26}X_{61} + X_{35}X_{58}X_{86}X_{63}$		

Toric Diagram	Brane Tiling	Quiver
		
$W = -X_{12}X_{23}X_{31} - X_{16}X_{64}X_{45}X_{51} - X_{27}X_{74}X_{48}X_{82} - X_{13}X_{37}X_{71} - X_{35}X_{56}X_{63} - X_{57}X_{78}X_{85} + X_{13}X_{35}X_{51} + X_{45}X_{57}X_{74} + X_{12}X_{27}X_{71} + X_{16}X_{63}X_{31} + X_{48}X_{85}X_{56}X_{64} + X_{23}X_{37}X_{78}X_{82}$		
		
$W = -X_{46}X_{65}X_{54} - X_{45}X_{57}X_{74} - X_{68}X_{87}X_{76} - X_{16}X_{67}X_{71} - X_{25}X_{53}X_{38}X_{82} - X_{13}X_{34}X_{42}X_{21} + X_{46}X_{67}X_{74} + X_{57}X_{76}X_{65} + X_{16}X_{68}X_{82}X_{21} + X_{13}X_{38}X_{87}X_{71} + X_{25}X_{54}X_{42} + X_{34}X_{45}X_{53}$		
		
$W = -X_{26}X_{64}X_{45}X_{52} - X_{37}X_{74}X_{48}X_{83} - X_{16}X_{63}X_{35}X_{51} - X_{17}X_{72}X_{28}X_{81} + X_{28}X_{83}X_{35}X_{52} + X_{17}X_{74}X_{45}X_{51} + X_{26}X_{63}X_{37}X_{72} + X_{16}X_{64}X_{48}X_{81}$		

Toric Diagram	Brane Tiling	Quiver
		
$W = -X_{15}X_{54}X_{46}X_{61} - X_{14}X_{47}X_{71} - X_{28}X_{87}X_{75}X_{52} - X_{38}X_{84}X_{46}X_{63} - X_{23}X_{34}X_{42} + X_{15}X_{52}X_{23}X_{38}X_{87}X_{71} + X_{47}X_{75}X_{54} + X_{28}X_{84}X_{42} + X_{14}X_{46}X_{61} + X_{34}X_{46}X_{63}$		
		
$W = -X_{13}X_{32}X_{24}X_{41} - X_{15}X_{56}X_{61} - X_{27}X_{75}X_{56}X_{68}X_{82} - X_{36}X_{64}X_{43} - X_{48}X_{87}X_{74} + X_{13}X_{36}X_{61} + X_{56}X_{68}X_{87}X_{75} + X_{27}X_{74}X_{43}X_{32} + X_{15}X_{56}X_{64}X_{41} + X_{24}X_{48}X_{82}$		
		
$W = -X_{34}X_{45}X_{53} - X_{36}X_{67}X_{73} - X_{18}X_{86}X_{61} - X_{24}X_{48}X_{82} - X_{47}X_{75}X_{54} - X_{13}X_{37}X_{71} - X_{16}X_{62}X_{21} - X_{28}X_{85}X_{52} + X_{34}X_{47}X_{73} + X_{16}X_{67}X_{71} + X_{28}X_{86}X_{62} + X_{48}X_{85}X_{54} + X_{37}X_{75}X_{53} + X_{13}X_{36}X_{61} + X_{18}X_{82}X_{21} + X_{24}X_{45}X_{52}$		

Toric Diagram	Brane Tiling	Quiver
		
$W = -X_{13}X_{32}X_{24}X_{41} - X_{16}X_{62}X_{25}X_{51} - X_{37}X_{74}X_{48}X_{83} - X_{58}X_{86}X_{67}X_{75} \\ + X_{13}X_{37}X_{75}X_{51} + X_{25}X_{58}X_{83}X_{32} + X_{16}X_{67}X_{74}X_{41} + X_{24}X_{48}X_{86}X_{62}$		
		
$W = -X_{46}X_{65}X_{54} - X_{45}X_{57}X_{74} - X_{68}X_{87}X_{76} - X_{16}X_{67}X_{71} - X_{24}X_{43}X_{38}X_{82} - X_{13}X_{35}X_{52}X_{21} \\ + X_{46}X_{67}X_{74} + X_{57}X_{76}X_{65} + X_{16}X_{68}X_{82}X_{21} + X_{13}X_{38}X_{87}X_{71} + X_{24}X_{45}X_{52} + X_{35}X_{54}X_{43}$		
		
$W = -X_{34}X_{45}X_{53} - X_{36}X_{67}X_{73} - X_{18}X_{86}X_{61} - X_{28}X_{84}X_{42} - X_{47}X_{75}X_{54} - X_{13}X_{37}X_{71} - X_{16}X_{62}X_{21} - X_{25}X_{58}X_{82} \\ + X_{34}X_{47}X_{73} + X_{16}X_{67}X_{71} + X_{28}X_{86}X_{62} + X_{25}X_{54}X_{42} + X_{37}X_{75}X_{53} + X_{13}X_{36}X_{61} + X_{18}X_{82}X_{21} + X_{45}X_{58}X_{84}$		

Toric Diagram	Brane Tiling	Quiver
		
$W = -X_{12}X_{23}X_{32}X_{21} - X_{34}X_{45}X_{54}X_{43} - X_{56}X_{67}X_{76}X_{65} - X_{78}X_{81}X_{18}X_{87} \\ + X_{23}X_{34}X_{43}X_{32} + X_{45}X_{56}X_{65}X_{54} + X_{67}X_{78}X_{87}X_{76} + X_{81}X_{12}X_{21}X_{18}$		
		
$W = -X_{11}X_{12}X_{21} - X_{22}X_{23}X_{32} - X_{34}X_{45}X_{54}X_{43} - X_{56}X_{67}X_{76}X_{65} - X_{78}X_{81}X_{18}X_{87} \\ + X_{11}X_{18}X_{81} + X_{22}X_{21}X_{12} + X_{23}X_{34}X_{43}X_{32} + X_{45}X_{56}X_{65}X_{54} + X_{67}X_{78}X_{87}X_{76}$		
		
$W = -X_{11}X_{12}X_{21} - X_{22}X_{23}X_{32} - X_{33}X_{34}X_{43} - X_{44}X_{45}X_{54} - X_{56}X_{67}X_{76}X_{65} - X_{78}X_{81}X_{18}X_{87} \\ + X_{11}X_{18}X_{81} + X_{22}X_{21}X_{12} + X_{33}X_{32}X_{23} + X_{44}X_{43}X_{34} + X_{45}X_{56}X_{65}X_{54} + X_{67}X_{78}X_{87}X_{76}$		

Toric Diagram	Brane Tiling	Quiver
		
$W = -X_{11}X_{12}X_{21} - X_{22}X_{23}X_{32} - X_{33}X_{34}X_{43} - X_{44}X_{45}X_{54} - X_{55}X_{56}X_{65} - X_{66}X_{67}X_{76} - X_{67}X_{78}X_{87}X_{76} \\ + X_{11}X_{18}X_{81} + X_{22}X_{21}X_{12} + X_{33}X_{32}X_{23} + X_{44}X_{43}X_{34} + X_{55}X_{54}X_{45} + X_{66}X_{65}X_{56} + X_{78}X_{81}X_{18}X_{87}$		
		
$W = -X_{11}X_{12}X_{21} - X_{22}X_{23}X_{32} - X_{33}X_{34}X_{43} - X_{44}X_{45}X_{54} \\ - X_{55}X_{56}X_{65} - X_{66}X_{67}X_{76} - X_{77}X_{78}X_{87} - X_{88}X_{81}X_{18} \\ + X_{11}X_{18}X_{81} + X_{22}X_{21}X_{12} + X_{33}X_{32}X_{23} + X_{44}X_{43}X_{34} \\ + X_{55}X_{54}X_{45} + X_{66}X_{65}X_{56} + X_{77}X_{76}X_{67} + X_{88}X_{87}X_{78}$		

3.5.4 Examples: GLSM data for Area 6, 7, 8

In this section, we take some examples from results in section 3.5 to elucidate the relation between toric geometry and GLSM. This relation is entirely based on the central object: charge matrix Q_t . Specifically, we would like to look at diagram 5, 10, 11 in area 6 list, diagram 7, 8 in area 7 list and diagram 1, 3 in area 8 list from tables 3.5, 3.5 and 3.7. Before we proceed, it is worthwhile to present some background materials on this interesting relation. The desire to implement both F-terms and D-terms conditions of supersymmetric gauge theory on the same footing as it is done in GLSM has led literatures [69, 139, 140] to develop the Forward Algorithm. Within these procedures, a new set of basis of fields are chosen from the set of quiver fields and these new fields are exactly the perfect matchings of a brane tiling [49, 50, 52]. These fields have the following properties:

- As described in section 3.2.2, a **perfect matching** p_α is a set of bifundamental fields which connects to all node precisely once inside a brane tiling. More importantly, they are collected inside the perfect matching matrix $P_{E \times c}$ with E being the number of matter fields and c the number of perfect matching.
- **F-term** constraints are encapsulated in the perfect matching matrix $P_{E \times c}$ with the charges under F-terms given by the kernel,

$$Q_{F(c-G-2) \times c} = \ker(P_{E \times c}) . \quad (3.14)$$

- **D-terms** [35] are given

$$D_i = -e^2 \left(\sum_a d_{ia} |X_a|^2 - \zeta_i \right) , \quad (3.15)$$

where X_a is a bifundamental matter field represented by the a -th column of the incidence matrix $d_{G \times E}$ as defined in section 2.2, i is the label for quiver gauge groups, e is the gauge coupling and ζ_i is the Fayet-Iliopoulos parameter. Specifically, D-terms are

related to the perfect matchings as follows

$$\Delta_{(G-1) \times E} = Q_{D(G-1) \times c} \cdot P_{c \times E}^t, \quad (3.16)$$

where $\Delta_{(G-1) \times E}$ is the reduced incidence matrix of the quiver since each column of $d_{G \times E}$ sums up to zero identically and $Q_{D(G-1) \times c}$ is the charge matrix under D-terms constraints.

With such two matrices at our disposal, we can concatenate them to form a $(c-3) \times c$ matrix

$$Q_t = \begin{pmatrix} Q_F \\ Q_D \end{pmatrix}. \quad (3.17)$$

Here we see that the charge matrix Q_t gives information on how the GLSM fields are charged under various $U(1)$ factors. Furthermore, the transpose of the kernel of charge matrix

$$G_t = [\ker(Q_t)]^t, \quad (3.18)$$

provides the coordinates of the **toric diagram** points with its columns.

We can see that the charge matrix Q_t is of dimension $(c-3) \times c$ and it is exactly the same matrix defined in section 2.3.2. The columns of the matrix gives perfect matchings *i.e.*, GLSM chiral fields, whereas the rows show how these fields are charged under the $U(1)^{c-3}$ gauge factors. Now we turn to some specific examples to elucidate this relation.

Area 6 Examples

We take diagrams 5, 10, 11, 12 from the area 6 list with the point in mind that toric diagrams with no internal points are associated with non-chiral gauge theories. Hence only diagrams with internal points shall be taken as examples for calculating its charge matrix Q_t . Furthermore, since triangulation of the toric diagram is of area 6, the total number of $U(1)$ gauge nodes of the resulting quiver gauge theory should also be 6.

Diagram 5 This toric diagram is not inside any known catalogue of geometries such as $L^{a,b,c}$, $Y^{p,q}$, $X^{p,q}$ due to the presence of only 3 external edges. It is also obvious that it is not inside the classes of del Pezzo surfaces and orbifolds. Its superpotential is comprised of 12 degree 3 monomial terms, which are themselves functions of 18 bifundamental fields.

The perfect matching for this particular brane-tiling is

$$P = \begin{pmatrix} \begin{array}{c|cccccccccccccccccccc} & p_1 & p_2 & p_3 & p_4 & p_5 & p_6 & p_7 & p_8 & p_9 & p_{10} & p_{11} & p_{12} & p_{13} & p_{14} & p_{15} & p_{16} & p_{17} \\ \hline X_1 & 0 & 0 & 1 & 0 & 1 & 1 & 1 & 0 & 0 & 1 & 0 & 0 & 0 & 0 & 0 & 0 & 0 \\ X_2 & 1 & 0 & 0 & 0 & 0 & 0 & 0 & 1 & 1 & 0 & 0 & 1 & 1 & 0 & 0 & 1 & 0 \\ X_3 & 1 & 1 & 0 & 1 & 0 & 1 & 0 & 0 & 0 & 0 & 0 & 0 & 1 & 1 & 0 & 0 & 0 \\ X_4 & 0 & 0 & 1 & 0 & 1 & 0 & 1 & 0 & 0 & 0 & 0 & 1 & 0 & 0 & 0 & 1 & 0 \\ X_5 & 1 & 1 & 0 & 1 & 0 & 0 & 0 & 1 & 1 & 0 & 1 & 0 & 0 & 0 & 0 & 0 & 0 \\ X_6 & 0 & 0 & 0 & 1 & 1 & 0 & 0 & 1 & 0 & 0 & 1 & 0 & 0 & 0 & 1 & 0 & 0 \\ X_7 & 0 & 1 & 0 & 1 & 0 & 0 & 0 & 0 & 0 & 1 & 0 & 0 & 0 & 1 & 1 & 0 & 1 \\ X_8 & 0 & 0 & 1 & 0 & 1 & 0 & 1 & 0 & 1 & 0 & 1 & 0 & 0 & 0 & 0 & 0 & 0 \\ X_9 & 1 & 0 & 0 & 0 & 0 & 1 & 1 & 0 & 1 & 0 & 0 & 0 & 1 & 0 & 0 & 1 & 0 \\ X_{10} & 0 & 0 & 0 & 0 & 0 & 0 & 1 & 0 & 1 & 0 & 1 & 0 & 0 & 0 & 1 & 1 & 1 \\ X_{11} & 1 & 1 & 1 & 0 & 0 & 0 & 0 & 0 & 0 & 0 & 0 & 1 & 1 & 1 & 0 & 0 & 0 \\ X_{12} & 0 & 0 & 0 & 1 & 1 & 1 & 0 & 1 & 0 & 1 & 0 & 0 & 0 & 0 & 0 & 0 & 0 \\ X_{13} & 0 & 0 & 0 & 0 & 0 & 1 & 0 & 0 & 0 & 1 & 0 & 0 & 1 & 1 & 0 & 0 & 1 \\ X_{14} & 1 & 1 & 1 & 0 & 0 & 0 & 1 & 0 & 1 & 0 & 1 & 0 & 0 & 0 & 0 & 0 & 0 \\ X_{15} & 0 & 1 & 1 & 0 & 0 & 0 & 0 & 0 & 0 & 1 & 1 & 0 & 0 & 1 & 0 & 0 & 1 \\ X_{16} & 0 & 0 & 0 & 1 & 1 & 1 & 1 & 0 & 0 & 0 & 0 & 0 & 0 & 1 & 0 & 0 & 0 \\ X_{17} & 0 & 0 & 0 & 0 & 0 & 0 & 0 & 1 & 1 & 1 & 1 & 0 & 0 & 0 & 1 & 1 & 1 \\ X_{18} & 0 & 0 & 0 & 0 & 0 & 0 & 0 & 0 & 0 & 0 & 1 & 1 & 1 & 1 & 1 & 1 & 1 \end{array} \end{pmatrix}. \quad (3.19)$$

The F-term charge matrix $Q_F = \ker(P)$ is

$$Q_F = \begin{pmatrix} \begin{array}{cccccccccccccccccccc} p_1 & p_2 & p_3 & p_4 & p_5 & p_6 & p_7 & p_8 & p_9 & p_{10} & p_{11} & p_{12} & p_{13} & p_{14} & p_{15} & p_{16} & p_{17} \\ \hline 2 & -3 & 2 & 2 & 0 & -1 & -1 & -1 & 0 & 0 & 0 & -1 & 0 & 0 & 0 & 0 & 1 \\ 1 & -2 & 2 & 2 & 0 & -1 & -1 & -1 & 0 & 0 & 0 & -1 & 0 & 0 & 0 & 0 & 1 \\ 1 & -1 & 1 & 0 & 0 & 0 & -1 & 0 & 0 & 0 & 0 & -1 & 0 & 0 & 1 & 0 & 0 \\ 1 & -2 & 1 & 1 & 0 & -1 & 0 & 0 & 0 & 0 & 0 & -1 & 0 & 1 & 0 & 0 & 0 \\ 0 & -1 & 1 & 1 & 0 & -1 & 0 & 0 & 0 & 0 & 0 & -1 & 1 & 0 & 0 & 0 & 0 \\ 1 & -2 & 1 & 1 & 0 & 0 & -1 & -1 & 0 & 0 & 1 & 0 & 0 & 0 & 0 & 0 & 0 \\ 1 & -1 & 0 & 1 & 0 & -1 & 0 & -1 & 0 & 1 & 0 & 0 & 0 & 0 & 0 & 0 & 0 \\ 0 & -1 & 1 & 1 & 0 & 0 & -1 & -1 & 1 & 0 & 0 & 0 & 0 & 0 & 0 & 0 & 0 \\ 0 & 1 & -1 & -1 & 1 & 0 & 0 & 0 & 0 & 0 & 0 & 0 & 0 & 0 & 0 & 0 & 0 \end{array} \end{pmatrix}. \quad (3.20)$$

The D-term charge matrix is given by

$$Q_D = \begin{pmatrix} \begin{array}{cccccccccccccccccccc} p_1 & p_2 & p_3 & p_4 & p_5 & p_6 & p_7 & p_8 & p_9 & p_{10} & p_{11} & p_{12} & p_{13} & p_{14} & p_{15} & p_{16} & p_{17} \\ \hline 0 & 0 & 0 & 0 & 0 & 0 & 0 & 0 & 0 & 0 & 0 & -1 & 0 & 0 & 1 & 1 & -1 \\ 0 & 0 & 0 & 0 & 0 & 0 & 0 & -1 & 0 & 1 & 1 & 0 & 0 & 0 & 0 & 0 & -1 \\ 0 & 0 & 0 & 0 & 0 & 0 & 0 & 1 & 0 & -1 & 0 & 0 & 0 & 0 & 0 & 0 & -1 \\ 0 & 0 & 0 & 0 & 0 & 0 & 0 & -1 & 0 & 0 & 0 & 1 & 0 & 0 & 0 & 0 & 0 \\ 0 & 0 & 0 & 0 & 0 & 0 & 0 & 0 & 0 & 0 & 0 & 1 & 0 & -1 & -1 & 0 & 1 \end{array} \end{pmatrix}. \quad (3.21)$$

The total charge matrix Q_t is of dimension 14×17 , which is indeed of the form $(c - 3) \times c$ with c being the number of perfect matchings or the GLSM fields. The charge matrix Q_t has its rows summing up to 0 as it is the condition for the variety to be Calabi-Yau as shown in

proposition 2.

Diagram 10 This diagram encodes precisely the geometry of $L^{3,3,3}$. We briefly remind the reader that the $L^{a,b,c}$ family of geometry has the following conditions on its toric diagram:

- $a + b = c + d$ where (a, b, c, d) are the GLSM charges and they satisfy the constraint $a \leq c \leq b$. The charges $a, b, c, d \in \mathbb{Z}^+$ are pairwise coprime: $\gcd(a, c) = 1$, $\gcd(a, d) = 1$, $\gcd(b, c) = 1$ and $\gcd(b, d) = 1$.
- The 4 corner points of the toric diagram are specified by the vector $(0, 0)$, $(1, 0)$, (P, d) and (F, b)
- The coordinates of four corners obey the relation

$$dF - bP + c = 0 .$$

The perfect matching for this particular brane tiling is

$$P = \begin{pmatrix} & P_1 & P_2 & P_3 & P_4 & P_5 & P_6 & P_7 & P_8 & P_9 & P_{10} & P_{11} & P_{12} & P_{13} & P_{14} & P_{15} & P_{16} & P_{17} & P_{18} \\ X_1 & 1 & 0 & 0 & 0 & 1 & 0 & 0 & 1 & 0 & 0 & 0 & 0 & 1 & 0 & 0 & 0 & 1 & 0 \\ X_2 & 0 & 0 & 1 & 0 & 0 & 0 & 0 & 0 & 0 & 1 & 1 & 0 & 0 & 0 & 1 & 0 & 0 & 0 \\ X_3 & 1 & 1 & 0 & 0 & 0 & 0 & 1 & 1 & 1 & 0 & 0 & 1 & 1 & 1 & 0 & 0 & 0 & 0 \\ X_4 & 1 & 1 & 1 & 1 & 1 & 1 & 0 & 0 & 0 & 0 & 0 & 0 & 0 & 0 & 0 & 0 & 0 & 0 \\ X_5 & 0 & 0 & 0 & 0 & 0 & 0 & 1 & 0 & 0 & 0 & 1 & 1 & 0 & 0 & 0 & 1 & 0 & 0 \\ X_6 & 0 & 0 & 0 & 1 & 0 & 0 & 1 & 0 & 0 & 0 & 0 & 1 & 0 & 0 & 0 & 1 & 0 & 0 \\ X_7 & 0 & 1 & 0 & 0 & 0 & 1 & 0 & 0 & 1 & 0 & 0 & 0 & 0 & 1 & 0 & 0 & 0 & 1 \\ X_8 & 0 & 0 & 1 & 1 & 0 & 0 & 0 & 0 & 1 & 0 & 0 & 0 & 0 & 0 & 1 & 0 & 0 & 0 \\ X_9 & 0 & 0 & 0 & 0 & 1 & 1 & 0 & 0 & 0 & 0 & 1 & 0 & 0 & 0 & 0 & 1 & 1 & 1 \\ X_{10} & 1 & 1 & 1 & 0 & 0 & 0 & 0 & 0 & 0 & 0 & 1 & 1 & 1 & 1 & 1 & 0 & 0 & 0 \\ X_{11} & 0 & 0 & 0 & 1 & 0 & 0 & 1 & 1 & 1 & 1 & 0 & 0 & 0 & 0 & 0 & 0 & 0 & 0 \\ X_{12} & 0 & 0 & 0 & 0 & 0 & 0 & 1 & 1 & 1 & 0 & 0 & 1 & 1 & 1 & 0 & 1 & 1 & 1 \\ X_{13} & 1 & 1 & 1 & 0 & 1 & 1 & 0 & 0 & 0 & 0 & 1 & 0 & 0 & 0 & 0 & 0 & 0 & 0 \\ X_{14} & 0 & 0 & 0 & 1 & 1 & 1 & 0 & 0 & 0 & 0 & 0 & 0 & 0 & 0 & 1 & 1 & 1 & 1 \\ X_{15} & 0 & 0 & 0 & 0 & 0 & 0 & 1 & 1 & 1 & 1 & 1 & 0 & 0 & 0 & 0 & 0 & 0 & 0 \\ X_{16} & 0 & 0 & 0 & 0 & 0 & 0 & 0 & 0 & 0 & 0 & 1 & 1 & 1 & 1 & 1 & 1 & 1 & 1 \end{pmatrix} . \quad (3.22)$$

The charge matrix for F-terms is

$$Q_F = \begin{pmatrix} P_1 & P_2 & P_3 & P_4 & P_5 & P_6 & P_7 & P_8 & P_9 & P_{10} & P_{11} & P_{12} & P_{13} & P_{14} & P_{15} & P_{16} & P_{17} & P_{18} \\ 2 & -1 & 0 & 0 & -1 & 0 & 1 & -1 & 0 & 0 & 0 & -1 & 0 & 0 & 0 & 0 & 0 & 1 \\ 1 & 0 & 0 & 0 & -1 & 0 & 1 & -1 & 0 & 0 & 0 & -1 & 0 & 0 & 0 & 0 & 1 & 0 \\ 1 & 0 & 0 & 0 & -1 & 0 & 0 & 0 & 0 & 0 & 0 & -1 & 0 & 0 & 0 & 1 & 0 & 0 \\ 1 & 0 & -1 & 0 & 0 & 0 & 1 & -1 & 0 & 0 & 0 & -1 & 0 & 0 & 1 & 0 & 0 & 0 \\ 1 & -1 & 0 & 0 & 0 & 0 & 1 & -1 & 0 & 0 & 0 & -1 & 0 & 1 & 0 & 0 & 0 & 0 \\ 0 & 0 & 0 & 0 & 0 & 0 & 1 & -1 & 0 & 0 & 0 & -1 & 1 & 0 & 0 & 0 & 0 & 0 \\ 1 & 0 & -1 & 1 & -1 & 0 & -1 & 0 & 0 & 0 & 1 & 0 & 0 & 0 & 0 & 0 & 0 & 0 \\ 1 & 0 & -1 & 0 & 0 & 0 & 0 & -1 & 0 & 1 & 0 & 0 & 0 & 0 & 0 & 0 & 0 & 0 \\ 1 & -1 & 0 & 0 & 0 & 0 & 0 & -1 & 1 & 0 & 0 & 0 & 0 & 0 & 0 & 0 & 0 & 0 \\ 1 & -1 & 0 & 0 & -1 & 1 & 0 & 0 & 0 & 0 & 0 & 0 & 0 & 0 & 0 & 0 & 0 & 0 \end{pmatrix} . \quad (3.23)$$

The charge matrix for D-terms is

$$Q_D = \begin{pmatrix} P_1 & P_2 & P_3 & P_4 & P_5 & P_6 & P_7 & P_8 & P_9 & P_{10} & P_{11} & P_{12} & P_{13} & P_{14} & P_{15} & P_{16} & P_{17} & P_{18} \\ 0 & 0 & 0 & 0 & 0 & 0 & 0 & 0 & 0 & 0 & 0 & 0 & 0 & -1 & 1 & 0 & 0 & 0 \\ 0 & 0 & 0 & 0 & 0 & 0 & 0 & 0 & 0 & 0 & 0 & 0 & 0 & 0 & 0 & 1 & -1 & 0 \\ 0 & 0 & 0 & 0 & 0 & 0 & 0 & 0 & 0 & 0 & 0 & 0 & 0 & -1 & 0 & 1 & 0 & 0 \\ 0 & 0 & 0 & 0 & 0 & 1 & 0 & 0 & 0 & 0 & 0 & 0 & 0 & 0 & 0 & -1 & 0 & 0 \\ 0 & 0 & 0 & 0 & 0 & 0 & 0 & 0 & 0 & -1 & 0 & 0 & 0 & 0 & 1 & 0 & 0 & 0 \end{pmatrix} . \quad (3.24)$$

The total charge matrix Q_t therefore specifies how the 18 GLSM fields are charged under $U(1)^{15}$.

Diagram 11 This diagram contains three external edges, which excludes itself from being included in any of the classes of $L^{a,b,c}$, $Y^{p,q}$, $X^{p,q}$. It is also obvious that it is not any of the del Pezzo surfaces of abelian orbifolds. Therefore, this diagram is of new type of geometry that does not afford any known description. On the other hand, the perfect matching matrix for this particular brane tiling is

$$P = \begin{pmatrix} X_1 & P_1 & P_2 & P_3 & P_4 & P_5 & P_6 & P_7 & P_8 & P_9 & P_{10} & P_{11} & P_{12} & P_{13} & P_{14} & P_{15} & P_{16} & P_{17} & P_{18} & P_{19} & P_{20} \\ X_2 & 1 & 1 & 0 & 0 & 0 & 1 & 1 & 0 & 1 & 1 & 0 & 0 & 0 & 0 & 1 & 0 & 0 & 0 & 0 & 0 \\ X_3 & 1 & 1 & 1 & 1 & 1 & 0 & 0 & 0 & 0 & 0 & 0 & 0 & 0 & 0 & 1 & 1 & 1 & 1 & 0 & 0 \\ X_4 & 0 & 0 & 0 & 0 & 0 & 0 & 0 & 0 & 0 & 0 & 0 & 1 & 0 & 1 & 1 & 1 & 1 & 1 & 1 & 0 \\ X_5 & 0 & 1 & 0 & 0 & 1 & 0 & 1 & 0 & 0 & 1 & 0 & 0 & 0 & 1 & 0 & 0 & 0 & 0 & 0 & 1 \\ X_6 & 0 & 0 & 1 & 0 & 0 & 0 & 0 & 1 & 0 & 0 & 1 & 0 & 1 & 0 & 0 & 1 & 0 & 0 & 1 & 0 \\ X_7 & 1 & 0 & 0 & 1 & 0 & 1 & 0 & 0 & 1 & 0 & 0 & 1 & 0 & 0 & 1 & 0 & 1 & 1 & 1 & 0 \\ X_8 & 0 & 0 & 0 & 1 & 1 & 0 & 0 & 0 & 0 & 0 & 1 & 0 & 1 & 0 & 0 & 1 & 0 & 0 & 1 & 0 \\ X_9 & 0 & 0 & 0 & 0 & 0 & 1 & 1 & 1 & 0 & 0 & 0 & 0 & 1 & 0 & 0 & 0 & 0 & 1 & 1 & 0 \\ X_{10} & 1 & 1 & 1 & 0 & 0 & 0 & 0 & 0 & 1 & 1 & 1 & 0 & 0 & 0 & 1 & 1 & 0 & 0 & 0 & 0 \\ X_{11} & 0 & 0 & 0 & 0 & 0 & 0 & 0 & 0 & 1 & 1 & 1 & 0 & 1 & 0 & 0 & 0 & 0 & 0 & 0 & 0 \\ X_{12} & 1 & 1 & 1 & 1 & 1 & 1 & 1 & 0 & 0 & 0 & 0 & 0 & 0 & 0 & 0 & 0 & 0 & 0 & 0 & 0 \\ X_{13} & 0 & 1 & 0 & 0 & 1 & 0 & 1 & 0 & 0 & 1 & 0 & 0 & 1 & 1 & 0 & 0 & 0 & 0 & 0 & 0 \\ X_{14} & 0 & 0 & 1 & 0 & 0 & 0 & 0 & 1 & 0 & 0 & 0 & 0 & 0 & 0 & 1 & 0 & 0 & 0 & 1 & 0 \\ X_{15} & 0 & 0 & 0 & 1 & 1 & 0 & 0 & 0 & 0 & 0 & 1 & 1 & 1 & 1 & 0 & 0 & 0 & 1 & 1 & 0 \\ X_{16} & 0 & 0 & 0 & 0 & 0 & 1 & 1 & 1 & 0 & 0 & 0 & 0 & 0 & 0 & 0 & 0 & 0 & 0 & 1 & 1 & 1 \\ X_{17} & 0 & 0 & 0 & 0 & 0 & 0 & 0 & 0 & 1 & 1 & 1 & 1 & 1 & 1 & 0 & 0 & 0 & 0 & 0 & 0 & 0 \\ X_{18} & 0 & 0 & 0 & 0 & 0 & 0 & 0 & 0 & 0 & 0 & 0 & 0 & 0 & 0 & 1 & 1 & 1 & 1 & 1 & 1 & 1 \end{pmatrix}. \quad (3.25)$$

The charge matrix for F-terms is

$$Q_F = \begin{pmatrix} P_1 & P_2 & P_3 & P_4 & P_5 & P_6 & P_7 & P_8 & P_9 & P_{10} & P_{11} & P_{12} & P_{13} & P_{14} & P_{15} & P_{16} & P_{17} & P_{18} & P_{19} & P_{20} \\ 4 & -1 & -1 & -1 & 0 & -1 & 0 & 0 & -1 & 0 & 0 & 0 & 1 & 0 & -1 & 0 & 0 & 0 & 0 & 1 \\ 2 & 0 & -1 & 0 & 0 & -1 & 0 & 0 & 0 & 0 & 0 & 0 & 0 & 0 & -1 & 0 & 0 & 0 & 1 & 0 \\ 1 & 0 & 0 & 0 & -1 & 0 & 0 & 0 & 0 & 0 & 0 & 0 & 0 & 0 & -1 & 0 & 0 & 1 & 0 & 0 \\ 1 & 0 & 0 & -1 & 0 & 0 & 0 & 0 & 0 & 0 & 0 & 0 & 0 & 0 & -1 & 0 & 1 & 0 & 0 & 0 \\ 2 & -1 & 0 & -1 & 0 & 0 & 0 & 0 & -1 & 0 & 0 & 0 & 0 & 1 & 0 & 0 & 0 & 0 & 0 & 0 \\ 1 & 0 & 0 & -1 & 0 & 0 & 0 & 0 & -1 & 0 & 0 & 1 & 0 & 0 & 0 & 0 & 0 & 0 & 0 & 0 \\ 1 & 0 & -1 & 0 & 0 & 0 & 0 & 0 & -1 & 0 & 1 & 0 & 0 & 0 & 0 & 0 & 0 & 0 & 0 & 0 \\ 1 & -1 & 0 & 0 & 0 & 0 & 0 & 0 & -1 & 1 & 0 & 0 & 0 & 0 & 0 & 0 & 0 & 0 & 0 & 0 & 0 \\ 1 & 0 & -1 & 0 & 0 & -1 & 0 & 1 & 0 & 0 & 0 & 0 & 0 & 0 & 0 & 0 & 0 & 0 & 0 & 0 & 0 \\ 1 & -1 & 0 & 0 & 0 & -1 & 1 & 0 & 0 & 0 & 0 & 0 & 0 & 0 & 0 & 0 & 0 & 0 & 0 & 0 & 0 \\ 1 & -1 & 0 & -1 & 1 & 0 & 0 & 0 & 0 & 0 & 0 & 0 & 0 & 0 & 0 & 0 & 0 & 0 & 0 & 0 & 0 \end{pmatrix}. \quad (3.26)$$

The charge matrix for D-terms is

$$Q_D = \begin{pmatrix} P_1 & P_2 & P_3 & P_4 & P_5 & P_6 & P_7 & P_8 & P_9 & P_{10} & P_{11} & P_{12} & P_{13} & P_{14} & P_{15} & P_{16} & P_{17} & P_{18} & P_{19} & P_{20} \\ 0 & 0 & 0 & 0 & 0 & 0 & 0 & 0 & 0 & 0 & 0 & 0 & -1 & 0 & 1 & 0 & 0 & 0 & -1 & 0 \\ 0 & 0 & 0 & 0 & 0 & 0 & 0 & 0 & 0 & 0 & 0 & 0 & 0 & -1 & 0 & 0 & 0 & -1 & 1 & 0 \\ 0 & 0 & 0 & 0 & 0 & 0 & 0 & -1 & 0 & 0 & 0 & 1 & 0 & 0 & 0 & 1 & -1 & 0 & 0 & 0 \\ 0 & 0 & 0 & 0 & 0 & 0 & 0 & 0 & 0 & 0 & 0 & 0 & 0 & 0 & 0 & -1 & 1 & 0 & 0 & 0 \end{pmatrix}. \quad (3.27)$$

We can easily see that each row of the charge matrix Q_t sums up to zero, which indeed checks out to be a toric Calabi-Yau threefold. The 20 GLSM fields are thus charged under $U(1)^{17}$.

Area 7 Examples

We shall also present some examples from area 7 diagrams with their charge matrices in this section. The principle for selection of candidate is also the same as that in area 6: diagrams with no internal points are not chosen since they give non-chiral gauge theories.

Diagram 7 This diagram corresponds to the geometry prescribed by $X^{3,1}$, which has the required 5 external edges. The perfect matching matrix is given by

$$P = \begin{pmatrix} X_1 & P_1 & P_2 & P_3 & P_4 & P_5 & P_6 & P_7 & P_8 & P_9 & P_{10} & P_{11} & P_{12} & P_{13} & P_{14} & P_{15} & P_{16} & P_{17} & P_{18} & P_{19} & P_{20} & P_{21} & P_{22} & P_{23} & P_{24} \\ X_2 & 1 & 1 & 1 & 0 & 0 & 0 & 0 & 0 & 0 & 0 & 0 & 1 & 1 & 0 & 0 & 0 & 1 & 1 & 0 & 0 & 0 & 0 & 1 & 0 \\ X_3 & 1 & 0 & 1 & 1 & 0 & 1 & 1 & 0 & 0 & 0 & 1 & 0 & 0 & 0 & 0 & 0 & 0 & 1 & 0 & 1 & 0 & 1 & 0 & 0 \\ X_4 & 0 & 1 & 0 & 0 & 1 & 0 & 0 & 1 & 1 & 1 & 0 & 0 & 0 & 0 & 0 & 0 & 1 & 0 & 1 & 0 & 1 & 0 & 0 & 0 \\ X_5 & 1 & 0 & 0 & 1 & 0 & 0 & 1 & 0 & 0 & 0 & 0 & 1 & 0 & 1 & 1 & 0 & 0 & 0 & 0 & 0 & 0 & 0 & 0 & 0 \\ X_6 & 0 & 0 & 0 & 1 & 0 & 0 & 0 & 0 & 1 & 0 & 0 & 0 & 0 & 1 & 0 & 0 & 0 & 0 & 1 & 1 & 0 & 0 & 0 & 1 \\ X_7 & 1 & 0 & 0 & 0 & 0 & 0 & 1 & 1 & 0 & 0 & 0 & 1 & 0 & 0 & 0 & 0 & 1 & 1 & 0 & 0 & 1 & 1 & 1 & 0 \\ X_8 & 0 & 0 & 0 & 0 & 0 & 0 & 1 & 0 & 0 & 1 & 1 & 0 & 0 & 0 & 1 & 0 & 0 & 0 & 0 & 0 & 1 & 1 & 0 & 0 \\ X_9 & 0 & 0 & 0 & 0 & 0 & 0 & 0 & 1 & 1 & 0 & 0 & 1 & 1 & 1 & 0 & 1 & 0 & 0 & 0 & 0 & 0 & 0 & 1 & 1 \\ X_{10} & 1 & 1 & 1 & 1 & 1 & 1 & 0 & 0 & 0 & 0 & 0 & 0 & 0 & 0 & 0 & 0 & 1 & 1 & 1 & 1 & 0 & 0 & 0 & 0 \\ X_{11} & 0 & 1 & 0 & 0 & 1 & 0 & 0 & 0 & 0 & 1 & 0 & 0 & 0 & 0 & 1 & 0 & 1 & 0 & 1 & 0 & 1 & 0 & 1 & 0 & 0 \\ X_{12} & 0 & 0 & 1 & 0 & 0 & 1 & 0 & 0 & 0 & 1 & 0 & 1 & 0 & 1 & 0 & 1 & 0 & 1 & 0 & 1 & 0 & 1 & 0 & 1 & 1 \\ X_{13} & 1 & 0 & 0 & 1 & 0 & 0 & 1 & 1 & 1 & 0 & 0 & 1 & 0 & 1 & 0 & 0 & 0 & 0 & 0 & 0 & 0 & 0 & 0 & 0 & 0 \\ X_{14} & 0 & 1 & 1 & 0 & 1 & 1 & 0 & 0 & 0 & 1 & 1 & 0 & 1 & 0 & 1 & 1 & 0 & 0 & 0 & 0 & 0 & 0 & 0 & 0 & 0 \\ X_{15} & 0 & 1 & 1 & 0 & 0 & 0 & 0 & 0 & 1 & 1 & 1 & 0 & 1 & 0 & 0 & 0 & 0 & 0 & 0 & 0 & 0 & 0 & 0 & 0 & 0 \\ X_{16} & 0 & 0 & 0 & 1 & 1 & 1 & 0 & 0 & 0 & 0 & 0 & 0 & 1 & 1 & 1 & 0 & 0 & 1 & 1 & 0 & 0 & 0 & 0 & 0 & 1 \\ X_{17} & 0 & 0 & 0 & 0 & 0 & 0 & 1 & 1 & 1 & 1 & 1 & 0 & 0 & 0 & 0 & 0 & 0 & 0 & 0 & 0 & 1 & 1 & 0 & 0 & 0 \\ X_{18} & 0 & 0 & 0 & 0 & 0 & 0 & 0 & 0 & 0 & 0 & 0 & 1 & 1 & 1 & 1 & 1 & 0 & 0 & 0 & 0 & 0 & 0 & 1 & 1 & 1 \\ X_{19} & 0 & 0 & 0 & 0 & 0 & 0 & 0 & 0 & 0 & 0 & 0 & 0 & 0 & 0 & 0 & 0 & 1 & 1 & 1 & 1 & 1 & 1 & 1 & 1 & 1 \end{pmatrix}. \quad (3.28)$$

Taking the kernel of matrix P , we have the charge matrix for F-terms

$$Q_F = \begin{pmatrix} P_1 & P_2 & P_3 & P_4 & P_5 & P_6 & P_7 & P_8 & P_9 & P_{10} & P_{11} & P_{12} & P_{13} & P_{14} & P_{15} & P_{16} & P_{17} & P_{18} & P_{19} & P_{20} & P_{21} & P_{22} & P_{23} & P_{24} \\ 2 & 1 & -1 & -1 & 0 & 0 & 0 & 0 & 0 & 0 & 0 & -1 & 0 & 0 & 0 & 0 & -1 & 0 & 0 & 0 & 0 & 0 & 0 & 1 \\ 1 & 1 & -1 & 0 & 0 & 0 & 0 & 0 & 0 & 0 & 0 & -1 & 0 & 0 & 0 & 0 & -1 & 0 & 0 & 0 & 0 & 0 & 1 & 0 \\ 1 & 1 & -1 & 0 & 0 & 0 & -1 & 0 & 0 & 0 & 0 & 0 & 0 & 0 & 0 & 0 & -1 & 0 & 0 & 0 & 0 & 0 & 1 & 0 \\ 1 & 0 & 0 & 0 & 0 & 0 & -1 & 0 & 0 & 0 & 0 & 0 & 0 & 0 & 0 & 0 & -1 & 0 & 0 & 0 & 1 & 0 & 0 & 0 \\ 1 & 1 & -1 & -1 & 0 & 0 & 0 & 0 & 0 & 0 & 0 & 0 & 0 & 0 & 0 & 0 & -1 & 0 & 0 & 1 & 0 & 0 & 0 & 0 \\ 1 & 0 & 0 & -1 & 0 & 0 & 0 & 0 & 0 & 0 & 0 & 0 & 0 & 0 & 0 & 0 & -1 & 0 & 1 & 0 & 0 & 0 & 0 & 0 \\ 0 & 1 & -1 & 0 & 0 & 0 & 0 & 0 & 0 & 0 & 0 & 0 & 0 & 0 & 0 & 0 & -1 & 1 & 0 & 0 & 0 & 0 & 0 & 0 \\ 1 & 1 & -1 & 0 & -1 & 0 & 0 & 0 & 0 & 0 & 0 & -1 & 0 & 0 & 0 & 1 & 0 & 0 & 0 & 0 & 0 & 0 & 0 & 0 & 0 \\ 1 & 0 & 0 & -1 & 0 & 0 & 0 & 0 & 0 & 0 & 0 & -1 & 0 & 0 & 1 & 0 & 0 & 0 & 0 & 0 & 0 & 0 & 0 & 0 & 0 \\ 1 & 0 & -1 & 0 & 0 & 0 & 0 & 0 & 0 & 0 & 0 & -1 & 1 & 0 & 0 & 0 & 0 & 0 & 0 & 0 & 0 & 0 & 0 & 0 & 0 \\ 1 & 0 & -1 & 0 & 0 & 0 & -1 & 0 & 0 & 0 & 1 & 0 & 0 & 0 & 0 & 0 & 0 & 0 & 0 & 0 & 0 & 0 & 0 & 0 & 0 \\ 1 & -1 & 0 & 0 & 0 & 0 & -1 & 0 & 0 & 1 & 0 & 0 & 0 & 0 & 0 & 0 & 0 & 0 & 0 & 0 & 0 & 0 & 0 & 0 & 0 \\ 1 & -1 & 0 & -1 & 1 & 0 & 0 & -1 & 1 & 0 & 0 & 0 & 0 & 0 & 0 & 0 & 0 & 0 & 0 & 0 & 0 & 0 & 0 & 0 & 0 \\ 0 & 1 & -1 & 0 & -1 & 1 & 0 & 0 & 0 & 0 & 0 & 0 & 0 & 0 & 0 & 0 & 0 & 0 & 0 & 0 & 0 & 0 & 0 & 0 & 0 \end{pmatrix}. \quad (3.29)$$

The charge matrix for D-terms is then

$$Q_D = \begin{pmatrix} P_1 & P_2 & P_3 & P_4 & P_5 & P_6 & P_7 & P_8 & P_9 & P_{10} & P_{11} & P_{12} & P_{13} & P_{14} & P_{15} & P_{16} & P_{17} & P_{18} & P_{19} & P_{20} & P_{21} & P_{22} & P_{23} & P_{24} \\ 0 & -1 & 1 & 0 & 0 & 0 \\ 0 & 0 & 0 & 0 & 0 & 0 & 0 & 0 & 0 & 0 & 0 & 0 & 0 & 0 & 0 & 0 & 0 & 0 & 0 & -1 & 0 & 1 & 0 & 0 & 0 \\ 0 & 0 & 0 & 0 & 0 & 0 & 0 & 0 & 0 & 0 & 0 & 0 & 1 & 0 & 0 & 0 & 0 & 0 & 0 & 0 & 0 & 0 & -1 & 0 & 0 \\ 0 & 0 & 0 & 0 & 0 & 0 & 0 & 0 & 0 & 0 & 0 & 0 & -1 & 0 & 0 & 1 & 0 & 0 & 0 & 0 & 0 & 0 & 0 & 0 & 0 \\ 0 & 0 & 0 & 0 & 0 & 0 & 0 & 0 & 0 & 0 & 0 & 0 & 0 & -1 & 0 & 0 & 0 & 0 & 1 & 1 & -1 & 0 & 0 & 0 & 0 \\ 0 & -1 & 1 & 0 & 0 & 0 \end{pmatrix}. \quad (3.30)$$

As we can see from above, the total charge matrix Q_t has its rows summing up to zero. This is within the description of a toric Calabi-Yau threefold. The 24 GLSM fields are then charged under $U(1)^{21}$ according to the charge matrix Q_t .

Diagram 8 This diagram corresponds to $X^{3,2}$ as we can see that it has 5 external edges.

The perfect matching matrix is

$$P = \begin{pmatrix} & P_1 & P_2 & P_3 & P_4 & P_5 & P_6 & P_7 & P_8 & P_9 & P_{10} & P_{11} & P_{12} & P_{13} & P_{14} & P_{15} & P_{16} & P_{17} & P_{18} & P_{19} & P_{20} & P_{21} & P_{22} \\ X_1 & 1 & 0 & 1 & 0 & 0 & 0 & 0 & 1 & 0 & 1 & 0 & 0 & 0 & 1 & 1 & 0 & 0 & 0 & 0 & 0 & 0 & 0 \\ X_2 & 0 & 1 & 0 & 0 & 0 & 0 & 1 & 1 & 0 & 1 & 0 & 0 & 0 & 0 & 0 & 0 & 0 & 0 & 0 & 0 & 1 & 0 \\ X_3 & 1 & 0 & 1 & 1 & 1 & 1 & 0 & 0 & 0 & 0 & 0 & 0 & 0 & 0 & 1 & 0 & 1 & 0 & 1 & 0 & 1 & 0 \\ X_4 & 0 & 1 & 0 & 0 & 0 & 0 & 0 & 0 & 0 & 0 & 0 & 0 & 0 & 1 & 0 & 1 & 0 & 1 & 0 & 1 & 0 & 0 \\ X_5 & 1 & 0 & 0 & 1 & 1 & 0 & 1 & 0 & 1 & 0 & 0 & 1 & 1 & 0 & 0 & 0 & 0 & 0 & 0 & 0 & 0 & 0 \\ X_6 & 0 & 1 & 0 & 1 & 0 & 0 & 0 & 0 & 1 & 0 & 1 & 0 & 0 & 0 & 0 & 1 & 1 & 0 & 0 & 0 & 0 & 0 \\ X_7 & 1 & 0 & 0 & 0 & 1 & 0 & 1 & 0 & 1 & 0 & 0 & 0 & 1 & 0 & 1 & 1 & 0 & 0 & 1 & 1 & 1 & 0 \\ X_8 & 0 & 0 & 0 & 0 & 0 & 0 & 0 & 1 & 0 & 1 & 1 & 1 & 1 & 1 & 1 & 0 & 1 & 0 & 1 & 0 & 0 & 1 \\ X_9 & 0 & 0 & 0 & 0 & 0 & 0 & 0 & 0 & 1 & 0 & 0 & 0 & 0 & 0 & 1 & 0 & 1 & 0 & 1 & 0 & 1 & 1 \\ X_{10} & 1 & 1 & 1 & 1 & 1 & 1 & 1 & 1 & 0 & 0 & 0 & 0 & 0 & 0 & 0 & 0 & 0 & 0 & 0 & 0 & 0 & 0 \\ X_{11} & 0 & 0 & 1 & 0 & 0 & 1 & 0 & 1 & 0 & 0 & 1 & 0 & 0 & 1 & 0 & 0 & 0 & 0 & 0 & 0 & 0 & 1 \\ X_{12} & 0 & 1 & 1 & 0 & 0 & 1 & 0 & 1 & 0 & 1 & 1 & 0 & 0 & 1 & 0 & 0 & 0 & 0 & 0 & 0 & 0 & 0 \\ X_{13} & 0 & 0 & 0 & 1 & 0 & 0 & 0 & 0 & 0 & 0 & 1 & 0 & 0 & 0 & 0 & 1 & 1 & 0 & 0 & 0 & 0 & 1 \\ X_{14} & 0 & 0 & 0 & 0 & 1 & 1 & 0 & 0 & 0 & 0 & 0 & 1 & 1 & 0 & 0 & 0 & 0 & 1 & 1 & 0 & 0 & 1 \\ X_{15} & 0 & 0 & 0 & 0 & 0 & 0 & 1 & 1 & 0 & 0 & 0 & 0 & 0 & 0 & 0 & 0 & 0 & 0 & 0 & 0 & 1 & 1 \\ X_{16} & 0 & 0 & 0 & 0 & 0 & 0 & 0 & 0 & 1 & 1 & 1 & 1 & 1 & 1 & 0 & 0 & 0 & 0 & 0 & 0 & 0 & 0 \\ X_{17} & 0 & 0 & 0 & 0 & 0 & 0 & 0 & 0 & 0 & 0 & 0 & 0 & 0 & 1 & 1 & 1 & 1 & 1 & 1 & 1 & 1 & 1 \end{pmatrix}. \quad (3.31)$$

The kernel of P then gives us the charge matrix for F-terms

$$Q_F = \begin{pmatrix} P_1 & P_2 & P_3 & P_4 & P_5 & P_6 & P_7 & P_8 & P_9 & P_{10} & P_{11} & P_{12} & P_{13} & P_{14} & P_{15} & P_{16} & P_{17} & P_{18} & P_{19} & P_{20} & P_{21} & P_{22} \\ 2 & 1 & -1 & -1 & 0 & 0 & -1 & 0 & 0 & 0 & 0 & 0 & 0 & 0 & -1 & 0 & 0 & 0 & 0 & 0 & 0 & 1 \\ 0 & 1 & 0 & 0 & 0 & 0 & -1 & 0 & 1 & -1 & 0 & 0 & 0 & 0 & -1 & 0 & 0 & 0 & 0 & 0 & 1 & 0 \\ 0 & 1 & 0 & 0 & -1 & 0 & 0 & 0 & 1 & -1 & 0 & 0 & 0 & 0 & -1 & 0 & 0 & 0 & 0 & 1 & 0 & 0 \\ 1 & 0 & 0 & 0 & -1 & 0 & 0 & 0 & 0 & 0 & 0 & 0 & 0 & -1 & 0 & 0 & 0 & 1 & 0 & 0 & 0 & 0 \\ 0 & 1 & 0 & -1 & 0 & 0 & 0 & 0 & 1 & -1 & 0 & 0 & 0 & 0 & -1 & 0 & 0 & 1 & 0 & 0 & 0 & 0 \\ 1 & 0 & 0 & -1 & 0 & 0 & 0 & 0 & 0 & 0 & 0 & 0 & 0 & -1 & 0 & 1 & 0 & 0 & 0 & 0 & 0 & 0 \\ -1 & 1 & 0 & 0 & 0 & 0 & 0 & 0 & 1 & -1 & 0 & 0 & 0 & 0 & -1 & 1 & 0 & 0 & 0 & 0 & 0 & 0 \\ 2 & 0 & -1 & 0 & -1 & 0 & 0 & 0 & -1 & 0 & 0 & 0 & 0 & 1 & 0 & 0 & 0 & 0 & 0 & 0 & 0 & 0 \\ 1 & 0 & 0 & 0 & -1 & 0 & 0 & 0 & -1 & 0 & 0 & 0 & 1 & 0 & 0 & 0 & 0 & 0 & 0 & 0 & 0 & 0 \\ 1 & 0 & 0 & -1 & 0 & 0 & 0 & 0 & -1 & 0 & 0 & 1 & 0 & 0 & 0 & 0 & 0 & 0 & 0 & 0 & 0 & 0 \\ 1 & 0 & -1 & 0 & 0 & 0 & 0 & 0 & -1 & 0 & 1 & 0 & 0 & 0 & 0 & 0 & 0 & 0 & 0 & 0 & 0 & 0 \\ 1 & 0 & -1 & 0 & 0 & 0 & -1 & 1 & 0 & 0 & 0 & 0 & 0 & 0 & 0 & 0 & 0 & 0 & 0 & 0 & 0 & 0 \\ 1 & 0 & -1 & 0 & -1 & 1 & 0 & 0 & 0 & 0 & 0 & 0 & 0 & 0 & 0 & 0 & 0 & 0 & 0 & 0 & 0 & 0 \end{pmatrix}. \quad (3.32)$$

Correspondingly, we obtain the charge matrix for D-terms

$$Q_D = \begin{pmatrix} P_1 & P_2 & P_3 & P_4 & P_5 & P_6 & P_7 & P_8 & P_9 & P_{10} & P_{11} & P_{12} & P_{13} & P_{14} & P_{15} & P_{16} & P_{17} & P_{18} & P_{19} & P_{20} & P_{21} & P_{22} \\ 0 & 0 & 0 & 0 & 0 & 0 & 0 & 0 & 0 & 0 & 0 & 0 & 0 & 0 & 0 & 0 & 0 & -1 & 1 & 0 & 0 & 0 \\ 0 & 0 & 0 & 0 & 0 & 0 & 0 & 0 & 0 & 0 & 0 & 0 & 0 & 0 & 0 & 0 & 0 & 0 & 0 & 1 & 0 & 0 \\ 0 & 0 & 0 & 0 & 0 & 0 & 0 & 1 & 0 & 0 & 0 & 0 & 0 & 0 & 0 & 0 & 0 & 0 & 0 & 0 & -1 & 0 \\ 0 & 0 & 0 & 0 & 0 & 0 & 0 & 0 & 0 & 0 & 0 & 1 & -1 & 0 & -1 & 0 & 1 & 0 & 0 & 0 & 0 & 0 \\ 0 & 0 & 0 & 0 & 0 & 0 & 0 & -1 & 0 & 0 & 0 & 0 & 1 & 0 & 1 & 0 & 0 & 0 & -1 & 0 & 0 & 0 \\ 0 & 0 & 0 & 0 & 0 & 0 & 0 & 0 & 0 & 0 & 0 & 0 & 0 & 0 & 0 & 0 & 0 & 0 & -1 & 1 & 0 & 0 \end{pmatrix}. \quad (3.33)$$

Assuringly, this example also gives us the charge matrix of a toric Calabi-Yau threefold. The corresponding 22 GLSM fields are therefore charged under $U(1)^{19}$ with charges specified by Q_t .

we have to full information on how the $U(1)$ gauge groups acts on the GLSM fields. The resulting variety is a toric Calabi-Yau threefold as shown by the fact that the charge matrix has its rows adding up to 0.

Chapter 4

Conclusions

In chapter 2, we have reviewed the foundations of string theory and saw that the need to make contact with low-energy four-dimensional gauge dynamics from string theory is natural and it led us to consider the construction of $\mathcal{N} = 1$ gauge theories using D-branes probing background singular geometry. Since the initialisation of quiver gauge theory in [24], efforts are devoted to construction of $\mathcal{N} = 1$ superconformal quiver gauge theories living on D3-branes probing singular Calabi-Yau. This has led to a series of unifying application of concepts such as Hyper-Kähler quotients, McKay correspondence finite group representations. However, after the introduction of brane tilings, the connection between gauge theories on D3-branes and toric CY 3-folds they probe is greatly simplified. While given an arbitrary toric singularity there are well-defined methods for obtaining the corresponding brane tiling, it is of great interest to work out catalogues of explicit examples. Such databases are useful, for example, for uncovering general properties of these theories and for identifying the best models for specific applications.

In chapter 3, we classified all toric CY 3-folds with toric diagrams up to area 8 and constructed a brane tiling for each of them. To do so, we developed implementations of dimer model techniques specifically tailored for partial resolution. We also created computational modules for a wide range of manipulations and computations involving brane tilings. They can be accessed at [158].

There are various directions for future investigation. First, additional information can be added to our catalogue. We found one brane tiling for every toric CY_3 but, generically,

each geometry is associated to more than one brane tiling. These so-called *toric phases* are related to each other by Seiberg duality and it would be interesting to provide a complete classification of them for the geometries in our list. Ideally, we would also like to determine extra data such as R -charges, j -invariants for the dessins, etc.

In future work, we plan to use our classification of brane tilings as the starting point for local model building of Standard Model (SM)-like theories with realistic spectra, hierarchies of masses, flavor mixings, etc. The main idea of this kind of construction is to consider a singularity that gives rise to a reasonable spectrum, such as the cone over dP_0 and embed it into a slightly larger one, such as the cone over dP_3 . This particular example was studied in great detail in [86, 87], with encouraging results. The finite size of the resolved cycles map to non-vanishing vevs for the scalar components of some bifundamental chiral multiplets. By construction, the resulting low energy theory is the desired SM quiver, but with the vevs appearing as new parameters that can be tuned to control the flavor structure. These vevs appear in very specific ways in the superpotential, leading to a constrained and predictive scenario. We will undertake a systematic large scale investigation of local model building using the entire set of area 6 to 8 toric CY 3-folds as parent geometries. We will identify those that are phenomenologically promising and work out the detailed features of the low energy theories.

Appendix A

A.1 Quick Review on String Theory

A.1.1 The Bosonic String

In this section, let us reiterate some basic elements of string theory[1, 3, 4] . As with point particle physics, the evolution of point particle is recorded in world line and we analyse the system using Feynman diagram that captures possible configuration of world lines as well as junction of world lines to represent the interactions. In string theory, the counterpart of world line is *world sheet* of a string and the perturbation expansions collect world sheets of different topologies. These topologies have important consequences to differentiate string theory from QFT. The interaction structure is uniquely determined by free theory and the interactions do not come from singularities in joining world sheets, which protects it from UV divergences. For the world sheet of the string under discussion, we can construct the string sigma-model as in eq. (A.1) which reduces to the Nambu-Goto action in ?? using classical equation of motion,

$$S_\sigma = -\frac{T}{2} \int \sqrt{-h} h^{\alpha\beta} \eta_{\mu\nu} \partial_\alpha X^\mu \partial_\beta X^\nu d\sigma d\tau , \quad (\text{A.1})$$

$$S_{\text{NG}} = -T \int d\sigma d\tau \sqrt{(\dot{X} \cdot X')^2 - \dot{X}^2 X'^2} = -T \int d\sigma d\tau \sqrt{|\det G(X)|} , \quad (\text{A.2})$$

where $h_{\alpha\beta}(\sigma, \tau)$ is the auxiliary world-sheet metric, $h = \det(h_{\alpha\beta})$, $h^{\alpha\beta}$ is the inverse and $G_{\alpha\beta} = \partial_\alpha X^\mu \partial_\beta X^\nu \eta_{\mu\nu}$ is the pull-back metric on world sheet. The spacetime coordinates $X^\mu(\sigma, \tau)$ are the embeddings of world-sheet inside spacetime. To quantize this classical

action, one needs to use Feynman path integral with gauge fixing and local symmetries. Most importantly, when one keeps conformal symmetry in quantum level, the space-time dimension is required to be $D = 26$ and analogous analysis shows that $D = 10$ for superstring. The parameter τ is the world-sheet time and σ parametrises the string at a given time. For closed string, the periodicity is chosen to be π and one then identifies the both ends of the string $X^\mu(\sigma, \tau) = X^\mu(\sigma + \pi, \tau)$. For open strings, we have Neumann and Dirichlet boundary conditions. The Dirichlet boundary condition then chooses us a spacetime hypersurface on which open strings can end. These physical objects are called D-branes which will be the main object under discussion in our first chapter.

The action in eq. (A.1) consists of the following symmetries that can be used to bring the metric $h_{\alpha\beta}$ into a simpler form:

- *Poincaré transformations.* These are global symmetries from the view of world-sheet

$$\delta X^\mu = a_\nu^\mu X^\nu + b^\mu, \quad (\text{A.3})$$

where the constants a_ν^μ represent infinitesimal Lorentz transformations and they are anti-symmetric. The parameters b^μ are from spacetime translation.

- *Reparametrisations.* The world-sheet is described by two coordinates τ and σ and the change in the parametrisation should leave the action invariant. Specifically, they are *diffeomorphisms*:

$$\sigma^\alpha \rightarrow f^\alpha(\sigma) = \sigma'^\alpha, \quad h_{\alpha\beta}(\sigma) = \frac{\partial f^\gamma}{\partial \sigma^\alpha} \frac{\partial f^\delta}{\partial \sigma^\beta} h_{\gamma\delta}(\sigma'). \quad (\text{A.4})$$

- *Weyl transformations.* The action is also invariant under local rescaling

$$h_{\alpha\beta} \rightarrow e^{\phi(\sigma, \tau)} h_{\alpha\beta}. \quad (\text{A.5})$$

The reparametrisation and Weyl rescaling then can be used to fix the gauge to bring the

metric into

$$h_{\alpha\beta} = \eta_{\alpha\beta} = \begin{pmatrix} -1 & 0 \\ 0 & 1 \end{pmatrix}. \quad (\text{A.6})$$

After this choice of gauge fixing, the action has a simple form

$$S = \frac{T}{2} \int d^2\sigma (\dot{X}^2 - X'^2), \quad (\text{A.7})$$

from which we can derive the equation of motion for field X with the assumption that there are no topological obstruction to the choice of flat metric $\eta_{\alpha\beta}$. The EoM is then

$$\partial_\alpha \partial^\alpha X^\mu = 0 \quad \text{or} \quad \left(\frac{\partial^2}{\partial \sigma^2} - \frac{\partial^2}{\partial \tau^2} \right) X^\mu = 0.$$

Now we can solve for its solutions with constraints from imposing $T_{\alpha\beta} = 0$. Since the EoM is a wave equation, therefore we can switch to *light-cone* coordinates $\sigma^\pm = \tau \pm \sigma$ that will give us solutions in terms of independent *left-mover* and *right-mover*

$$X^\mu(\tau, \sigma) = X_R^\mu(\tau - \sigma) + X_L^\mu(\tau + \sigma), \quad (\text{A.8})$$

with constraints $T_{\alpha\beta} = 0$ becoming

$$\begin{aligned} T_{++} &= \partial_+ X^\mu \partial_+ X_\mu = 0, \\ T_{--} &= \partial_- X^\mu \partial_- X_\mu = 0, \end{aligned} \quad (\text{A.9})$$

and vanishing of trace goes to $T_{+-} = T_{-+} = 0$. Following the route of canonical quantisation, one needs to find the classical Poisson brackets from the action in terms of field X^μ and its momentum, then substitute mode expansions for left and right movers to obtain the Poisson bracket in terms of modes for left and right mover α_m^μ and $\tilde{\alpha}_m^\mu$. After this, one gets

$$\begin{aligned} [\alpha_m^\mu, \alpha_n^\mu]_{\text{P.B.}} &= [\tilde{\alpha}_m^\mu, \tilde{\alpha}_n^\mu]_{\text{P.B.}} = im\eta^{\mu\nu} \delta_{m+n,0}, \\ [\alpha_m^\mu, \tilde{\alpha}_n^\mu]_{\text{P.B.}} &= 0. \end{aligned} \quad (\text{A.10})$$

Replacing the Poisson brackets by commutators, we have

$$[\alpha_m^\mu, \alpha_n^\mu] = [\tilde{\alpha}_m^\mu, \tilde{\alpha}_n^\mu] = m\eta^{\mu\nu}\delta_{m+n,0}, \quad (\text{A.11})$$

which becomes the following after rescaling $a_m^\mu = \frac{1}{\sqrt{m}}\alpha_m^\mu$ and $a_m^{\mu\dagger} = \frac{1}{\sqrt{m}}\alpha_{-m}^\mu$ for $m > 0$,

$$[a_m^\mu, a_n^\mu] = [\tilde{a}_m^\mu, \tilde{a}_n^\mu] = \eta^{\mu\nu}\delta_{m,n} \quad \text{for } m, n > 0. \quad (\text{A.12})$$

The higher vibrational states are then obtained by applying the ground state $|0\rangle$ the raising operators $a_m^{\mu\dagger}$. Note here we get the negative norm state by observing that $[a_m^0, a_m^{0\dagger}] = -1$. These states indicate instability of the vacuum, therefore they need to be removed. We will shortly review how this is done and the introduction of supersymmetry on the world-sheet and space-time thus becomes necessary.

The above analysis seems to have exhausted the symmetries within the theory by choosing the gauge to fix the metric. However, there is one more residual symmetry from varying metric reparametrisation simultaneously:

$$\partial^\alpha \xi^\beta + \partial^\beta \xi^\alpha = \Lambda \eta^{\alpha\beta}, \quad (\text{A.13})$$

where Λ is the infinitesimal parameter for Weyl rescaling and ξ^α is that for reparametrisation. In other words, these are reparametrisations that can be compensated by Weyl rescalings. More importantly, the generators for these symmetries satisfy the *Virasoro algebra* classically:

$$[L_m, L_n]_{\text{P.B.}} = i(m-n)L_{m+n},$$

where L_m and \tilde{L}_m comes from the Fourier expansions of T_{--} and T_{++} :

$$L_m = \frac{1}{2} \sum_{n=-\infty}^{+\infty} \alpha_{m-n} \cdot \alpha_n \quad \text{and} \quad \tilde{L}_m = \frac{1}{2} \sum_{n=-\infty}^{+\infty} \tilde{\alpha}_{m-n} \cdot \tilde{\alpha}_n. \quad (\text{A.14})$$

On the other hand, the quantum version of this algebra is

$$[L_m, L_n] = (m - n)L_{m+n} + \frac{c}{12}m(m^2 - 1)\delta_{m+n,0}, \quad (\text{A.15})$$

where c is the dimension of spacetime as we shall see later. This addition of c -number to the classical Virasoro algebra essentially comes from the fact that we need normal order when $m + n = 0$ when quantising the theory. Thus any quantum corrections to the classical algebra should only give a term of the form $A(m)\delta_{m+n,0}$, where $A(m)$ is an m -dependent c -number. This algebra is called the central extension of the classical one and the c -number is called the anomaly term in the algebra. The determination of the specific form of $A(m)$ ¹ can be found in [1] Quantum mechanically, we need to fix the normal ordering ambiguity. Specifically, by observing eq. (A.12) and eq. (A.14) carefully, we see that we only need to consider L_0 and \tilde{L}_0 whose correction needs a constant a . If we impose the condition that the zero mode of energy momentum tensor to vanish as in the classical counter-part, we need the following condition

$$(L_0 - a)|\phi\rangle = 0 \quad \text{and} \quad (\tilde{L}_0 - a)|\phi\rangle = 0, \quad (\text{A.16})$$

where $|\phi\rangle$ can be any physical on-shell state. Before we move onto the definition of spurious state and the determination of constant a and dimension D , let us motivate the reason we study the so called *spurious states* and the importance of them in eliminating negative norm states.

First, let us denote the open-string ground state of momentum k^μ as $|0; k\rangle$. The mass-shell condition eq. (A.16) implies that $\alpha'k^2 = a$. Now consider the first excited state $\zeta \cdot \alpha_{-1}|0; k\rangle$, where $\zeta^\mu(k)$ is the polarisation vector with D independent components before applying gauge constraints. The mass-shell condition now becomes $\alpha'k^2 = a - 1$ and the condition $L_1(\zeta \cdot \alpha_{-1})|0; k\rangle = 0$ implies $\zeta \cdot k = 0$ using Virasoro algebra. The norm of these states is given by $\zeta \cdot \zeta$ and each state has $D - 1$ allowed polarisations. Now we have the

¹In short, we can find some recursion relation of $A(m)$ using Jacobi identity of L_m whose solution is $A(m) = c_3m^3 + c_1m$. Then we can inspect the commutators $\langle 0|[L_1, L_{-1}]|0\rangle$ and $\langle 0|[L_2, L_{-2}]|0\rangle$ to determine the $A(m)$.

liberty of choosing k to lie within the plane $(0, 1)$ and ζ normal to k have positive norm since they are now space-like. On the other hand, if we choose a such that $k^2 > 0$ meaning first excited state being a tachyon, k can be chosen to have no time component. Then ζ becomes time like and has negative norm. If a is chosen to make $k^2 < 0$, k can be chosen to only have time component and ζ has positive norm. Finally, if $k^2 = 0$, ζ also has zero norm. Therefore, we can see that the choice of constant a has a direct impact in elimination of zero norm states.

Together with the conditions for a physical state $|\phi\rangle$

$$(L_m - a\delta_{m,0})|\phi\rangle = 0 \quad m \geq 0, \quad (\text{A.17})$$

and the definition of *spurious* states $|\psi\rangle^2$

$$(L_0 - a)|\psi\rangle = 0 \quad \text{and} \quad \langle\phi|\psi\rangle = 0, \quad (\text{A.18})$$

one can obtain the value of $a = 1$. [3, 1, 4] Following this route, we can find that the spacetime dimension³ $D = 26$. This choice of $D = 26$ and $a = 1$ essentially gives the boundary between (1) regions containing negative norm states and (2) regions where the negative norm states are absent. The theory with extra set of zero-norm states is the most interesting one to study. This is because the zero-norm states must decouple from S matrix describing physical processes by some underlying principle analogous to gauge invariance in the field theory. So the occurrence of extra zero-norm states indicates an enhanced gauge invariance in this theory.

It is also worthwhile to do a short review on the spectrum of bosonic string with the choice of values $a = 1$ and $D = 26$. Let us concentrate on the closed string. We know that

²One such example can be $|\psi\rangle = \sum_{n=1}^{\infty} L_{-n}|\chi_n\rangle$ with $(L_0 - a + n)|\chi_n\rangle$ and any such state can be written as $|\psi\rangle = L_{-1}|\chi_1\rangle + L_{-2}|\chi_2\rangle$ as a result of Virasoro algebra. One can check that states of such form indeed has zero norm and is orthogonal to any physical states.

³Here we consider some zero-norm spurious states of the form $|\psi\rangle = (L_{-2} + \gamma L_{-1}^2)|\tilde{\chi}\rangle$, with the requirements $(L_0 + 1)|\tilde{\chi}\rangle$ and $L_m|\tilde{\chi}\rangle = 0$ for $m > 0$ to ensure the mass-shell condition $(L_0 - 1)|\psi\rangle = 0$. The constants γ and D are determined to be $3/2$ and 26 by imposing the conditions $L_1|\psi\rangle = 0$ and $L_2|\psi\rangle = 0$

the mass of states are given by

$$\alpha' M^2 = 4(N - 1) = 4(\tilde{N} - 1), \tag{A.19}$$

with N and \tilde{N} being number operators for left and right movers. The first few excited states are as follows:

- The ground state $|0; k\rangle$ is a tachyon with $\alpha' M^2 = -4$.
- At the level of $N = 1$, there are $24^2 = 576$ states of the form

$$|\Omega^{ij}\rangle = \alpha_{-1}^i \tilde{\alpha}_{-1}^j |0; k\rangle ,$$

which is a tensor product of two massless vectors from left and right mover respectively. The important observation is that the symmetric traceless part of this tensor product transforms under $SO(24)$ as a massless spin-two particle which we identify with the *graviton*. The trace is then a massless scalar, which we recognise as the *dilaton*. The anti-symmetric part is then a second-rank tensor under $SO(24)$.

A.1.2 Strings with World-Sheet Supersymmetry

In previous section, we briefly sketched some elementary aspects of bosonic string theory. This theory is unsatisfactory in two respects. Firstly, the closed-string spectrum contains a tachyon which has an imaginary mass. If one decides to include open string, then we have an additional open string tachyons. Tachyons are unphysical since they indicate in unstable vacuum. However, the fate of open-string tachyons is understood as the decay of D-branes into closed string radiation.[7]. The counter-part for closed-string has not yet been offered clear interpretation. Lastly, the bosonic string theory does not contain fermions in its spectrum for which we need to make contact with Standard Model. It turns out that the inclusion of fermions in the spectrum of string theory require *supersymmetry*, a symmetry that relates fermions and bosons. The extended theory is called *superstring theory*.

There are two formalisms present to infuse supersymmetry into bosonic string theory

- *The Ramond-Neveu-Schwarz* (RNS) formalism introduces supersymmetry on the world-sheet.
- *The Green-Schwarz* (GS) formalism is supersymmetric in 10D Minkowski spacetime and this can be generalised into other background geometries.

In this section, we shortly review the RNS formalism, which is equivalent to GS formalism in 10D Minkowski spacetime.

The starting point of this approach is to pair each bosonic field $X^\mu(\sigma, \tau)$ with a fermionic super-partner $\psi^\mu(\sigma, \tau)$. This new field is a 2-component spinor on the world-sheet and a vector under Lorentz transformation in the target spacetime. To incorporate fermions on the 2D world-sheet, we supplement the action in eq. (A.7) with a 2D Dirac action

$$S = -\frac{1}{2\pi} \int d^2\sigma (\partial_\alpha X_\mu \partial^\alpha X^\mu + \bar{\psi}^\mu \rho^\alpha \partial_\alpha \psi_\mu), \quad (\text{A.20})$$

where we set $\alpha' = 1/2$ or $T = 1/\pi$. The 2D Dirac matrices obey the Dirac algebra

$$\{\rho^\alpha, \rho^\beta\} = 2\eta^{\alpha\beta}, \quad (\text{A.21})$$

and the fermionic fields obey normal anti-commutation relations.

The action in eq. (A.20) can also be written in terms of light-cone coordinates

$$S = \frac{1}{\pi} \int d^2\sigma (2\partial_+ X \partial_- X + i\psi_- \partial_+ \psi_- + i\psi_+ \partial_- \psi_+), \quad (\text{A.22})$$

using the fermionic field $\psi^\mu = \begin{pmatrix} \psi_-^\mu \\ \psi_+^\mu \end{pmatrix}$ and Dirac conjugation for a spinor being $\bar{\psi} = \psi^\dagger \beta$ and $\beta = i\rho^0$ with appropriate choice of basis for Dirac matrices. Such arrangement of action gives the equation of motion for spinors to be

$$\partial_+ \psi_- = 0 \quad \text{and} \quad \partial_- \psi_+ = 0, \quad (\text{A.23})$$

which simply describes left and right moving waves. With these EoM, we can derive the mode expansion of the spinor fields and use canonical quantisation to find the spectrum of

the theory as in the bosonic string case. However, the negative-norm states also appear. The decoupling of negative norm states in the bosonic string theory requires the Virasoro constraints in eq. (A.16) and eq. (A.17) which in turn require special values for $a = 1$ and spacetime dimension $D = 26$. Following the similar strategy, we can use the *superconformal symmetry* to eliminate these negative norm states. The constraints used here are the super-Virasoro constraints which upon quantising requires the spacetime dimension to be $D = 10$.

To construct the super-Virasoro conditions, we need to find the conserved currents associated to global symmetries. In this case, they are the energy momentum tensor from translation symmetry and the supercurrent from supersymmetry. The energy momentum tensor is

$$T_{\alpha\beta} = \partial_\alpha X^\mu \partial_\beta X_\mu + \frac{1}{4} \bar{\psi}^\mu \rho_\alpha \partial_\beta \psi_\mu + \frac{1}{4} \bar{\psi}^\mu \rho_\beta \partial_\alpha \psi_\mu - (\text{trace}) . \quad (\text{A.24})$$

On the other hand, the supercurrent can be found using Nöether method by taking the supersymmetry parameter ϵ to be non-constant. We have the current to take the specific form

$$J_A^\alpha = -\frac{1}{2} (\rho^\beta \rho_\alpha \psi_\mu)_A \partial_\beta X^\mu . \quad (\text{A.25})$$

These currents can be written in terms of light-cone coordinates can used to eliminate negative norm states with the conditions from superconformal symmetry. In such spirit, we have the conditions to be

$$J_+ = J_- = T_{++} = T_{--} = 0 . \quad (\text{A.26})$$

Before we discuss the actual quantisation and elimination of negative norm states of the theory, we need to know that there are different boundary conditions for world-sheet spinors that lead to different sectors in the final theory. These are the periodic and anti-periodic boundary conditions from the spinors. The boundary term from variation of the action shows how this arises

$$\delta S \sim \int d\tau [(\psi_+ \delta\psi_+ - \psi_- \delta\psi_-)|_{\sigma=\pi} - (\psi_+ \delta\psi_+ - \psi_- \delta\psi_-)|_{\sigma=0}] . \quad (\text{A.27})$$

Therefore, we have 2 ways for the above term to vanish $\psi_+^\mu = \pm \psi_-^\mu$.

- *Ramond boundary condition:* In this case, we have $\psi_+^\mu|_{\sigma=\pi} = \psi_-^\mu|_{\sigma=\pi}$. They give rise

to target spacetime fermions and the mode expansion is as follows

$$\begin{aligned}\psi_-^\mu(\sigma, \tau) &= \frac{1}{\sqrt{2}} \sum_{n \in \mathbb{Z}} d_n^\mu e^{-in(\tau-\sigma)}, \\ \psi_+^\mu(\sigma, \tau) &= \frac{1}{\sqrt{2}} \sum_{n \in \mathbb{Z}} d_n^\mu e^{-in(\tau+\sigma)},\end{aligned}\tag{A.28}$$

where the Majorana condition requires $d_{-n}^\mu = d_n^{\mu\dagger}$.

- *Neveu-Schwarz boundary condition*: This has a relative minus sign between components of the spinor: $\psi_+^\mu|_{\sigma=\pi} = -\psi_-^\mu|_{\sigma=\pi}$. This boundary condition gives rise to spacetime boson. The mode expansion is then

$$\begin{aligned}\psi_-^\mu(\sigma, \tau) &= \frac{1}{\sqrt{2}} \sum_{r \in \mathbb{Z}+1/2} b_r^\mu e^{-in(\tau-\sigma)}, \\ \psi_+^\mu(\sigma, \tau) &= \frac{1}{\sqrt{2}} \sum_{r \in \mathbb{Z}+1/2} b_r^\mu e^{-in(\tau+\sigma)}.\end{aligned}\tag{A.29}$$

On the other hand, the closed string has left and right movers. We have periodic and anti-periodic for both movers, therefore we have four different sectors. States in NS-NS and R-R sectors are spacetime bosons and states in the NS-R and R-NS sectors are spacetime fermions. To see how spacetime boson and fermions correspond to different sectors, we first need the anti-commutation relations for the Fourier coefficients

$$\{b_r^\mu, b_s^\nu\} = \eta^{\mu\nu} \delta_{r+s,0} \quad \text{and} \quad \{d_m^\mu, d_n^\nu\} = \eta^{\mu\nu} \delta_{m+n,0}.\tag{A.30}$$

Because r and s are half-integers, we can find a unique ground state without degeneracies and identify it with spin zero state. The integer m and n prevent us finding a non-degenerate ground state due to the fact that d_0^μ obey algebra $\{d_0^\mu, d_0^\nu\} = \eta^{\mu\nu}$ and commute with the number operator N . As a result, the set of ground states in R sector must furnish an irreducible representation of this algebra, which is just Dirac algebra $\{\Gamma^\mu, \Gamma^\nu\} = -2\eta^{\mu\nu}$ in disguise, with a normalisation $\Gamma^\mu = i\sqrt{2}d_0^\mu$.

On top of this, we can proceed to obtain the super-Virasoro generators, which are simply the modes for energy-momentum tensor $T_{\alpha\beta}$ and the supercurrent J_A^α . For the open string,

we have the modes for $T_{\alpha\beta}$ given by

$$L_m = \frac{1}{\pi} \int_{-\pi}^{\pi} d\sigma e^{im\sigma} T_{++} = L_m^{(b)} + L_m^{(f)}, \quad (\text{A.31})$$

with contribution from

- bosonic modes

$$L_m^{(b)} = \frac{1}{2} \sum_{n \in \mathbb{Z}} : \alpha_{-n} \cdot \alpha_{m+n} : \quad m \in \mathbb{Z}, \quad (\text{A.32})$$

- fermionic modes in the NS sector

$$L_m^{(f)} = \frac{1}{2} \sum_{r \in \mathbb{Z} + 1/2} \left(r + \frac{m}{2} \right) : b_{-r} \cdot b_{m+r} : \quad m \in \mathbb{Z}, \quad (\text{A.33})$$

- fermionic modes in the R sector

$$L_m^{(f)} = \frac{1}{2} \sum_{n \in \mathbb{Z}} \left(n + \frac{m}{2} \right) : d_{-n} \cdot d_{m+n} : \quad m \in \mathbb{Z}. \quad (\text{A.34})$$

On the other hand, we also have the modes for supercurrent in different sectors:

- In the NS sector, it is given by

$$G_r = \frac{\sqrt{2}}{\pi} \int_{-\pi}^{\pi} d\sigma e^{ir\sigma} J_+ = \sum_{n \in \mathbb{Z}} \alpha_{-n} \cdot b_{r+n} \quad r \in \mathbb{Z} + \frac{1}{2}. \quad (\text{A.35})$$

- In the R sector, it is given by

$$F_m = \frac{\sqrt{2}}{\pi} \int_{-\pi}^{\pi} d\sigma e^{im\sigma} J_+ = \sum_{n \in \mathbb{Z}} \alpha_{-n} \cdot d_{m+n} \quad m \in \mathbb{Z}. \quad (\text{A.36})$$

With the above definitions, one can then calculate the super-Virasoro algebra in different sectors to be:

- In R sector

$$\begin{aligned}
[L_m, L_n] &= (m - n)L_{m+n} + \frac{D}{8}m^3\delta_{m+n,0} , \\
[L_m, F_n] &= \left(\frac{m}{2} - n\right) F_{m+n} , \\
\{F_m, F_n\} &= 2L_{m+n} + \frac{D}{2}m^2\delta_{m+n,0} .
\end{aligned} \tag{A.37}$$

- In NS sector

$$\begin{aligned}
[L_m, L_n] &= (m - n)L_{m+n} + \frac{D}{8}m(m^2 - 1)\delta_{m+n,0} , \\
[L_m, G_r] &= \left(\frac{m}{2} - r\right) G_{m+r} , \\
\{G_r, G_s\} &= 2L_{r+s} + \frac{D}{2}\left(r^2 - \frac{1}{4}\right)\delta_{r+s,0} .
\end{aligned} \tag{A.38}$$

In terms of quantisation of RNS string, we need to require all positive modes of the Virasoro generators annihilate the physical state. In different sectors, they respectively are:

- NS sector

$$\begin{aligned}
G_r |\phi\rangle &= 0 \quad r > 0 , \\
L_m |\phi\rangle &= 0 \quad m > 0 , \\
(L_0 - a_{\text{NS}}) |\phi\rangle &= 0 .
\end{aligned} \tag{A.39}$$

- R sector

$$\begin{aligned}
F_n |\phi\rangle &= 0 \quad n \geq 0 , \\
L_m |\phi\rangle &= 0 \quad m > 0 , \\
(L_0 - a_{\text{R}}) |\phi\rangle &= 0 .
\end{aligned} \tag{A.40}$$

The constants a_{NS} and a_{R} above are from the normal ordering ambiguity and need to be determined later. Using the relation $L_0 = F_0^2$ and $F_0 |\phi\rangle = 0$, one can immediately obtain that $a_{\text{R}} = 0$.

To find the critical values of a_{NS} , we first consider the ground state $|0; p\rangle$ whose on-

shell condition gives $p_0^2 = a_{\text{NS}}$. When acted with $G_{-1/2}$, it gives $p^2 = a - 1/2$. If we take $a_{\text{NS}} = 1/2$, this state is a physical state with $G_{1/2}|\phi\rangle = 0$ for which it is also a zero norm state $\langle\phi|\phi\rangle = \langle 0;p|G_{1/2}G_{-1/2}|0;p\rangle = 0$. It has negative norm if $a_{\text{NS}} > 1/2$. Therefore, $a_{\text{NS}} = 1/2$ is a preferred value, similar to $a = 1$ in bosonic case. However, this also gives rise to the problem of ground state being tachyon and first excited state $b_{-1/2}^\mu$ being massless vector. Lastly, we would like to find the critical value of dimension D . Let us consider a family of zero-norm states of the form

$$|\phi\rangle = (G_{-3/2} + \lambda G_{-1/2}L_{-1})|\tilde{\phi}\rangle, \quad (\text{A.41})$$

where

$$G_{1/2}|\tilde{\phi}\rangle = G_{3/2}|\tilde{\phi}\rangle = (L_0 + 1)|\tilde{\phi}\rangle. \quad (\text{A.42})$$

For $|\phi\rangle$ to be a physical state, both $G_{1/2}|\phi\rangle$ and $G_{3/2}|\phi\rangle$ have to vanish as

$$\begin{aligned} G_{1/2}|\phi\rangle &= (2 - \lambda)L_{-1}|\tilde{\phi}\rangle, \\ G_{3/2}|\phi\rangle &= (D - 2 - 4\lambda)L_{-1}|\tilde{\phi}\rangle. \end{aligned} \quad (\text{A.43})$$

This give $\lambda = 2$ and $D = 10$.

On the other hand, we can confirm the value of $D = 10$ in the R sector using a new set of zero norm spurious states.

$$|\psi\rangle = F_0F_{-1}|\chi\rangle, \quad (\text{A.44})$$

with $F_1|\chi\rangle = (L_0 + 1)|\chi\rangle = 0$. Using (anti-)commutations for R sector, we can verify that $F_0|\psi\rangle = 0$. If this is also annihilated by L_1 , it is then a physical state with zero-norm. This can be seen as follows

$$L_1|\psi\rangle = \left(\frac{1}{2}F_1 + F_0L_1\right)F_{-1}|\chi\rangle = \frac{1}{4}(D - 10)|\chi\rangle. \quad (\text{A.45})$$

This again confirms the critical dimension of superstring theory is $D = 10$.

Analysis of the Spectrum

Before we move to the classification of different types of superstring, it is important that there is no tachyon present in the spectrum. Take the open string as an example in light-cone gauge $X^+(\sigma, \tau) = x^+ + p^+ \tau$.

- The NS-sector with $a_{\text{NS}} = 1/2$ has the mass formula as

$$\alpha' M^2 = \sum_{n=1}^{\infty} \alpha_n^i \alpha_{-n}^i + \sum_{r=1/2}^{\infty} r b_r^i b_{-r}^i - \frac{1}{2}. \quad (\text{A.46})$$

The ground state of this sector $|0; k\rangle_{\text{NS}}$ has the following properties

$$\alpha_n^i |0; k\rangle_{\text{NS}} = b_r^i |0; k\rangle_{\text{NS}} = 0 \quad \text{for } n, r > 0, \quad (\text{A.47})$$

$$\alpha_0^\mu |0; k\rangle_{\text{NS}} = \sqrt{2\alpha'} k^\mu |0; k\rangle_{\text{NS}}. \quad (\text{A.48})$$

From eq. (A.46), we can see that the ground state has mass $\alpha' M^2 = -1/2$. This again confirms our previous assertion that the ground state has tachyon present in its NS-sector spectrum. The first excited state is then obtained by acting the ground state with the smallest frequency creation operator.

$$b_{-1/2}^i |0; k\rangle_{\text{NS}}, \quad (\text{A.49})$$

with i labelling the $D - 2 = 8$ spacetime dimensions since we are in the light-cone gauge. We can see that the operator $b_{-1/2}^i$ raise the mass $\alpha' M^2$ by $1/2$. Similarly, the operator b_m^i raises the mass by a positive m unit. In general, the mass of the first excited state is given by $\alpha' M^2 = 1/2 - a_{\text{NS}}$. Note that the ground state is bosonic and acting on it with b_m^i gives a spacetime vector of $SO(8)$.

- The Ramond sector in light-cone gauge has its mass described by

$$\alpha' M^2 = \sum_{n=1}^{\infty} \alpha_{-n}^i \alpha_n^i + \sum_{n=1}^{\infty} n d_{-n}^i d_n^i. \quad (\text{A.50})$$

The ground state $|0; k\rangle_{\text{R}}$ is defined by $\alpha_n^i |0; k\rangle_{\text{R}} = d_n^i |0; k\rangle_{\text{R}} = 0$ for $n > 0$. It is also a

solution to the massless Dirac equation. This solution is not unique as described earlier since the zero modes satisfy the 10D Dirac algebra. The solution is thus a $Spin(9, 1)$ spinor. Therefore, the ground state of the R-sector is a 32-component spinor. Taking into account of the Majorana, Weyl and Dirac equation constraints, the spinor in $Spin(9, 1)$ is turned into one in $Spin(8)$.

The spectrum discussed above has several problems. Firstly, the NS-sector contains tachyonic ground state. Secondly, the spectrum is not supersymmetric in target spacetime. For example, there is not fermion with the same mass as the tachyon. Spacetime supersymmetry is required for a consistent interacting theory, which in this case the quantum of local supersymmetry, gravitino is present in the spectrum. Therefore, we need to truncate (project) the spectrum in a specific way to make it supersymmetric. This is the content of GSO (Gliozzi, Scherk, Olive) projection [11], which we briefly review in next paragraph.

GSO Projection

Before we perform this project, we to define an operator called G -parity. It has different forms depending on which sector is it in.

- In the NS-sector, it is defined as

$$G = (-1)^{F+1} = (-1)^{\sum_{r=1}^{\infty} (b_{-r}^i b_r^{i+1})} , \quad (\text{A.51})$$

where F is the number operator for b -oscillator excitations, which gives world-sheet fermion number.

- In the R sector, it is defined

$$G = \Gamma_{11} (-1)^{\sum_{n=1}^{\infty} d_{-n}^i d_n^i} , \quad (\text{A.52})$$

with $\Gamma_{11} = \Gamma_0 \Gamma_1 \cdots \Gamma_9$, $\Gamma_{11}^2 = 1$ and $\{\Gamma_{11}, \Gamma^\mu\} = 0$ for $\mu = 0, \dots, 9$. With such Dirac

matrices, we can then define chirality according to

$$\Gamma_{11}\psi = \pm\psi , \tag{A.53}$$

$$P_{\pm} = \frac{1}{2}(1 \pm \Gamma_{11}) . \tag{A.54}$$

where positive sign means a spinor ψ has positive chirality as stated in appendix A.1.2

The GSO projection by definition, only keeps the states with a positive G -parity in the NS sector, *i.e.*

$$(-1)^{F_{\text{NS}}} = -1 .$$

This means we only keep excitations states with odd number of b -oscillator. In the R sector, we can make any projection depending on the chirality of the spinor ground state. Now, let us look at the ground state of the NS sector

$$G |0; k\rangle_{\text{NS}} = - |0; k\rangle_{\text{NS}} , \tag{A.55}$$

where we can see that it has negative G -parity. Hence the tachyonic ground state in NS sector is eliminated. The ground state of NS sector now consists of a massless vector boson, which matches with the ground state in the R sector with a massless spinor occupying its ground state. The GSO projection now may seem rather *ad hoc*, but this can actually be seen in one-loop or two-loop modular invariance. We quickly sketch its contents below.

Modular invariance In the RNS model, without GSO projection or similar one that eliminates the massless spin 3/2 particle or engenders spacetime supersymmetry, lacks modular invariance at one-loop level.

Firstly, we take the right-moving fermions for a closed string with $0 \leq \sigma \leq \pi$ in the RNS model, where the fermions may obey either periodic and anti-periodic conditions. They are referred as $+$ for periodic (even) and $-$ for anti-periodic (odd) and remember that they give rise to fermions and bosons in the target spacetime, respectively. If one performs a path integral on a torus, their boundary conditions are shown in fig. A-1. If we parametrise the torus by $\nu = \sigma_1 + \sigma_2\tau$ such that the two fundamental periods are $\sigma_1 \rightarrow \sigma_1 + 1$. The boundary

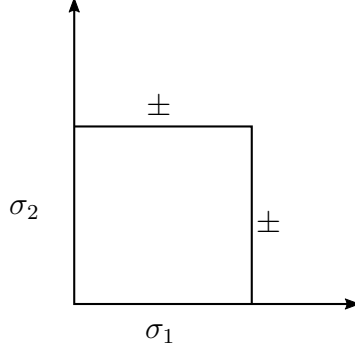


Figure A-1: Path integral on a torus where the fermions may obey + or - boundary conditions in the σ_1 and σ_2 directions respectively.

conditions in each of the two directions σ_1 and σ_2 can have two choices separately. There are 4 choices in total $(+, +)$, $(+, -)$, $(-, +)$ and $(-, -)$. The first entry is for the choice in σ_1 direction and the second for σ_2 . These four choices are referred to as *spin structure*.

Secondly, we consider loop amplitudes with a factor of the form

$$\text{Tr}e^{-yH} , \tag{A.56}$$

with $\tau = (x + iy)/2\pi$. This specifies the propagation through imaginary time y . It is also important to recall that the partition function for a fermion in quantum statistical mechanics requires anti-periodic boundary condition in σ_2 direction⁴. Therefore, the trace in the amplitude is naturally endowed with $(-)$ in σ_2 direction. On the other hand, if we wish to calculate the following

$$\text{Tr}(-1)^F e^{-yH} , \tag{A.57}$$

with $(-1)^F$ defined in eq. (A.51), we have to use + in the σ_2 direction. Therefore, in the absence of GSO projection, the NS sector contributes to the loop amplitude with $(-, -)$ boundary condition and R sector contributes similarly with boundary condition $(+, -)$. Now if we take the combination of partition functions from the two sectors, *i.e.* $(-, -)$ and $(+, -)$, we see that it is not modular invariant. Since S transformation in modular group has its

⁴In the path integral approach to quantum statistical mechanics, the Euclidean time direction is taken to lie on a circle with circumference proportional to the inverse of the temperature of the system. It is shown that free fermions must take anti-periodic boundary condition around time direction to reproduce Fermi-Dirac distribution.

action as $(\sigma_1, \sigma_2) \rightarrow (\sigma_2, -\sigma_1)$ and it turns $(+, -)$ into $(-, +)$. To have a modular invariant RNS model, one must supplement it with $(-, +)$. $(-, +)$ is the partition function for NS states with $(-1)^F$ inserted in the path integral. Therefore, the NS-sector has its modular invariant partition function

$$\text{Tr}(1 + (-1)^F r^{-yH};, \tag{A.58}$$

where we can see that it is exactly the GSO projection operator eq. (A.51) inserted in the trace. We can see from the above that the modular invariance at 1-loop level only requires NS sector to be considered, which means one does not need to make GSO projection in the R sector. This shows that at 1-loop level, GSO projection is made for bosons. GSO projection for fermions will require the addition of $(+, +)$ boundary condition, which is modular invariant by itself. It can be shown at 2-loop level, GSO projection is required for both fermions and bosons.

Checking degrees of freedom The requirement of modular invariance of partition function on a torus requires the GSO projection has its geometric interpretation of summing over spin structures. On top of this, we can see the necessity of this projection by counting physical degrees of freedom at the ground state from both sectors.

- The ground state in the NS sector is a massless vector. After GSO projection, it is $b_{-1/2}^\mu |0; k\rangle$, which has 8 transverse propagating degrees of freedom.
- The ground state in the R sector is a spinor. In ten dimensions, it has $2^{10/2} = 32$ complex components. In ten dimensions, the Majorana and Weyl conditions are compatible, therefore, Majorana condition leaves 32 real components. Weyl condition splits the spinor into definite chirality, thus this leaves 16 real components. Finally, the Dirac equation further reduces the degrees of freedom by half to give 8 real components transforming as a spinor in $Spin(8)$.

Even though this counting does not guarantee a spacetime supersymmetry, it still serves as a strong evidence as the equal number of bosonic and fermionic is a prerequisite for

supersymmetry. However, the Green-Schwarz formalism is developed to make the spacetime supersymmetry manifest.

The massless spectrum for type II superstring

Since the closed string has left and right movers, there are four different sectors we have to analyse separately: R-R, R-NS, NS-R and NS-NS. As described in the previous section, we can eliminate NS sector tachyons by projecting the states onto a positive G -parity spectrum. The R sector on the other hand, can be projected onto either parity depending on the chirality of the ground state on which excitations are built. Therefore, two different theories can be obtained depending on the relative chirality between two movers.

In type IIB superstring theory, the left- and right- moving R-sector ground states have the same positive chirality. This means the two R sectors have the same G -parity, denoted by $|+\rangle_{\text{R}}$. In such setting, the massless spectrum of type IIB is

$$|+\rangle_{\text{R}} \otimes |+\rangle_{\text{R}} , \quad (\text{A.59})$$

$$\tilde{b}_{-1/2}^i |0\rangle_{\text{NS}} \otimes b_{-1/2}^j |0\rangle_{\text{NS}} , \quad (\text{A.60})$$

$$\tilde{b}_{-1/2}^i |0\rangle_{\text{NS}} \otimes |+\rangle_{\text{R}} , \quad (\text{A.61})$$

$$|+\rangle_{\text{R}} \otimes b_{-1/2}^j |0\rangle_{\text{NS}} . \quad (\text{A.62})$$

All of these four sectors contain $8 \times 8 = 64$ physical degrees of freedom.

Type IIA theory has its left- and right- moving R-sector ground state in opposing chirality. Its spectrum is

$$|-\rangle_{\text{R}} \otimes |+\rangle_{\text{R}} , \quad (\text{A.63})$$

$$\tilde{b}_{-1/2}^i |0\rangle_{\text{NS}} \otimes b_{-1/2}^j |0\rangle_{\text{NS}} , \quad (\text{A.64})$$

$$\tilde{b}_{-1/2}^i |0\rangle_{\text{NS}} \otimes |+\rangle_{\text{R}} , \quad (\text{A.65})$$

$$|-\rangle_{\text{R}} \otimes b_{-1/2}^j |0\rangle_{\text{NS}} . \quad (\text{A.66})$$

The massless spectrum each of the type II theory contains two gravitinos to form $\mathcal{N} = 2$

supergravity multiplets. Let us now list all 64 states in each of the 4 massless sectors.

- NS-NS sector: This sector is the same for both type IIB theory. The spectrum contains a scalar called the dilaton (the trace from the symmetric tensor), an anti-symmetric two-form gauge field ($8 \times 7/2 = 28$ states) and a symmetric traceless rank 2 tensor, *i.e.* the graviton ($8 \times 9/2 - 1 = 35$ states).
- NS-R or R-NS sector: All of the type II theories have two spin 3/2 gravitinos (Γ -traceless anti-symmetric part) with 56 states and a spin 1/2 fermion (Γ -trace), dilatino with 8 states. In the IIB case, the two gravitinos have same chirality and IIA case has opposite chirality.
- R-R sector: These states are bosons built by pairing two Majorana-Weyl spinors.⁵ In the IIA case, the two Majorana-Weyl spinors have opposite chirality. We obtain a 1-form gauge field (8 states), and an antisymmetric 3-form (56 states). In the IIB case, the two spinors have same chirality. We obtain a 0-form, which is simply a scalar, a 2-form (28 states) and 4-form with a self-dual field strength (35 states).

To summarise our discussion of type II string theory, we note the following features of it:

- Type II string theory consists of two parts: (1) type IIA with two conserved supercharges of opposite chirality, thus it is non-chiral (*i.e.* left-right symmetric), (2) type IIB of oriented closed strings with same chirality on the ground state of R sector for both left- and right-mover.
- The difference in chirality of the R-sector ground states from left- and right-movers results in a different field strength in R-R sector thus leads to different allowed dimension of D-branes.

⁵To build anti-symmetric n -forms from two spinors, we need spinors bilinears in different sectors as follows:

$$\text{IIA : } F^{\mu_1 \dots \mu_{d+1}} = \bar{\psi}_-^L \gamma^{\mu_1 \dots \mu_{d+1}} \psi_+^R, \quad \text{IIB : } F^{\mu_1 \dots \mu_{d+1}} = \bar{\psi}_+^L \gamma^{\mu_1 \dots \mu_{d+1}} \psi_+^R, \quad (\text{A.67})$$

where $\bar{\psi}_\pm^L$ is from the left movers and ψ_\pm^R is from the right movers. We also have

$$\gamma^{\mu_1 \dots \mu_{d+1}} = \gamma^{[\mu_1 \dots \mu_{d+1}]}, \quad (\text{A.68})$$

being antisymmetric product of $(d + 1)$ gamma matrices.

Type I superstring

Having briefly reviewed the basics in type II superstring theory, we move on to the type I superstring, which consists of both open and closed strings. It can be understood as a result of a projection from type IIB superstring theory. The world-sheet parity transformation

$$\Omega : \sigma \rightarrow -\sigma \tag{A.69}$$

is a symmetry of IIB theory since the left- and right-moving fermions have the same space-time chirality. When we gauge this symmetry we have the resulting type I theory. Consider the projection operator

$$P = \frac{1}{2}(1 + \Omega) , \tag{A.70}$$

the type I spectrum is then obtain by keeping states that are even under parity transformation. Therefore, let us iterate the spectrum in each sector separately

- NS-NS sector: Only the states that are symmetric in the two vectors survive this projection. They are the dilaton and graviton with the antisymmetric B_2 being projected out.
- NS-R or R-NS sector: The 2 gravitinos in the type IIB, Ψ_1^μ and Ψ_2^μ , are exchanged upon the parity transformation. Therefore, only the sum $\Psi_1^\mu + \Psi_2^\mu$ is invariant under this projection. Using similar argument, the one of the two dilatinos survives projection. Therefore, the total massless fermionic degrees of freedom becomes $56 + 8 = 64$. With only one gravitino after projection, we see that type I theory has half amount of supersymmetry as type IIB theory (16 supercharges as opposed to 32).
- R-R sector: Since type I theory has to be supersymmetric, the bosonic degrees of freedom from R-R sector have to match with those from fermionic side. The only way to achieve this is to project out C_4 and C_0 while keeping C_2 . The bosonic fields are then graviton and dilaton from NS-NS sector and C_2 from R-R sector. The total bosonic degrees of freedom are thus $35 + 1 + 28 = 64$. All the fields described above then together form the $\mathcal{N} = 1$ supergravity multiplet.

To construct gauge theory in type I theory, Chan-Paton method is used to give rise to gauge group. Quantum mechanically, the cancellation of anomaly as reviewed in appendix A.2 requires the gauge group to be $SO(32)$.

Heterotic superstring

Heterotic superstring theory is also a theory of closed strings only, with the exception that left- and right- moving modes are decoupled. It is therefore legitimate to envisage a closed-string theory in which the left-moving modes are of one type, and the right-moving modes are of another type altogether. To accommodate space-time supersymmetry, we take the right-moving modes to be superstring modes and the left-moving modes to incorporate gauge degrees of freedom with suitable current algebra. The following action is an example of such construction:

$$S = -\frac{1}{2\pi} \int d^2\sigma \left(\sum_{\mu=0}^9 (\partial_\alpha X^\mu \partial^\alpha X_\mu - 2\psi_+^\mu \partial_- \psi_{\mu+}) - 2 \sum_{A=1}^n \lambda_-^A \partial_+ \lambda_-^A \right), \quad (\text{A.71})$$

where ψ^μ , $\mu = 0, \dots, 9$ are Lorentz vectors; λ^A , $A = 1, \dots, n$ are Lorentz singlets but the indices A are for some internal quantum numbers. Both ψ^μ and λ^A are Majorana-Weyl fermions.

The right-moving modes are ψ_+^μ and the right moving part of X^μ . They are the same in the other type II theories, which means the critical dimension in the right-moving sector is $D = 10$ and this is why we set μ to $0, \dots, 9$ in eq. (A.71). The left-moving modes are from the left-moving parts of X^μ and λ^A . As there is no supersymmetry in left-moving sector, the only left-moving ghosts are from reparametrisation, which are enough to cancel the contribution of 26 bosons. But we only have ten X^μ in eq. (A.71), the rest of Virasoro anomaly must be cancelled by the λ^A . From bosonisation of fermions we know that two Majorana fermions or one Dirac fermion make up the Virasoro anomaly of a boson, therefore we need $32 \lambda^A$ in the action. If all fermions obey the same boundary condition, they carry $SO(32)$, which is in fact a gauge symmetry since massless gauge meson of $SO(32)$ occurs as well as anomaly cancellation also requires such group. On the other hand, if not all fermions obey the same boundary conditions, one get $E_8 \times E_8$.

The $SO(32)$ theory In this setting for the heterotic string theory, we set all the 32 λ^A to have the same boundary condition, *i.e.* periodic or anti-periodic. Recall from previous discussion that the decoupling of negative norm states requires the normal-ordering constant a to be zero as the same in the Ramond sector due to inclusion of world-sheet supersymmetry. As for \tilde{a} , the contribution to normal-ordering constant from a bosonic coordinate is $1/24$ while that from a half-integrally moded fermionic coordinate is $1/48$, and that from an integrally moded fermionic sector is $-1/24$.⁶ Therefore, we can combine these values to obtain the value of \tilde{a} for two sectors:

$$\begin{aligned}\tilde{a}_A &= \frac{8}{24} + \frac{32}{48} = 1 \\ \tilde{a}_P &= \frac{8}{24} + \frac{32}{24} = -1.\end{aligned}\tag{A.72}$$

Thus the Virasoro constraints

$$(L_0 - a) |\Omega\rangle = (\tilde{L}_0 - \tilde{a}) |\Omega\rangle = 0$$

combine to give

$$\frac{1}{4}(\text{mass})^2 = N + \tilde{N} - \tilde{a},$$

where $L_0 = p^2/8 + N$ and similarly for \tilde{N} .

As $a = 0$, we have $N = 0$ since $p^2 = -8N$. Therefore, we have $N = 0$ and $\tilde{N} = 1$ in anti-periodic sector for massless states. On the other hand, similar arguments give $\tilde{N} = -1$, which is in contradiction with \tilde{N} being non-negative as it is the number operator. This shows there are no massless states in periodic sector. The massless spectrum is then made of tensor products of the right-moving modes of $N = 0$ with the left-moving modes of $\tilde{N} = 1$ in anti-periodic sector. Finally, the gauge symmetry is in fact $Spin(32)/\mathbb{Z}_2$ rather than $SO(32)$ described above for the following reasons. Firstly, the representations of $Spin(2n)$ falls into four conjugacy classes. The anti-periodic sector consists of entirely tensor representation of even rank because there are always an even number of λ excitations. All such representations belong to the same conjugacy class as the adjoint representation. Secondly, the periodic left-

⁶These particular values can be derived by looking at the Hamiltonian after bosonisation of fermions with different boundary conditions.(c.f. §3.2.4 [1])

moving sector only contains one of the two fundamental spinor representations. All other excitations can be obtained from this state by acting with even number of λ excitations. This means higher mass states at in the same conjugacy class as the fundamental representation. Therefore, the complete spectrum falls into two conjugacy class, hence, the group symmetry is now $Spin(32)/\mathbb{Z}_2$.

The $E_8 \times E_8$ theory For the $Spin(32)/\mathbb{Z}_2$ theory, we demanded all the 32 λ^A to have the same boundary condition: periodic or anti-periodic, in order to not break the symmetry group. However, we can arrive at a far more interesting symmetry group of $E_8 \times E_8$ by splitting the fermions into two groups that belong to the representation of $Spin(n) \times Spin(32-n)$. This means the 32 fermions are divided into a group of n and another of group of $32-n$. This allows us to assign P and A boundary conditions separately to the two sets of fermions. There are four such possibilities: AA , AP , PA and PP , where the first label denotes the boundary condition for the n fermions and the second denotes that for the $32-n$ fermions. The normal ordering constants for these different choices are $\tilde{a}_{AA} = 1$, $\tilde{a}_{AP} = (n-16)/16$, $\tilde{a}_{PA} = (16-n)/16$ and $\tilde{a}_{PP} = -1$. From the relation for massless spectrum $N = \tilde{N} - \tilde{a}$, we see that for values of n not divisible by 8, there are no physical states in AP and PA sector. Discarding all these sectors, we are back to the $Spin(32)/\mathbb{Z}_2$ case. For n divisible by 8, there are 3 possibilities: (i) $n = 32$ or 0, (ii) $n = 16$, (iii) $n = 24$ or 8. Case (i) is in the $Spin(32)/\mathbb{Z}_2$ scenario. Case (ii) gives $Spin(16) \times Spin(16)$ and case (iii) give $Spin(24) \times Spin(8)$ which gives one-loop anomalies and will not be discussed here.

Let us consider the case of $Spin(16) \times Spin(16)$. For the AA sector, we have $\tilde{a} = 1$ which translates to $\tilde{N} = 1$ for massless left-moving states. Therefore, when acted by two $\lambda_{-1/2}^i$, each contributing $+1/2$ to the eigenvalue of \tilde{N} , we have $\tilde{N} = 1$. The resulting states are in the form

$$\lambda_{-1/2}^i \lambda_{-1/2}^j |\Omega\rangle ,$$

which transform under $Spin(16) \times Spin(16)$ as

$$\begin{aligned}
(\mathbf{120}, \mathbf{1}) & \text{ if } i, j = 1, \dots, 16, \\
(\mathbf{1}, \mathbf{120}) & \text{ if } i, j = 17, \dots, 32, \\
(\mathbf{16}, \mathbf{16}) & \text{ if } i = 1, \dots, 16, j = 17, \dots, 32.
\end{aligned}$$

The $\mathbf{16}$ and $\mathbf{120}$ are the vector and adjoint representation of $SO(32)$ respectively. In addition, since the normal ordering constant $\tilde{a} = 0$ for AP and PA sectors, there are extra massless states than the above ones. These are the states of $\tilde{N} = 0$ with fermion zero modes transforming as spinors of $Spin(16)$ (c.f. ground states for Ramond sector). So if we denote the two spinor representations of $Spin(16)$ as $\mathbf{128}$ and $\mathbf{128}'$, the massless left-moving states in PA and AP sectors are

$$\begin{aligned}
PA & : (\mathbf{128}, \mathbf{1}) \oplus (\mathbf{128}', \mathbf{1}), \\
AP & : (\mathbf{1}, \mathbf{128}) \oplus (\mathbf{1}, \mathbf{128}').
\end{aligned}$$

The combined massless states described by $\mathbf{120} \oplus \mathbf{128}$ of $Spin(16)$ from left- and right-moving sectors actually form the E_8 algebra. Hence, we have $E_8 \times E_8$ as the gauge group for heterotic theory.

A.2 Notes on Anomalies in Superstring Theory

A.2.1 Chiral Anomaly

In this section, we review anomalies in string theory with a pedagogical perspective.

Symmetries of classical field theories can be broken by quantum effects are known as anomalies. The origin of these effects can be traced back to ill-behaved Feynman diagrams that have classically conserved currents attached that do not admit a regulator compatible with simultaneous conservation of all attached currents. Global conservation laws with anomalies are acceptable since the physical content of the theory is intact. Anomalies in local conservation laws such as gauge invariance or general covariance cause the theory to be inconsistent. In particular, gauge invariance is crucial in decoupling longitudinal states in physical processes if the theory is to be unitary.

Firstly, let us consider the global chiral anomaly to illustrate the essential contents on how anomaly can arise in QFT in 4D. Take the example from the theory of a single massless fermion with lagrangian $\mathcal{L} = \bar{\psi}i\gamma^\mu\partial_\mu\psi$. The transformations $\psi \rightarrow e^{i\theta}\psi$ and $\psi \rightarrow e^{i\theta\gamma^5}\psi$ corresponding to conserved currents $J^\mu = \bar{\psi}\gamma^\mu\psi$ and $J_5^\mu = \bar{\psi}\gamma^\mu\gamma^5\psi$ are symmetries of the theory. Now consider the amplitude give by

$$\langle 0|T J_5^\lambda(0)J^\mu(x_1)J^\nu(x_2)|0\rangle ,$$

whose Feynman diagrams are given by the two “triangle” diagrams: where we see that these

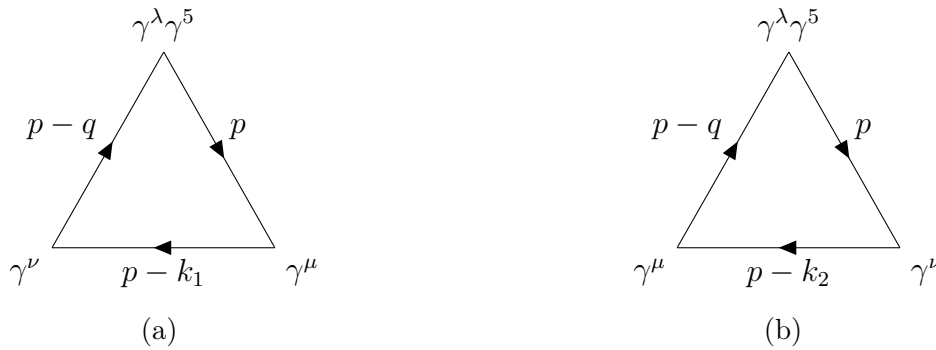


Figure A-2: The two triangle diagrams to illustrate chiral anomaly. Note that these two diagrams are required by bose statistics and $q = k_1 + k_2$.

two diagrams are required by Bose statistics. This amplitude is given by the integral as

$$\Delta^{\lambda\mu\nu}(k_1, k_2) = (-1)i^3 \int \frac{d^34}{(2\pi)^4} \text{tr} \left(\gamma^\lambda \gamma^5 \frac{1}{\not{p} - \not{q}} \gamma^\nu \frac{1}{\not{p} - \not{k}'_1} \gamma^\mu \frac{1}{\not{p}} + \gamma^\lambda \gamma^5 \frac{1}{\not{p} - \not{q}} \gamma^\mu \frac{1}{\not{p} - \not{k}'_2} \gamma^\nu \frac{1}{\not{p}} \right), \quad (\text{A.73})$$

where the overall -1 comes from the fermion loop. Classically, the conservation of vector and axial currents implies $\partial_\mu J^\mu$ and $\partial_\mu J_5^\mu$. Quantum mechanically, if we demand the vector symmetry to be anomaly free, we require $k_{1\mu} \Delta^{\lambda\mu\nu} = 0$ and $k_{2\mu} \Delta^{\lambda\mu\nu} = 0$. Similarly, for axial symmetry we have $q_\lambda \Delta^{\lambda\mu\nu} = 0$. Before we proceed, it is essential to understand the physical significance of the two currents not being conserved quantum mechanically. The charge $Q = \int d^3x J^0$ counts the number of fermions and the non-conservation of this means fermion number being not conserved. In addition, we need $\partial_\mu J^\mu$ to prove why photons have only two transverse degrees of freedom. Also if we couple the vertex labelled by μ with a photon with propagator proportional to $(i/k_1^2)[\xi(k_{1\mu}k_{2\rho}/k_1^2) - g_{\mu\rho}]$. The gauge dependent term $\xi(k_{1\mu}k_{2\rho}/k_1^2)$ can only disappear if the vector current is conserved to ensure photon has two degrees of freedom. Now let us see how $k_{1\mu} \Delta^{\lambda\mu\nu}$ and $k_{2\mu} \Delta^{\lambda\mu\nu}$ behave when we hit them with $k_{1\mu}$ and $k_{2\mu}$. Replacing k'_1 with $\not{p} - (\not{p} - k'_1)$ in the first term of eq. (A.73) and with $(\not{p} - k'_2) - (\not{p} - \not{q})$ in the second term, we have

$$k_{1\mu} \Delta^{\lambda\mu\nu}(k_1, k_2) = i \int \frac{d^4p}{(2\pi)^4} \text{tr} \left(\gamma^\lambda \gamma^5 \frac{1}{\not{p} - \not{q}} \gamma^\nu \frac{1}{\not{p} - \not{k}'_1} - \gamma^\lambda \gamma^5 \frac{1}{\not{p} - \not{k}'_2} \gamma^\nu \frac{1}{\not{p}} \right). \quad (\text{A.74})$$

The integrand actually vanishes when shift the variable $p \rightarrow p - k_1$. However, this shift of variables will result in the following difference in the integral. Consider a generic Feynman integral in d -dimension, we see that it is

$$\int d_E^d p [f(p+a) - f(p)] = \int d_E^d p [a^\mu \partial_\mu f(p) + \dots];,$$

which by is given by a surface integral over an infinitely large sphere enclosing all of spacetime

$$\lim_{P \rightarrow \infty} a^\mu \left(\frac{P_\mu}{P} \right) f(P) S_{d-1}(P),$$

where $S_{d-1}(P)$ is the area of a $(d-1)$ -dimensional sphere. Rotating back to Minkowski

spacetime, we have

$$\int d^4p [f(p+a) - f(p)] = \lim_{P \rightarrow \infty} ia^\mu \left(\frac{P_\mu}{P} \right) (2\pi^2 P^3); \quad (\text{A.75})$$

Using this for $f(p)$ given by the integrand in our example

$$f(p) = \text{tr} \left(\gamma^\lambda \gamma^5 \frac{1}{\not{p} - \not{k}_2} \gamma^\nu \frac{1}{\not{p}} \right) = \frac{\text{tr}[\gamma^5 (\not{p} - \not{k}_2) \gamma^\nu \not{p} \gamma^\lambda]}{(p - k_2)^2 p^2} = \frac{4i\epsilon^{\tau\nu\sigma\lambda} k_{2\tau} p_\sigma}{(p - k_2)^2 p^2},$$

with identity $\text{tr}(\gamma^\mu \gamma^\nu \gamma^\rho \gamma^\sigma \gamma^5) = 4\epsilon^{\mu\nu\rho\sigma}$, we have

$$k_{1\mu} \Delta^{\lambda\mu\nu} = \frac{i}{(2\pi)^4} \lim_{P \rightarrow \infty} i(-k_1)^\mu \frac{P_\mu}{P} \frac{4i\epsilon^{\tau\nu\sigma\lambda} k_{2\tau} P_\sigma}{P^4} 2\pi^2 P^3 = \frac{i}{8\pi^2} \epsilon^{\lambda\nu\tau\sigma} k_{1\tau} k_{2\sigma}. \quad (\text{A.76})$$

However, the previous calculation does not take into account of the fact that the integral is linearly divergent and thus not well defined for an infinitely large sphere. In addition, if we consider $\Delta^{\lambda\mu\nu}$ with another linear shift in momentum p by a vector a

$$\Delta^{\lambda\mu\nu}(a, k_1, k_2) = (-1)i^3 \int \frac{d^34}{(2\pi)^4} \text{tr} \left(\gamma^\lambda \gamma^5 \frac{1}{\not{p} + \not{a} - \not{q}} \gamma^\nu \frac{1}{\not{p} + \not{a} - \not{k}_1} \gamma^\mu \frac{1}{\not{p} + \not{a}} + \{\mu, k_1 \rightarrow \nu, k_2\} \right),$$

this choice of vector enables us to make $k_{1\mu} \Delta^{\lambda\mu\nu}(a, k_1, k_2)$ and $k_{2\nu} \Delta^{\lambda\mu\nu}(a, k_1, k_2)$ vanish. Now we can apply eq. (A.75) to $f(p) = \text{tr}(\gamma^\lambda \gamma^5 \frac{1}{\not{p}-\not{q}} \gamma^\nu \frac{1}{\not{p}-\not{k}_1} \gamma^\mu \frac{1}{\not{p}})$

$$\begin{aligned} f(P) &= \lim_{P \rightarrow \infty} \frac{\text{tr}(\gamma^\lambda \gamma^5 \not{P} \gamma^\nu \not{P} \gamma^\mu \not{P})}{P^6} \\ &= \frac{2P^\mu \text{tr}(\gamma^\lambda \gamma^5 \not{P} \gamma^\nu \not{P}) - P^2 \text{tr}(\gamma^\lambda \gamma^5 \not{P} \gamma^\nu \gamma^\mu)}{P^6} \\ &= \frac{4iP^2 P_\sigma \epsilon^{\sigma\nu\mu\lambda}}{P^6}, \end{aligned} \quad (\text{A.77})$$

where q and k_1 are ignored since we take the limit of $P \rightarrow \infty$. Using eq. (A.75) we have

$$\begin{aligned} \Delta^{\lambda\mu\nu}(a, k_1, k_2) - \Delta^{\lambda\mu\nu}(k_1, k_2) &= \frac{4i}{8\pi^2} \lim_{P \rightarrow \infty} a^\omega \frac{P_\omega P_\sigma}{P^2} \epsilon^{\sigma\nu\mu\lambda} + \{\mu, k_1 \rightarrow k\nu, k_2\} \\ &= \frac{i}{8\pi^2} \epsilon^{\sigma\nu\mu\lambda} a_\sigma + \{\mu, k_1 \rightarrow \nu, k_2\}. \end{aligned}$$

Note here we have two independent momenta k_1 and k_2 , so we can take $a = \alpha(k_1 + k_2) +$

$\beta(k_1 - k_2)$ to obtain

$$\Delta^{\lambda\mu\nu}(a, k_1, k_2) = \Delta^{\lambda\mu\nu}(k_1, k_2) + \frac{i\beta}{4\pi^2} \epsilon^{\lambda\mu\nu\sigma} (k_1 - k_2)_\sigma, \quad (\text{A.78})$$

where we note that α drops out due to the antisymmetric tensor $\epsilon^{\lambda\mu\nu\sigma}$. Since we want $k_{1\mu} \Delta^{\lambda\mu\nu}(a, k_1, k_2) = 0$, we can set $\beta = -1/2$ with the result in eq. (A.76) to achieve this result. Therefore, the vector current is conserved with a particular choice of shift in internal momenta.

To check the conservation of axial current, we simply have to compute the following

$$q_\lambda \Delta^{\lambda\mu\nu}(a, k_1, k_2) = q_\lambda \Delta^{\lambda\mu\nu}(k_1, k_2) + \frac{i}{4\pi^2} \epsilon^{\mu\nu\lambda\sigma} k_{1\lambda} k_{2\sigma}, \quad (\text{A.79})$$

where we used both eq. (A.78) and $q = k_1 + k_2$. So replacing $\not{q} \rightarrow \not{p} - (\not{p} - \not{q})$, we obtain

$$\begin{aligned} q^\lambda \Delta^{\lambda\mu\nu}(k_1, k_2) &= i \int \frac{d^4 p}{(2\pi)^4} \text{tr} \left(\gamma^5 \frac{1}{\not{p} - \not{q}} \gamma^\nu \frac{1}{\not{p} - \not{k}_1} \gamma^\mu - \gamma^5 \frac{1}{\not{p} - \not{k}_2} \gamma^\nu \frac{1}{\not{p}} \gamma^\mu \right) + \{\mu, k_1 \rightarrow \nu, k_2\} \\ &= \frac{i}{4\pi^2} \epsilon^{\mu\nu\lambda\sigma} k_{1\lambda} k_{2\sigma}. \end{aligned} \quad (\text{A.80})$$

Plugging this back into eq. (A.79), we obtain the anomaly as

$$q_\lambda \Delta^{\lambda\mu\nu}(a, k_1, k_2) = \frac{i}{2\pi^2} \epsilon^{\mu\nu\lambda\sigma} k_{1\lambda} k_{2\sigma}. \quad (\text{A.81})$$

This result can actually be expressed in terms of field strength $F_{\mu\nu}$ for a simple QED theory with Lagrangian $\mathcal{L} = \bar{\psi} i \gamma^\mu (\partial_\mu - ie A_\mu) \psi$, where the two vertices labelled by μ and ν can be thought as two photon lines coming out

$$\partial_\mu J_5^\mu = \frac{e^2}{(4\pi)^2} \epsilon^{\mu\nu\lambda\sigma} F_{\mu\nu} F_{\lambda\sigma}.$$

In addition, the anomaly can also be derived by looking at the Jacobian for transformation $\psi(x) \rightarrow e^{i\alpha(x)\gamma_5} \psi(x)$ (c.f. [6]). Furthermore, if we have a mass term for the Lagrangian $\mathcal{L} = \bar{\psi} (i\gamma^\mu \partial_\mu - m) \psi$, the classical axial current conservation is already not conserved $\partial_\mu J_5^\mu =$

$2m\bar{\psi}i\gamma^5\psi$. For theory $\mathcal{L} = \bar{\psi}[(i\gamma^\mu(\partial_\mu - ieA_\mu) - m)]\psi$, quantum fluctuations correct the conservation of axial current by an additional anomaly term

$$\partial_\mu J_5^\mu = 2m\bar{\psi}i\gamma^5\psi + \frac{e^2}{(4\pi)^2}\epsilon^{\mu\nu\lambda\sigma}F_{\mu\nu}F_{\lambda\sigma}.$$

On top of the simple fermion Lagrangian, we can couple the fermions to scalar field by adding $f\phi\bar{\psi}\psi$ to the Lagrangian. If we want to calculate higher order diagram to the tree loop diagram in fig. A-2, we would expect eq. (A.76) to be multiplied by some correction term $1 + h(f, e, \dots)$ with h being some unknown function of all couplings in the theory. However, Adler and Bardeen proved that $h = 0$ to all orders and this is known as the nonrenormalisation of the anomaly. Particularly, this allowed the decay amplitude for $\pi^0 \rightarrow \gamma + \gamma$ to be calculated with great accuracy. This amplitude originally required an infinite number of diagrams, but the nonrenormalisation of the anomaly shows that only the tree amplitude contributes and it does not depend on the details of the strong interaction. It actually came out a factor of 3 too small, which means quarks come in 3 copies.

A.2.2 Anomalies in Gauge Theory

Before we move on to the full picture on anomalies in superstring theory, it is illustrative to consider the anomaly from field theory perspective. The Yang-Mills gauge anomaly in $D = 10$ is interesting to us since it is a part of a low-energy approximation to the superstring theories in our discussion. First, let us consider the loop amplitude illustrated in the Fig. fig. A-3. The vector bosons and Majorana-Weyl fermions are both in the adjoint representation of the gauge group. For the case when fermions being massless, the formal expression for the amplitude is given by

$$A_M \sim T \int d^{10}p \operatorname{tr} \left[\frac{\Gamma \cdot p_1}{p_1^2} \Gamma \cdot \zeta_1 \frac{\Gamma \cdot p_2}{p_2^2} \cdots \Gamma \cdot \zeta_M \left(\frac{1 + \Gamma_{11}}{2} \right) \right]. \quad (\text{A.82})$$

The factor $T = \operatorname{tr}(t^{a_1} t^{a_2} \cdots t^{a_M})$ comes from the summing over gauge group indices and a_i labels the charge of the i -th boson and the t 's are in the adjoint representation of the gauge group. The vector $\zeta_i^\mu(k_i)$ is from the polarisation of the i -th boson, which is required to

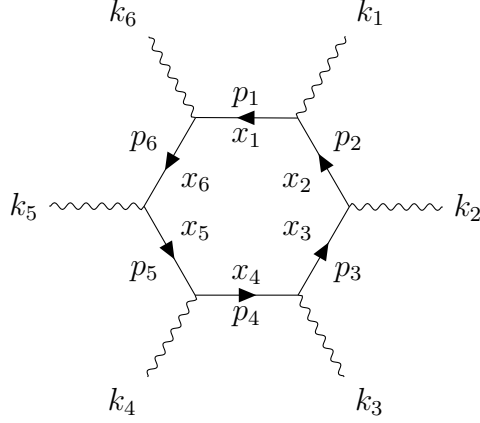


Figure A-3: The Feynman diagram for hexagonal loop amplitude.

be on-shell and physical, *i.e.* $k_i \cdot \zeta_i = k_i \cdot k_i = 0$. The internal fermions have momenta constrained by $p_i = p - \sum_{j=1}^{i-1} k_j$. The projection operator $(1 + \Gamma_{11})/2$ is used to fix the chirality of the internal fermions. There will be a totally anti-symmetric tensor ϵ coming out from summing over all the gamma matrices as from eq. (A.76) and the final result must be a contraction between the ϵ tensor and 10 of the momenta and polarisation vectors. But the constraint $\sum k_i = 0$ reduces the number of independent momenta k_i into $M - 1$. Therefore, the simplest diagram for potential anomaly is when $M = 6$, which is the reason why we analyse the hexagonal diagram. The anomaly can be calculated using Pauli-Villars regulator by subtracting an identical equation as eq. (A.82) with massless propagator $\Gamma \cdot p/p^2$ replaced by massive ones $(\Gamma \cdot p)/(p^2 + m^2)$. The final anomaly is found by setting one of the polarisation vector to be longitudinal $\zeta_6^\mu = k_6^\mu$ and letting regulator mass $m \rightarrow \infty$. We then have

$$A_5 \sim T \epsilon_{\mu_1 \dots \mu_5 \nu_1 \dots \nu_5} \zeta_1^{\mu_1} \dots \zeta_5^{\mu_5} k_1^{\nu_1} \dots k_5^{\nu_5} .$$

We note here the factor T can only identically vanish when the gauge group is abelian. In addition, T has a total symmetry in the five external vector bosons and this implies that there is a permutation symmetry in the five external lines. This in total, signifies that only totally symmetric trace can contribute to the amplitude. For A_6 , only symmetrised trace contribute to $\text{Tr}(t^6)$. Finally, before we move onto anomalies of superstring theory, we note some relation between matrices in fundamental and adjoint representations for classical groups. For t in adjoint representation of $SO(n)$ and λ^a in its fundamental representation,

we have the following relation

$$t_{ab,cd} = \frac{1}{2}(\lambda_{ac}\delta_{bd} - \lambda_{bc}\delta_{ad} - \lambda_{ad}\delta_{bc} + \lambda_{bd}\delta_{ac}) ,$$

taking traces ('Tr' stands for trace in adjoint representation and 'tr' for that in fundamental representation), we have

$$\text{Tr } t^6 = (n - 32)\text{tr}\lambda^6 + 15\text{tr}\lambda^4 \text{tr}\lambda^2 . \quad (\text{A.83})$$

Similarly we have $\text{Tr } t^6 = (n + 32)\text{tr}\lambda^6 + 15\text{tr}\lambda^4 \text{tr}\lambda^2$ for $USp(n)$ and $\text{Tr } t^6 = n\text{tr}\lambda^6 + 15\text{tr}\lambda^4 \text{tr}\lambda^2$ for $U(n)$. We see here the $\text{tr}(\lambda^6)$ term can be eliminated only in $SO(32)$. But Super-Yang-Mills in such case is still anomalous since the term $\text{tr}\lambda^4 \text{tr}\lambda^2$ is still present. We shall see later in this section that superstring offers new effects to cancel contributions from such terms in type I theory.

Now we take a two-dimensional example in which gauge fields couple to left- and right-moving currents with same current algebra \mathfrak{g} . The action is then written as

$$S_{\text{int}} = \int d^2z (j_z^a A_{\bar{z}}^a + j_{\bar{z}}^a A_z^a) , \quad (\text{A.84})$$

where the coefficients of the Schwinger terms is given by $\hat{k}_{L,R}\delta^{ab}$. Since the operator product expansion (OPE) determines the expectation value of jj , the path integral to second order is therefore

$$Z[A] = \frac{1}{2} \int d^2z_1 d^2z_2 \left[\frac{\hat{k}_L}{z_{12}^2} A_{\bar{z}_1}^a(z_1, \bar{z}_1) A_{\bar{z}_2}^a(z_2, \bar{z}_2) + \frac{\hat{k}_R}{\bar{z}_{12}^2} A_{\bar{z}_1}^a(z_1, \bar{z}_1) A_{\bar{z}_2}^a(z_2, \bar{z}_2) \right] . \quad (\text{A.85})$$

If we make a gauge transformation with leading order being $\delta A_1^a = d\lambda^a$ and integrate by parts, we have the following

$$\delta Z[A] = 2\pi \int d^2z \lambda^a(z, \bar{z}) [\hat{k}_L \partial_z A_{\bar{z}}^a(z, \bar{z}) + \hat{k}_R \partial_{\bar{z}} A_z^a(z, \bar{z})] . \quad (\text{A.86})$$

Now consider the case that $\hat{k}_L = \hat{k}_R = \hat{k}$ with $\delta Z[A] = -2\pi\hat{k} \delta \int d^2z A_z^a(z, \bar{z}) A_{\bar{z}}^a(z, \bar{z})$. We

have the gauge invariant path integral

$$\begin{aligned}
Z'[A] &= Z[A] + 2\pi\hat{k} \int d^2_z A_z^a(z, \bar{z}) A_{\bar{z}}^a(z, \bar{z}) \\
&= \frac{\hat{k}}{2} \int d^2 z_1 d^2 z_2 \ln|z_{12}^2| F_{z\bar{z}}^a(z_1, \bar{z}_1) F_{z\bar{z}}^a(z_2, \bar{z}_2) .
\end{aligned}
\tag{A.87}$$

Here we start with a non-local path integral and its local gauge variation. Note that this local variation is not necessarily for a local operator, when this is the case as in $\hat{k}_L = \hat{k}_R$, one can subtract this local operator to restore gauge invariance. The OPE above is for non-zero separation only, therefore it is not sensitive to local terms. The final form of gauge invariant path integral contains field strength and the full path integral for abelian theory is just the exponential of this. The non-abelian case still requires $\hat{k}_L = \hat{k}_R$ to preserve the gauge symmetry. For parity-symmetric theories, one can define the path integral invariantly using a Pauli-Villars regulator. The anomalies are also unaffected if additional massive degrees of freedom are added. These degrees of freedom give contributions to $Z[A]$ which look local from long distance. Any such gauge variations can thus be written as variations of local operator and removed by local counterterms. From such reasoning, the anomalies in superstring theory are determined by massless spectrum that is independent of short distance stringy effects.

Now consider a single fermion of charge q coupling to a $U(1)$ gauge field. It contributes q^2 to the above jj OPE. The anomaly cancellation conditions for this free fermion is then

$$\text{gauge anomaly : } \sum_L q^2 - \sum_R q^2 = 0 , \tag{A.88}$$

$$\text{gravitational anomaly : } \sum_L 1 - \sum_R 1 = 0 , \tag{A.89}$$

$$\text{mixed anomaly : } \sum_L q - \sum_R q = 0 . \tag{A.90}$$

In four dimensional theories, the potential anomalous amplitudes have three currents as in appendix A.2.1 and the anomaly is quadratic in field strength and curvature tensors. The particle and anti-particle then have charges q and $-q$ respectively. Therefore, the two terms in anomaly are equal for odd power of q and opposite for even powers. The anomaly

cancellation condition is then

$$\text{gauge anomaly : } \sum_L q^3 = 0 , \quad (\text{A.91})$$

$$\text{mixed anomaly : } \sum_L q = 0 . \quad (\text{A.92})$$

The IIA theory is parity-symmetric and thus anomaly-free. In ten dimensions the anomaly amplitude comes from the hexagon diagram which has six currents and it is of fifth order in the field strength and curvatures. This calculation can be found in literatures with greater details. The anomaly can be written in terms of an *anomaly polynomial* which is a formal $(d + 2)$ -form $\hat{I}_{d+1}(R_2, F_2)$. The anomalous variation including gauge and gravitational transformations is give by

$$\delta \ln Z = \frac{-i}{(2\pi)^5} \int \hat{I}_d(F_2, R_2) ,$$

where \hat{I}_d is connected to anomaly polynomial through $\hat{I}_{d+2} = d\hat{I}_{d+1}$ and $\delta\hat{I}_{d+1} = d\hat{I}_d$. This simply says that the polynomial equation is an exterior derivative of a $(d + 1)$ -form whose variation is the exterior derivative of a d -form. In addition, the R_2 is the Reimann tensor and F_2 is the gauge field strength. The anomaly cancellation condition is that the total anomaly polynomial vanishes.

The $10D$ supergravity has three kinds of chiral fields that we need to take into consideration: spinors $\mathbf{8}$ and $\mathbf{8}'$, gravitinos $\mathbf{56}$ and $\mathbf{56}'$ and self-dual 5-form field strength $[5]_+$ and $[5]_-$ from the IIB theory. Parity reversal interchanges two two in each pair, they therefore make opposite contribution to the anomaly. There anomalies have been calculated in literatures.

For Majorana-Weyl $\mathbf{8}$,

$$\begin{aligned} \hat{I}_{\mathbf{8}}(F_2, R_2) = & -\frac{\text{Tr}(F_2^6)}{1440} + \frac{\text{Tr}(F_2^4)\text{tr}(R_2^2)}{2304} - \frac{\text{Tr}(F_2^2)\text{tr}(R_2^4)}{23040} - \frac{\text{Tr}(F_2^2)[\text{tr}(R_2^2)]^2}{18432} \\ & + \frac{n \text{tr}(R_2^6)}{725760} + \frac{n \text{tr}(R_2^4)\text{tr}(R_2^2)}{552960} + \frac{n[\text{tr}(R_2^2)]^3}{1327104} . \end{aligned} \quad (\text{A.93})$$

For Majorana-Weyl **56**

$$\hat{I}_{\mathbf{56}}(F_2, R_2) = -495 \frac{\text{tr}(R_2^6)}{725760} + 225 \frac{\text{tr}(R_2^4)\text{tr}(R_2^2)}{552960} - 63 \frac{[\text{tr}(R_2^2)]^3}{1327104}. \quad (\text{A.94})$$

The self-dual 5 form,

$$\hat{I}_{SD}(R_2) = 992 \frac{\text{tr}(R_2^6)}{725760} - 448 \frac{\text{tr}(R_2^4)\text{tr}(R_2^2)}{552960} + 128 \frac{[\text{tr}(R_2^2)]^3}{1327104}. \quad (\text{A.95})$$

The ‘tr’ is over the Riemann curvature indices, *i.e.* over the tangent space indices of a local coordinate patch. The products within the traces are explicitly exterior wedge products \wedge . The ‘Tr’ is over the field strength indices for the representation carried by the fermions.

Type IIB anomalies There are two **8**'s, two **56**s and one $[5]_+$. The total anomaly polynomial is then given by

$$\hat{I}_{\text{IIB}}(R_2) = -2\hat{I}_{\mathbf{8}}(R_2) + 2\hat{I}_{\mathbf{56}}(R_2) + \hat{I}_{SD}(R_2) = 0.$$

There are no gauge fields so only gravitational anomalies enter and the coefficients conspire to give a cancellation of anomaly. This existence of chiral theory is one of the reasons that string theory becomes the main candidate for unifying theory which connects with Standard Model. This anomaly free low energy effective theory can be viewed as a manifestation of internal consistency of string theory.

Type I and heterotic anomalies Since type I and heterotic string have the same low energy limits, so they are put together under discussion. One immediate problem arises since there is only one charge chiral field **8**, which implies that there is no apparent cancellation of mixed and gauge anomalies. This problem led Green and Schwarz to study the structure of the string amplitude and found a previous unknown mechanism of anomaly cancellation. Previously, we only checked counterterms built from gauge field and metric. It

is also important to look at Chern-Simons interaction

$$S' = \int B_2 \text{Tr}(F_2^4) . \quad (\text{A.96})$$

The variation of this action under gauge transformation of vector potential is

$$\delta S' \sim \int \text{Tr}(\lambda dA_1) \text{Tr}(F_2^4) . \quad (\text{A.97})$$

Therefore, we can convert this variation to $(n + 2)$ -form for anomaly polynomial through descendent equations.

$$\begin{aligned} \hat{I} &\sim \text{Tr}(\lambda dA_1) \text{Tr}(F_2^4) , \\ \hat{I}_{d+1} &\sim \text{Tr}(A_1 F_2) \text{Tr}(F_2^4) , \\ \hat{I}_{d+2} &\sim \text{Tr}(F_2^2) \text{Tr}(F_2^4) . \end{aligned} \quad (\text{A.98})$$

Therefore, the inclusion of this Chern-Simons term can cancel anomaly of this particular form. Similarly, the variation of action

$$S'' = \int B_2 [\text{Tr}(F_2^2)]^2$$

can cancel anomaly polynomial of the form $[\text{Tr}(F_2^2)]^3$. Now since fermions in supergravity theory are always in the adjoint representation, we want to convert the traces in adjoint representation into vector representation. Some useful relations in addition to eq. (A.83) are

$$\begin{aligned} \text{Tr}_a(t^2) &= (n - 2) \text{Tr}_V t^2 , \\ \text{Tr}_a(t^4) &= (n - 8) \text{Tr}_V t^4 + 3 \text{Tr}_V(t^2) \text{Tr}_V(t^2) , \\ \text{Tr}_a(t^6) &= (n - 32) \text{Tr}_V t^6 + 15 \text{Tr}_V(t^2) \text{Tr}_V(t^4) . \end{aligned} \quad (\text{A.99})$$

The last identity shows that for $SO(32)$ the gauge anomaly $\text{Tr}_a(F_2^6)$ is equal to traces of lower power and it can be cancelled by the variation of S' and S'' . This is the famous *Green-Schwarz mechanism*.

For the group E_8 , the sixth order traces reduce to

$$\mathrm{Tr}_a(t^4) = \frac{1}{100}[\mathrm{Tr}_a(t^2)]^2, \quad \mathrm{Tr}_a(t^6) = \frac{1}{7200}[\mathrm{Tr}_a(t^2)]^3. \quad (\text{A.100})$$

Now we can consider the full anomaly by including gravitational contribution. Generalising S' and S'' to

$$\int B_2 X_8(F_2, R_2), \quad (\text{A.101})$$

makes it possible to cancel anomaly of the form $\mathrm{Tr}(F_2^2)X_8(F_2, R_2)$ for arbitrary 8-form $X_8(F_2, R_2)$. Therefore, the variation of this action cancels anomaly of the form

$$[c \mathrm{Tr}(F_2^2) + c' \mathrm{Tr}(R_2^2)]X_8(F_2, R_2).$$

The total anomaly for $\mathcal{N} = 1$ supergravity with gauge group G for chiral fields: gravitino **56**, fermion **8'** and gaugino **8** in the adjoint representation, is the following

$$\begin{aligned} \hat{I}_1 &= \hat{I}_{\mathbf{56}}(R_2) - \hat{I}_{\mathbf{8}}(R_2) + \hat{I}(F_2, R_2) \\ &= \frac{1}{1440} \left\{ -\mathrm{Tr}(F_2^6) + \frac{1}{48} \mathrm{Tr}_a(F_2^2) \mathrm{Tr}_a(F_2^4) - \frac{[\mathrm{Tr}_a(F_2^2)]^3}{1440} \right\} \\ &\quad + (n - 496) \left\{ \frac{\mathrm{tr}(R_2^6)}{725760} + \frac{\mathrm{tr}(R_2^4) \mathrm{tr}(R_2^2)}{552960} + \frac{[\mathrm{tr}(R_2)]^3}{1327104} \right\} + \frac{Y_4 X_8}{768}, \end{aligned} \quad (\text{A.102})$$

with

$$\begin{aligned} Y_4 &= \mathrm{tr}(R_2^2) - \frac{1}{30} \mathrm{Tr}_a(F_2^2), \\ X_8 &= \mathrm{tr}(R_2^4) + \frac{[\mathrm{tr}(R_2)]^2}{4} - \frac{\mathrm{Tr}_a(F_2^2) \mathrm{tr}(R_2^2)}{30} + \frac{\mathrm{Tr}_a(F_2^4)}{3} - \frac{[\mathrm{Tr}_a(F_2^2)]^2}{900}. \end{aligned} \quad (\text{A.103})$$

Then anomaly is separated into three terms. The first one has to vanish for adjoint representation of the gauge group G . The second term can only vanish for the number of generator of gauge group being 496. These two requirements are both satisfied by groups $SO(32)$ and $E_8 \times E_8$. The remaining anomaly is then

$$\frac{Y_4 X_8}{768}.$$

This can be cancelled through Green-Schwarz mechanism by variation of action of the form eq. (A.101).

A.3 McKay Correspondence

In this appendix, we quickly review some rudiments of classification of discrete subgroups of finite group and its connection with that of *affine* Lie algebra for the completeness of this article.

A large class of Gorenstein canonical singularities are quotients of flat spaces by discrete groups. More importantly, when the groups are discrete subgroups of $SU(N)$, *i.e.* the holonomy groups of Calabi-Yau manifolds and when resolution of singularities are possible, these quotient spaces are singular limits of CY's and serve as local models of CY's. Such quotients of flat spaces by discrete finite subgroups are called **orbifolds**. As these orbifolds provide local CY's, we should give a closer look at these orbifolds and in particular, the orbifold of the type $\mathbb{C}^3/\Gamma \simeq \mathbb{C} \times \mathbb{C}^2/(\Gamma \subset SU(2))$. In 1884, F. Klein made classification of discrete subgroups of $SU(2)$ as a part of finding transcendental solutions to the quintic problem [120]. Note that $SU(2)$ is a double cover of $SO(3)$, which is simply the rotational group in \mathbb{R}^3 and they are the symmetries of perfectly regular shapes in \mathbb{R}^3 viz. the **Platonic Solids**. This group also affords an ADE classification: two infinite series of regular polygons and three exceptionals associated with give regular polyhedra: the tetrahedron, the cube (and its dual octahedral) and the icosahedron (and its dual dodecahedron). This classification is recorded in table A.1. Nearly a century later until 1980s, McKay [19] found another

Group	Name	Order
$A_n \simeq \mathbb{Z}_{n+1}$	Cyclic	$n + 1$
D_n	Binary Dihedral	$2n$
E_6	Binary Tetrahedral	24
E_7	Binary Octahedral (Cubic)	48
E_8	Binary Icosahedral (Dodecahedron)	120

Table A.1: The classification of discrete subgroups of $SU(2)$. As we can see that this has an ADE pattern. Note the 'binary' essentially comes from the fact that $SU(2)$ is a double cover of $SO(3)$

remarkable correspondence between these groups and the Lie algebras. His observation goes

as follows. Take the Clebsch-Gordan decomposition for \mathcal{R} , the fundamental $\mathbf{2}$ of $\Gamma \subset SU(2)$ and irreps $\{\mathcal{R}_i\}$. In another word, we take

$$\mathbf{2} \otimes \mathcal{R}_i = \bigoplus_j a_{ij}^2 \mathcal{R}_j, \quad (\text{A.104})$$

and a_{ij}^2 is taken as the adjacency matrix for some finite graph. These graphs are precisely the Dynkin diagrams of the affine simply-laced Lie algebra (the central extension of Lie algebras). The diagrams are presented in fig. A-4. The McKay correspondence shows that

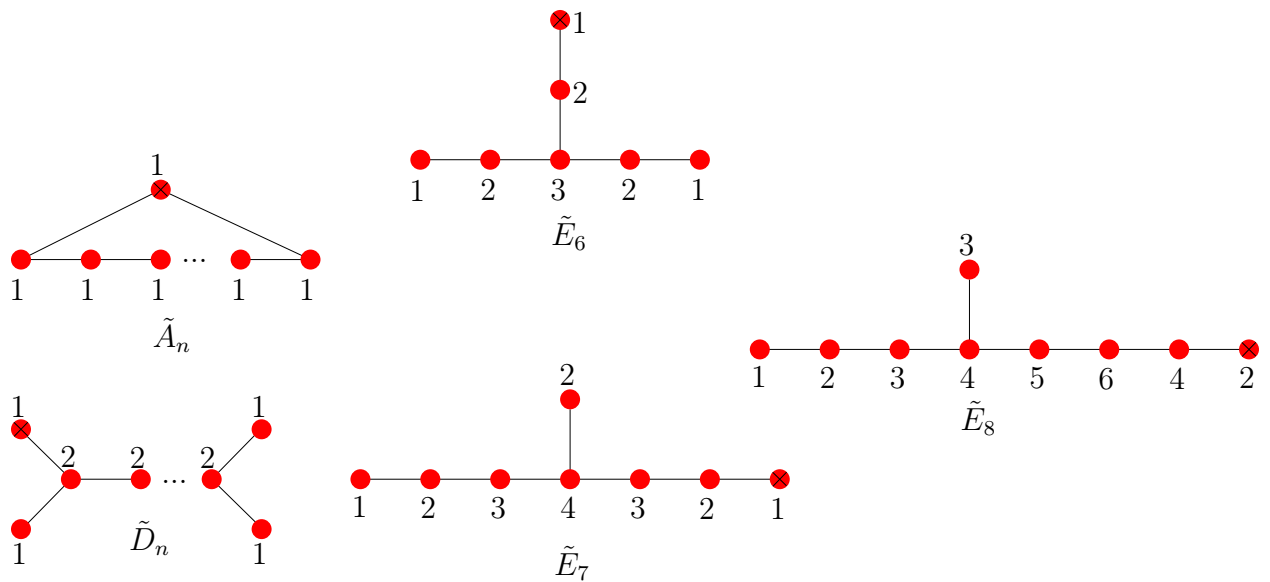


Figure A-4: The dynkin diagrams for affine simply-laced Lie algebras. The nodes are labelled by comarks of each simple roots. These diagrams have an extra affine node (marked with crosses) due to the central extension.

the node labels for affine Lie algebras correspond to the dimensions of the irreps of discrete finite subgroups of $SU(2)$. The matrices a_{ij}^2 are precisely the Cartan matrices of associated algebra.

A.4 D-branes as Probes of ALE Spaces

Before we discuss D-branes as a probe to recover the short-distance details of the background geometry, or the metric geometry of the resolved singular orbifold spaces, we shortly review an example of the string propagating on a smooth hyper-Kähler K3 manifold by ‘blowing-up’ 16 fixed points of the T^4/\mathbb{Z}_2 orbifold compactification.

Let us take a type II closed string theory compactified on a four torus T^4 , with the simplest setting where the torus is a product of four circles S^1 with radius R . Say we choose the four directions x^6, x^7, x^8, x^9 to be periodic with period $2\pi R$. The resulting 6D theory has $\mathcal{N} = 4$ supersymmetry since torus does not break any supersymmetry. Now we start orbifolding the theory with a \mathbb{Z}_2 symmetry

$$\mathbf{R}: \quad x^6, x^7, x^8, x^9 \rightarrow -x^6, -x^7, -x^8, -x^9. \quad (\text{A.105})$$

Since the isometry of \mathbb{R}^4 of the compactified directions is $SO(4) \sim SU(2)_L \times SU(2)_R$, we have the liberty to put \mathbf{R} inside $SU(2)_L$. This leaves the $SU(2)_R$ intact and it descends to a global R-symmetry of the remaining 6D $\mathcal{N} = 2$.

A.4.1 The Orbifold Spectrum

We construct the resulting 6D spectrum in this section first by obtaining the left-moving spectrum under \mathbf{R} and then tensor it with another copy from the right to get the closed string spectrum. First, we set some notations. The Roman indices $m = 6, 7, 8, 9$ are for the orbifolding directions and Greek indices are then for the remaining $\mu = 0, \dots, 5$. In addition, the 10D Lorentz group also factors as $SO(1, 9) \supset SO(1, 5) \times SO(4)$. The massless states in the theory shall be labelled under the $SU(2)_L \times SU(2)_R = SO(4)$ little group. In particular the vector representation decomposes into $\mathbf{4} = (\mathbf{2}, \mathbf{2})$ and spinor representation on the other hand decomposes into $\mathbf{2} = (\mathbf{2}, \mathbf{1})$ and $\mathbf{2}' = (\mathbf{1}, \mathbf{2})$. So we choose a labelling of the states in the Ramond sector according to rotations in the planes $(x^0, x^1), (x^2, x^3), \dots$ as eigenstates s_0, s_1, \dots, s_4 of the operators S^{01}, S^{23}, \dots , etc.⁷ We can therefore see which states survive GSO

⁷These operators are defined to find possible Weyl condition for Dirac matrices in certain dimension d . See §B.1 in [5] for more technical details.

projection in table A.2. On top of this untwisted sector, we also need to include the twisted

Sector	State	\mathbf{R}	$SU(2)_L \times SU(2)_R$
NS	$\psi_{-1/2}^\mu 0; k\rangle$	+	$(\mathbf{2}, \mathbf{2})$
	$\psi_{-1/2}^m 0; k\rangle$	-	$4 \times (\mathbf{1}, \mathbf{1})$
R	$ s_1, s_2, s_3, s_4\rangle; s_1 = +s_2, s_3 = -s_4$	+	$2 \times (\mathbf{2}, \mathbf{1})$
	$ s_1, s_2, s_3, s_4\rangle; s_1 = -s_2, s_3 = +s_4$	-	$2 \times (\mathbf{1}, \mathbf{2})$

Table A.2: Transformation properties of massless states in the untwisted sector.

sector to make the resulting theory modular invariant. In this twisted sector, the moding for the fields in the x^m directions is changed and the bosons are now half-integer moded. We recall that integer moded sectors will give us degenerate vacua, therefore, we only have states $|s_1 s_2\rangle$ from the R-sector (they are half-integer moded in the x^m directions due to orbifolding) and the NS sector, which is integer moded in the x^m directions, has states $|s_3 s_4\rangle$. Therefore, the spectrum from the twisted sector after GSO projection is in table A.3 In addition, the

Sector	State	\mathbf{R}	$SU(2)_L \times SU(2)_R$
NS	$ 0, 0, s_3 s_4\rangle; s_3 = -s_4$	+	$2 \times (\mathbf{1}, \mathbf{1})$
R	$ s_1, s_2, 0, 0\rangle; s_1 = -s_2$	-	$(\mathbf{1}, \mathbf{2})$

Table A.3: Transformation properties of massless states in the untwisted sector.

zero point energy for each sector is as follows

$$\begin{aligned}
 \text{NS sector: } & 4\left(-\frac{1}{24}\right) + 4\left(-\frac{1}{48}\right) + 4\left(\frac{1}{48}\right) + 4\left(\frac{1}{24}\right) = 0 \\
 \text{R sector: } & 4\left(-\frac{1}{24}\right) + 4\left(\frac{1}{24}\right) + 4\left(\frac{1}{48}\right) + 4\left(-\frac{1}{48}\right) = 0 .
 \end{aligned}
 \tag{A.106}$$

In the NS sector, the bosons from the twisted sector has zero point energy (z.p.e) $1/48$ (since it is half-integrally moded) and the 4 in front signifies that there are four orbifold directions. The un-twisted bosons as usual have $-1/24$ z.p.e. In the 4 directions that are not orbifolded, the z.p.e is as usual, therefore this gives the total zero in eq. (A.106). The fermions give $-1/48$ and $1/24$ respectively and they add up to zero when combined with contribution from bosons. The similar argument is applied to R sector to achieve 0 z.p.e.

With the previous results for the left-moving sector, we can tensor up an identical copy to get the spectrum Since we have 2 twisted sectors for each orbifold S^1 , we thus have 16

Sector	Untwisted	Twisted
	$SU(2)_L \times SU(2)_R$	$SU(2)_L \times SU(2)_R$
NS-NS	$(\mathbf{3}, \mathbf{3}) + (\mathbf{1}, \mathbf{3}) + (\mathbf{3}, \mathbf{1}) + (\mathbf{1}, \mathbf{1})$ $10 \times (\mathbf{1}, \mathbf{1}) + 6 \times (\mathbf{1}, \mathbf{1})$	$3 \times (\mathbf{1}, \mathbf{1}) + (\mathbf{1}, \mathbf{1})$
R-R (IIB)	$3 \times (\mathbf{3}, \mathbf{1}) + 4 \times (\mathbf{1}, \mathbf{1})$ $3 \times (\mathbf{1}, \mathbf{3}) + 4 \times (\mathbf{1}, \mathbf{1})$	$(\mathbf{1}, \mathbf{3}) + (\mathbf{1}, \mathbf{1})$
R-R (IIA)	$4 \times (\mathbf{2}, \mathbf{2})$ $4 \times (\mathbf{2}, \mathbf{2})$	$(\mathbf{2}, \mathbf{2})$

Table A.4: The bosonic spectrum for the untwisted and twisted sectors.

twisted sectors for T^4/\mathbb{Z}_2 . So we need to take 16 copies of the above twisted sector to make the complete spectrum. Let us make the identification with different pieces in the spectrum.

- Gravity multiplet $G_{\mu\nu} + B_{\mu\nu} + \Psi$ is the first line in our NS-NS untwisted sector as we expected. The $B_{\mu\nu}$ field is decomposed into self-dual and anti-self-dual parts, $B_{\mu\nu}^+$ and $B_{\mu\nu}^-$, transforming as $(\mathbf{1}, \mathbf{3})$ and $(\mathbf{3}, \mathbf{1})$. There are 16 other scalar fields in the un-twisted NS-NS sector. The twisted sector has $4 \times 16 = 64$ scalars. Including dilaton, there are 80 scalars from the NS-NS sector alone.
- The R-R sector in IIA has 8 one-forms (vectors in $SO(4)$) from untwisted sector and 16 from twisted sector. This gives a total of 24 vectors that give a generic $U(1)^{24}$.
- The R-R sector in IIB has 3 self-dual and 3 anti-self-dual tensors in the untwisted sector with additional 16 self-dual tensors $(\mathbf{1}, \mathbf{3})$ coming from twisted sector. There are 8 scalars from untwisted sector and 16 from twisted sector. Including dilaton, we have 105 scalars for IIB case.

An important note to include here is that this IIB theory is chiral and we should check if it is anomaly free. A more detailed analysis can be found in §7.6.2 in [8]. It is a miraculous fact these anomalies do cancel.

A.4.2 Spectrum on K3 Manifold

With the spectrum presented in the previous subsection, we can proceed to find the emergence of K3 manifold through these data. K3 manifold is complex two dimensional (four real dimensions) manifold containing 22 independent two-cycles, which are topologically two

spheres S^2 as complex surface $\mathbb{C}\mathbb{P}^1$. The corresponding two-forms that can be integrated on these two cycles form a 22 dimensional space. This space can have a basis built out of the data we just encountered: 19 of them are self-dual and 3 of them are anti-self-dual. The space of metric on K3 is in fact parametrised by 58 numbers. By compactifying type II theories on K3, the ten dimensional gravity multiplets and other R-R fields give rise to six dimensional fields through dimensional reduction with components of fields in K3 giving other fields. The six dimensional gravity multiplets are from reduction of NS-NS sector. The 58 scalars arise from ways the internal parts of the metric G_{mn} can choose to parametrise the space of K3 metrics. Similarly, the existence of 22 scalars is from the 19 + 3 ways to place the internal components of anti-symmetric tensor B_{mn} on the manifold.

The R-R sector on the other hand of IIB on the other had had one scalar in ten dimension reduces to a scalar in six dimension. There is a two-form to give 22 scalars in a similar fashion as NS-NS two-form. The self-dual four-form can be integrated over the 22 two cycles to give 22 two-forms in six dimensions. 19 of them are self-dual and 3 of them anti-self-dual. The last scalar comes from wrapping the four form entirely on the K3. This is the exactly the spectrum in table A.4.

For type IIA, the NS-NS sector is the same as that from IIB. There are one-form, three-form and five-form distinct for type IIA. The one-form directly descends to six dimensions as one-form. The three-form gives 22 one forms by integrating over K3 in six dimensions, while the five-form produces a single one-form. Therefore, we have 24 one-forms in six dimensions. As we can see again, this spectrum is the same as we obtained from T^4/\mathbb{Z}_2 orbifold.

A.4.3 Singular Limit of K3 Manifold

The connection between K3 manifold and our orbifold T^4/\mathbb{Z}_2 can be found through singular resolution of the orbifold [123, 124, 125, 126, 127]. The K3 manifold can reach its singular limit by choosing appropriate vacuum expectation values of various scalar field. For the orbifold T^4/\mathbb{Z}_2 , we have 16 fixed points which are locally $\mathbb{R}^4/\mathbb{Z}^2$ with infinite curvature. The 58 parameters of K3 can be seen as follows. 10 of them are from symmetric G_{mn} constant components in the internal directions. There are enough to specify the four-torus since the hypercube in \mathbb{R}^4 is specified by ten angles between its unit vectors. In addition, each of the

16 fixed-points has three scalars associated to its metric.

These three metric scalars can be tuned to resolve or ‘blow-up’ the fixed point to smooth it to \mathbb{CP}^1 . These correspond to the 16 two-cycles of the K3. The other six come from the six \mathbb{Z}_2 invariant forms $dX^m \wedge dX^n$ on the T^4 . This resolved space has the Eguchi-Hanson metric [128] which is locally asymptotically to $\mathbb{R}^4/\mathbb{Z}_2$. The explicit metric is

$$ds^2 = \left(1 - \left(\frac{a}{r}\right)^4\right)^{-1} dr^2 + r^2 \left(1 - \left(\frac{a}{r}\right)^4\right) \sigma_3^2 + r^2(\sigma_1^2 + \sigma_2^2), \quad (\text{A.107})$$

where σ_i are defined in terms of the S^3 Euler angles (θ, ϕ, ψ) with $4(\sigma_1^2 + \sigma_2^2) = d\theta^2 + \sin^2\theta d\phi^2$. The point where $r = a$ is called the ‘bolt’ singularity. The space has a topology of $\mathbb{R}_{r\psi}^2 \times S_{\theta\phi}^2$ with the radius of S^2 being $a/2$. This is actually a coordinate singularity if ψ has period of 2π . However, ψ has period of 4π , the space at infinity is S^3/\mathbb{Z}_2 . For small a , the Eguchi-Hanson space can be put onto the space after we take out the neighbourhood of the fixed point. The ‘bolt’ is in fact \mathbb{CP}^1 and the parameter a controls the size of the bolt with other two parameters correspond to how \mathbb{R}^2 is oriented in \mathbb{R}^4 .

The Eguchi-Hanson space is the simplest example of ‘Asymptotically Locally Euclidean’ (ALE) space which K3 can be tuned to resemble locally. These ALE spaces are classified according to their identification at infinity by the discrete finite subgroups Γ of $SU(2)$, which acts on S^3 at infinity to give S^3/Γ . These subgroups have an ADE pattern due to the observation by McKay [19]. The A-series correspond to Gibbons-Hawking metrics and Eguchi-Hanson is the simplest of such series corresponding to A_1 .

A.5 D-brane Probes

After the construction of type II string, we see that by resolving singular orbifold T^2/\mathbb{Z}_2 , one can reconstruct the same spectrum for strings compactified on the smooth hyper-Kähler manifold K3. But to be strict, we only recovered the spectrum or the algebraic data of the K3 manifold but the full geometric data is still not fully present. In this subsection, we review a powerful and central technique to this article to recover the geometric details. This is done by using D-brane as a probe to singular background geometry.

To illustrate the central idea behind the original idea [24], we focus on a single orbifolded point and type IIB theory. The full theory is propagating in the space of $\mathbb{R}^6 \times (\mathbb{R}^4/\mathbb{Z}_2)$ which has the same reflection \mathbf{R} as that in appendix A.4.1: $\mathbf{R} : (x^6, x^7, x^8, x^9) \rightarrow (-x^6, -x^7, -x^8, -x^9)$. The D1-brane is placed in this plane at $x^2, \dots, x^9 = 0$. For this setup, we have the table A.5. The D1-brane needs to include an image if it is to move off the fixed

	x^0	x^1	x^2	x^3	x^4	x^5	x^6	x^7	x^8	x^9
D1	–	–								
ALE	–	–	–	–	–	–				

Table A.5: The coordinate arrangement for D1-brane probing ALE.

point of the action \mathbf{R} to respect the \mathbb{Z}_2 symmetry. This requires us to include two Chan-Paton indices for the D1-brane and its image. This gets us to start with a $U(2)$ symmetry for D-brane system living at the fixed point. Since the \mathbf{R} action exchanges the two D-branes, it can be seen as acting on the open string states as the exchange represented by matrix $\gamma = \sigma^1$, where σ^i are the Pauli matrices since we are considering $U(2)$. The representation of the action of \mathbf{R} can therefore be written as

$$\mathbf{R} |\psi, ij\rangle = \sigma_{ii'} |\mathbf{R}\psi, i'j'\rangle \sigma_{j'j}^{-1}. \quad (\text{A.108})$$

It acts on the oscillator as usually but also switches the Chan-Paton indices of the D1-branes. We therefore must make sure that the orbifold action also acts on the Chan-Paton indices when D-branes are present [45].

Now we can look at the spectrum. In the NS sector, the massless \mathbf{R} -invariant states are (in terms of vertex operator)

$$\begin{aligned} \partial_t X^\mu \sigma^{0,1}, \quad \mu = 0, 1 \\ \partial_n X^i \sigma^{0,1}, \quad i = 2, 3, 4, 5 \\ \partial_n X^m \sigma^{2,3}, \quad i = 6, 7, 8, 9. \end{aligned} \quad (\text{A.109})$$

Note here the Pauli matrices essentially signify the structure of the Chan-Paton indices. Since the first row has its spacetime indices of the D1-brane, it is therefore a gauge field for the $U(1) \times U(1)$ world-volume gauge group. The next row are four scalars in the adjoint

representation of the gauge group, describing the position of D1-brane inside \mathbb{R}^6 . The last row is the four scalars in the bifundamental charges $(\pm 1, \mp 1)$ of the gauge group. They can also be interpreted as transverse position of the D1-brane in x^6, x^7, x^8, x^9 . These D-string fields are denoted by A^μ, X^i, X^m , which are all 2×2 matrices. The gauge group and matter content are all recorded in the ‘quiver diagram’ drawn in fig. A-5.

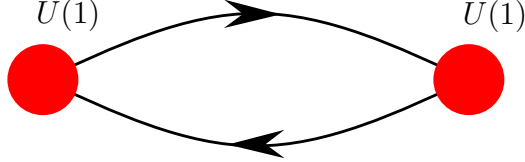


Figure A-5: The quiver diagram for the $U(1) \times U(1)$ gauge theory on D1-brane.

Quiver diagrams of such type has nodes representing the gauge group $U(n_i)$ and the arrows representing bifundamental fields which are usually matrix valued as our $U(1) \times U(1)$ gives fields in 2×2 matrices. Note that this diagram is simply the affine Dynkin diagram of A_1 , with one node being the trivial representation which physically represents the centre of mass of the D-brane system.

The bosonic action for these fields is the $D = 10$ $U(2)$ Yang-Mills action with a dimensional reduction and \mathbb{Z}_2 projection.

$$\begin{aligned} \text{Kinetic term : } & -\frac{1}{4g_{YM}^2} \left(F_{\mu\nu}F^{\mu\nu} + \sum_i \mathcal{D}_\mu X^i \mathcal{D}^\mu X^i + \sum_m \mathcal{D}_\mu X^m \mathcal{D}^\mu X^m \right) \\ \text{Potential term : } & -\frac{1}{4g_{YM}^2} \left(2 \sum_{i,m} \text{Tr}[X^i, X^m]^2 + \sum_{m,n} \text{Tr}[X^m, X^n]^2 \right), \end{aligned} \quad (\text{A.110})$$

where $g_{YM}^2 = (2\pi)^{-1} \alpha'^{-1/2} g_s$. The resulting theory has $\mathcal{N} = (4, 4)$ supersymmetry in $D = 2$ with a $SU(2)$ R-symmetry which can be interpreted as the remnant $SU(2)_R$ from parent $SO(4)$ by including the orbifold action \mathbb{Z}_2 inside $SU(2)_L$.

Now we want to find the moduli space, the *family* of vacua, of this dimensionally reduced theory. There are two different ‘branches’ in the moduli space.

- The ‘Coulomb branch’ is defined by $X^m = 0$ and $X^i = u^i \sigma^0 + v^i \sigma^1$. This has a geometric meaning of two D1-branes moving independently inside the \mathbb{R}^6 with positions $u^i \pm v^i$

but staying at the fixed point in $\mathbb{R}^4/\mathbb{Z}^2$. In this branch, the gauge symmetry stays intact giving independent $U(1)$ group on each D-brane.

- The ‘Higgs branch’ on the other hand, is defined by non-zero X^m and $X^i = u^i \sigma^0$, the σ^1 gauge invariance is broken and we can choose a gauge in which $X^m = w^m \sigma^3$. This corresponds to the D1-brane moving off the fixed plane with string and its image being at $(u^i, \pm w^m)$. This branch has the $\mathbb{R}^6 \times \mathbb{R}^4/\mathbb{Z}_2$ we started with.
- The orbifold requires the twisted sector to make the theory modular invariant as we covered in table A.4. These twisted sectors are essential to resolve the orbifold singularity. Now let us define a complex variable q^m by $X^m = \sigma^3 \text{Re}(q^m) + \sigma^2 \text{Im}(q^m)$ and two doublets of the remaining $SU(2)_R$ made out of them

$$\Phi_0 = \begin{pmatrix} q^6 + iq^7 \\ q^8 + iq^9 \end{pmatrix} \quad \Phi_1 = \begin{pmatrix} \bar{q}^6 + i\bar{q}^7 \\ \bar{q}^8 + i\bar{q}^9 \end{pmatrix}. \quad (\text{A.111})$$

These doublets have charges ± 1 respectively under the σ^1 of $U(1)$. The three NS-NS moduli can thus be written as a vector ξ of the $SU(2)_R$, and the potential is proportional to

$$(\xi - \mu)^2 \equiv (\Phi_0^\dagger \tau \Phi_0 - \Phi_1^\dagger \tau \Phi_1 + \xi)^2, \quad (\text{A.112})$$

where the Pauli matrices are collected into a vector $\tau = (\tau^1, \tau^2, \tau^3)$ to emphasise that they now act on a different space. the vector μ is what mathematician call a ‘momentum map’ which we shall come to a bit more detail in next section. The form of this potential comes from the supersymmetric construction of the ‘D-term’. The vanishing of this is called the ‘D-flat’ condition and the vector ξ is the ‘Fayet–Iliopoulos’ parameter in the D-term, and the presence of this parameter comes from the existence of abelian $U(1)$ factors in the gauge group. Also the $SU(2)_R$ requires that the FI term and the D-term to come in as a vector. One can check that this form reduces to the second term in the potential of eq. (A.110) when $\xi = 0$. A further discussion on this can be found in literature [9, 10]. For the case when $\xi \neq 0$, the moduli space of the gauge theory is the set of possible locations of the D1-brane probe, which is the blown-up smooth ALE space. The X^m contain eight scalar fields. Three

of them are removed by the ‘D-flatness’ condition that the superpotential should vanish. With the fourth one being a gauge degree of freedom, we have four moduli in total. Thus the theory has the amount of supersymmetry equivalent to $D = 6 \mathcal{N} = 1$.

A.5.1 ALE Space as the Moduli Space

The metric for this moduli space should have the metric of the smooth ALE space as its metric [46]. Since there are eight supercharges, the space should be a hyper-Kähler manifold [47]. The three coordinates on the moduli space afford the definition (normalisation absorbs the dimensionful constants)

$$\mathbf{y} = \Phi_0^\dagger \tau \Phi_0 , \tag{A.113}$$

and the fourth coordinate z is defined as $z = 2\arg(\Phi_{0,1}\Phi_{1,1})$. The D-flatness condition gives

$$\Phi_1^\dagger \tau \Phi_1 = \mathbf{y} + \boldsymbol{\xi} , \tag{A.114}$$

where we can determine Φ_0 and Φ_1 in terms of \mathbf{y} and z .

The original metric of the space of hypermultiplet VEVs is the flat metric

$$ds^2 = d\Phi_0^\dagger d\Phi_0 + d\Phi_1^\dagger d\Phi_1 . \tag{A.115}$$

We have to project this metric onto the space orthogonal to the $U(1)$ gauge action. We have to project this onto the space orthogonal to the $U(1)$ gauge transformation. This can be done via coupling Φ_0 and Φ_1 to two dimensional gauge field and integrate out the gauge fields. Thus we have

$$ds^2 = d\Phi_0^\dagger d\Phi_0 + d\Phi_1^\dagger d\Phi_1 - \frac{(\omega_0 + \omega_1)^2}{4(\Phi_0^\dagger \Phi_0 + \Phi_1^\dagger \Phi_1)} , \tag{A.116}$$

with $\omega_i = i(\Phi_i^\dagger d\Phi_i - d\Phi_i^\dagger \Phi_i)$. To rewrite the metric in terms of \mathbf{y} and t for arbitrary $SU(2)$

doublets $\alpha, \beta, \gamma, \delta$,⁸ we find the metric is the $\mathcal{N} = 2$ Gibbons-hawking metric

$$ds^2 = V^{-1}(dz - \mathbf{A} \cdot d\mathbf{y})^2 + V d\mathbf{y} \cdot d\mathbf{y}$$

$$V = \sum_{i=0}^{N-1} \frac{1}{|\mathbf{y} - \mathbf{y}_i|}, \quad \nabla V = \nabla \times \mathbf{A} . \quad (\text{A.119})$$

Up to an overall normalisation, we have $y_0 = 0$, $y_1 = \xi$ and the vector potential is

$$\mathbf{A}(\mathbf{y}) \cdot d\mathbf{y} = |\mathbf{y}|^{-1}\omega_0 + |\mathbf{y} + \boldsymbol{\xi}|^{-1}\omega_1 + dz . \quad (\text{A.120})$$

The field strength is thus obtained by taking exterior derivative. With a change of variable [17], this metric for $\mathcal{N} = 2$ thus becomes the Eguchi-Hanson metric. The three parameters in vector $y_1 = \boldsymbol{\xi}$ are the NS-NS fields characterising the size and orientation of the \mathbb{CP}^1 blow-up.

A.5.2 Hyper-Kähler Quotient Construction of ALE Spaces

The construction we just described is the *hyper-Kähler quotient* [18], which was used in [16] to construct the full family of ALE metrics. Hyper-Kähler spaces are complex $4k$ -dimensional manifolds with three complex structures that transform under an $SU(2)$ symmetry, which in physical language, often becomes the $SU(2)$ R-symmetry for a system with eight supercharges. These complex structures are in fact, quaternionic in nature. In this subsection, we draw out attention to quickly review this quotient construction of ALE spaces as a small detour.

A Riemannian manifold X with three covariantly constant complex structures $i := I, J, K$ satisfying the quaternionic algebra is call **Hyper-Kähler**. We can thus construct closed

⁸The identity to use here is

$$(\alpha^\dagger \tau^a \beta)(\gamma^\dagger \tau^a \delta) = 2(\alpha^\dagger \delta)(\gamma^\dagger \beta) - (\alpha^\dagger \beta)(\gamma^\dagger \delta) . \quad (\text{A.117})$$

Thus we have

$$\begin{aligned} \Phi_0^\dagger \Phi_0 &= |\mathbf{y}|, & \Phi_1^\dagger \Phi_1 &= |\mathbf{y} + \boldsymbol{\xi}|, \\ d\mathbf{y} \cdot d\mathbf{y} &= |\mathbf{y}| d\Phi_0^\dagger d\Phi_0 - \omega_0^2 = |\mathbf{y} + \boldsymbol{\xi}| d\Phi_1^\dagger d\Phi_1 - \omega_1^2 . \end{aligned} \quad (\text{A.118})$$

Kähler 2-forms:

$$\omega_i(V, W) := g(V, iW) \quad \text{for } i = I, J, K, \quad (\text{A.121})$$

mapping tangent vectors $V, W \in T(X)$ to \mathbb{R} with g being the metric tensor.

On such a manifold with Killing vectors V ($\mathcal{L}_V g = 0$), we can impose the **triholomorphicity** condition as: $\mathcal{L}_V \omega_i = V^\nu (d\omega_i)_\nu + d(V^\nu (\omega_i)_\nu) = 0$. This condition joined with the closedness of Kähler form $d\omega_i = 0$ implies the existence of potentials μ_i , such that $d\mu_i = V^\nu (\omega_i)_\nu$. As the dual of the Lie algebra \mathfrak{g} of the group of symmetries G generated by the Killing vectors V is identifiable with left-invariant forms, we have the following induced map of such potentials

$$\mu_i : X \rightarrow \mu_i^a \in \mathbb{R}^3 \otimes \mathfrak{g}^* \quad i = 1, 2, 3; \quad a = 1, \dots, \dim(G). \quad (\text{A.122})$$

These maps are the (hyper-Kähler) **moment maps** and usually groups as $\mu_{\mathbb{R}} = \mu_3$ and $\mu_{\mathbb{C}} = \mu_1 + i\mu_2$. Therefore, any hyper-Kähler manifold Ξ of dimension $4n$ with k freely acting triholomorphic symmetries can be used to construct another, X_ζ , of dimension $4n - 4k$ by the following steps

1. For $3k$ moment maps, we can define level set of dimension $4n - 3k$:

$$P_\zeta := \{\xi \in \Xi \mid \mu_i^a(\xi) = \zeta_i^a\} \quad (\text{A.123})$$

2. When $\zeta \in \mathbb{R}^3 \otimes \text{Centre}(\mathfrak{g}^*)$, P_ζ is a principal G -bundle over a new hyper-Kähler manifold

$$X_\zeta := P_\zeta / G \simeq \{\xi \in \Xi \mid \mu_i^a(\xi) = \zeta_{\mathbb{C}}^a\}. \quad (\text{A.124})$$

This quotient construct is the celebrated **Hyper-Kähler quotient** construction [122, 16].

Now we can review this construction for ALE spaces in Kronheimer's work. Recall that an ALE space is the orbifold $\mathbb{C}^2 / (\Gamma \in SU(2))$. Before we apply this to ALE spaces, we clarify some notations

- $\Gamma \in SU(2)$: discrete finite subgroups of $SU(2)$ with ADE pattern.

- $Q :=$ The defining \mathbb{C}^2 representation.
- $R :=$ The regular $|\Gamma|$ -dimensional complex representation. $R_{i=0,\dots,r} :=$ Irreps(Γ) of dimension n_i with 0 being the trivial affine node (trivial representation).
- $(\)_\Gamma :=$ the Γ -invariant part, a_{ij} The adjacency matrix McKay quiver for Γ . They have a relation defined as $Q \otimes R_i = \oplus_j a_{ij} R_j$.
- $T := \{x_0 + x_1i + x_2j + x_3k | x_i \in \mathbb{R}\}$: A one-dimensional quaternion vector space; $\Lambda^+ T^* = \text{Span}\{\text{hyper-Kähler two-forms } \omega_{i=I,J,K}\}$: The self-dual part of the second exterior power of the dual space.
- $[y \wedge y] := (T^* \wedge T^*) \otimes [\text{End}(V), \text{End}(V)]$, for $y \in T^* \otimes \text{End}(V)$; $\text{Endkew}(R) :=$ The anti-Hermitian endomorphism of R ; $Z :=$ Traceless part of the Centre($\text{Endskew}_\Gamma(R)$).
- $G := \prod_{i=1}^r U(n_i) =$ The group of unitary automorphisms of R commuting with the action of Γ , modded out by $U(1)$ scaling. This will correspond to the nodes (fractional branes) in our quiver diagram as we have seen.
- $X_\zeta := \{y \in (T^* \otimes_{\mathbb{R}} \text{Endskew}(R))_\Gamma | [y \wedge y]^+ = \zeta\} / G$ for generic $\zeta \in \Lambda^+ T^* \otimes Z$.
- $\mathcal{R} := Y_\zeta \times_G R$ with $Y_\zeta := \{y | [y \wedge y]^+ = \zeta\}$: The natural bundle over X_ζ .
- $\xi :=$ A tautological vector-bundle endomorphism as an element in $T^* \otimes_{\mathbb{R}} \text{Endskew}(\mathcal{R})$.

Now we can apply hyper-Kähler quotient construction to the ALE manifold

$$\begin{aligned}
\Xi &:= (Q \otimes \text{End}(R))_\Gamma = \left\{ \xi = \begin{pmatrix} \alpha \\ \beta \end{pmatrix} \right\} \\
&= \oplus_{ij} a_{ij} \text{Hom}(\mathbb{C}^{n_i}, \mathbb{C}^{n_j}) \\
&\simeq (T^* \times_{\mathbb{R}} \text{Endskew}(R))_\Gamma = \left\{ \xi = \begin{pmatrix} \alpha & -\beta^\dagger \\ \beta & \alpha^\dagger \end{pmatrix} \right\}, \tag{A.125}
\end{aligned}$$

where α and β are $|\Gamma| \times |\Gamma|$ matrices satisfying

$$\begin{pmatrix} R_\gamma \alpha R_{\gamma^{-1}} \\ R_\gamma \beta R_{\gamma^{-1}} \end{pmatrix} = Q_\gamma \begin{pmatrix} \alpha \\ \beta \end{pmatrix},$$

for $\gamma \in \Gamma$. This is simply the Γ -invariance condition or in terms of physical language, the projection of matter content by the action of orbifold. In the second line, we have used the definition of McKay quiver matrices for a_{ij} . The third line is the canonical isomorphism between \mathbb{C}^4 and the quaternions. The hyper-Kähler two-forms are $\omega_{\mathbb{R}} = \text{Tr}(d\alpha \wedge d\alpha^\dagger) + \text{Tr}(d\beta \wedge d\beta^\dagger)$ and $\omega_{\mathbb{C}} = \text{Tr}(d\alpha \wedge d\beta)$. The moment map is $\mu_{\mathbb{R}} = [\alpha, \alpha^\dagger] + [\beta, \beta^\dagger]$ and $\mu_{\mathbb{C}} = [\alpha, \beta]$. The group of trihomomorphic isometries is $G = \prod_{i=1}^r U(n_i)$ with trivial $U(n_0) = U(1)$ modded out. Then we have the theorem due to Kronheimer

Theorem. *The space*

$$X_\zeta := \{\xi \in \Xi \mid \mu_i^a(\xi) = \zeta_i^a\} / G \tag{A.126}$$

is a smooth hyper-Kähler manifold of dimension four diffeomorphic to the resolution of the ALE orbifold \mathbb{C}^2/Γ . And all ALE hyper-Kähler four-folds are obtained through such resolution.

Remark. In the metric, $\zeta_{\mathbb{C}}$ is the complex deformation while $\zeta_{\mathbb{R}} = 0$ corresponds to the singular limit \mathbb{C}^2/Γ .

A.6 Computational Modules

We created various *Mathematica* modules that implement the ideas presented in this paper. Their applicability goes well beyond the classification of brane tilings we presented and should be useful for a wide community. They are publicly available at [158]. Here we summarize some of the basic commands.

So far the package is for a standard **Unix** environment, where the default directory for storing the intermediate output is the user's home directory `$HOME`.

The $m \times n$ rectangular brane tilings for $\mathcal{C}/\mathbb{Z}_m \times \mathbb{Z}_n$ play a central role in our studies, since we use them as simple starting points for partial resolution. For this reason, we created a module called `RecDimerModels[m,n]`, which generates the brane tiling for $\mathcal{C}/(\mathbb{Z}_m \times \mathbb{Z}_n)$ with all its elements properly labeled and generates its Kasteleyn matrix. The intermediate data is stored in the file `$HOME.dimer.model.tmp.txt`.

Next, the `ToricInfo[KM]` module takes a Kasteleyn matrix as input and produces the corresponding perfect matchings and toric diagram.

For triangulating toric diagrams, we provide `TriangDimer[ToricPts]`, which is a modified version of the `DelaunayMesh[]` command in *Mathematica*.

The module `RemovePoints[KM,Ptsremove]` generates all possible collections of vevs, or equivalently edges to be removed, that give rise to a desired partial resolution defined by a starting toric diagram and the points we want to delete from it (*Ptsremove*). The data is loaded in `$HOME.dimer.model.tmp.txt`. This is the most computationally intensive module, even though we use parallel computing and an optimized algorithm to enumerate all collections of removed edges. The output is in the form of a list containing all the possible higgsings (*PossibleHiggsings*). With this information, it is straightforward to determine the brane tiling resulting from any of these higgsings using `HiggsingDimerSU[Kmatrix,possiblehiggsing]`. This module also produces the quiver and superpotential for the brane tiling.

Algorithm 1 provides a brief summary of how these modules were exploited for the classification of brane tilings carried out in this paper.

Algorithm 1 Classification of dimer models for all toric diagrams with a given area

Initialise *Models* as empty set. ▷ used as storing physical models.

Load *PSets* as all the inequivalent toric diagrams with a given area.

for *toric* in *PSets* **do**

 Define *Kmatrix* by using `RecDimerModels[m,n]`. The integers *m* and *n* must define a rectangular toric diagram in which *toric* can be embedded.

 Define *ptsremove* as the set containing points to be removed from the rectangular toric diagram.

 Determine *PossibleHiggsings*, the collections of vevs that produce a given partial resolution, using `RemovePoints[Kmatrix,ptsremove]`.

for *possiblehiggsing* in *PossibleHiggsings* **do**

 Use `HiggsingDimer[Kmatrix,higgsantz]` to compute the brane tiling, quiver and superpotential for every *possiblehiggsing*.

 Save this information into *Models*.

end for

end for

Bibliography

- [1] M. B. Green, J. H. Schwarz and E. Witten, "Superstring Theory Vol. 1 : 25th Anniversary Edition." doi:10.1017/CBO9781139248563
- [2] M. B. Green, J. H. Schwarz and E. Witten, "Superstring Theory Vol. 2 : 25th Anniversary Edition," doi:10.1017/CBO9781139248570
- [3] K. Becker, M. Becker and J. H. Schwarz, "String theory and M-theory: A modern introduction."
- [4] J. Polchinski, "String theory. Vol. 1: An introduction to the bosonic string."
- [5] J. Polchinski, "String theory. Vol. 2: Superstring theory and beyond," doi:10.1017/CBO9780511618123
- [6] Fujikawa, K. and Suzuki, H., "Path Integrals and Quantum Anomalies." International Series of Monographs on Physics, 2004, OUP Oxford, **ISBN 9780191523816**
- [7] A. Sen, "Tachyon dynamics in open string theory," Int. J. Mod. Phys. A **20**, 5513 (2005) doi:10.1142/S0217751X0502519X [hep-th/0410103].
- [8] C.V. Johnson, "D-Branes," Cambridge Monographs on Mathematical Physics 2006, Cambridge University Press, **ISBN 9780521030052**
- [9] S. Weinberg, "The Quantum Theory of Fields, Vol 3," Cambridge Monographs on Mathematical Physics 2000, Cambridge University Press
- [10] M. F. Sohnius, "Introducing Supersymmetry," Phys. Rept. **128**, 39 (1985). doi:10.1016/0370-1573(85)90023-7

- [11] F. Gliozzi, J. Scherk and D. I. Olive, “Supergravity and the Spinor Dual Model,” *Phys. Lett.* **65B** (1976) 282. doi:10.1016/0370-2693(76)90183-0
- [12] J.E. Paton and H.M Chan, “Generalized veneziano model with isospin”. *Nuclear Physics B*, 10(3):516520, 1969.
- [13] E. Witten, “String theory dynamics in various dimensions,” *Nucl. Phys. B* **443**, 85 (1995) doi:10.1016/0550-3213(95)00158-O [hep-th/9503124].
- [14] P. Candelas, G. T. Horowitz, A. Strominger and E. Witten, “Vacuum Configurations for Superstrings,” *Nucl. Phys. B* **258**, 46 (1985). doi:10.1016/0550-3213(85)90602-9
- [15] M. Kreuzer and H. Skarke, “Complete classification of reflexive polyhedra in four-dimensions,” *Adv. Theor. Math. Phys.* **4**, 1209 (2002) doi:10.4310/ATMP.2000.v4.n6.a2 [hep-th/0002240].
- [16] P. Kronheimer, “The construction of ale spaces as hyper-kähler quotients,” *Journal of differential geometry*, 29(3):665683, 1989.
- [17] M. K. Prasad, *Phys. Lett.* **83B**, 310 (1979). doi:10.1016/0370-2693(79)91114-6
- [18] N. J. Hitchin, A. Karlhede, U. Lindstrom and M. Rocek, “Hyperkahler Metrics and Supersymmetry,” *Commun. Math. Phys.* **108**, 535 (1987). doi:10.1007/BF01214418
- [19] G. Mackey, “Graphs, singularities, and finite groups,” *Uspekhi Matematicheskikh Nauk*, 38(3):159162, 1983.
- [20] Y. Ito and M. Reid, “The McKay correspondence for finite subgroups of $SL(3, \mathbb{C})$,” *alg-geom/9411010*.
- [21] A. Hanany and Y. H. He, “NonAbelian finite gauge theories,” *JHEP* **9902**, 013 (1999) doi:10.1088/1126-6708/1999/02/013 [hep-th/9811183].
- [22] S. Govindarajan and T. Jayaraman, “D-branes, exceptional sheaves and quivers on Calabi-Yau manifolds: From Mukai to McKay,” *Nucl. Phys. B* **600**, 457 (2001) doi:10.1016/S0550-3213(01)00062-1 [hep-th/0010196].

- [23] A. Tomasiello, “D-branes on Calabi-Yau manifolds and helices,” JHEP **0102**, 008 (2001) doi:10.1088/1126-6708/2001/02/008 [hep-th/0010217].
- [24] M. R. Douglas and G. W. Moore, “D-branes, quivers, and ALE instantons,” hep-th/9603167.
- [25] C. V. Johnson and R. C. Myers, “Aspects of type IIB theory on ALE spaces,” Phys. Rev. D **55**, 6382 (1997) doi:10.1103/PhysRevD.55.6382 [hep-th/9610140].
- [26] A. E. Lawrence, N. Nekrasov and C. Vafa, “On conformal field theories in four-dimensions,” Nucl. Phys. B **533**, 199 (1998) doi:10.1016/S0550-3213(98)00495-7 [hep-th/9803015].
- [27] M. R. Douglas, B. R. Greene and D. R. Morrison, “Orbifold resolution by D-branes,” Nucl. Phys. B **506**, 84 (1997) doi:10.1016/S0550-3213(97)00517-8 [hep-th/9704151].
- [28] D. R. Morrison and M. R. Plesser, “Nonspherical horizons. 1.,” Adv. Theor. Math. Phys. **3**, 1 (1999) doi:10.4310/ATMP.1999.v3.n1.a1 [hep-th/9810201].
- [29] C. Beasley, B. R. Greene, C. I. Lazaroiu and M. R. Plesser, “D3-branes on partial resolutions of Abelian quotient singularities of Calabi-Yau threefolds,” Nucl. Phys. B **566**, 599 (2000) doi:10.1016/S0550-3213(99)00646-X [hep-th/9907186].
- [30] R. von Unge, “Branes at generalized conifolds and toric geometry,” JHEP **9902**, 023 (1999) doi:10.1088/1126-6708/1999/02/023 [hep-th/9901091].
- [31] K. Oh and R. Tatar, “Branes at orbifolded conifold singularities and supersymmetric gauge field theories,” JHEP **9910**, 031 (1999) doi:10.1088/1126-6708/1999/10/031 [hep-th/9906012].
- [32] J. Park, R. Rabadan and A. M. Uranga, “Orientifolding the conifold,” Nucl. Phys. B **570**, 38 (2000) doi:10.1016/S0550-3213(99)00700-2 [hep-th/9907086].
- [33] D. Berenstein and R. G. Leigh, “Discrete torsion, AdS / CFT and duality,” JHEP **0001**, 038 (2000) doi:10.1088/1126-6708/2000/01/038 [hep-th/0001055].

- [34] I. R. Klebanov and E. Witten, “Superconformal field theory on three-branes at a Calabi-Yau singularity,” Nucl. Phys. B **536**, 199 (1998) doi:10.1016/S0550-3213(98)00654-3 [hep-th/9807080].
- [35] E. Witten, Nucl. Phys. B **403**, 159 (1993) [AMS/IP Stud. Adv. Math. **1**, 143 (1996)] doi:10.1016/0550-3213(93)90033-L [hep-th/9301042].
- [36] A. M. Uranga, “Brane configurations for branes at conifolds,” JHEP **9901**, 022 (1999) doi:10.1088/1126-6708/1999/01/022 [hep-th/9811004].
- [37] O. Aharony and A. Hanany, “Branes, superpotentials and superconformal fixed points,” Nucl. Phys. B **504**, 239 (1997) doi:10.1016/S0550-3213(97)00472-0 [hep-th/9704170].
- [38] O. Aharony, A. Hanany and B. Kol, “Webs of (p,q) five-branes, five-dimensional field theories and grid diagrams,” JHEP **9801**, 002 (1998) doi:10.1088/1126-6708/1998/01/002 [hep-th/9710116].
- [39] A. Hanany and A. Iqbal, “Quiver theories from D6 branes via mirror symmetry,” JHEP **0204**, 009 (2002) doi:10.1088/1126-6708/2002/04/009 [hep-th/0108137].
- [40] P. Gabriel, “Unzerlegbare Darstellungen. I,” Manuscripta Math. **6** (1972) 71103; correction, *ibid.* **6** (1972), 309.
- [41] K. D. Kennaway, “Brane Tilings,” Int. J. Mod. Phys. A **22**, 2977 (2007) doi:10.1142/S0217751X07036877 [arXiv:0706.1660 [hep-th]].
- [42] M. Yamazaki, Fortsch. Phys. **56**, 555 (2008) doi:10.1002/prop.200810536 [arXiv:0803.4474 [hep-th]].
- [43] Y. H. He, “Calabi-Yau Varieties: from Quiver Representations to s d’Enfants,” arXiv:1611.09398 [math.AG].
- [44] S. Benvenuti and A. Hanany, “New results on superconformal quivers,” JHEP **0604**, 032 (2006) doi:10.1088/1126-6708/2006/04/032 [hep-th/0411262].
- [45] E. G. Gimon and J. Polchinski, “Consistency conditions for orientifolds and d manifolds,” Phys. Rev. D **54**, 1667 (1996) doi:10.1103/PhysRevD.54.1667 [hep-th/9601038].

- [46] M. R. Douglas, “Gauge fields and D-branes,” *J. Geom. Phys.* **28**, 255 (1998) doi:10.1016/S0393-0440(97)00024-7 [hep-th/9604198].
- [47] L. Alvarez-Gaume and D. Z. Freedman, “Geometrical Structure and Ultraviolet Finiteness in the Supersymmetric Sigma Model,” *Commun. Math. Phys.* **80**, 443 (1981). doi:10.1007/BF01208280
- [48] H. Ooguri and C. Vafa, “Two-dimensional black hole and singularities of CY manifolds,” *Nucl. Phys. B* **463**, 55 (1996) doi:10.1016/0550-3213(96)00008-9 [hep-th/9511164].
- [49] A. Hanany and K. D. Kennaway, “Dimer models and toric diagrams,” hep-th/0503149.
- [50] A. Hanany and D. Vegh, “Quivers, tilings, branes and rhombi,” *JHEP* **0710**, 029 (2007) doi:10.1088/1126-6708/2007/10/029 [hep-th/0511063].
- [51] S. Franco, A. Hanany, K. D. Kennaway, D. Vegh and B. Wecht, “Brane dimers and quiver gauge theories,” *JHEP* **0601**, 096 (2006) doi:10.1088/1126-6708/2006/01/096 [hep-th/0504110].
- [52] S. Franco, A. Hanany, D. Martelli, J. Sparks, D. Vegh and B. Wecht, *Gauge theories from toric geometry and brane tilings*, *JHEP* **01** (2006) 128, [hep-th/0505211].
- [53] Y. Imamura, “Global symmetries and ’t Hooft anomalies in brane tilings,” *JHEP* **0612**, 041 (2006) doi:10.1088/1126-6708/2006/12/041 [hep-th/0609163].
- [54] Y. Imamura, K. Kimura and M. Yamazaki, “Anomalies and O-plane charges in orientifolded brane tilings,” *JHEP* **0803**, 058 (2008) doi:10.1088/1126-6708/2008/03/058 [arXiv:0801.3528 [hep-th]].
- [55] S. Franco, Y. H. He, C. Sun and Y. Xiao, “A Comprehensive Survey of Brane Tilings,” *Int. J. Mod. Phys. A* **32**, no. 23n24, 1750142 (2017) doi:10.1142/S0217751X17501421 [arXiv:1702.03958 [hep-th]].
- [56] D. R. Gulotta, “Properly ordered dimers, R-charges, and an efficient inverse algorithm,” *JHEP* **0810**, 014 (2008) doi:10.1088/1126-6708/2008/10/014 [arXiv:0807.3012 [hep-th]].

- [57] R. Kenyon, A. Okounkov and S. Sheffield, “Dimers and amoebae,” math-ph/0311005.
- [58] J. P. Gauntlett, D. Martelli, J. Sparks and D. Waldram, “Sasaki-Einstein metrics on $S^2 \times S^3$ ” Adv. Theor. Math. Phys. **8**, no. 4, 711 (2004) doi:10.4310/ATMP.2004.v8.n4.a3 [hep-th/0403002].
- [59] J. P. Gauntlett, D. Martelli, J. Sparks and D. Waldram, *Supersymmetric AdS(5) solutions of M theory*, *Class. Quant. Grav.* **21** (2004) 4335–4366, [hep-th/0402153].
- [60] M. Cvetič, H. Lu, D. N. Page and C. N. Pope, “New Einstein-Sasaki spaces in five and higher dimensions,” Phys. Rev. Lett. **95** (2005) 071101 doi:10.1103/PhysRevLett.95.071101 [hep-th/0504225].
- [61] D. Martelli and J. Sparks, *Toric Sasaki-Einstein metrics on $S^{**2} \times S^{**3}$* , *Phys. Lett. B* **621** (2005) 208–212, [hep-th/0505027].
- [62] P Kasteleyn, “The statistics of dimers on a lattice: I. the number of dimer arrangements on a quadratic lattice,” *Physica* 27 (1961), no. 12 1209–1225.
- [63] P. Kasteleyn, “Graph theory and crystal physics,” *Graph theory and theoretical physics* 1 (1967) 43110.
- [64] A. Hanany and A. Zaffaroni, “On the realization of chiral four-dimensional gauge theories using branes,” *JHEP* **9805**, 001 (1998) doi:10.1088/1126-6708/1998/05/001 [hep-th/9801134].
- [65] A. Hanany and E. Witten, “Type IIB superstrings, BPS monopoles, and three-dimensional gauge dynamics,” *Nucl. Phys. B* **492**, 152 (1997) doi:10.1016/S0550-3213(97)00157-0, 10.1016/S0550-3213(97)80030-2 [hep-th/9611230].
- [66] S. Elitzur, A. Giveon and D. Kutasov, “Branes and N=1 duality in string theory,” *Phys. Lett. B* **400**, 269 (1997) doi:10.1016/S0370-2693(97)00375-4 [hep-th/9702014].
- [67] A. Giveon and D. Kutasov, “Brane dynamics and gauge theory,” *Rev. Mod. Phys.* **71**, 983 (1999) doi:10.1103/RevModPhys.71.983 [hep-th/9802067].

- [68] N. Seiberg, “Electric - magnetic duality in supersymmetric nonAbelian gauge theories,” Nucl. Phys. B **435**, 129 (1995) doi:10.1016/0550-3213(94)00023-8 [hep-th/9411149].
- [69] B. Feng, A. Hanany and Y. H. He, “D-brane gauge theories from toric singularities and toric duality,” Nucl. Phys. B **595**, 165 (2001) doi:10.1016/S0550-3213(00)00699-4 [hep-th/0003085].
- [70] C. E. Beasley and M. R. Plesser, “Toric duality is Seiberg duality,” JHEP **0112**, 001 (2001) doi:10.1088/1126-6708/2001/12/001 [hep-th/0109053].
- [71] B. Feng, A. Hanany, Y. H. He and A. M. Uranga, “Toric duality as Seiberg duality and brane diamonds,” JHEP **0112**, 035 (2001) doi:10.1088/1126-6708/2001/12/035 [hep-th/0109063].
- [72] F. Cachazo, B. Fiol, K. A. Intriligator, S. Katz and C. Vafa, “A Geometric unification of dualities,” Nucl. Phys. B **628**, 3 (2002) doi:10.1016/S0550-3213(02)00078-0 [hep-th/0110028].
- [73] B. Feng, A. Hanany and Y. H. He, “Phase structure of D-brane gauge theories and toric duality,” JHEP **0108**, 040 (2001) doi:10.1088/1126-6708/2001/08/040 [hep-th/0104259].
- [74] B. Feng, Y. H. He and F. Lam, “On correspondences between toric singularities and (p,q) webs,” Nucl. Phys. B **701**, 334 (2004) doi:10.1016/j.nuclphysb.2004.08.048 [hep-th/0403133].
- [75] V. A. Novikov, M. A. Shifman, A. I. Vainshtein and V. I. Zakharov, “Exact Gell-Mann-Low Function of Supersymmetric Yang-Mills Theories from Instanton Calculus,” Nucl. Phys. B **229**, 381 (1983). doi:10.1016/0550-3213(83)90338-3
- [76] R. P. Stanley, “Hilbert functions of graded algebras,” *Adv. Math* **28** (1978), no.1 57-83
- [77] J. Harris, “Algebraic geometry: a first course,” Vol 133. Springer Verlag, 1992.
- [78] S. Benvenuti, B. Feng, A. Hanany and Y. H. He, “Counting BPS Operators in Gauge Theories: Quivers, Syzygies and Plethystics,” JHEP **0711**, 050 (2007) doi:10.1088/1126-6708/2007/11/050 [hep-th/0608050].

- [79] B. Feng, A. Hanany and Y. H. He, “Counting gauge invariants: The Plethystic program,” *JHEP* **0703**, 090 (2007) doi:10.1088/1126-6708/2007/03/090 [hep-th/0701063].
- [80] A. Butti, D. Forcella, A. Hanany, D. Vegh and A. Zaffaroni, “Counting Chiral Operators in Quiver Gauge Theories,” *JHEP* **0711**, 092 (2007) doi:10.1088/1126-6708/2007/11/092 [arXiv:0705.2771 [hep-th]].
- [81] A. Hanany and A. Zaffaroni, “The master space of supersymmetric gauge theories,” *Adv. High Energy Phys.* **2010**, 427891 (2010). doi:10.1155/2010/427891
- [82] D. Forcella, A. Hanany, Y. H. He and A. Zaffaroni, “Mastering the Master Space,” *Lett. Math. Phys.* **85**, 163 (2008) doi:10.1007/s11005-008-0255-6 [arXiv:0801.3477 [hep-th]].
- [83] D. Forcella, A. Hanany and A. Zaffaroni, “Master Space, Hilbert Series and Seiberg Duality,” *JHEP* **0907**, 018 (2009) doi:10.1088/1126-6708/2009/07/018 [arXiv:0810.4519 [hep-th]].
- [84] A. Zaffaroni, “The master space of N=1 quiver gauge theories: Counting BPS operators,” Prepared for 8th Workshop on Continuous Advances in QCD (CAQCD-08), Minneapolis, Minnesota, 15-18 May 2008.
- [85] D. Forcella, “Master Space and Hilbert Series for N=1 Field Theories,” arXiv:0902.2109 [hep-th].
- [86] S. Krippendorf, M. J. Dolan, A. Maharana and F. Quevedo, “D-branes at Toric Singularities: Model Building, Yukawa Couplings and Flavour Physics,” *JHEP* **1006**, 092 (2010) doi:10.1007/JHEP06(2010)092 [arXiv:1002.1790 [hep-th]].
- [87] M. J. Dolan, S. Krippendorf and F. Quevedo, *Towards a Systematic Construction of Realistic D-brane Models on a del Pezzo Singularity*, *JHEP* **10** (2011) 024, [1106.6039].
- [88] M. Yamazaki, “Geometry and Combinatorics of Crystal Melting,” *RIMS Kokyuroku Bessatsu B* **28**, 193 (2011) [arXiv:1102.0776 [math-ph]].
- [89] M. Yamazaki, “Crystal Melting and Wall Crossing Phenomena,” *Int. J. Mod. Phys. A* **26**, 1097 (2011) doi:10.1142/S0217751X11051482 [arXiv:1002.1709 [hep-th]].

- [90] M. Yamazaki, “Quivers, YBE and 3-manifolds,” JHEP **1205**, 147 (2012) doi:10.1007/JHEP05(2012)147 [arXiv:1203.5784 [hep-th]].
- [91] A. B. Goncharov and R. Kenyon, “Dimers and cluster integrable systems,” arXiv:1107.5588 [math.AG].
- [92] S. Franco, “Dimer Models, Integrable Systems and Quantum Teichmuller Space,” JHEP **1109**, 057 (2011) doi:10.1007/JHEP09(2011)057 [arXiv:1105.1777 [hep-th]].
- [93] R. Eager, S. Franco and K. Schaeffer, “Dimer Models and Integrable Systems,” JHEP **1206**, 106 (2012) doi:10.1007/JHEP06(2012)106 [arXiv:1107.1244 [hep-th]].
- [94] N. Arkani-Hamed, J. L. Bourjaily, F. Cachazo, A. B. Goncharov, A. Postnikov and J. Trnka, “Grassmannian Geometry of Scattering Amplitudes,” doi:10.1017/CBO9781316091548 arXiv:1212.5605 [hep-th].
- [95] S. Franco, D. Galloni, A. Mariotti and J. Trnka, “Anatomy of the Amplituhedron,” JHEP **1503**, 128 (2015) doi:10.1007/JHEP03(2015)128 [arXiv:1408.3410 [hep-th]].
- [96] B. Feng, Y. H. He, K. D. Kennaway and C. Vafa, “Dimer models from mirror symmetry and quivering amoebae,” Adv. Theor. Math. Phys. **12**, no. 3, 489 (2008) doi:10.4310/ATMP.2008.v12.n3.a2 [hep-th/0511287].
- [97] G. Mikhalkin, “Amoebas of algebraic varieties and tropical geometry,” ArXiv Mathematics e-prints (Feb., 2004) [math/0403].
- [98] N. Broomhead, “Dimer models and Calabi-Yau algebras,” arXiv:0901.4662 [math.AG].
- [99] A. Ishii and K. Ueda, “On moduli spaces of quiver representations associated with dimer models,” ArXiv e-prints (Oct., 2007) [arXiv:0710.1898].
- [100] A. Ishii and K. Ueda, “Dimer models and the special McKay correspondence,” ArXiv e-prints (Oct., 2007) [arXiv:0710.1898].
- [101] H. Derksen, J. Weyman and A. Zelevinsky, *Quivers with potentials and their representations I: Mutations*, 0704.0649.

- [102] H. Derksen, J. Weyman and A. Zelevinsky, *Quivers with potentials and their representations II: Applications to cluster algebras*, 0904.0676.
- [103] K. Baur, A. D. King and R. J. Marsh, *Dimer models and cluster categories of Grassmannians*, *Proc. Lond. Math. Soc. (3)* **113** (2016) 213–260, [1309.6524].
- [104] V. Ginzburg, *Calabi-Yau algebras*, math/0612139.
- [105] R. Bocklandt, *Graded calabi yau algebras of dimension 3*, *Journal of pure and applied algebra* **212** (2008) 14–32, [math/0603558].
- [106] J. Stienstra, “Hypergeometric Systems in two Variables, Quivers, Dimers and Dessins d’Enfants,” arXiv:0711.0464 [math.AG].
- [107] Y. H. He and J. Read, “Hecke Groups, Dessins d’Enfants and the Archimedean Solids,” *Front. in Phys.* **3**, 91 (2015) doi:10.3389/fphy.2015.00091 [arXiv:1309.2326 [math.AG]].
- [108] S. Bose, J. Gundry and Y. H. He, “Gauge theories and dessins d’enfants: beyond the torus,” *JHEP* **1501**, 135 (2015) doi:10.1007/JHEP01(2015)135 [arXiv:1410.2227 [hep-th]].
- [109] V. Jejjala, S. Ramgoolam and D. Rodriguez-Gomez, *Toric CFTs, Permutation Triples and Belyi Pairs*, *JHEP* **03** (2011) 065, [1012.2351].
- [110] A. Hanany, Y.-H. He, V. Jejjala, J. Pasukonis, S. Ramgoolam and D. Rodriguez-Gomez, *The Beta Ansatz: A Tale of Two Complex Structures*, *JHEP* **06** (2011) 056, [1104.5490].
- [111] A. Hanany, Y.-H. He, V. Jejjala, J. Pasukonis, S. Ramgoolam and D. Rodriguez-Gomez, *Invariants of Toric Seiberg Duality*, *Int. J. Mod. Phys. A* **27** (2012) 1250002, [1107.4101].
- [112] R. Vidunas and Y.-H. He, *Composite Genus One Belyi Maps*, 1610.08075.
- [113] J. M. Maldacena, “The Large N limit of superconformal field theories and supergravity,” *Int. J. Theor. Phys.* **38**, 1113 (1999) [*Adv. Theor. Math. Phys.* **2**, 231 (1998)] doi:10.1023/A:1026654312961, 10.4310/ATMP.1998.v2.n2.a1 [hep-th/9711200].

- [114] S. S. Gubser, I. R. Klebanov and A. M. Polyakov, “Gauge theory correlators from non-critical string theory,” *Phys. Lett. B* **428**, 105 (1998) doi:10.1016/S0370-2693(98)00377-3 [hep-th/9802109].
- [115] E. Witten, “Anti-de Sitter space and holography,” *Adv. Theor. Math. Phys.* **2**, 253 (1998) doi:10.4310/ATMP.1998.v2.n2.a2 [hep-th/9802150].
- [116] B. S. Acharya, J. M. Figueroa-O’Farrill, C. M. Hull and B. J. Spence, “Branes at conical singularities and holography,” *Adv. Theor. Math. Phys.* **2**, 1249 (1999) doi:10.4310/ATMP.1998.v2.n6.a2 [hep-th/9808014].
- [117] S. Benvenuti, S. Franco, A. Hanany, D. Martelli and J. Sparks, *An Infinite family of superconformal quiver gauge theories with Sasaki-Einstein duals*, *JHEP* **06** (2005) 064, [hep-th/0411264].
- [118] A. Butti, D. Forcella and A. Zaffaroni, *The Dual superconformal theory for L^{**pqr} manifolds*, *JHEP* **09** (2005) 018, [hep-th/0505220].
- [119] S. Benvenuti and M. Kruczenski, *From Sasaki-Einstein spaces to quivers via BPS geodesics: $L^{**p,q/r}$* , *JHEP* **04** (2006) 033, [hep-th/0505206].
- [120] F. Klein, *Vorlesungen u ber das Ikosaeder und die Auflö sung der Gleichungen vom fünften Grade*, Leipzig, 1884.
- [121] G. Gonzales-Sprinberg and J. Verdier, “Construction g eometrique de la Correspondence de McKay,” *Ann. Sci. Ecole Norm. Sup.* **16** (1983), 409-449.
- [122] P. Kronheimer, *Instantons Gravitationnels et Singularit e de Klein*. *C. R. Acad. Sci. Paris*, **303** Serie I (1986) 53-55.
- [123] D. N. Page, “A Physical Picture of the K3 Gravitational Instanton,” *Phys. Lett.* **80B**, 55 (1978). doi:10.1016/0370-2693(78)90305-2
- [124] M. A. Walton, “The Heterotic String on the Simplest Calabi-yau Manifold and Its Orbifold Limits,” *Phys. Rev. D* **37**, 377 (1988). doi:10.1103/PhysRevD.37.377

- [125] D. Anselmi, M. Billo, P. Fre, L. Girardello and A. Zaffaroni, “ALE manifolds and conformal field theories,” *Int. J. Mod. Phys. A* **9**, 3007 (1994) doi:10.1142/S0217751X94001199 [hep-th/9304135].
- [126] N. Seiberg, “Observations on the Moduli Space of Superconformal Field Theories,” *Nucl. Phys. B* **303**, 286 (1988). doi:10.1016/0550-3213(88)90183-6
- [127] P. S. Aspinwall and D. R. Morrison, “String theory on K3 surfaces,” *AMS/IP Stud. Adv. Math.* **1**, 703 (1996) [hep-th/9404151].
- [128] T. Eguchi and A. J. Hanson, “Selfdual Solutions to Euclidean Gravity,” *Annals Phys.* **120**, 82 (1979). doi:10.1016/0003-4916(79)90282-3
- [129] W. Fulton, “Introduction to Toric Varieties,” Princeton University Press, 1993
- [130] B. R. Greene, “String theory on Calabi-Yau manifolds,” hep-th/9702155.
- [131] K. Hori, S. Katz, A. Klemm, R. Pandharipande, R. Thomas, C. Vafa, R. Vakil, and E. Zaslow, “Mirror Symmetry,” vol. 1 of Clay Mathematics Monographs. American Mathematical Society, 2003. 929p.
- [132] H. Skarke, “String dualities and toric geometry: An Introduction,” *Chaos Solitons Fractals* **10**, 543 (1999) doi:10.1016/S0960-0779(98)00161-1 [hep-th/9806059].
- [133] M. Aganagic, A. Klemm, M. Marino and C. Vafa, “The Topological vertex,” *Commun. Math. Phys.* **254**, 425 (2005) doi:10.1007/s00220-004-1162-z [hep-th/0305132].
- [134] A. Butti and A. Zaffaroni, “From toric geometry to quiver gauge theory: The Equivalence of a-maximization and Z-minimization,” *Fortsch. Phys.* **54**, 309 (2006) doi:10.1002/prop.200510276 [hep-th/0512240].
- [135] A. Butti and A. Zaffaroni, “R-charges from toric diagrams and the equivalence of a-maximization and Z-minimization,” *JHEP* **0511**, 019 (2005) doi:10.1088/1126-6708/2005/11/019 [hep-th/0506232].

- [136] D. Martelli, J. Sparks and S. T. Yau, “The Geometric dual of a-maximisation for Toric Sasaki-Einstein manifolds,” *Commun. Math. Phys.* **268**, 39 (2006) doi:10.1007/s00220-006-0087-0 [hep-th/0503183].
- [137] L. E. Ibanez, R. Rabadan and A. M. Uranga, “Anomalous U(1)’s in type I and type IIB $D = 4$, $N=1$ string vacua,” *Nucl. Phys. B* **542** (1999) 112 doi:10.1016/S0550-3213(98)00791-3 [hep-th/9808139].
- [138] K. A. Intriligator and N. Seiberg, “The Runaway quiver,” *JHEP* **0602**, 031 (2006) doi:10.1088/1126-6708/2006/02/031 [hep-th/0512347].
- [139] B. Feng, S. Franco, A. Hanany and Y. H. He, “Symmetries of toric duality,” *JHEP* **0212**, 076 (2002) doi:10.1088/1126-6708/2002/12/076 [hep-th/0205144].
- [140] B. Feng, S. Franco, A. Hanany and Y. H. He, “UnHiggsing the del Pezzo,” *JHEP* **0308**, 058 (2003) doi:10.1088/1126-6708/2003/08/058 [hep-th/0209228].
- [141] S. Franco and D. Vegh, “Moduli spaces of gauge theories from dimer models: Proof of the correspondence,” *JHEP* **0611**, 054 (2006) doi:10.1088/1126-6708/2006/11/054 [hep-th/0601063].
- [142] T. H. Buscher, “Path Integral Derivation of Quantum Duality in Nonlinear Sigma Models,” *Phys. Lett. B* **201**, 466 (1988). doi:10.1016/0370-2693(88)90602-8
- [143] S. Franco, *Bipartite Field Theories: from D-Brane Probes to Scattering Amplitudes*, *JHEP* **11** (2012) 141, [1207.0807].
- [144] D. Xie and M. Yamazaki, *Network and Seiberg Duality*, *JHEP* **09** (2012) 036, [1207.0811].
- [145] S. Franco, D. Galloni and R.-K. Seong, *New Directions in Bipartite Field Theories*, *JHEP* **06** (2013) 032, [1211.5139].
- [146] S. Franco, *Cluster Transformations from Bipartite Field Theories*, *Phys. Rev.* **D88** (2013) 105010, [1301.0316].

- [147] J. J. Heckman, C. Vafa, D. Xie and M. Yamazaki, *String Theory Origin of Bipartite SCFTs*, *JHEP* **05** (2013) 148, [1211.4587].
- [148] S. Franco and A. Uranga, *Bipartite Field Theories from D-Branes*, *JHEP* **04** (2014) 161, [1306.6331].
- [149] S. Franco, D. Galloni and A. Mariotti, *Bipartite Field Theories, Cluster Algebras and the Grassmannian*, *J. Phys.* **A47** (2014) 474004, [1404.3752].
- [150] R. Bocklandt, *Generating toric noncommutative crepant resolutions*, *Journal of Algebra* **364** (2012) 119–147, [1104.1597].
- [151] S. Mozgovoy and M. Reineke, *On the noncommutative donaldson–thomas invariants arising from brane tilings*, *Advances in mathematics* **223** (2010) 1521–1544, [0809.0117].
- [152] C. Beil, *The geometry of noncommutative singularity resolutions*, 1102.5741.
- [153] R. Bocklandt, A. Craw and A. Q. Véléz, *Geometric reids recipe for dimer models*, *Mathematische Annalen* **361** (2015) 689–723, [1305.0156].
- [154] R. Eager and S. Franco, *Colored BPS Pyramid Partition Functions, Quivers and Cluster Transformations*, *JHEP* **09** (2012) 038, [1112.1132].
- [155] G. Musiker, R. Schiffler and L. Williams, *Bases for cluster algebras from surfaces*, *Compositio Mathematica* **149** (2013) 217–263, [1110.4364].
- [156] T. Lai and G. Musiker, *Beyond Aztec Castles: Toric Cascades in the dP_3 Quiver*, 1512.00507.
- [157] A. B. Goncharov and R. Kenyon, *Dimers and cluster integrable systems*, in *Annales scientifiques de l'École Normale Supérieure*, vol. 46, pp. 747–813, Société mathématique de France, 2013. 1107.5588.
- [158] <https://github.com/DimerSystem/Tilings>.
- [159] A. Ishii and K. Ueda, *A note on consistency conditions on dimer models*, 1012.5449.

- [160] B. Davison, *Consistency conditions for brane tilings*, *Journal of Algebra* **338** (2011) 1–23, [0812.4185].
- [161] R. Bocklandt, *Consistency conditions for dimer models*, *Glasgow Mathematical Journal* **54** (2012) 429–447, [1104.1592].
- [162] A. Hanany, V. Jejjala, S. Ramgoolam and R.-K. Seong, *Consistency and Derangements in Brane Tilings*, *J. Phys.* **A49** (2016) 355401, [1512.09013].
- [163] A. Hanany, D. Orlando and S. Reffert, *Sublattice Counting and Orbifolds*, *JHEP* **06** (2010) 051, [1002.2981].
- [164] J. Davey, A. Hanany and R.-K. Seong, *Counting Orbifolds*, *JHEP* **06** (2010) 010, [1002.3609].
- [165] A. Hanany and R.-K. Seong, *Symmetries of Abelian Orbifolds*, *JHEP* **01** (2011) 027, [1009.3017].
- [166] J. Davey, A. Hanany and R.-K. Seong, *An Introduction to Counting Orbifolds*, *Fortsch. Phys.* **59** (2011) 677–682, [1102.0015].
- [167] A. Hanany, V. Jejjala, S. Ramgoolam and R.-K. Seong, *Calabi-Yau Orbifolds and Torus Coverings*, *JHEP* **09** (2011) 116, [1105.3471].
- [168] A. Hanany, P. Kazakopoulos and B. Wecht, *A New infinite class of quiver gauge theories*, *JHEP* **08** (2005) 054, [hep-th/0503177].
- [169] J. Davey, A. Hanany and J. Pasukonis, *On the Classification of Brane Tilings*, *JHEP* **01** (2010) 078, [0909.2868].
- [170] P. Candelas and X. C. de la Ossa, “Comments on Conifolds,” *Nucl. Phys. B* **342**, 246 (1990). doi:10.1016/0550-3213(90)90577-Z